UNIVERSITY OF LIVERPOOL

UNDERSTANDING THE SELF-ASSEMBLY PROCESS AND TUNABILITY OF THE FINAL PROPERTIES OF DIPEPTIDE-BASED LOW MOLECULAR WEIGHT HYDROGELS

Thesis submitted in accordance with the requirements of the **University of Liverpool** for the degree of **Doctor of Philosophy** by Jaclyn Raeburn

May 2014

Contents

Acknowledgements

Firstly, I would like to say thank you to all of the people who contributed to the experimental data in this thesis, including Dr Tom McDonald (SEM), Dr Petra Cameron (SPR and electrochemistry work), Dr Jonathan Howse (electrochemistry work), Dr Yann Cesbron (confocal microscopy) and Christopher Hill (cell culture study) and all of the technical staff in the Department of Chemistry (University of Liverpool). In particular, I would like to thank Dr Lin Chen for all of her help and guidance in the lab throughout my PhD.

I would also like to mention all of the great people that I have met and worked with during my time in Liverpool. At the risk of insulting anyone by forgetting to mention their name, I will simply say that the group of Scousers (and honorary Scousers) that I have become friends with have made me feel very welcome from the beginning and have contributed to making all aspects of my PhD life very enjoyable. I also say thank you to my family and friends "north of the wall" for supporting and encouraging me from afar.

Finally, and most importantly, I would like to say a huge thank you to Dr Dave Adams for not only giving me the opportunity to work in his group, but for being like a mentor to me throughout my PhD. He always encouraged me to do the absolute best I could and was always very approachable and happy to help me at any time. I really appreciate the invaluable knowledge gained from his supervision, which was paramount to the success of my PhD.

Abstract

Reported in this thesis is the ability to prepare a number of dipeptide-conjugate hydrogels with tunable final properties, through judicious choice of the assembly conditions and gelator structure. Gelation of these materials can be triggered by solvent-mediated, pH-triggered, UV-triggered and electrochemically-induced means to give different mechanical properties. Subtle changes in the assembly conditions can evoke changes in the final properties - something that was evident across a range of gelator systems and methods of triggering gelation. UV and electrochemical methods demonstrated the ability to spatially and temporally control gelation, which could be of potential use to biosensor and cell culturing applications. Molecular rotors could be employed to monitor the kinetics of the gelation process, indicating an evolution in self-assembled structure around the pK_a of a gelator. This thesis highlights the importance of the self-assembly process on the final properties of dipeptide-conjugate gels. A better understanding of this process will be beneficial for gelator design. Where specific hydrogel properties are needed, the gelator will be tunable for a desired application by manipulating the assembly conditions.

Publication List

1. **J. Raeburn**, B. Alston, J. Kroeger, T. O. McDonald, J. R. Howse, P. J. Cameron and D. J. Adams, *Mater. Horiz.*, 2014, **1**, 241-246.
2. **J. Raeburn**, A. Zamith Cardoso and D. J. Adams, *Chem. Soc. Rev.*, 2013, **42**, 5143-5156.
3. K. L. Morris, L. Chen, **J. Raeburn**, O. R. Sellick, P. Cotanda, A. Paul, P. C. Griffiths, S. M. King, R. K. O'Reilly, L. C. Serpell and D. J. Adams, *Nat. Commun.*, 2013, **4**, 1480-1485.
4. J. Huang, C. L. Hastings, G. P. Duffy, H. M. Kelly, **J. Raeburn**, D. J. Adams and A. Heise, *Biomacromolecules*, 2013, **14**, 200-206.
5. **J. Raeburn**, T. O. McDonald and D. J. Adams, *Chem. Commun.*, 2012, **48**, 9355-9357.
6. M. Hughes, P. Frederix, **J. Raeburn**, L. S. Birchall, J. Sadownik, F. C. Coomer, I. H. Lin, E. J. Cussen, N. T. Hunt, T. Tuttle, S. J. Webb, D. J. Adams and R. V. Ulijn, *Soft Matter*, 2012, **8**, 5595-5602.
7. **J. Raeburn**, G. Pont, L. Chen, Y. Cesbron, R. Levy and D. J. Adams, *Soft Matter*, 2012, **8**, 1168-1174.
8. L. Chen, **J. Raeburn**, S. Sutton, D. G. Spiller, J. Williams, J. S. Sharp, P. C. Griffiths, R. K. Heenan, S. M. King, A. Paul, S. Furzeland, D. Atkins and D. J. Adams, *Soft Matter*, 2011, **7**, 9721-9727.

Abbreviations

A	Alanine	**G'**	Storage Modulus
AFM	Atomic Force Microscopy	**G"**	Loss Modulus
CCVJ	9-(2-Carboxy-2-cyanovinyl)julolidine	**GdL**	Glucono-δ-lactone
CD	Circular Dichroism	**HFIP**	Hexafluoroisopropanol
CV	Cyclic Voltammetry	**HPTS**	8-Hydroxypyrene-1,3,6-trisulfonic Acid
DCVJ	9-(2,2-Dicyanovinyl)julolidine	**HQ**	Hydroquinone
DMEM	Dulbecco's Modified Eagle Medium	**L**	Leucine
DMSO	Dimethylsulfoxide	**Log P**	Partition Coefficient
DPIC	Diphenyliodonium Carboxylate	**LVE**	Linear Viscoeleastic
DPIN	Diphenyliodonium Nitrate	**PAG**	Photoacid Generator
DPNDS	Dipotassium 2-Naphthol-6,8-disulfonate Hydrate	**pXRD**	Powder X-Ray Diffraction
F	Phenylalanine	**SEM**	Scanning Electron Microscopy
Fmoc	Fluorenylmethoxycarbonyl	**SPR**	Surface Plasmon Resonance Spectroscopy
FT-IR	Fourier Transform-Infrared Spectroscopy	**ThT**	Thioflavin T
FTO	Fluorine-Doped Tin Oxide	**V**	Valine
G	Glycine	**$\Phi_{solvent}$**	Volume Fraction of Solvent

CHAPTER 1

Introduction

1.1 Hydrogels

Hydrogels are a class of viscoelastic materials consisting primarily of water yet possessing properties more reminiscent of a solid material.[1, 2] The reason for this behaviour is that a hydrogel consists of a fibrous network capable of immobilising water. These materials are widely studied and are gaining ever-increasing interest as a consequence of their potential to be used in an array of applications. Hydrogels have shown promise in many biological applications due to the biocompatibility of the hydrogel systems, allowing for applications in drug delivery[3], tissue engineering and cell culturing.[4, 5] The fibrous matrix of a hydrogel can be formed from a range of different materials including synthetic polymers such as crosslinked poly(ethylene oxide) (PEO)[6] and poly(sodium acrylate) (PSA)[7], naturally occurring biopolymers (including alginate[8, 9] and pectin[9]) and low molecular weight gelators (LMWG) (discussed in detail below and are the focus of this Thesis). Synthetic polymeric materials form hydrogels by way of crosslinking in water, which in turn renders the polymer insoluble, causing this crosslinked network to entrap water in the polymer matrix (Figure 1). Crosslinking is usually induced by a UV-initiated method. For example, poly(acetic acid) (PAAc)/chitosan gels have been prepared by photo-initiated crosslinking of PAAc to afford PAAc/chitosan gels with high mechanical strengths in the MPa range.[10] The amino acid chains of chitosan are thought to form a polyelectrolyte complex with the carboxylic acid groups of the crosslinked PAAc network.[10 11] The major limitations with polymeric hydrogels when the desired applications are biological are that the presence of radical materials from the polymerisation process can damage cells and if a controlled release application is desired, encapsulation of the drug material may also be affected by presence of these radical materials.[12] In some cases, this would require drug loading to occur post-crosslinking.[13] Biopolymers are an alternative to synthetic hydrogels in a bid to increase the bioavailability. However, in another attempt to overcome the pitfalls associated with polymer hydrogels, LMWG have emerged as a promising class of materials (Figure 1).

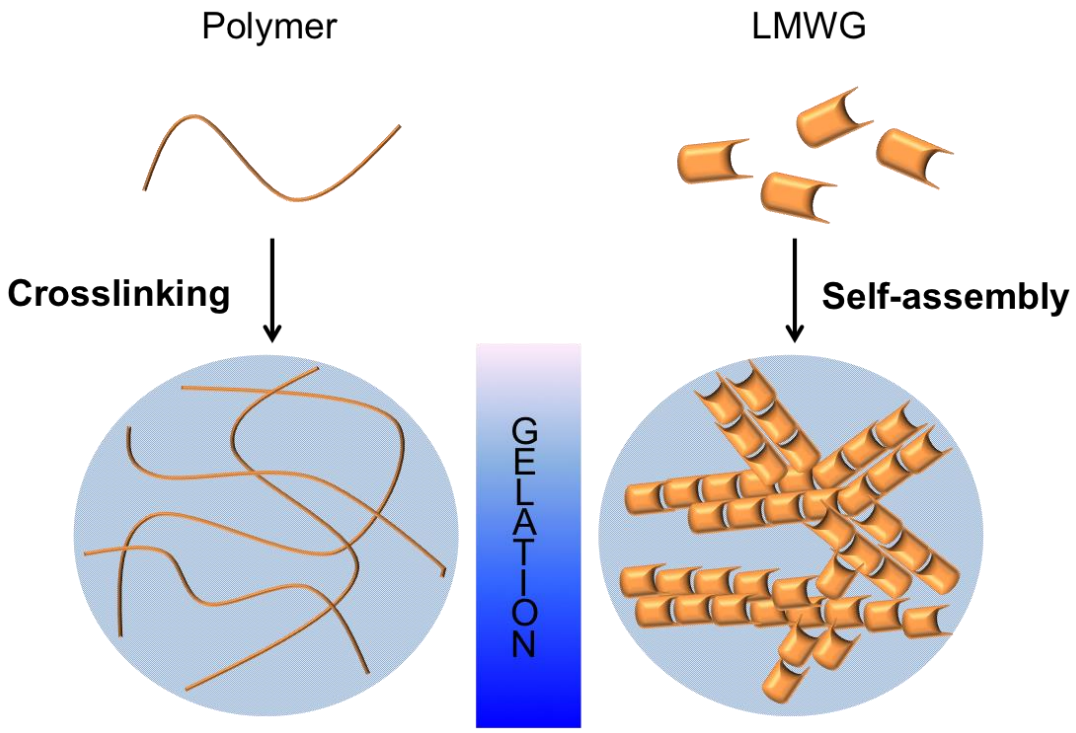

Figure 1 Schematic highlighting the differences in structure between a) polymer hydrogels and b) low molecular weight hydrogels

1.2 Low Molecular Weight Gelators (LMWG)

LMWG are small molecules (typically with a molecular weight < 1000 Da) that self-assemble in water to form a hydrogel.[1, 2, 14, 15] These differ from polymer hydrogels in that the interactions between gelator molecules upon assembly consist of non-covalent interactions, rather than chemical (covalently-bonded) crosslinks (Figure 2). LMWG tend to be mechanically different as a result, with LMWG exhibiting hydrogel breakdown at much lower strains. When LMWG assemble, assembly is driven by hydrogen-bonding, van der Waals interactions, π-π stacking and electrostatic interactions.[1, 2, 16] The one-dimensional structures formed *via* these interactions, grow and entangle to form a fibrous matrix that ultimately entraps the water to form a hydrogel (Figure 2). The distinct difference in bonding between these classes of materials (LMWG and polymeric) impacts the reversibility of the gels. A gel-sol transition for LMWG is relatively easily achieved compared to polymeric gels containing chemically bonded crosslinks[9, 12], thus, the use of a LMWG hydrogel as a temporary scaffold for *in vivo* applications is more attractive than using a

polymer hydrogel scaffold, as the former could easily be released and removed when no longer needed.

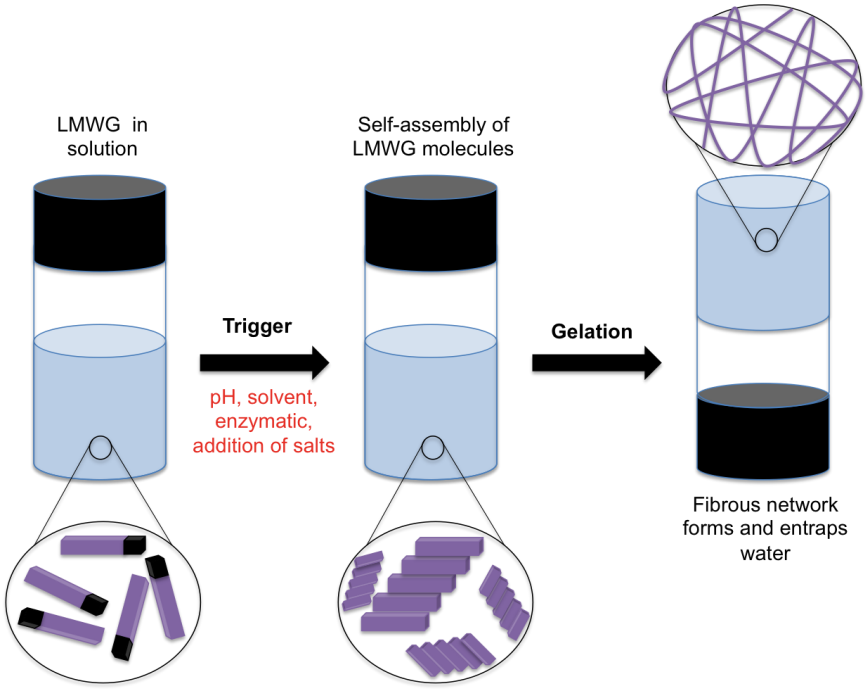

Figure 2 Schematic showing the self-assembly of a gelator *via* non-covalent interactions leading to a fibrous network that entangles to produce a self-supporting gel

1.3 Design of LMWG

Numerous examples of LMWG gelators exist in the literature.[1, 2, 15] Examples include functionalised sugars[17] and oligopeptides.[18] A common theme also exists between these molecules: the ability to H-bond and have specific regions capable of directionally bonding *via* other non-covalent interactions. More specifically, LMWG tend to consist of a hydrophilic region to allow for compatibility with water and a hydrophobic region that drives the self-assembly in water. LMWG consisting of peptides are very common. A system devised by Zhang and co-workers utilised a β-sheet-based fibrous system created by a pattern of hydrophobic amino acid residues and complementary charges between peptides to give the gelator RADA16-I (amongst others).[19, 20] Once gelled, this material has been shown to maintain its supramolecular structure after being subjected to mechanical stress (sonication). Atomic force microscopy (AFM) indicated that upon subjection to mechanical stress, the long fibres of the self-assembled peptide material break down to smaller fibrous

fragments, but reform after cessation of the mechanical stress. Circular dichroism (CD) measurements showed no change at the molecular level of the peptide at any time during the experiment.[20] Based on the concept proposed by Zhang and co-workers, similar ionic-complimentary peptides have been synthesised and successfully used to form hydrogels. Saiani *et al*. prepared phenylalanine-based octa-peptides that formed β-sheets in solution before forming gels upon cooling the peptide-solution from 90 °C to room temperature.[21] Pochan and Schneider developed a 20 amino acid gelator gelator consisting of two strands with an alternating sequence of valine (V) and lysine (K) residues that are connected with a tetrapeptide type II' turn sequence (–VDPPT–) to give the gelator MAX1.[22-24] This gelator forms a β-hairpin conformation preceding gelation (Figure 3). Folding of MAX1 occurs as a result of diminished electrostatic repulsion between positively-charged lysine residues leading to self-assembly of MAX1 – facilitated *via* both H-bonding between β -hairpins and hydrophobic association of valine-rich faces of the folded peptide.

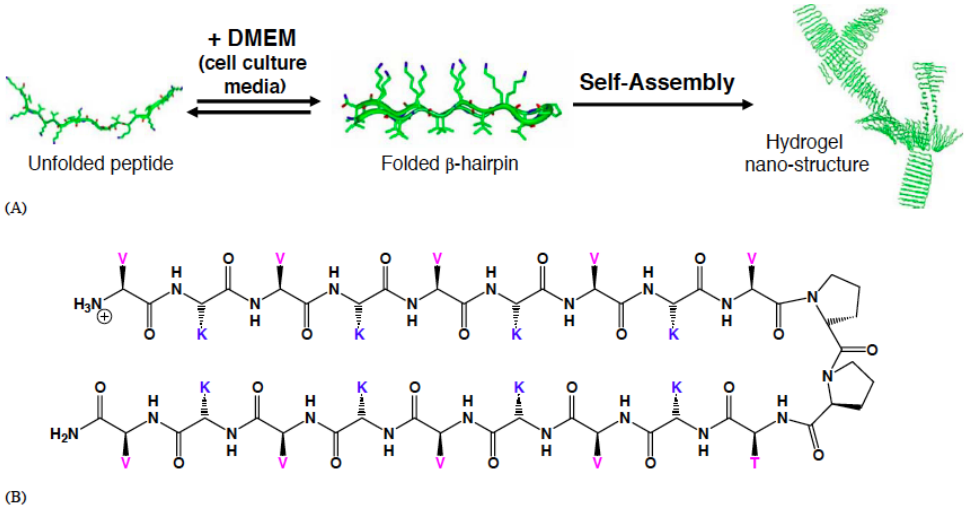

Figure 3 a) Schematic for the assembly of MAX 1 and b) the folded sequence of MAX1[23]

1.3.1 Amino Acids

As mentioned briefly above, peptide gelators are commonly studied and are becoming increasingly popular. The development of materials of biological origin is of interest to many areas in science. The fabrication of such biomaterials at the molecular scale from ''the bottom up'', *via* synthesis one molecule at a time, to the

self-assembly of one unit at a time is advantageous. This approach is not only flexible and possible using relatively simple building blocks, but these materials can also be specifically designed to incorporate desired chemical functionality, thus having the potential to cater to biochemically and medically desired features. The simple building blocks that can serve as a means of designing biocompatible gelator materials are amino acids. Amino acids are the natural building blocks for peptide and proteins in nature. There are twenty naturally occurring amino acids (Figure 4). With the exception of glycine (G), all amino acids are chiral in nature and exist in the $_{L}$-conformation. Amino acids have the same basic structure: a carboxylic acid end group (C-terminus); a primary amine end group (N-terminus) and an R-group on the central carbon connecting the termini. Depending on the group of the amino acid, they can be classified as either hydrophobic, hydrophilic, charged or "other".[15]

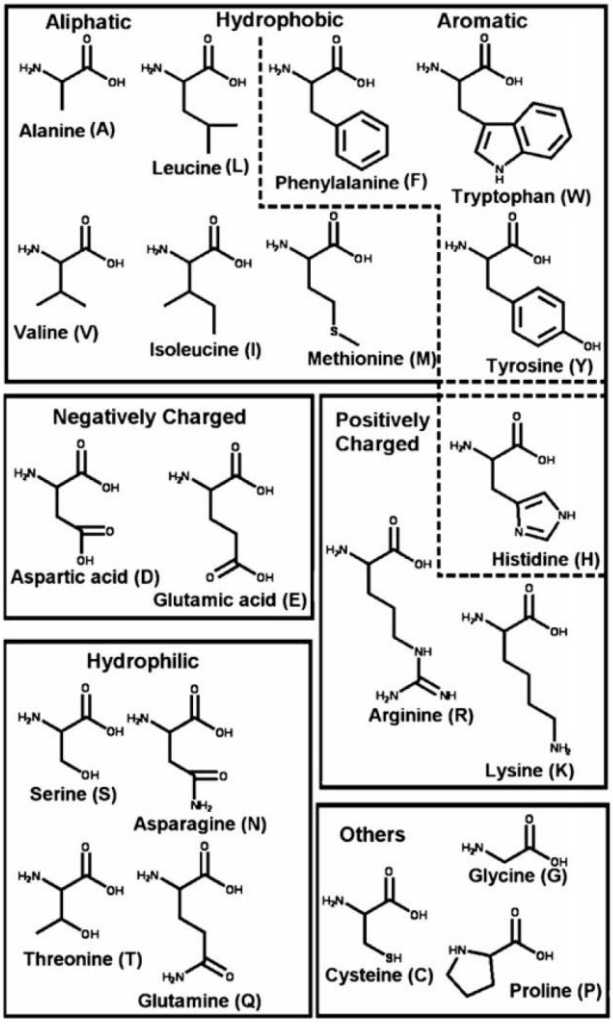

Figure 4 Structures of the 20 naturally occurring amino acids[15]

Sequences of amino acids provide the primary structure for peptide materials, with amino acids chains being synthesised *via* condensation reactions to give peptide bonds between each coupled amino acid pair (Scheme 1).[15]

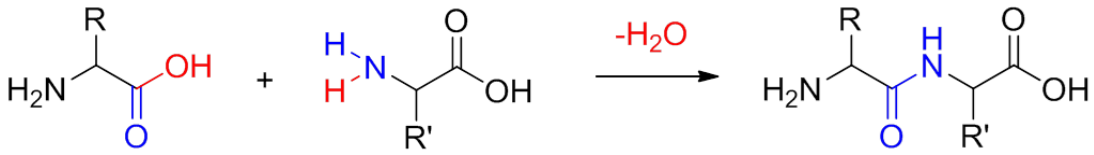

Scheme 1 Condensation reaction showing the coupling of amino acids to form a peptide chain joined *via* a peptide bond

The conformation adopted by these peptide chains is dependent on the interaction and functionality of neighbouring amino acids.[15] Amino acids can interact with one another *via* H-bonding between C- and N-termini of nearby molecules. Aromatic amino acid residues can further interact with other aromatic amino acids via π-π interactions where π-orbital overlap occurs in these π-conjugated systems. Charged residues can be manipulated to create electrostatic interactions/repulsions between residues to influence assembly between residues. Assembly of amino acid residues into natural secondary peptidic structures such as α-helices and coiled coils (Woolfson[25, 26]), β-sheets (Zhang[19, 27, 28]) and turns (Schneider and Pochan[22, 24, 29]) can be the basis for self-assembling hydrogelator molecules. Utilising the knowledge of the conformational properties of these building blocks allows some basic design rules to be ascertained for developing new gelator systems.

1.3.2 Peptide Amphiphiles

Beyond the scope of basic secondary structures of amino acids as the principals for designing assembling gelator molecules, extensive studies have been carried out on a modified class of materials. Peptide amphiphiles (PA) are a class of oligopeptides that incorporate a hydrophobic alkyl tail onto a peptide chain to give distinct hydrophobic and hydrophilic regions, much like surfactant molecules. Both the alkyl chain and amino acid sequence can be altered in an attempt to design a successful gelator. Stupp and his group utilised a sixteen-carbon alkyl chain coupled to a peptide chain consisting of several main components.[18, 30] The first component is a robust chain of four cysteine residues that are adjoined to the alkyl chain. These cysteine residues can form disulfide bonds with nearby molecules upon oxidation,

allowing the supramolecular structure to be locked in. Coupled to the cysteine residues is a chain of three glycine residues, giving flexibility to the hydrophilic head region of the molecule. To add functionality to the molecule, the next component on the chain is a phosphorylated serine residue which is needed to interact with calcium ions – this molecule is designed to mineralise hydroxyapatite (HA), and phosphorylated proteins are closely related to collagen extracellular matrix (ECM) which is known to play a role in the mineralisation of HA. Upon self-assembly, a highly phosphorylated surface will be visible. The final component of this molecule is the cell adhesion motif; arg-gly-asp (RGD). When self-assembled, this molecule adopts a configuration where the hydrophobic alkyl chain makes up the core of cylindrical micelle (Figure 5), the robust cysteine portion of the molecule is the β-sheet, hydrogen bonding region, whereas the outer core consists of the remainder of the peptide chain and is not constrained to a specific conformation. This region forms the interface of the assembled material.[30]

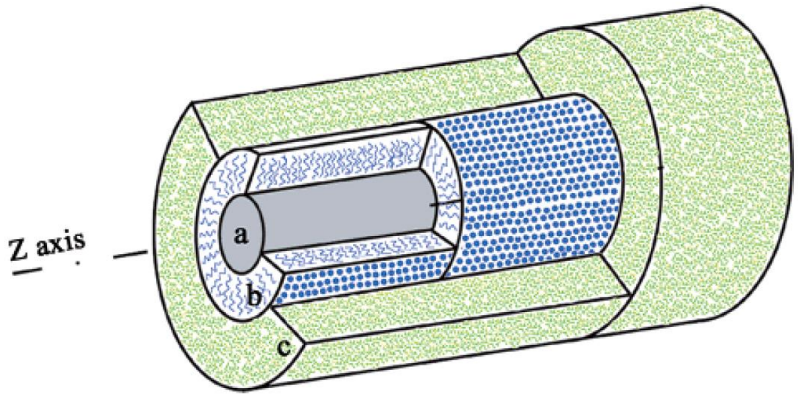

Figure 5 Basic structure of a self-assembled PA devised by Stupp and his group. a) the hydrophobic alkyl chain makes up the core of the cylindrical micelle, b) the four cysteine residues constitute the hydrogen bonding, β-sheet forming portion of the molecule and c) consists of the rest of the peptide chain[30]

From the work of Stupp and his co-workers, there are certain principles for the design of PA (that can self-assemble) which have become apparent. Extrapolating the knowledge gained here enabled an emerging subclass of PA to becoming widely studied: dipeptide-conjugates. Dipeptide-conjugate gelators consist of a dipeptide unit joined to a large aromatic group.[15, 31] These aromatic groups include fluorenylmethoxycarbonyl (Fmoc), naphthalene and pyrene (Scheme 2).

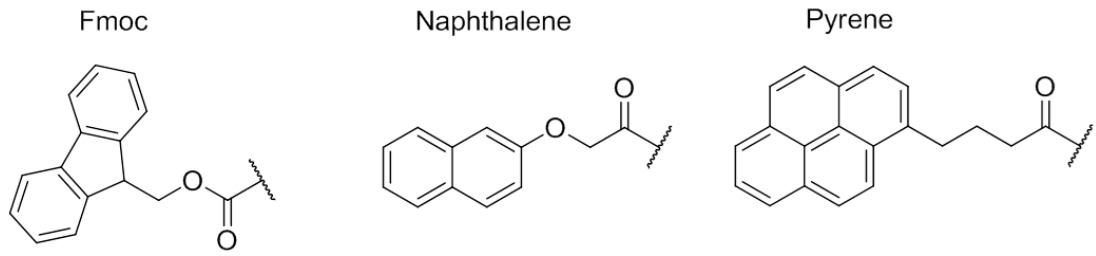

Scheme 2 Structures of aromatic groups commonly joined to dipeptide units to form dipeptide-conjugate gelators

Numerous examples of this class of material exist in the literature[15, 31, 32] but the absolute design rules for a successful gelator molecule are still not fully understood.[33] Subtle variations in the structure and choice of amino acid can be the difference between a gelling and non-gelling material.[34]

1.3.3 Dipeptide-Conjugate Gelators

1.3.3.1 Fmoc Gelators

The most extensively studied dipeptide gelators contain the aromatic group Fmoc. Many Fmoc-dipeptide hydrogels exist in the literature[35-37], but the most commonly reported of all is FmocFF (Scheme 3).

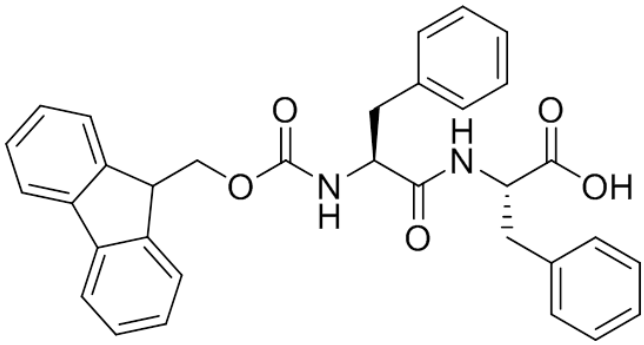

Scheme 3 Structure of the gelator FmocFF

FmocFF is such an attractive gelator as it has been known to form homogenous, transparent hydrogels at physiological pH.[38] This gives the potential for FmocFF gels to be used for a myriad of biological applications, in particular, as a temporary scaffold for cell culturing[5] or controlled drug release.[3] The use of this gelator was first reported by Gazit and his co-workers, who had previously shown the self-assembly of diphenylalanine alone.[39] Diphenylalanine makes up the aromatic core

recognition motif of β-amyloid fibrils, and aromatic residues are thought to play a key role in the self-assembly of into these fibrils *via* aromatic stacking interactions.[39] On this basis, Gazit and his co-workers investigated the contribution of aromatic interactions by incorporating an aromatic group onto the N-terminus of diphenylalanine. They prepared FmocFF gels (and gels with the Fmoc replaced with the protecting group tert-butyloxycarbonyl (Boc)) and found that they self-assembled into amyloid-like fibrils. They also found that diphenylalanine modified with a non-aromatic group on the N-terminus did self-assemble but to form highly ordered, tubular structures rather than smaller, amyloid-like fibrils.[40] FmocFF was found to be the smallest unit known to self-assemble into fibrillar structures similar to amyloid fibrils. The (smaller) diphenylalanine unit alone has also been shown to self-assemble, but into tubular structures, rather than amyloid-like fibrous structures.[40] Gazit's group prepared gels from FmocFF with less than 1 % peptide material in the final hydrogel. Ulijn and his group have also studied FmocFF extensively and have shown that FmocFF gels have the composition and structure to suit the potential growth of cells in the gel matrix[5, 41] (as have other researchers[3, 42]). With FmocFF, a gelator with huge potential has been designed by applying basic principals for peptide assembly. Jayawarna *et al*. prepared a small library of Fmoc-dipeptide hydrogels and showed that the design of gelators is more complex and less understood than the simple principle adopted to successfully design FmocFF. They found that the sequence of amino acid residues joined to the Fmoc group can mean the difference between a gelling and non-gelling material. For instance, FmocFG can form a hydrogel under the conditions used but FmocGF cannot.[37] This was also verified later by Orbach *et al*. who encountered the same result under different assembly conditions.[34] Another publication by Orbach *et al*. also demonstrated the complexity of gelator design by showing that the sequence of amino acids was vital in Fmoc-peptide gelator containing four amino acid residues. Again, one sequence (FmocRGDF) could successfully self-assemble to give a network capable of forming a hydrogel but a similar molecule (FmocFRGD) could not under certain conditions.[43] The amino acid sequence order can lead to different assembled structures in a number of Fmoc-tripeptides.[44] Zhang *et al*. have also shown that in the specific case of FmocAA, the choice of amino acid enantiomer does not affect hydrogelation.[36]

Although FmocFF was found to be the smallest unit to form amyloid fibrils upon assembly, smaller Fmoc gelator molecules have been made. Fmoc conjugated to single amino acids such as tyrosine have been commonly reported in the literature.[45-50]

1.3.3.2 Naphthalene Gelators

The understanding that aromatic π-π stacking interactions play a vital role in directing the assembly of peptide molecules has been applied to many other dipeptide-conjugate materials. Upon looking for an alternative to Fmoc, Bing Xu pioneered a class of dipeptide gelator that contains a naphthalene ring on the N-terminus as the aromatic directing group.[51, 52] Xu used a library-based approach to investigate the rules for designing these gelator molecules. Due to the ease of synthesis of naphthalene-dipeptide molecules, a wider number of molecules could be studied in a bid to gain an insight into what makes a successful gelator and what results in a non-gelling material. A similar approach was also adopted later by our group for naphthalene-dipeptide gelator molecules.[53] Yang *et al*. were able to prepare stable, mechanically strong hydrogels from many naphthalene-dipeptides; with some gelators forming gels at a concentration as low as 0.07 %.[52] Our group expanded on the library of these materials by introducing functional groups such as bromo and cyano groups onto the naphthalene ring to increase the hydrophobicity of the gelator. More hydrophobic gelators have shown to be better gelators – with greater stability and mechanical properties.[52-54] The efficiency of naphthalene to produce a successful gelator allowed it to be considered a versatile motif for the development and design of new gelator molecules.[52-54] Furthermore, the instability of the Fmoc group under basic conditions[55], which are necessary to dissolve the gelator, can pose a problem which would not be expected for naphthalene-based gelator materials.[53] Both Fmoc and naphthalene-based gelators will be the basis for this thesis.

1.4 Gelation of LMWG

Although it has been found that subtle changes in the gelator structure can result in no gelation, there are many different methods by which gelation can induced. By changing the solution conditions in some way (Figure 2), the gelator molecules can be triggered to nucleate and grow into a fibrous entangled network capable of

entrapping water i.e. self-assemble. The gelator molecules transition from a soluble state into insoluble, fibrous structures.

1.4.1 Temperature Trigger

Due to the hydrophobic nature of many LMWG, they tend to be soluble in water only at low concentration and at high temperature. As solubility is reducing as the temperature is decreased, non-covalent interactions drive assembly of the gelator to give fibrous structures. The first example of temperature-triggered gelation of Fmoc-dipeptide based LMWG was demonstrated by Vegners *et al*.[56] By cooling solutions of gelator, gelation occurred. The minimum gelation concentration was found be much higher for the most hydrophilic gelator tested (FmocAD). Debnath *et al*. have prepared gels by lowering the temperature of various solutions containing Fmoc-dipeptides with cationic C-termini.[57] Not many examples of temperature-triggered gelation of LMWG exist in the literature despite a heat-cool cycle of a gel being a common way of demonstrating the healable properties of a gel.[24, 58] The gelation formation and melting temperatures have been known to be affected by the solvent used.[59] The use of temperature to induce assembly is more widely reported for polymer hydrogelation due to the lower solubility of certain longer polymer chains.[59, 60]

1.4.2 Solvent-Mediated Gelation

As LMWG contain a hydrophobic component, solubility in water to prepare the gel may be a problem, even at low gelator concentrations. A way to overcome this is to dissolve the gelator in another solvent to give a saturated solution of LMWG. Upon dilution of the solution with water to produce the hydrogel, the hydrophobic interactions take precedence and trigger assembly of the gelator molecules, forming fibrous structures. This has become an increasingly popular method due to the ease of preparation, as many cases reported have described little or no mixing of the gelator being required in certain solvents.[58, 61] Also, this method demonstrates very quick gelation times when compared to other assembly methods.[38, 58, 61] Furthermore, hydrogels prepared in this way have been known to be stable over a wide pH range, including extreme acidic conditions, and in the presence of urea and guanidinium hydrochloride.[3, 61]

1.4.3 Enzymatically-Triggered Gelation

Due to the inherent biocompatibility of peptide-based LMWG[62], the application of hydrogels in biological applications is a common area of research. However, the main issue is the need for the self-assembly process to be triggered under physiological conditions. One possible way of overcoming this issue is the use of an enzyme to trigger gelation. Enzymes can serve as a catalytic tool used to convert a soluble, non-gelling precursor molecule to a self-assembling gelator *in situ*. Enzymatically-triggered self-assembly can be achieved by two methods. First, the removal of an enzyme-cleavable group from a solubilised molecule, resulting in the formation of the hydrogelator which is then capable of self-assembling. The other method involves the catalysis of the synthesis of a self-assembling hydrogelator molecule. Enzymatic assembly methods have been demonstrated by both Xu's group[47, 63] and Uljin's group.[64] Both groups have used tyrosine-phosphate attached to an Fmoc group, which is soluble in buffer solution. Addition of the enzyme alkaline phosphatase catalyses the dephosphorylation of the molecule to give the insoluble FmocY hydrogelator (Scheme 4). This change in hydrophobicity, as a result, leads to the self-assembly of FmocY. Xinming *et al*. have adopted this method to enzymatically prepare a hydrogelator from a naphthalene-conjugated short peptide motif. This contained a tyrosine-phosphate as before and utilised a dephosphorylation reaction, resulting in the gelator. This gelator contained an azobenzene group that could undergo a photo-switching reaction. Upon UV irradiation, *trans-cis* isomerisation of the azobenzene group occurred, leading to a gel-sol transition.[65]

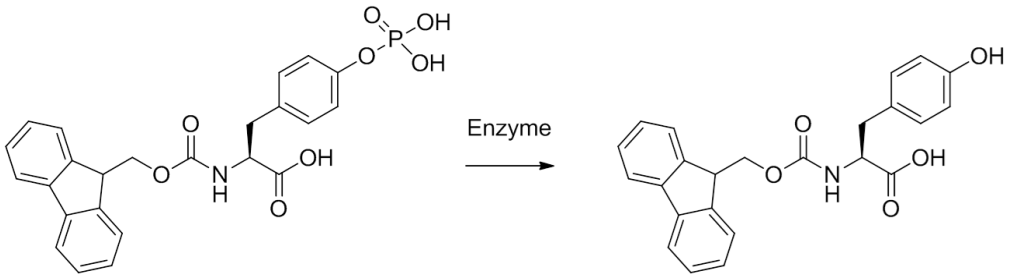

Scheme 4 Dephosphorylation of FmocY-phosphate to give the hydrogelator FmocY *via* enzyme action

Another example of gelation triggered by way of an enzyme-cleavable group involves the methyl ester hydrolysis from the C-terminus of an Fmoc-conjugated dipeptide, to produce a hydrogelator *in situ* using the enzyme subtilisin.[66] The use of a two-enzyme system to trigger both the gelation and gel-sol transition have also been demonstrated.[66]

The other enzymatic route for producing a hydrogelator from a solubilised non-gelling precursor *in situ* has been demonstrated for LMWG. Williams *et al*. prepared a small library of assembling materials by the reaction of an Fmoc-amino acid and a C-terminus protected amino acid *via* reversed hydrolysis (Scheme 5).[64, 67] Amide bond formation was thought to be favoured in these reactions over hydrolysis of the peptide bonds (using the enzyme thermolysin) due to the stabilisation of the amino component by the formation of assembled structures.[67] Williams *et al*. show that spatially controlled gelation using this enzymatic process is possible, as a result of hydrogelation occurring at the site of the enzyme.[67]

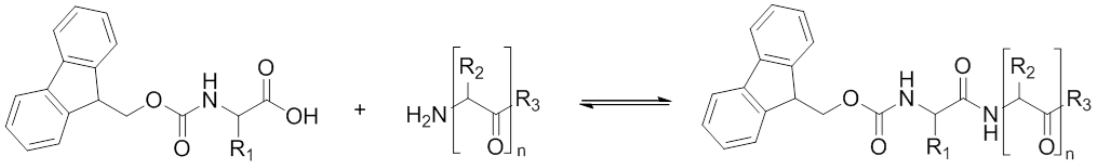

Scheme 5 Hydrogelator formation through the use of an enzymatic route *via* reversed hydrolysis, as described by Williams *et al*.[67]

Yang *et al*. have demonstrated a simple assay showing the potential of enzymatically-triggered gelation for use in bioanalytical applications. Using the tyrosine-phosphate system mentioned above, the presence of inhibitors that block the active site, which results in no enzyme action and hence, no gel formation could be detected. They showed that this visual assay provided efficient initial screening of several inhibitors without the need for spectroscopic assays.[68]

1.4.4 pH-Triggered Gelation

Perhaps the most widely studied method by which self-assembly and hence gelation is triggered for dipeptide-based LMWG is a pH trigger. Due to the use of charge interactions in the self-assembly process itself, many LMWG are inherently pH sensitive, therefore a pH trigger is relatively simple to utilise. The solubility of

gelator molecules tends to be pH dependent. Most of the dipeptide-conjugate gelators are coupled *via* the N-terminus of the dipeptide chain, leaving the C-terminus free and therefore charged at high pH and protonated (and hence, uncharged) at low pH. The charged C-terminus solubilises the gelator molecules in water and a decrease in pH decreases the solubility and results in self-assembly of the gelator to produce a hydrogel. Some gelators do form assembled structures at high pH, leading to higher viscosity, however no gel is formed unless the pH is lowered.[69, 70] Our group (and others[38]) recently reported that gelation does not occur until the pH is lower than the apparent pK_a of the C-termini of these materials. The pK_a values were found to be significantly higher than the pK_a of conventional peptides (approx. 3.5) and the pK_a values were also seen to be related to the hydrophobicity of the gelator.[53, 71] This is a result of the hydrophobicity of the whole molecule, as changing the amino acid or aromatic substituent can affect the hydrophobicity (and the pK_a). From the study produced by Chen *et al*., the most hydrophobic molecules generally have the highest pK_a values.[53] The LMWG with the higher pK_a values were later found to be assembled into worm-like micelles at high pH.[69] It is also known that the pK_a can shift dramatically in hydrophobic environments for proteins and peptides.[72]

The majority of researchers employ a pH trigger to their LMWG through the use of hydrochloric acid (HCl). When Yang *et al*. first prepared a small library of naphthalene-dipeptides; they dissolved the gelators at high pH to deprotonate the C-terminus. To trigger gelation, a small volume of 1 M HCl was added and transparent gels were formed. The final pH of the gels were ~ 2.[52] Ulijn has extensively reported pH-triggered gelation of FmocFF. His group have reported the pK_a of FmocFF as 9.9 and dissolved the gelator above this pH value. The Fmoc group is known to be unstable at high pH[55] and therefore Fmoc-dipeptide stock solutions would be unstable over time.[46] FmocFF has the highest reported pK_a value of any dipeptide-conjugate gelator[38], giving it potential for use in cell culturing. Ulijn has demonstrated that FmocFF is stable at physiological pH and can support chondrocytes in culture.[37] Ulijn and his co-workers add HCl to their stock solution to form a gel, sometimes utilising heating and cooling along with the addition of acid.[38] The latter may add to the widely reported array of mechanical properties for FmocFF gels prepared using HCl.[73] However, even when no heating is applied during the

gelation process, heterogeneity of the final gel is still observed.[74] Thus, HCl does not appear to be a very reproducible method for preparing gels from FmocFF.

Using this information, this group more recently reported an alternative method for inducing a pH decrease to trigger gelation: the use of the sugar glucono-δ-lactone (GdL). This molecule slowly hydrolyses in water to produce gluconic acid[75] (Figure 6).

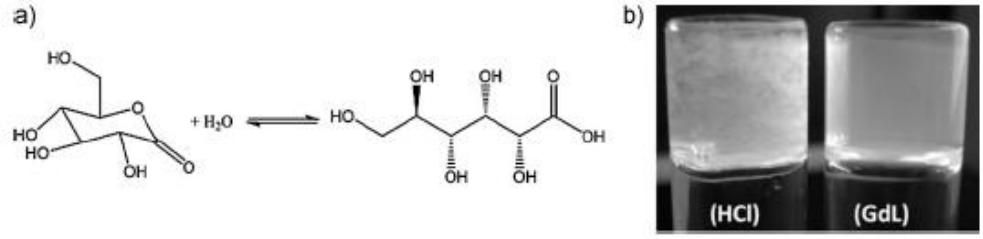

Figure 6 a) The hydrolysis of glucono-δ-lactone (GdL) to gluconic acid. b) Hydrogels of FmocLG prepared using HCl and GdL, showing that GdL produces a more homogeneous hydrogel[32]

Dissolution of GdL is quicker than the hydrolysis of GdL and a slow decrease in pH ensues as a result. This allows for a more homogeneous pH decrease throughout the bulk gelator solution and results in a visibly more homogeneous hydrogel being produced (Figure 6b). This method has been used on an array of gelators by this group[35, 53] and by others[50] and reproducible gels were formed.

1.4.5 Salt-Induced Gelation

Many reports (and mentioned above) show that dipeptide-conjugate gelators are insoluble in water unless the C-terminus is deprotonated to give an anionic molecule.[35, 38, 53] This requires the gelator to be under alkaline conditions and therefore above the apparent pK_a of the gelator molecule. Self-assembly to form a gel therefore does not occur until a pH value lower than the pK_a is reached.[54] Hence, the pH range at which gelation will occur is fairly restricted. Most gelators tend to have a pK_a below physiological pH, even with tuning of the hydrophobicity of gelators in a library.[53] For some gelators studied in this group, at high pH, gelators are above the critical micelle concentration (cmc) of that molecule which leads to the formation of assembled structures.[53] These structures were found to be worm-like micelles and this characteristic was apparent in the more hydrophobic gelators studied in a

library.[69] Through the addition of divalent cations (trivalent and polyvalent can be used in some cases[70]) from ionic salts, the charges on the C-termini of the gelator molecules could be screened which, in turn, led to crosslinking between worm-like micelles to form a network. From this hypothesis, the core of the worm-like micelles were assumed to be hydrophobic, with the carboxylate anions stabilising the micelle-water interface. The crosslinking points were "egg-box" junction type crosslinks (Figure 7), where the divalent cation was the foundation of the crosslink point.[69, 70] Ultimately, gelation occurs as a result of the crosslinking – and above the pK_a of the gelator. The egg-box model was originally proposed for alginate and pectin gels prepared using divalent calcium ions.[9] These crosslinks differ from the chemical crosslinks in polymer hydrogels, where all bonds formed are covalent.[76] Here, physical crosslinking between salt cations and gelator anions occurs and the interactions are electrostatic and non-covalent.

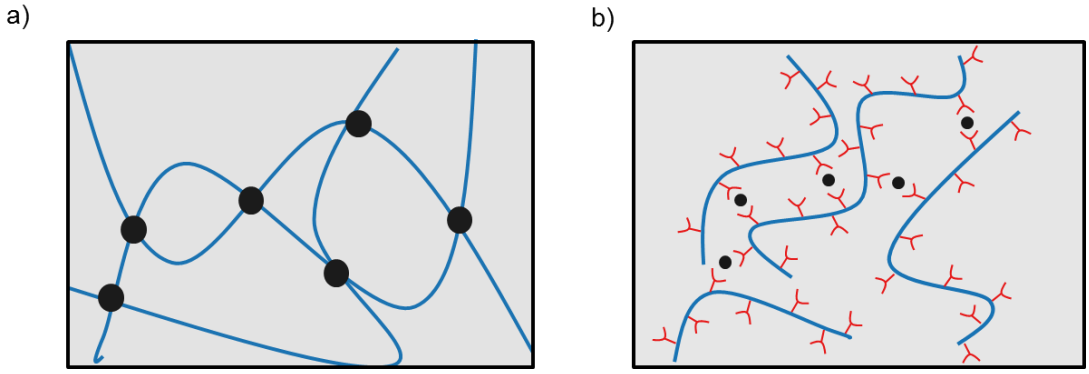

Figure 7 Hydrogel networks of a) polymer gel consisting of a covalently-bonded crosslinked network and b) a LMWG network where the charges on the gelator molecule are screened by salt ions, resulting in non-covalent crosslink points

Roy *et al*. have used ion complexation to screen the charge on an Fmoc-dipeptide. They used a combination of enzymatically-triggered gelation with the addition of salts and showed that the mechanical strength of the gels was increased with the presence of salts. They attributed the changes in the gel properties to increased electrostatic interactions, with the increasing interaction of different salts following the Hofmeister trend.[77] Shi *et al*. also demonstrated increased mechanical strength by orders of magnitude when the calcium salt concentration was increased in their oligopeptide gel systems, thus deducing that increased calcium salt bridges could increase mechanical strength.[78] Pochan and Schneider have studied the effects of the

addition of borate anions in their MAX1 gels. MAX1 assembles above a certain critical temperature. This is a reversible process, with unfolding of MAX1 occurring when the temperature is lowered. However, in the presence of borate anions, the folding and assembly process is irreversible. Complexation between the borate anions and lysine side chains of MAX1 allows physical crosslinking between MAX1 molecules to occur – in addition to the physical crosslinks already present above the transition temperature. The presence of borate anions led to a stiffening transition as a result.[79]

1.4.6 UV-Triggered Gelation

UV light is commonly used to trigger crosslinking in polymer materials which can lead to hydrogelation.[10] Again, this produces chemical crosslinks unlike those observed in LMWG. UV-triggered hydrogelation of LMWG has become an area of interest. The majority of self-assembly triggers result in bulk gelation, whereas UV light can be focused on a particular area; through the use of photolithography, where UV light and a UV mask are utilised. Thus, allowing spatial and temporal control over gelation.[80] Stupp and his group have used UV light to trigger gelation of a peptide amphiphile (PA). To do so, a non-gelling precursor containing a photo-cleavable 2-nitryl group was irradiated with UV light, resulting in a sol-gel transition. This transition upon UV irradiation triggered a significant change in the supramolecular structure of the PA, as nanofibres were produced from nanospheres.[81] UV light can also trigger the transition of a gel to a solution. Li *et al*. have used UV light to switch from a *trans* to a *cis* isomer, leading to the gelator becoming a non-gelling material.[65]

More recently, UV-triggered gelation *via* the use of a photoacid generator (PAG) has emerged as an efficient self-assembly method.[9] Upon UV irradiation, a PAG produces protons that lower the pH in solution to afford a gel, much in the same way as a pH trigger (mentioned above).[82] Raghavan's group demonstrated the use of a PAG to trigger the gelation of the biopolymers alginate and pectin. The protons liberated *in situ* reacted with $CaCO_3$ in the biopolymer solution to afford Ca^{2+} ions, which then crosslinked the biopolymer in solution to form a gel. The crosslink domains consisted of Ca^{2+} bridging neighbouring biopolymer chains in an "egg box"

junction.[9] Raghavan and his co-workers have also demonstrated that UV light and a PAG can be used to tune the rheological properties of a dispersion containing laponite, a poly(ethylene oxide)–poly(propylene oxide)–poly(ethylene oxide) triblock copolymer.[83]

1.4.7 Electrochemically-Triggered Gelation

Another method of triggering the self-assembly of LMWG that is an attractive method for spatially and temporally controlling gel growth is electrochemical-triggered gelation (or electroaddressing).[84-86] Electrochemically-driven gelation processes involve an application of current, which generates protons at the anode/cathode surface, leading to the hydrogelation at the electrode surface as the pH is lowered/increased, depending on the electrode. Therefore electrochemically-triggered gelation is essentially a pH-triggered method for inducing the self-assembly of hydrogelators. The difference being here that electrochemical methods have more spatial and temporal control as bulk gelation does not occur, rather nucleation and growth from an electrode surface.[87] Payne and his group have shown the electrodeposition of chitosan gels on an electrode surface. Gelation of chitosan occurs locally and as a result of a pH gradient produced by an applied current. The majority of the biopolymer remains in solution. Gelation can be controlled to the extent that thin hydrogel layers can be grown. Layer-by-layer assembly of alginate and chitosan could be grown (Figure 8). Fluorescent-labelled chitosan indicated that layers were grown as the fluorescent signal increased with each subsequent bilayer.[88] Alginate can also be electrodeposited onto an electrode surface in multiple layers of alginate, where cells can be entrapped in layers which have been grown by using the source of calcium ions in the previous layer to gel the next layer.[8]

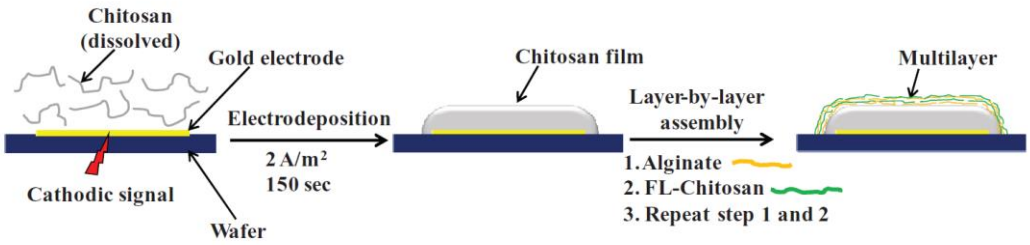

Figure 8 Layer-by-layer self-assembly of chitosan and alginate hydrogel layers onto a cathode electrode surface[88]

Another electrochemical method employed to trigger gelation has been used previously by Johnson *et al*. to form hydrogel films of FmocLG.[89] This method involves the addition of an oxidisable (and non-gelling) material to the gelator solution that can produce protons at the anode to trigger gelation. The material used here was hydroquinone (HQ). HQ produces two protons per molecule upon oxidation. Gelation ensues on a gold electrode surface as proton liberation occurs (Figure 9).

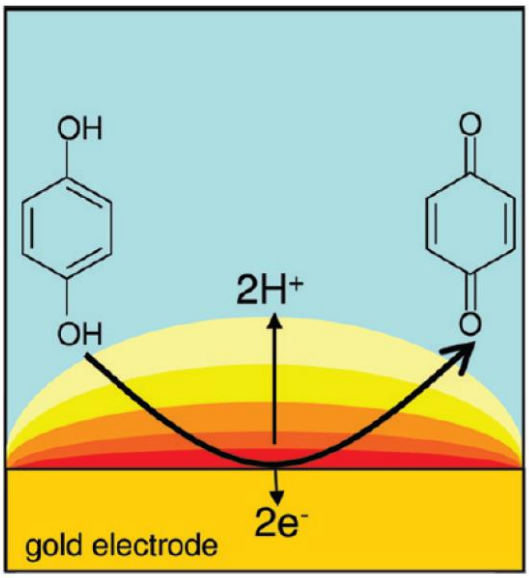

Figure 9 Oxidation of hydroquinone (HQ) at a gold electrode surface which produces 1, 4-benzoquinone and liberates protons, resulting in a pH decrease at the electrode surface[89]

Liu *et al*. have demonstrated another LMWG can be electrodeposited using similar principles.[90] Liu *et al*. showed that FmocF gels could be formed by applying a current to an anode, where a pH gradient results, and FmocF gelation occurs as a result of the pH decrease. Furthermore, they showed that separate electric signals can be applied on the same surface to both assemble and disassemble electrodeposited FmocF gels. Both these processes could occur simultaneously on a single surface.[90]

Beyond the scope of this understanding, the design rules for a successful LMWG are relatively unknown.[2, 33] Many researchers discover new gelators through library-based approaches. This approach has shown that subtle changes in molecular structure can be the difference between a gelling and non-gelling material.

1.5 Importance of Gelation Process

For many LMWG hydrogel systems, subtle changes in the assembly conditions can have an effect on the final hydrogel properties. For LMWG, the self-assembly process has been shown to be very important.[58, 61, 73] Many LMWG can be prepared by several of the self-assembly triggers mentioned above and each individual trigger can lead to different final mechanical properties of a gel Using a mineral acid (HCl) to lower the pH results in a rapid pH drop with inefficient mixing and an inhomogeneous gel. Tang *et al*. utilised an added heating process to improve the mixing after acid had been added to the solution of FmocFF.[38] Homogeneity of Fmoc-dipeptide hydrogel samples was further improved by utilising a GdL pH trigger rather than an HCl trigger.[35] As mentioned in Section 1.3.4, GdL lowers the pH of the bulk solution to afford a homogenous gel. The amount of GdL used to lower the pH can be changed to alter the final pH of the gel.[54] Ramachandran *et al*. have shown that the kinetics of the self-assembly process affected the mechanical properties of their complimentary oligopeptides. By studying the gelation process at 5 °C and 25 °C, they found that at the lower temperature gelation was slowed in comparison, and the resulting gels were mechanically weaker with thinner fibres formed.[91] Recently, Cardoso *et al*. also noted that altering the temperature did affect the kinetics of gelation but the final rheological properties measured were the same.[92]

1.5.1 Effects of Trigger

A particular gelator that has been well documented in the literature is a 20 amino acid β-hairpin molecule known as MAX1 (mentioned in Section 1.2). The extensive literature on this molecule allows the effects that changes in the assembly process have on the mechanical properties of the resulting gels to be highlighted.[22, 29, 93, 94] This gelator has been studied by Pochan and Schneider and consists of two strands with an alternating sequence of valine (V) and lysine (K) residues that are connected with a tetrapeptide type II' turn sequence (-V^{D}PPT-) (Figure 3) MAX1 is known to fold and consequently self-assemble under specific pH, temperature and/or salt concentrations.[22, 23, 29, 93, 94] At neutral to low pH, coupled with low ionic strength and temperature (~ 20 °C), the lysine residues of MAX1 are mainly positively charged with charge repulsion rendering peptide folding energetically unfavourable.

CD data collected for gels of MAX1, with varying assembly conditions, have shown that β-hairpin formation always precedes self-assembly. β-sheet formation is monitored by measuring the mean residue ellipticity at 216 nm ($[\theta]_{216}$). Under assembly conditions, $[\theta]_{216}$ values collected show that β-sheets are present and folding is triggered.[94] Similar data has been collected for all assembled states for MAX1 indicating that the assembly trigger has no effect on the type of molecular packing adopted.[22, 24, 29, 93-95] Furthermore, both cryo-TEM and TEM data show that on the nanometre level of the self-assembled MAX1, fibril widths of ~ 3 nm were measured.[95] Gels prepared with NaCl as the salt used to trigger gelation displayed such fibril widths, which were in agreement with MAX1 gels that used DMEM buffer as the salt in the trigger.[93] The concentration of gelator slightly varies in these cases, but as the assembly conditions also differ it can be deduced that intramolecular folding at the nanoscale is unaffected by the trigger used. Manipulation of the assembly conditions allows folding and subsequent self-assembly to occur with notable differences in the mechanical properties of the resulting gels.

At low pH, MAX1 remains unfolded and cannot form gels. This is largely due to electrostatic repulsion between positively charged lysine residues. When the pH is increased above the intrinsic pK_a of the molecule, lysine side chains will become neutral and intramolecular folding occurs – repulsion is diminished. Acidification can lead to unfolding and hence hydrogel dissolution, deeming this a reversible process. The first reported MAX1 gels by Pochan and Schneider were prepared at pH 9.0.[22] For gels prepared with 2 wt% peptide material in pH 9 buffer (125 mM borate and 10 mM NaCl) at 25 °C, rheological data was collected. After 30 minutes, the storage modulus (G') was greater than the loss modulus (G''), which is indicative of gel-like properties. A final G' value of ~ 1200 Pa was measured for such gels. These gels also displayed the ability to recover after shear cessation with 100 % recovery of G' (after 30 minutes) after application of 1000 % strain for 180 s.[22]

Using the conditions for the gels at pH 9, no gelation occurs if the pH is lowered. MAX1 forms coiled coils in solution at pH values lower than 9 under these solution conditions.[22] However, MAX1 gels have been reported at and around physiological pH by altering the temperature or salt conditions of the system. MAX1 can form gels at pH 7.4 using bispropane buffer.[29, 94, 96] At pH 7.4, MAX1 has a net positive charge

– suggesting that it cannot fold due to electrostatic repulsion. Increasing the concentration of NaCl in the buffer solution allows the chloride ions to screen the positive charges on the lysine residues and thus allow folding to proceed. Increased salt concentration (and therefore ionic strength) drives hydrophobic association of fibrils with faster hydrogelation kinetics. This can be studied using rheology. A 2 wt% MAX1 gel prepared at pH 7.4 with 20 mM NaCl shows no significant increase in *G′* in the first 3000 s of the gelation process (Figure 10). Increasing the salt concentration to 150 mM decreases the lag time by half and further increasing the salt concentration to 400 mM shows no lag in *G′* evolution during gelation. 20, 150 and 400 mM salt concentrations give final *G′* values of ~100, ~300 and ~3000 Pa at 20 °C, respectively (Figure 10).[29] Not only do higher salt concentrations provide faster gelation kinetics, they also produce stronger gels. It is possible that there are more crosslinks in the fibril network due to the faster kinetics, which would ultimately lead to stronger networks and stronger gel mechanical properties.

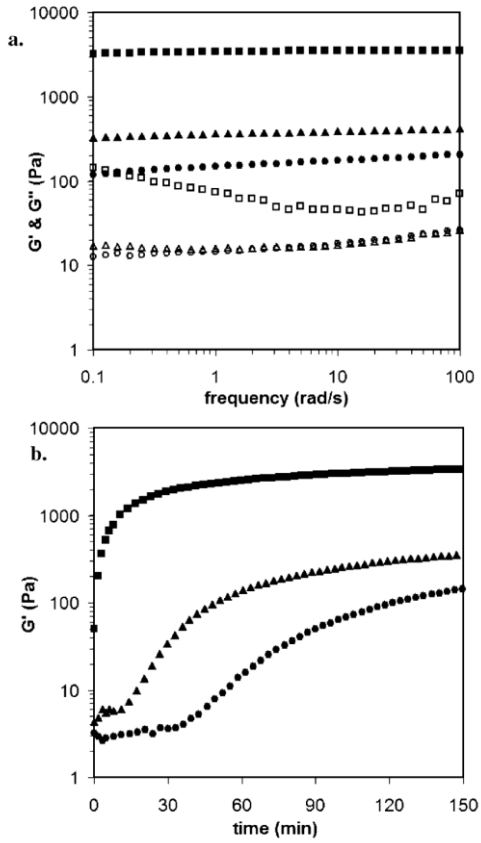

Figure 10 (a) Frequency sweep rheological data of 2 wt% MAX1 gels, pH 7.4 with 20 mM (*G′*, ●; *G″*, ○), 150 mM (*G′*, ▲; *G″*, △), and 400 mM NaCl (*G′*, ■; *G″*, □). (b) Frequency sweep data of 2 wt% MAX1 gels, pH 7.4 with DMEM in the presence and absence of 10 % calf serum[29]

The type of salts used in these systems can affect the mechanical properties of the hydrogels produced, not just the concentration. MAX1 gels prepared using NaCl have shown that stable gels at physiological conditions can be achieved. With potential biological applications in mind, cell culture media which contain salts have proven effective as a self-assembly trigger for MAX1.[23, 93] Utilising such data allowed MAX1 gels particularly applicable to the area of tissue regeneration to be prepared. With cell culture media already a component of the hydrogel itself, the number of additives needed is reduced. MAX1 gels (2 wt%) using serum-free DMEM (Dulbecco's Modified Eagle Medium), which contained 165 mM of salt produced gels at pH 7.4 and 37 °C. Kinetic rheological data for gelation showed that after 30 min, $G' > 1800$, and after 120 min, the $G' > 2500$ Pa (Figure 11).[23] After 24 hours, G' had increased further to ~ 10 kPa (Figure 11).[29] The 2 wt% gels containing DMEM also showed 50 % recovery of G' from shear (1000 %). Interestingly, the increase in G' in the recovery phase was quicker than in the initial gelation.[29] This recovery of gel strength is only half of that for MAX1 gels of the same concentration but using NaCl salt as a trigger at pH 9 (mentioned previously). These gels were significantly weaker than the gels with DMEM. Such variability in mechanical properties occurs for the same concentration of material with only the conditions of the trigger altered.

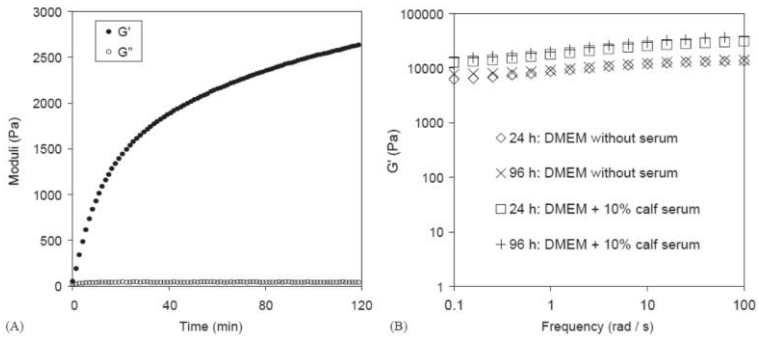

Figure 11 a) Time-dependent rheology of 2 wt% MAX1 hydrogel formed upon addition of DMEM to an aqueous solution of MAX1. ● represents the storage modulus (G') and ○ represents the loss modulus (G''). b) Frequency sweep rheology monitoring G' of hydrogels under cell culture conditions in the presence and absence of 10% calf serum[23]

Both peptide-conjugate and dipeptide-conjugate gelators have also demonstrated that the assembly conditions have an impact on the final properties of the gelator. FmocY has been widely studied as a hydrogelator that can form gels both enzymatically and by use of a pH trigger. The mechanical properties for FmocY gels reported are

variable as a result of differences in the assembly conditions. Unlike MAX1, there is also some indication that the molecular packing of FmocY upon assembly is dependent on the trigger used.[68] Yang *et al*. first demonstrated the enzymatic formation of FmocY *via* the dephosphorylation of Fmoc-Y-phosphate (as mentioned in Section 1.3.3).[47] Gelation occurred at high pH (9.6) and at 37 °C. For FmocY gels prepared using a pH trigger, gelation occurred at much lower pH values. The pK_a of FmocY was measured to be 5.5 at a gelator concentration of 1 wt%[50] but FmocY gels reported in the literature, that utilise a pH trigger, were prepared at a higher concentration.[97] Therefore, the pK_a may have shifted, thus allowing for an increased gelation pH. Thornton *et al*. demonstrated a pH-triggered FmocY gel (1.55 wt%) with a final pH of 7.4.[97]

Between these two methods of triggering gelation, the CD spectra measured were different (Figure 12). CD is used to detect the chiral orientation of the material and can probe the secondary peptide structure. At lower pH, the CD signals were stronger, with an intense peak at 275 nm present.[68] The stacking of the Fmoc groups was also analysed *via* fluorescence spectroscopy (Figure 12). Enzymatically-triggered gelation of FmocY afforded a slight red shift upon gelation (at pH 9.6).[68] A low intensity peak at 450 nm was observed due to stacked fluorenyl rings. For pH-triggered gels, an additional peak at 420 nm – attributed to aggregated Fmoc groups, was noted. Thus, there is evidence of changes in the molecular packing from both the CD and fluorescence spectra. Thornton *et al.* used an enzyme to form FmocY hydrogels under physiological conditions (pH 7.4, 37 °C).[97] The molecular packing observed here was comparable to that of a pH-triggered gel. Hence, pH has a clear impact on gelation properties.

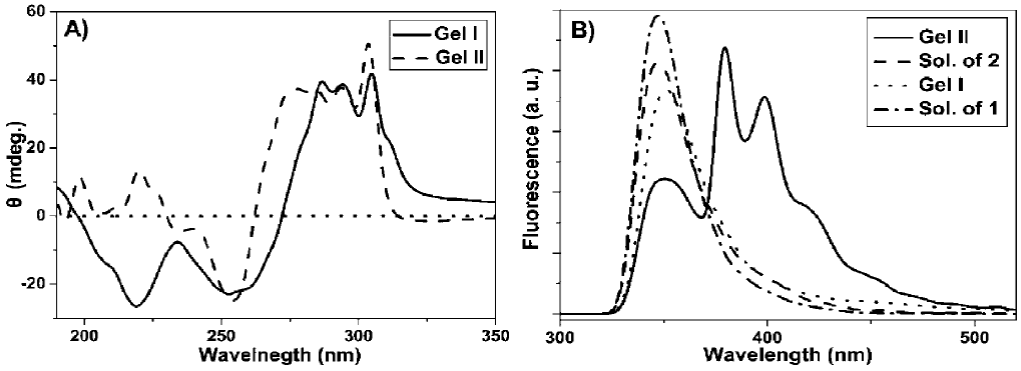

Figure 12 a) CD spectra of FmocY hydrogels and b) the corresponding fluorescence spectra of the gels and their solution form before self-assembly. Gel I is an enzymatically triggered gel and gel II is a pH-triggered gel[68]

Along with the molecular packing, the final mechanical properties of FmocY are vulnerable to changes in the assembly conditions. Both Yang *et al*. and Schnepp *et al*. have prepared FmocY gels under the same conditions (pH 9.6, 37 °C) using the enzymatic method. However, Yang *et al*. prepared their gels at higher gelator concentration (1.9 wt%) but measured a lower *G'* (1000 Pa)[47] compared to Schnepp *et al*., where the *G'* measured was > 10^5 Pa at a concentration of 1.55 wt%.[48] It may be expected that a higher concentration of gelator would in fact give a mechanically stronger gel. As this was not the case, the kinetics of assembly may have played a role in the increased mechanical strength for the 1.55 wt% gels.

Schnepp *et al*. also demonstrated that the addition of Ca^{2+} ions can increase mechanical strength.[48] This could also explain why enzymatically-triggered FmocY gels can successfully form at pH values above the pK_a. When FmocY-phosphate is dephosphorylated at high pH, the product obtained is the same molecule as that used to prepare an FmocY gel using a pH trigger. Reports for various other LMWG have shown that gelation is possible in the presence of salts (see above).[69, 70, 79] Presumably, once dephosphorylated, the FmocY carboxylate salt is present at high pH due to the salts contained in the buffers required to optimise enzyme action.

Recently Patil *et al*. reported a new method by which FmocY gels can be prepared.[49] Through the addition of cerium oxide nanoparticles at pH 10.2 (at room temperature), dephosphorylation of FmocY-phosphate could be catalysed. For these gels, a *G'* of 20000 Pa was measured which was higher than other triggers, despite

being at a pH value further away from the pK_a. These gels also had a melting temperature 40 °C higher than the enzymatically-triggered gels, and could form gels at lower concentrations.

Although FmocY appeared to be affected at both the molecular and bulk scale by altering the conditions of assembly, dipeptide-conjugate gelators display different behaviour. Dipeptide-conjugate gelators display behaviour more reminiscent of that observed for MAX1 gels i.e. the molecular packing is the same regardless of the trigger applied, but the rheological properties are not. FmocFF is the most widely studied dipeptide-conjugate gelator and by a range of different research groups (including our group). Naturally, a number of different assembly conditions have been employed. Whether it be a solvent-mediated trigger or a pH trigger, FmocFF gels all exhibit molecular packing in the form of β-sheets between the dipeptide chains of neighbouring molecules and π-π stacking interactions between Fmoc groups.[3, 5] Both Xu's group and Ulijn's group have also demonstrated the same molecular packing for gels of FmocGG, despite subtle differences between their pH-triggered assembly methods.[36, 37] Tang *et al*. measured two pK_a values for FmocFF, with the structures formed and resulting properties of the hydrogel system being pH dependent.[38]

Several researchers (including our group) have prepared FmocFF gels *via* a solvent-mediated method. FmocFF dissolved in DMSO at high concentration, before being diluted with water affords transparent gels at a pH ~ 4. Gazit's group prepared their FmocFF gels by diluting an FmocFF stock solution (with a concentration of 100 or 25 mg/mL) with water to give a final gelator concentration of 5 mg/mL and a *G'* of ~ 10000 Pa.[3] Our group has recently shown that the ratio of DMSO:water can affect the final mechanical properties (Chapter 3).[61] Huang *et al*. prepared FmocFF gels at a slightly lower concentration in DMSO and PBS buffer (also containing a surfactant) at pH 7.4.[98] These gels were mechanically weaker than Gazit's gels. FmocFF gels have been known to be affected by the presence of buffers.[42] However, Jayawarna *et al*. prepared mechanically stronger gels in DMEM (*G'* 21200 Pa) at pH 7.5 *via* a salt-trigger from the presence of DMEM.[41] In the absence of DMEM, weaker mechanical properties were observed for a gel prepared at the same concentration (*G'* 2000 Pa). The pH was slightly lower (pH 6).[99]

1.5.2 Effects of Additives

It is clear that the conditions of the trigger of self-assembly have an effect on the final mechanical properties. No difference is observed on a molecular level between triggers for several gelator systems.[3, 22, 38, 100] The triggers must therefore affect the self-assembly process on a larger scale. The mechanical properties may therefore be governed by microstructure arrangement of the fibres and/or the degree of inter-fibril branching and entanglements. The inclusion of additives within the gel matrix may support this idea. Additives are not a necessity for peptide folding and self-assembly but they may interfere in the degree of entanglements and hence, the network formation. The exception to this is for systems such as salt-triggered and enzyme-triggered gelation, where both the non-gelling precursor and salt/enzyme are both required for gelation to proceed (mentioned above and shown in Figure 13).

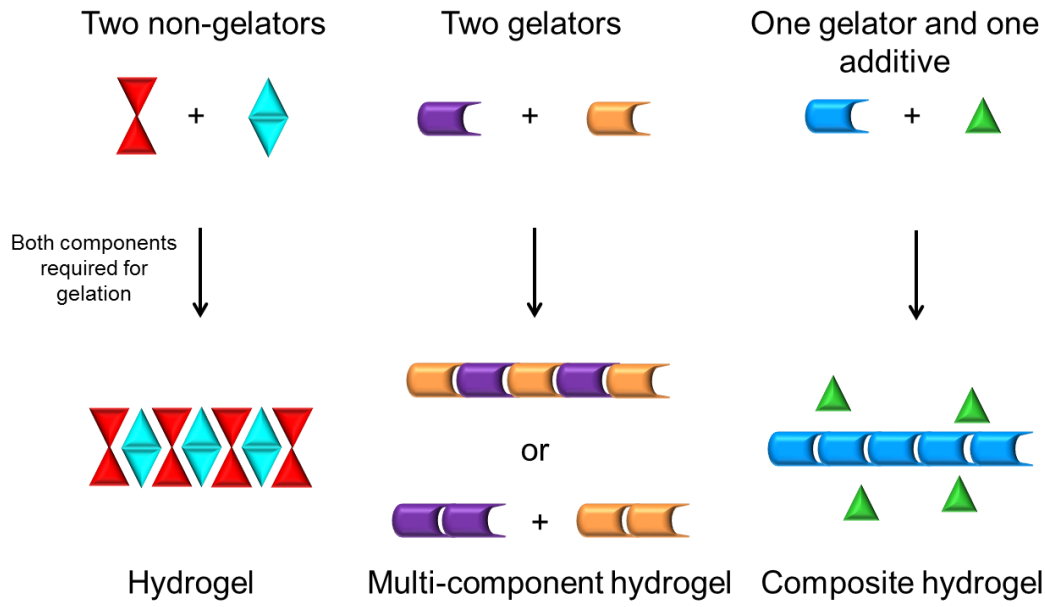

Figure 13 The three main classes of multiple component gels: two non-gelling components that combine to form a gel; two gelling materials that may co-assemble or self-sort and a gelator plus a non-gelling material that may influence the properties of the gel[101]

Additions to the gel system may alter the mesh size of the network due to crowding effects[102, 103] resulting from a smaller free volume, and at higher concentrations, viscosity effects and can affect the gel strength as a whole.[104] Several different additives have been demonstrated to have an influence on the gel properties in many hydrogel systems. Adhia *et al.* showed that polymeric additives decreased the critical

gelation concentration and assembly rates, whilst also increasing the final mechanical properties in pyridine-based gelator systems. They attributed this behaviour to the efficiency of the polymer additives to absorb onto the fibres. Polymers with complimentary functional groups led to lower critical gelation concentrations.[105] Our group previously added polymeric materials to dipeptide-gelators before gelling, and found that the nature of the polymer affected the gel properties.[104] Another material, graphene, has no effect on the gel morphology of FmocYD and FmocFD gels but the gels were mechanically more rigid when graphene was incorporated in the fibres.[106]

Biopolymer additives can influence the gelation properties of LMWG. Huang *et al.* prepared hybrid FmocFF gels containing the polysaccharide konjac glucomannan (KGM) and compared both the gelation kinetics and final gel properties with FmocFF gels with no additive.[98] The hybrid materials displayed slower gelation kinetics, as the rheological behaviour (*G'*) for an FmocFF-KGM gel reached a plateau after ~ 180 minutes whereas an FmocFF gel reached a plateau in the rheology after only ~ 20 minutes. Gels exhibited different final mechanical properties also. The hybrid gel was more rigid and also had smaller fibres. Similar molecular packing was observed on both types of gel. KGM acted as a stabiliser in the gel when monitoring the release of a drug material, harbouring more control over the release kinetics than an FmocFF gel with no additive.[98] Our group has shown behaviour in FmocFF gels and gels of a naphthalene-based dipeptide gelator (BrNapAV) are affected in the presence of dextran. More viscous solutions had more effect on the rheological properties in these gels. A solution viscosity lower than 10 mPa/s resulted in a *G'* value comparable with gels containing no additive. Above this viscosity, rheological properties were depleted. The same was observed for several different molecular weight dextrans.[104]

As mentioned, MAX1 gels have been prepared using DMEM cell culture media as the salt trigger for folding and self-assembly of the gelator molecules. These gels were also prepared as before but were additionally loaded with 10 % calf-serum – physiological conditions were used.[23] After 24 hours, a *G'* value of ~ 10 kPa was obtained for these gels (shown in Figure 11). On comparison of gels prepared under the same conditions (2 wt% MAX1, pH 7.4, 37 °C) minus cells, the *G'* values barely

differ (Figure 11). MAX1 gels containing calf-serum display a slight increase in *G'* but not a significant increase. One may expect additional material within a gel matrix to have some effect on the fibril network formation, in this particular example, however, the mechanical properties are generally unaffected.

The electrodeposition of chitosan has shown the effects of NaCl on the resulting gel properties.[107] Gels containing NaCl were more opaque, with the opacity increasing with increased NaCl concentration. These gels were also less homogeneous than gels which contained no salt. However, the film thickness was increased when the NaCl concentration was increased but these gels were less rigid.[107]

1.5.3 Mixed Gelator Systems

An emerging class of multi-component materials is one where the multi-components are both gelators themselves. Under certain conditions, each component can individually self-assemble to form a gel. When mixed together in solution, both gelators can either co-assemble, where the two gelators yield structures consisting of both components; or they could self-sort, where distinct architectures of independently self-assembled components make up the gel network (Figure 13). In reality, there is the possibility for a combination of both to occur to a certain degree.[101, 108]

Recently, Javid *et al.* reported hydrogels consisting of co-assembled Fmoc-dipeptide gelators and protein clusters.[109] They noted that the properties of these co-assembled gels could be enhanced or negatively affected and were dependent on the hydrophobicity of the gelator. It is plausible to expect that a system consisting of gelling materials with different binding motifs may encourage self-sorting, conversely, when the two components are similar, it may encourage co-assembly to occur. Smith's group have demonstrated self-sorting hydrogel systems prepared from sorbitol derivatives with agarose[110] and a cholesterol-based gelator.[111] The gels were prepared by heating a solution containing both components, cooled (to gel agarose) and GdL was added to gel LMWG. The resulting gels showed characteristics associated with individual sorbitol gels. The sorbitol gel was pH responsive, a quality which was retained in the multi-component gel – the LMWG could assemble/disassemble within the agarose network.[110] For the sorbitol

LMWG/cholesterol system, independent, self-sorted networks were detected from the molecular to the macro length scale. Alone, gels of the modified cholesterol exhibits aging effects that were transferred to the multi-component gel.[111] Our group has recently demonstrated the ability to self-sort multi-component gelator systems consisting of similar LMWG.[108] Using GdL to lower the pH of the multi-component gelator solution, gelation occurred sequentially based on the apparent pK_a of the gelators in solution. This was amongst the first examples of self-sorted gelation of similar multi-component LMWG.

The mechanical properties of MAX1 gels (1 wt%, 150 mM NaCl) have been known to be enhanced through racemic mixtures of the L-isomer and its D-enantiomer.[112] The D-isomer of MAX1 (known as DMAX1) can also undergo folding under the same conditions as that for the L-enantiomer (MAX1) and produces hydrogels with virtually the same mechanical properties (*G'* value of 200 Pa after 120 min). As before, these gels appear the same on a molecular level as the CD data for DMAX1 is a mirror image of MAX1, as expected, suggesting that β-sheet structures are formed. Altering the ratio of MAX1 to DMAX1 enhances the mechanical rigidity of the gels. Both 1:3 and 3:1 mixtures of MAX1:DMAX1 more than doubles the *G'* values of the gels of single enantiomers. An equal ratio of MAX1:DMAX1 further enhances the rheological properties with a *G'* value of 800 Pa after 120 min begin measured. On a nanoscale level, TEM shows that a fibril width of ~ 3 nm was also measured for these gels – the same as every other MAX1 gel. The increase in the mechanical strength of these gels by the addition of DMAX1 must occur from some favourable interactions between enantiomers. This may be either on the molecular or the network level. Although, the packing of the molecules is found to be the same for every other MAX1 gel made, there still could be some interactions between enantiomers at this lever that may guide the self-assembly and result in co-assembly of enantiomers to give fibrils that are homogenous. Conversely, if such favourable interactions are having an effect a higher level, perhaps in the network formation, then it could be possible that segregation of enantiomers may occur and lead to self-sorting of enantiomers. This could result in fibrils consisting of single enantiomers only.

Whilst not a hydrogel, related work by Dasgupta *et al.* demonstrated an interesting

example of self-sorting in multi-component organogels.[59] They prepared hybrid polymer gels from an oligo(p-phenylvinylene) molecule (OPV16) and poly(styrene)(PS). Atactic PS molecules are unable to form gels under the conditions described by Dasgupta, but it could be loaded into an OPV16 gel and have no effect on the final gel properties. However, when a stereo-regular, isotactic PS molecule was used, both individual and multi-component gelation were possible.[59] Furthermore, increasing the PS concentration in the multi-component gel results in a smaller mesh size which could have an effect on the growth of the OPV16 fibrils – when the polymer gel forms first. Dasgupta *et al.* have therefore demonstrated that changing the tacticity of one of the components can render a system containing a gel with an additive to a self-sorting, multi-component system.

1.6 Tunable Hydrogel Properties for Application

Although the absolute rules of design for LMWG are not fully understood[2, 33], the scope of knowledge gained over recent years has been paramount. Judicious choice of amino acid and aromatic substituent and/or self-assembly trigger conditions can be crucial to the final hydrogel properties. Using this information allows the properties to be tuned to suit a potential application.[113] The inherent biocompatibility of amino acid-based LMWG lends them to be studied for cell culture and tissue regeneration techniques. Uljin's group have shown the compatibility of gel mixtures of Fmoc-dipeptide and Fmoc-peptide differs when the amino acid on the single amino acid molecule is altered.[41] The compatibility with a number of different cell lines was affected by the choice of amino acid.

An important characteristic of LMWG is the wide range of mechanical properties that can be achieved. This is important as the *G'* of a gel has been demonstrated to influence the differentiation and growth of stem cells. This factor has been demonstrated in an acrylamide/poly(ethylene glycol) hydrogel system where altering the amount of acrylamide in the hybrid system can alter the rheological properties of the final gel.[114] The differentiation of stem cells where a neuronal marker was exhibited was optimal in the gels where the mechanical properties were in a range comparable with neural tissue (~ 500 Pa). Under the differentiation conditions for astrocytes, the astrocytes count decreased in softer gels.

The entangled fibrous network of a hydrogel is able to entrap external materials, as mentioned above. Utilising this attribute for controlled release in drug applications is plausible. Depending on the mesh size of the network, the entrapped molecule size and diffusion of that molecule, could affect the release of drug molecules from a gel.[115] The mesh size limits the diffusion rates of FITC-dextran from MAX1 and MAX8 hydrogel networks.[116] It could be expected that smaller molecules would diffuse out of a network first and conversely, larger molecules could be completely immobilised. However, interactions of functional groups on the entrapped molecules with the fibres of the gelator can affect the release rate of the entrapped material. Our group previously suggested that the release behaviour of model drugs from the peptide gelators FmocF and FmocY was related to the rheological properties of the gels. FmocY was mechanically stronger than FmocF and model drug molecules were released slower. FmocF did not show much difference in release rates between small and large molecules entrapped. This was attributed to the weaker mechanical properties of the gel.[46]

Along with being able to alter the molecular structure and composition to tune the mechanical properties of a hydrogel material, which in turn, can influence the growth of cells; the ability to control spatial and temporal growth of gels can be vital to tissue engineering applications. Both electro-addressing[8, 117] and photolithography[118] techniques have demonstrated the ability to spatially control gel growth. Such control can be of interest for cell culturing. Surface topology can have an effect on the differentiation and growth of cells. The surface topology of a gel can be easily manipulated by employing an imprinting technique (Figure 14). Here the gel is grown over a monolayer of cells (mammalian in this case) to create a complimentary gel topography into which gels can be attached and promoted to grow by the surface cues created from the gel "mould".[119]

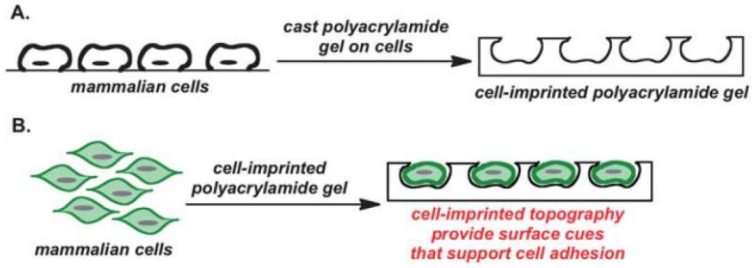

Figure 14 Programmed cell adhesion and growth *via* a cell-imprinting technique. a) A poly(acrylamide) gel is cast onto a monolayer of mammalian cells to create a complimentary topography and b) shows that the imprinted features support cell adhesion and growth[119]

As LMWG materials are reversible[24, 36, 120], they are vulnerable to certain external stimuli, and can evoke a response to a particular change in conditions. This enables hydrogels to be studied for their potential use as biosensor materials. Yang *et al.* showed that for the dipeptide-conjugate gelator; Fmoc-$_D$-Ala-$_D$-Ala, a gel-sol transition could be induced in the presence of the antibiotic vanmyocin. This was known to have an affinity for the $_D$-Ala-$_D$-Ala motif and in its presence, the delicate, non-covalently bound self-assembled network was disturbed. The same was not reported for the gelator prepared from the $_L$-enantiomer (Fmoc-$_L$-Ala-$_L$-Ala).[36]

The chemical potential of LMWG does not just limit them to biological applications. Many hydrogels materials have found emerging interest in applications such as energy transfer[121] and catalysis.[122] Such versatility in both design and control of material properties, coupled with the wide potential future application, ensures the continued interest in LMWG.

1.7 Present Study

Previously, there has been an indication that the final properties of a hydrogel material are variable given subtle changes in the assembly conditions and that the gelation process could play a vital role in the variability. In the study discussed in this Thesis, gelation kinetics and final hydrogel properties are investigated for a number of dipeptide-conjugate gelator systems self-assembled *via* different triggers. Past work on these systems has been reported in our group by Chen *et al.*.[53, 54, 58] The ability to tune the material properties with different triggers is discussed and is utilised to demonstrate hydrogels with spatial and temporal control over

hydrogelation and with more complex composition. By scrutinising the gelation process, a better understanding of the dynamics of the process and the factors which affect the gelation process can be gained in a bid to enable gelator design and gelation parameters to be exploited to benefit the desired hydrogel properties.

Chapter 3 investigates the application of a solvent-mediated method of triggering gelation in FmocFF and compares the varied final mechanical properties that can be achieved with subtle changes in the assembly conditions. The same methodology is applied to a small number of other Fmoc-dipeptides and the correlation between gelators (if any) is noted.

Chapter 4 demonstrates the first example of UV-triggered gelation of LMWG using a photoacid generator (PAG). A PAG liberates protons upon UV-initiated breakdown and gelation ensues when a pH decrease below the pK_a of the gelator is reached. The properties of the gels prepared in this way are compared to the same gels prepared using other triggers. Application of this UV-triggered method to employ a simple lithography technique to spatially control gelation is also studied.

Chapter 5 looks at spatially and temporally controlling the growth of single and multi-component gelator systems using an electrochemically triggered gelation method. By utilising the oxidation of HQ to generate protons, gelation is triggered *via* a pH change at an electrode surface. Multiple electrode systems on one surface are studied to grow multiple gels simultaneously to alter the hydrogel surface topography across the whole substrate. The current applied in the systems investigated is controlled to manipulate the growth of both single and multi-component systems, with the latter having self-sorting promoted.

Chapter 6 studies the gelation kinetics of a number of dipeptide-conjugates using known molecular rotors; DCVJ and CCVJ, and also investigates the role of Thioflavin T as molecular rotor rather than a stain for β-sheets. The evolution of rheological properties, the decrease in pH and fluorescent response from the rotors are all measured for each hydrogel system, and correlations between the data discussed. The effects of additives on the kinetics of gelation are also demonstrated.

1.8 References

1. P. Terech and R. G. Weiss, *Chem. Rev.*, 1997, **97**, 3133-3160.
2. M. de Loos, B. L. Feringa and J. H. van Esch, *Eur. J. Org. Chem.*, 2005, **17**, 3615-3631.
3. A. Mahler, M. Reches, M. Rechter, S. Cohen and E. Gazit, *Adv. Mater.*, 2006, **18**, 1365-1370.
4. E. S. Place, J. H. George, C. K. Williams and M. M. Stevens, *Chem. Soc. Rev.*, 2009, **38**, 1139-1151.
5. M. Zhou, A. M. Smith, A. K. Das, N. W. Hodson, R. F. Collins, R. V. Ulijn and J. E. Gough, *Biomaterials*, 2009, **30**, 2523-2530.
6. E. Alexandre, K. Boudjema, B. Schmitt, J. Cinqualbre, D. Jaeck and P. J. Lutz, in *Polymeric Drug Delivery II*, American Chemical Society, 2006, vol. 924, pp. 135-149.
7. M. Backer, M. Raue, S. Schusser, C. Jeitner, L. Breuer, P. Wagner, A. Poghossian, A. Forster, T. Mang and M. J. Schoning, *Phys. Status Solidi. A-Appl. Mat.*, 2012, **209**, 839-845.
8. J. F. Betz, Y. Cheng, C.-Y. Tsao, A. Zargar, H.-C. Wu, X. Luo, G. F. Payne, W. E. Bentley and G. W. Rubloff, *Lab Chip*, 2013, **13**, 1854-1858.
9. V. Javvaji, A. G. Baradwaj, G. F. Payne and S. R. Raghavan, *Langmuir*, 2011, **27**, 12591-12596.
10. J. W. Lee, S. Y. Kim, S. S. Kim, Y. M. Lee, K. H. Lee and S. J. Kim, *J. Appl. Polym. Sci.*, 1999, **73**, 113-120.
11. R. R. Vincent and M. A. K. Williams, *Carbohyd. Res.*, 2009, **344**, 1863-1871.
12. J. L. Ifkovits, Burdick, Jason A., *Tissue Eng.*, 2007, **13**, 2369-2385.
13. Q. G. David, B. N. Zorraquin-Cornejo, A. Ganem-Rondero, E. Pinon-Segundo, M. G. Nava-Arzaluz and J. M. Cornejo-Bravo, *J. Mex. Chem. Soc.*, 2008, **52**, 272-278.
14. L. A. Estroff and A. D. Hamilton, *Chem. Rev.*, 2004, **104**, 1201-1218.
15. R. V. Ulijn and A. M. Smith, *Chem. Soc. Rev.*, 2008, **37**, 664-675.
16. S. G. Zhang, *Nat. Biotechnol.*, 2003, **21**, 1171-1178.
17. J. Cui, Z. Shen and X. Wan, *Langmuir*, 2009, **26**, 97-103.
18. J. D. Hartgerink, E. Beniash and S. I. Stupp, *Science*, 2001, **294**, 1684-1688.
19. H. Yokoi, T. Kinoshita and S. G. Zhang, *Proc. Nat. Acad. Sci. USA*, 2005, **102**, 8414-8419.
20. C. A. E. Hauser and S. Zhang, *Chem. Soc. Rev.*, 2010, **39**, 2780-2790.
21. A. Saiani, A. Mohammed, H. Frielinghaus, R. Collins, N. Hodson, C. M. Kielty, M. J. Sherratt and A. F. Miller, *Soft Matter*, 2009, **5**, 193-202.
22. J. P. Schneider, D. J. Pochan, B. Ozbas, K. Rajagopal, L. Pakstis and J. Kretsinger, *J. Am. Chem. Soc.*, 2002, **124**, 15030-15037.
23. J. K. Kretsinger, L. A. Haines, B. Ozbas, D. J. Pochan and J. P. Schneider, *Biomaterials*, 2005, **26**, 5177-5186.
24. D. J. Pochan, J. P. Schneider, J. Kretsinger, B. Ozbas, K. Rajagopal and L. Haines, *J. Am. Chem. Soc.*, 2003, **125**, 11802-11803.
25. M. J. Pandya, G. M. Spooner, M. Sunde, J. R. Thorpe, A. Rodger and D. N. Woolfson, *Biochemistry*, 2000, **39**, 8728-8734.

26. E. F. Banwell, E. S. Abelardo, D. J. Adams, M. A. Birchall, A. Corrigan, A. M. Donald, M. Kirkland, L. C. Serpell, M. F. Butler and D. N. Woolfson, *Nat. Mater.*, 2009, **8**, 596-600.
27. S. Zhang, D. M. Marini, W. Hwang and S. Santoso, *Current Opinion in Chem. Biol.*, 2002, **6**, 865-871.
28. Y. Nagai, L. D. Unsworth, S. Koutsopoulos and S. Zhang, *J. Control. Release*, 2006, **115**, 18-25.
29. B. Ozbas, J. Kretsinger, K. Rajagopal, J. P. Schneider and D. J. Pochan, *Macromolecules*, 2004, **37**, 7331-7337.
30. S. E. Paramonov, H.-W. Jun and J. D. Hartgerink, *J. Am. Chem. Soc.*, 2006, **128**, 7291-7298.
31. D. J. Adams and P. D. Topham, *Soft Matter*, 2010, **6**, 3707-3721.
32. D. J. Adams, *Macromol. Biosci.*, 2011, **11**, 160-173.
33. J. H. van Esch, *Langmuir*, 2009, **25**, 8392-8394.
34. R. Orbach, L. Adler-Abramovich, S. Zigerson, I. Mironi-Harpaz, D. Seliktar and E. Gazit, *Biomacromolecules*, 2009, **10**, 2646-2651.
35. D. J. Adams, M. F. Butler, W. J. Frith, M. Kirkland, L. Mullen and P. Sanderson, *Soft Matter*, 2009, **5**, 1856-1862.
36. Y. Zhang, H. W. Gu, Z. M. Yang and B. Xu, *J. Am. Chem. Soc.*, 2003, **125**, 13680-13681.
37. V. Jayawarna, M. Ali, T. A. Jowitt, A. F. Miller, A. Saiani, J. E. Gough and R. V. Ulijn, *Adv. Mater.*, 2006, **18**, 611-614.
38. C. Tang, A. M. Smith, R. F. Collins, R. V. Ulijn and A. Saiani, *Langmuir*, 2009, **25**, 9447-9453.
39. M. Reches and E. Gazit, *Science*, 2003, 625-627.
40. M. Reches and E. Gazit, *Israel J. Chem.*, 2005, **45**, 363-371.
41. V. Jayawarna, S. M. Richardson, A. R. Hirst, N. W. Hodson, A. Saiani, J. E. Gough and R. V. Ulijn, *Acta Biomater.*, 2009, **5**, 934-943.
42. T. Liebmann, S. Rydholm, V. Akpe and H. Brismar, *BMC Biotechnol.*, 2007, **7**, 88-98.
43. R. Orbach, I. Mironi-Harpaz, L. Adler-Abramovich, E. Mossou, E. P. Mitchell, V. T. Forsyth, E. Gazit and D. Seliktar, *Langmuir*, 2012, **28**, 2015-2022.
44. G. Cheng, V. Castelletto, C. M. Moulton, G. E. Newby and I. W. Hamley, *Langmuir*, 2010, **26**, 4990-4998.
45. D. M. Ryan, S. B. Anderson and B. L. Nilsson, *Soft Matter*, 2010, **6**, 3220-3231.
46. S. Sutton, N. L. Campbell, A. I. Cooper, M. Kirkland, W. J. Frith and D. J. Adams, *Langmuir*, 2009, **25**, 10285-10291.
47. Z. Yang, H. Gu, D. Fu, P. Gao, J. K. Lam and B. Xu, *Adv. Mater.*, 2004, **16**, 1440-1444.
48. Z. A. C. Schnepp, R. Gonzalez-McQuire and S. Mann, *Adv. Mater.*, 2006, **18**, 1869-1872.
49. A. J. Patil, R. K. Kumar, N. J. Barron and S. Mann, *Chem. Commun.*, 2012, **48**, 7934-7936.
50. A. Aufderhorst-Roberts, W. J. Frith and A. M. Donald, *Soft Matter*, 2012, **8**, 5940-5946.
51. Z. Yang, G. Liang and B. Xu, *Chem. Commun.*, 2006, 738-740.
52. Z. Yang, G. Liang, M. Ma, Y. Gao and B. Xu, *J. Mater. Chem.*, 2007, **17**, 850-854.

53. L. Chen, S. Revel, K. Morris, L. C. Serpell and D. J. Adams, *Langmuir*, 2010, **26**, 13466-13471.
54. L. Chen, K. Morris, A. Laybourn, D. Elias, M. R. Hicks, A. Rodger, L. Serpell and D. J. Adams, *Langmuir*, 2010, **26**, 5232-5242.
55. A. K. Tickler, C. J. Barrow and J. D. Wade, *J. Pept. Sci.*, 2001, **7**, 488-494.
56. R. Vegners, I. Shestakova, I. Kalvinsh, R. M. Ezzell and P. A. Janmey, *J. Pept. Sci*, 1995, **1**, 371-378.
57. S. Debnath, A. Shome, D. Das and P. K. Das, *J. Phys. Chem. B*, 2010, **114**, 4407-4415.
58. L. Chen, J. Raeburn, S. Sutton, D. G. Spiller, J. Williams, J. S. Sharp, P. C. Griffiths, R. K. Heenan, S. M. King, A. Paul, S. Furzeland, D. Atkins and D. J. Adams, *Soft Matter*, 2011, **7**, 9721-9727.
59. D. Dasgupta, S. Srinivasan, C. Rochas, A. Ajayaghosh and J. M. Guenet, *Langmuir*, 2009, **25**, 8593-8598.
60. J. Huang, C. L. Hastings, G. P. Duffy, H. M. Kelly, J. Raeburn, D. J. Adams and A. Heise, *Biomacromolecules*, 2013, **14**, 200-206.
61. J. Raeburn, G. Pont, L. Chen, Y. Cesbron, R. Levy and D. J. Adams, *Soft Matter*, 2012, **8**, 1168-1174.
62. B. Xu, *Langmuir*, 2009, **25**, 8375-8377.
63. Z. Yang, G. Liang and B. Xu, *Accounts Chem. Res.*, 2008, **41**, 315-326.
64. S. Toledano, R. J. Williams, V. Jayawarna and R. V. Ulijn, *J. Am. Chem. Soc.*, 2006, **128**, 1070-1071.
65. X. Li, Y. Gao, Y. Kuang and B. Xu, *Chem. Commun.*, 2010, **46**, 5364-5366.
66. A. K. Das, R. Collins and R. V. Ulijn, *Small*, 2008, **4**, 279-287.
67. R. J. Williams, A. M. Smith, R. Collins, N. Hodson, A. K. Das and R. V. Ulijn, *Nat. Nano.*, 2009, **4**, 19-24.
68. Z. Yang and B. Xu, *Chem. Commun.*, 2004, 2424-2425.
69. L. Chen, G. Pont, K. Morris, G. Lotze, A. Squires, L. C. Serpell and D. J. Adams, *Chem. Commun.*, 2011, **47**, 12071-12073.
70. L. Chen, T. O. McDonald and D. J. Adams, *RSC Adv.*, 2013, **3**, 8714-8720.
71. C. Tang, R. Ulijn and A. Saiani, *Eur. Phys. J. E*, 2013, **36**, 1-11.
72. D. W. Urry, S. Q. Peng, T. M. Parker, D. C. Gowda and R. D. Harris, *Angew. Chem. Int. Ed.*, 1993, **32**, 1440-1442.
73. J. Raeburn, A. Zamith Cardoso and D. J. Adams, *Chem. Soc. Rev.*, 2013, **42**, 5143-5156.
74. A. M. Smith, R. J. Williams, C. Tang, P. Coppo, R. F. Collins, M. L. Turner, A. Saiani and R. V. Ulijn, *Adv. Mater.*, 2008, **20**, 37-41.
75. Y. Pocker and E. Green, *J. Am. Chem. Soc.*, 1973, **95**, 113-119.
76. S. R. Raghavan and J. F. Douglas, *Soft Matter*, 2012, **8**, 8539-8546.
77. S. Roy, N. Javid, J. Sefcik, P. J. Halling and R. V. Ulijn, *Langmuir*, 2012, **28**, 16664-16670.
78. J. Shi, Y. Gao, Y. Zhang, Y. Pan and B. Xu, *Langmuir*, 2011, **27**, 14425-14431.
79. B. Ozbas, K. Rajagopal, L. Haines-Butterick, J. P. Schneider and D. J. Pochan, *J. Phys. Chem. B*, 2007, **111**, 13901-13908.
80. K. Tamaki, T. Utaka, H. Takase, Y. Eriyama and T. Ukachi, *J. Photopolym. Sci.*, 2002, **15**, 103-108.
81. T. Muraoka, C.-Y. Koh, H. Cui and S. I. Stupp, *Angew. Chem. Int. Ed.*, 2009, **48**, 5946-5949.

82. J. Raeburn, T. O. McDonald and D. J. Adams, *Chem. Commun.*, 2012, **48**, 9355-9357.
83. K. Sun, R. Kumar, D. E. Falvey and S. R. Raghavan, *J. Am. Chem. Soc.*, 2009, **131**, 7135-7141.
84. K. M. Gray, E. Kim, L. Q. Wu, Y. Liu, W. E. Bentley and G. F. Payne, *Soft Matter*, 2011, **7**, 9601-9615.
85. L.Q. Wu, A. P. Gadre, H. Yi, M. J. Kastantin, G. W. Rubloff, W. E. Bentley, G. F. Payne and R. Ghodssi, *Langmuir*, 2002, **18**, 8620-8625.
86. R. Fernandes, L.-Q. Wu, T. Chen, H. Yi, G. W. Rubloff, R. Ghodssi, W. E. Bentley and G. F. Payne, *Langmuir*, 2003, **19**, 4058-4062.
87. P. J. Bracher, M. Gupta, E. T. Mack and G. M. Whitesides, *ACS Appl. Mater.*, 2009, **1**, 1807-1812.
88. Y. Wang, Y. Liu, Y. Cheng, E. Kim, G. W. Rubloff, W. E. Bentley and G. F. Payne, *Adv. Mater.*, 2011, **23**, 5817-5821.
89. E. K. Johnson, D. J. Adams and P. J. Cameron, *J. Am. Chem. Soc.*, 2010, **132**, 5130-5136.
90. Y. Liu, E. Kim, R. V. Ulijn, W. E. Bentley and G. F. Payne, *Adv. Funct. Mater.*, 2011, **21**, 1575-1580.
91. S. Ramachandran, M. B. Taraban, J. Trewhella, I. Gryczynski, Z. Gryczynski and Y. B. Yu, *Biomacromolecules*, 2010, **11**, 1502-1506.
92. A. Z. Cardoso, A. E. Alvarez Alvarez, B. N. Cattoz, P. C. Griffiths, S. M. King, W. J. Frith and D. J. Adams, *Faraday Discuss.*, 2013, **166**, 101-116.
93. L. Haines-Butterick, K. Rajagopal, M. Branco, D. Salick, R. Rughani, M. Pilarz, M. S. Lamm, D. J. Pochan and J. P. Schneider, *Proc. Nat. Acad. Sci.*, 2007, **104**, 7791-7796.
94. K. Rajagopal, M. S. Lamm, L. A. Haines-Butterick, D. J. Pochan and J. P. Schneider, *Biomacromolecules*, 2009, **10**, 2619-2625.
95. T. Yucel, C. M. Micklitsch, J. P. Schneider and D. J. Pochan, *Macromolecules*, 2008, **41**, 5763-5772.
96. C. Yan, A. Altunbas, T. Yucel, R. P. Nagarkar, J. P. Schneider and D. J. Pochan, *Soft Matter*, 2010, **6**, 5143-5156.
97. K. S. Thornton, Andrew M.; Merry, Catherine L. R.; Ulijn, Rein V., *Biochem. Soc. T.*, 2009, **37**, 660-664.
98. R. L. Huang, W. Qi, L. B. Feng, R. X. Su and Z. M. He, *Soft Matter*, 2011, **7**, 6222-6230.
99. W. Helen, P. de Leonardis, R. V. Ulijn, J. Gough and N. Tirelli, *Soft Matter*, 2011, **7**, 1732-1740.
100. R. V. Rughani, D. A. Salick, M. S. Lamm, T. Yucel, D. J. Pochan and J. P. Schneider, *Biomacromolecules*, 2009, **10**, 1295-1304.
101. L. E. Buerkle and S. J. Rowan, *Chem. Soc. Rev.*, 2012, **41**, 6089-6102.
102. L. A. Munishkina, E. M. Cooper, V. N. Uversky and A. L. Fink, *J. Mol. Recognit.*, 2004, **17**, 456-464.
103. D. M. Hatters, A. P. Minton and G. J. Howlett, *J. Bio. Chem.*, 2002, **277**, 7824-7830.
104. G. Pont, L. Chen, D. G. Spiller and D. J. Adams, *Soft Matter*, 2012, **8**, 7797-7802.
105. Y. J. Adhia, T. H. Schloemer, M. T. Perez and A. J. McNeil, *Soft Matter*, 2012, **8**, 430-434.
106. B. Adhikari and A. Banerjee, *Soft Matter*, 2011, **7**, 9259-9266.

107. Y. Liu, B. Zhang, K. M. Gray, Y. Cheng, E. Kim, G. W. Rubloff, W. E. Bentley, Q. Wang and G. F. Payne, *Soft Matter*, 2013, **9**, 2703-2710.
108. K. L. Morris, L. Chen, J. Raeburn, O. R. Sellick, P. Cotanda, A. Paul, P. C. Griffiths, S. M. King, R. K. O'Reilly, L. C. Serpell and D. J. Adams, *Nat. Commun.*, 2013, **4**, 1480-1485.
109. N. Javid, S. Roy, M. Zelzer, Z. Yang, J. Sefcik and R. V. Ulijn, *Biomacromolecules*, 2013, **14**, 4368-4376.
110. D. J. Cornwell, B. O. Okesola and D. K. Smith, *Soft Matter*, 2013, 8730-8736.
111. M. M. Smith and D. K. Smith, *Soft Matter*, 2011, **7**, 4856-4860.
112. K. J. Nagy, M. C. Giano, A. Jin, D. J. Pochan and J. P. Schneider, *J. Am. Chem. Soc.*, 2011, **133**, 14975-14977.
113. D. Seliktar, *Science*, 2012, **336**, 1124-1128.
114. K. Saha, A. J. Keung, E. F. Irwin, Y. Li, L. Little, D. V. Schaffer and K. E. Healy, *Biophys. J.*, 2008, **95**, 4426-4438.
115. M. Wallace, D. J. Adams and J. A. Iggo, *Soft Matter*, 2013, **9**, 5483-5491.
116. M. C. Branco, D. J. Pochan, N. J. Wagner and J. P. Schneider, *Biomaterials*, 2009, **30**, 1339-1347.
117. N. Kojic, M. J. Panzer, G. G. Leisk, W. K. Raja, M. Kojic and D. L. Kaplan, *Soft Matter*, 2012, **8**, 6897-6905.
118. A. Revzin, R. G. Tompkins and M. Toner, *Langmuir*, 2003, **19**, 9855-9862.
119. S. M. DePorter, I. Lui and B. R. McNaughton, *Soft Matter*, 2012, **8**, 10403-10408.
120. J. W. Chung, B.-K. An and S. Y. Park, *Chem. Mat.*, 2008, **20**, 6750-6755.
121. L. Chen, S. Revel, K. Morris and D. J. Adams, *Chem. Commun.*, 2010, **46**, 4267-4269.
122. Q. Wang, Z. Yang, Y. Gao, W. Ge, L. Wang and B. Xu, *Soft Matter*, 2008, **4**, 550-553.

CHAPTER 2

Experimental

2.1 Materials

All dipeptide materials except FmocFF/LG/VG/AG (synthesised by Dr D. J. Adams as described previously[1]) were prepared as described below. Unless characterised below, dipeptide gelators were synthesised by Dr D. J. Adams using the same procedure as described below (and elsewhere[2, 3]). Deionised water was used throughout. All other chemicals were purchased from Sigma-Aldrich (unless stated otherwise) and used as received.

2.2 Low Molecular Weight Gelator (LMWG) Synthesis

All dipeptide gelators were prepared as described previously[2] from either 6-bromo-2-naphthol, 2-naphthol or 1-bromo-2-naphthol. These were reacted as follows: 6-bromo-2-naphthol (10.1 g, 45.2 mmol) was dissolved in acetone (150 mL) before adding potassium carbonate (31.2 g, 226 mmol) and finally *tert*-butyl chloroacetate (7.1 mL, 49.7 mmol). The solution was heated to reflux for 24 hours. Upon cooling, chloroform (100 mL) was added and the solution was washed with 4 x 100 mL water, dried with magnesium sulfate and the solvent removed *in vacuo* to afford a colourless oil. The crude product was directly used in the next step of the reaction.

Tert-butyl 2-(6-bromonaphthalen-2-yloxy)acetate ^{1}H NMR ($CDCl_3$): 7.94 (d, ArH, 1H, J = 2.3 Hz), 7.69 (d, ArH, 2H, J = 9.0 Hz), 7.60 (d, ArH, 1H, J = 8.7 Hz), 7.52 (d, ArH, 1H, J = 8.7 Hz), 7.27 (dd, ArH, 1H, J = 6.8 Hz, J = 4.0 Hz), 7.04 (d, ArH, 1H, J = 2.7 Hz), 4.64 (s, OCH_2), 1.51 (s, $OC(CH_3)_3$, 9H) ppm.

Tert-butyl 2-(naphthalen-2-yloxy)acetate ^{1}H NMR ($CDCl_3$): 7.77 (d, ArH, 1H, J = 8.0 Hz), 7.76 (d, ArH, 1H, J = 9.0 Hz), 7.70 (d, ArH, 1H, J = 8.2 Hz), 7.43 (t, ArH, 1H, J = 6.9 Hz), 7.34 (t, ArH, 1H, J = 7.0 Hz), 7.23 (dd, ArH, 1H, J = 9.0 Hz, J = 2.6 Hz) , 7.06 (d, ArH, 1H, J = 2.4 Hz), 4.63 (s, OCH_2, 2H), 1.49 (s, $C(CH_3)_3$, 9H) ppm.

Tert-butyl 2-(1-bromonaphthalen-2-yloxy)acetate ^{1}H NMR ($CDCl_3$): 8.27 (d, ArH,

1H, J = 8.6 Hz), 7.81 (d, ArH, 1H, J = 9.0 Hz), 7.60 (t, ArH, 1H, J = 7.1 Hz), 7.44 (d, ArH, 1H, J = 8.0 Hz), 7.18 (d, ArH, 1H, J = 9.0 Hz), 4.75 (s, OCH_2, 2H), 1.50 (s, $C(CH_3)_3$, 9H) ppm.

The *tert*-butyl protecting group was then removed as follows: All of the *tert*-butyl 2-(6-bromonaphthalen-2-yloxy)acetate from the previous step was dissolved in 30 mL chloroform. Trifluoroacetic acid (~ 10 mL) was added and the solution was left to stir overnight. Hexane (200 mL) was added to precipitate out the solid product. The solid material was washed with hexane to give the product 2-(6-bromonaphthalen-2-yloxy)acetic acid product in an 85 % yield.2-(6-bromonaphthalen-2-yloxy)acetic acid ^{1}H NMR (d_6-DMSO) – 85 % yield: 8.12 (d, ArH, 1H, J = 1.8 Hz), 7.84 (d, ArH, 1H, J = 9.0 Hz), 7.77 (d, ArH, 1H, J = 8.8 Hz), 7.56 (dd, ArH, 1H, J = 6.8 Hz, J = 2.0 Hz), 7.32 (d, ArH, 1H, J = 2.4 Hz), 7.26 (dd, ArH, 1H, J = 6.4 Hz, J = 2.6 Hz), 4.81 (s, OCH_2, 2H), 3.39 (bs, OH, 1H) ppm.

2-(Naphthalen-2-yloxy)acetic acid ^{1}H NMR (d_6-DMSO) – 81 % yield: 7.85 (d, ArH, 1H, J = 9.1 Hz), 7.79 (d, ArH, 1H, J = 8.1 Hz), 7.46 (t, ArH, 1H, J = 6.7 Hz), 7.36 (t, ArH, 1H, J = 6.9 Hz), 7.27 (d, ArH, 1H, J = 2.5 Hz), 7.22 (dd, ArH, 1H, J = 8.9 Hz, J = 2.6 Hz), 4.81 (s, OCH_2, 2H) ppm.

2-(1-Bromonaphthalen-2-yloxy)acetic acid ^{1}H NMR (d_6-DMSO) – 87 % yield: 8.10 (d, ArH, 1H, J = 8.6 Hz), 7.94 (d, ArH, 1H, J = 9.1 Hz), 7.91 (d, ArH, 1H, J = 8.2 Hz), 7.63 (d, ArH, 1H, J = 7.6 Hz), 7.45 (t, ArH, 1H, J = 7.6 Hz), 7.36 (d, ArH, 1H, J = 9.1 Hz), 4.88 (s, OCH_2, 2H) ppm.

A C-ethyl-protected (or methyl) amino acid was coupled as follows: *N*-methylmorpholine (1.7 ml, 15.5 mmol) and isobutylchloroformate (2.2 mL, 17.0 mmol) were added to a solution of 2-(6-bromonaphthalen-2-yloxy)acetic acid (5.21 g, 15.5 mmol) in 100 mL chloroform and stirred for 5 min at 0 ºC. A solution of L-alanine ethyl ester (2.5 g, 16.3 mmol) and *N*-methylmorpholine (1.7 mL, 15.5 mmol) in chloroform (25 mL) was added. The solution was allowed to warm to room temperature with stirring overnight. The solution was washed with 4 x 100 mL water (and ~ 30 mL 0.1 M HCl) and dried with magnesium sulfate before removing the

solvent *in vacuo* to give ethyl 2-(2-(6-bromonaphthalen-2-yloxy)acetamido)propanoate as a colourless oil. The crude product was directly used in the next step of the reaction.

Ethyl 2-(2-(6-bromonaphthalen-2-yloxy)acetamido)propanoate ^{1}H NMR ($CDCl_3$): 7.96 (s, ArH, 1H), 7.72 (d, ArH, 1H, J = 9.0 Hz), 7.63 (d, ArH, 1H, J = 8.8 Hz), 7.53 (d, ArH, 1H, J = 8.9 Hz), 7.26 (m, ArH and NH, 2H), 7.15 (s, ArH, 1H), 4.74 (m, C*H*$_2$CH$_3$, 2H), 4.64 (s, OCH$_2$, 2H), 1.50 (t, CH$_2$C*H*$_3$, 3H, J = 7.2 Hz) ppm.

Ethyl 2-(2-(6-bromonaphthalen-2-yloxy)acetamido)-3-phenylpropanoate ^{1}H NMR ($CDCl_3$): 7.95 (d, ArH, 1H, J = 1.7 Hz), 7.69 (d, ArH, 1H, 9.0 Hz), 7.60 (d, ArH, 1H, J = 8.8 Hz), 7.53 (dd, ArH, 1H, J = 8.7 Hz, J = 1.9 Hz), 7.18 – 7.14 (m, ArH, 3H), 7.06 – 7.01 (m, ArH and NH, 5H), 4.96 (dt, C*H*NH, 1H, J = 6.0 Hz, J = 6.0 Hz), 4.60 (s, OCH$_2$, 2H), 4.17 (q, C*H*$_2$CH$_3$, 2H, J = 7.1 Hz), 3.14 (d, CH2Ph, 2H, J = 6.0 Hz), 1.23 (t, CH$_2$C*H*$_3$, 3H, J = 7.2 Hz) ppm.

Ethyl 2-(2-(naphthalen-2-yloxy)acetamido)propanoate ^{1}H NMR ($CDCl_3$): 7.72 (d, ArH, 1H, J = 7.4 Hz), 7.68 (d, ArH, 1H, J = 8.3 Hz), 7.64 (d, ArH, 1H, J = 7.9 Hz), 7.40 (t, ArH, 1H, J = 7.2 Hz), 7.31 (t, ArH, 1H, J = 8.0 Hz), 7.19 – 7.12 (m, ArH and NH, 2H), 7.09 (d, ArH, 1H, J = 2.4 Hz), 4.62 (m, C*H*NH, 1H), 4.56 (s, OCH$_2$, 2H), 4.14 (q, C*H*$_2$CH$_3$, 2H, J = 7.1 Hz), 1.40 (d, CHC*H*$_3$, 3H, J = 7.2 Hz), 1.20 (t, CH$_2$C*H*$_3$, 3H, J = 7.1 Hz) ppm.

Ethyl 2-(2-(naphthalen-2-yloxy)acetamido)-3-phenylpropanoate ^{1}H NMR ($CDCl_3$): 7.79 (d, ArH, 1H, J = 8.0 Hz), 7.78 (d, 1H, ArH, J = 8.9 Hz), 7.73 (d, ArH, 1H, J = 8.2 Hz), 7.47 (t, ArH, 1H, J = 7.0 Hz), 7.39 (t, ArH, 1H, J = 7.1 Hz), 7.03 – 7.17 (m, ArH and NH, 8H), 4.95 (dt, C*H*NH, 1H, J = 8.1, J = 6.0 Hz), 4.62 (s, OCH$_2$, 2H), 4.17 (q, C*H*$_2$CH$_3$, 2H, J = 7.1 Hz), 3.16 (d, C*H*$_2$Ph, 2H, J = 6.0 Hz), 1.22 (t, CH$_2$C*H*$_3$, 3H, J = 7.1 Hz) ppm.

Methyl 2-(2-(1-bromonaphthalen-2-yloxy)acetamido)-3-methylbutanoate ^{1}H NMR ($CDCl_3$): 8.23 (d, ArH, 1H, J = 7.6 Hz), 7.86 (d, ArH, 1H, J = 9.0 Hz), 7.82 (d, ArH, 1H, J = 8.2 Hz), 7.61 (m, 2H, ArH and NH), 7.46 (t, ArH, 1H, J = 7.4 Hz), 7.21 (d,

ArH, 1H, J = 9.0 Hz), 4.72 (s, OCH_2, 2H), 4.66 (m, C*H*NH, 1H), 2.79 (s, OCH_3, 3H), 2.28 (m, C*H*$(CH_3)_2$, 1H), 1.00 (t, CH$(CH_3)_2$, 6H, J = 6.6 Hz) ppm.

To deprotect the C-terminus, lithium hydroxide (0.25 g) was added to a solution of all of the ethyl 2-(2-(6-bromonaphthalen-2-yloxy)acetamido)propanoate from the previous step in a 4:1 THF:water (60 mL) solution and the solution was stirred overnight. Distilled water (200 mL) was added and then HCl (1 M) was added dropwise until the pH was lowered to ~ pH 3. The resulting precipitate was collected by filtration and washed with water before being dried *in vacuo* to afford the 2-(2-(6-bromonaphthalen-2-yloxy)acetamido)propanoic acid product in an 89 % yield.

2-(2-(6-Bromonaphthalen-2-yloxy)acetamido)propanoic acid ^{1}H NMR (d_6-DMSO) – 89 % yield: 12.70 (bs, OH, 1H), 8.45 (d, ArH, 1H, J = 7.5 Hz), 8.12 (d, ArH, 1H, J = 1.8 Hz), 7.86 (d, ArH, 1H, J = 8.9 Hz), 7.75 (d, ArH, 1H, J = 8.8 Hz), 7.58 (dd, ArH, 1H, J = 5.8 Hz, J = 2.1 Hz), 7.32 (m, ArH and NH, 2H), 4.66 (s, OCH_2, 2H), 4.34 (m, CH_3C*H*, 1H), 1.34 (d, C*H*$_3$CH, 3H, J = 7.3 Hz) ppm.

2-(2-(6-Bromonaphthalen-2-yloxy)acetamido)-3-phenylpropanoic acid ^{1}H NMR (d_6-DMSO) – 83 % yield: 8.36 (d, NH, 1H, J = 8.2 Hz), 8.13 (d, ArH, 1H, 1.9 Hz), 7.85 (d, ArH, 1H, J = 9.0 Hz), 7.70 (d, ArH, 1H, J = 8.8 Hz), 7.59 (dd, ArH, 1H, J = 8.8 Hz, J = 2.0 Hz), 7.29 – 7.14 (m, ArH, 8H), 4.61 (d, OCH_2, 2H, J = 2.3 Hz), 4.54 (m, OCH and C*H*NH, 2H), 3.14 (dd, CHPh, 1H, J = 13.4 Hz, J = 4.7 Hz), 2.98 (dd, CHPh, 1H, J = 13.9 Hz, J = 9.4 Hz) ppm.

2-(2-(Naphthalen-2-yloxy)acetamido)propanoic acid ^{1}H NMR (d_6-DMSO) – 80 % yield: 12.7 (bs, OH, 1H), 8.43 (d, ArH, 1H, J = 7.6 Hz), 7.87 (d, ArH, 1H, J = 8.9 Hz), 7.85 (d, ArH, 1H, J = 8.0 Hz), 7.78 (d, ArH, 1H, J = 8.4 Hz), 7.47 (t, ArH, 1H, J = 7.9 Hz), 7.37 (t, ArH, 1H, J = 8.0 Hz), 7.31 – 7.25 (m, ArH and NH, 2H), 4.65 (d, OCH_2, 2H, J = 3.2 Hz), 4.34 (m, C*H*NH, 1H), 1.35 (d, CHC*H*$_3$, 3H, J = 7.3 Hz) ppm.

2-(2-(Naphthalen-2-yloxy)acetamido)-3-phenylpropanoic acid ^{1}H NMR (d_6-DMSO) – 77 % yield: 8.36 (d, ArH, 1H, J = 8.2 Hz), 7.84, (d, ArH, 1H, J = 9.3 Hz), 7.73 (d, ArH, 1H, J = 8.2 Hz), 7.46 (t, ArH, 1H, J = 7.0 Hz), 7.37 (t, ArH, 1H, J = 8.0 Hz),

7.19 (m, ArH and NH, 7H), 4.60 (s, OCH_2, 2H), 4.53 (m, C*H*NH, 1H), 3.14 (dd, C*H*Ph, 1H, J = 13.8, J = 4.7 Hz), 3.01 (dd, C*H*Ph, 1H, J = 13.9 Hz, J = 9.4 Hz) ppm.

2-(2-(1-Bromonaphthalen-2-yloxy)acetamido)-3-methylbutanoic acid ^{1}H NMR (d_6-DMSO) – 72 % yield: 8.10 (d, ArH, 1H, J = 9.6 Hz), 8.02 – 7.93 (m, ArH and NH, 3H), 4.88 (d, OCH_2, 2H, J = 5.3 Hz), 4.28 (m, C*H*NH, 1H), 2.15 (m, C*H*$(CH_3)_2$, 1H), 0.90 (d, CH(C*H*$_3)_2$, 6H, J = 6.9) ppm.

A similar procedure to the above was followed for the addition of the second amino acid.

Ethyl 2-(2-(2-(6-bromonaphthalen-2-yloxy)acetamido)propanamido)-3-methylbutanoate ^{1}H NMR ($CDCl_3$): 7.93 (d, ArH, 1H, J = 1.8 Hz), 7.69 (d, ArH, 1H, J = 9.0 Hz), 7.60 (d, ArH, 1H, J = 7.8 Hz), 7.52 (dd, ArH, 1H, J = 8.7 Hz, J = 2.0 Hz), 7.25 (m, ArH and NH, 2H), 7.11 (d, ArH, 1H, J = 2.5 Hz), 6.69 (bd, NH, 1H), 4.69 (m, C*H*NH, 1H), 4.62 (d, OCH_2, 2H, J = 3.2 Hz), 4.52 (dd, C*H*NH, 1H, J = 8.7 Hz, J = 3.8 Hz), 4.09 (q, C*H*$_2$CH$_3$, 2H, J = 5.2 Hz), 2.34 (m, C*H*$(CH_3)_2$, 1H), 1.36 (d, CHC*H*$_3$, 3H, J = 6.9 Hz), 1.07 (t, CH_2C*H*$_3$, 3H, J = 6.8 Hz), 0.95 (d, CHC*H*$_3$, 3H, J = 5.2 Hz) ppm.

Methyl 2-(2-(2-(6-bromonaphthalen-2-yloxy)acetamido)-3-phenylpropanamido)-3-methylbutanoate ^{1}H NMR ($CDCl_3$): 7.94 (d, ArH, 1H, J = 1.7 Hz), 7.68 (d, ArH, 1H, J = 9.0 Hz), 7.58 (d, ArH, 1H, J = 8.8 Hz), 7.51 (dd, ArH, 1H, J = 8.8 Hz, J = 1.9 Hz), 7.22 – 7.13 (m, ArH and NH, 7H), 7.04 (d, ArH, 1H, J = 2.3 Hz), 6.33 (d, NH, 1H, J = 8.5 Hz), 4.79 (dt, C*H*NH, 1H, J = 7.2 Hz, J = 7.2 Hz), 4.59 (d, OCH_2, 2H, J = 5.2 Hz), 4.42 (dd, CHNH, 1H, J = 8.5 Hz, J = 5.1 Hz), 4.17 (q, C*H*$_2$CH$_3$, 2H, J = 7.1 Hz), 3.12 (m, CH_2Ph, 2H), 2.06 (m, C*H*$(CH_3)_2$, 1H), 1.23 (t, CH_2C*H*$_3$, 3H, J = 7.2 Hz), 0.83 (d, CHC*H*$_3$, 3H, J = 6.9 Hz), 0.79 (d, CHC*H*$_3$, 3H, J = 6.9 Hz)

Ethyl 2-(2-(2-(naphthalene-2-yloxy)acetamido)propanamido)acetate ^{1}H NMR ($CDCl_3$): 7.78 (m, ArH, 3H), 7.48 (t, ArH, 1H, J = 7.9 Hz), 7.38 (d, ArH, 1H, J = 7.1 Hz), 7.28 (bd, NH, 1H, J = 8.9 Hz), 7.24 (dd, ArH, 1H, J = 6.4 Hz, J = 2.5 Hz), 7.15 (d, ArH, 1H, J = 2.4 Hz), 6.55 (bs, NH, 1H), 4.67 (s, OCH_2, 2H), 4.59 (m, C*H*NH,

1H), 3.94 (q, C*H*$_2$CH$_3$, 2H, J = 6.8 Hz), 1.41 (d, CHC*H*$_3$, 3H, J = 7.2 Hz), 0.98 (d, CH$_2$C*H*$_3$, 3H, J = 6.7 Hz) ppm.

Ethyl 2-(2-(2-(naphthalen-2-yloxy)acetamido)-3-phenylpropanamido)-3-phenylpropanoate ^{1}H NMR ($CDCl_3$): 7.80 (d, ArH, 2H, J = 9.0 Hz), 7.72 (d, ArH, 1H, J = 8.3 Hz), 7.47, (t, ArH, 1H, J = 7.7 Hz), 7.39 (t, ArH, 1H, J = 7.0 Hz), 7.26 (bs, NH, 1H), 7.20 – 7.07 (m, ArH, 11H), 6.97 (d, ArH, 1H, J = 6.97 Hz), 6.28 (d, NH, 1H, J = 7.2 Hz), 4.73 (m, C*H*NH, 2H), 4.55 (s, OCH$_2$, 2H), 4.14 (q, C*H*$_2$CH$_3$, 2H, J = 7.1 Hz), 3.14 – 2.94 (m, C*H*$_2$Ph, 4H,), 1.22 (t, CH$_2$C*H*$_3$, 3H, J = 7.2 Hz) ppm.

Methyl 2-(2-(2-(1-bromonaphthalen-2-yloxy)acetamido)-3-methylbutanamido)acetate ^{1}H NMR ($CDCl_3$): 8.24 (d, ArH, 1H, J = 8.7 Hz), 7.86 (d, NH, 1H, J = 9.0 Hz), 7.82 (d, ArH, 1H, J = 8.2 Hz), 7.66 – 7.59 (m, ArH and NH, 2H), 7.47 (t, ArH, 1H, J = 8.0 Hz), 7.35 (d, ArH, 1H, J = 8.0 Hz), 7.21 (d, ArH, 1H, J = 9.0 Hz), 4.74 (s, OCH$_2$, 2H), 4.46 (dd, C*H*NH, 1H, J = 6.1 Hz, J = 2.6 Hz), 4.09 (d, C*H*$_2$NH, 2H, J = 5.2 Hz), 3.77 (s, CH$_3$, 3H), 2.34 (m, C*H*(CH$_3$)$_2$, 1H), 1.06 (d, CH(C*H*$_3$)$_2$, 6H, J = 6.8 Hz) ppm.

Deprotection was then carried out as described above.

2-(2-(2-(6-Bromonaphthanlen-2-yloxy)acetamido)propanamido)-3-methylbutanoic acid **(BrNapAV)** ^{1}H NMR (d$_6$-DMSO) – 82 % yield: 12.60 (br s, OH, 1H), 8.20 (d, NH, 1H, J = 7.7 Hz), 8.13 (d, ArH, 1H, J = 1.7 Hz), 8.06 (d, NH, 1H, J = 8.5 Hz), 7.86 (d, ArH, 1H, J = 8.9 Hz), 7.76 (d, ArH, 1H, J = 8.9 Hz), 7.58 (dd, ArH, 1H, J = 6.7 Hz, J = 2.0 Hz), 7.30 (m, ArH, 2H), 4.65 (d, OCH$_2$, 2H, J = 2.2 Hz), 4.53 (m, C*H*NH, 1H), 4.15 (dd, C*H*NH, 1H, J = 8.5 Hz, J = 5.7 Hz), 2.03 (m, C*H*(CH$_3$)$_2$, 1H), 1.27 (d, CHC*H*$_3$, 3H, J = 7.0 Hz), 0.84 (d, CH(C*H*$_3$)$_2$, 6H, J = 6.7 Hz) ppm.

2-(2-(2-(6-Bromonaphthanlen-2-yloxy)acetamido)-3-phenylpropanaamido)-3-methylbutanoic acid **(BrNapFV)** ^{1}H NMR (d$_6$-DMSO) – 88 % yield: 8.24 (d, NH, 1H, J = 8.4 Hz), 8.22 (d, NH, 1H, J = 8.5 Hz), 8.12 (d, ArH, 1H, J = 1.9 Hz), 7.83 (d, ArH, 1H, J = 8.9 Hz), 7.69 (d, ArH, 1H, J = 8.9), 7.57 (dd, ArH, 1H, J = 8.8 Hz, J = 2.0 Hz), 7.26 – 7.13 (m, ArH, 7H), 4.75 (m, C*H*NH, 1H), 4.58 (s, OCH$_2$, 2H), 4.16

(m, C*H*NH, 1H), 3.06 (dd, C*H*PH, 1H, J = 13.9 Hz, J = 4.0 Hz), 2.90 (dd, C*H*Ph, 1H, J = 13.8 Hz, J = 9.8 Hz), 2.06 (m, C*H*$(CH_3)_2$, 1H), 0.86 (m, CH(C*H*$_3)_2$, 6H) ppm.

2-(2-(2-(Naphthalen-2-yloxy)acetamido)propanamido)propanoic acid **(2NapAA)** ^{1}H NMR (d_6-DMSO) – 79 % yield: 12.52 (bs, OH, 1H), 8.28 (d, NH, 1H, J = 7.3 Hz), 8.18 (d, NH, 1H, J = 7.8 Hz), 7.81 (m, ArH, 3H), 7.47 (t, ArH, 1H, J = 8.0 Hz), 7.37 (t, ArH, 1H, J = 7.1 Hz), 7.31 (d, ArH, 1H, J = 2.4 Hz), 7.26 (dd, ArH, 1H, J = 8.9 Hz, J = 2.6 Hz), 4.65 (s, OCH_2, 2H), 4.44 (m, C*H*NH, 1H), 4.21 (m, C*H*NH, 1H), 1.29 (d, CHC*H*$_3$, 3H, J = 6.7 Hz), 1.25 (d, CHC*H3*, 3H, J = 6.9 Hz)

2-(2-(2-(Naphthalen-2-yloxy)acetamido)-3-phenylpropanamido)-3-phenylpropanoic acid **(2NapFF)** ^{1}H NMR (d_6-DMSO) – 89 % yield: 8.36 (d, NH, 1H, J = 7.9 Hz), 8.04, (d, NH, 1H, J = 8.5 Hz), 7.75 (d, ArH, 2H, J = 6.9 Hz), 7.64, (d, ArH, 1H, J = 8.1 Hz), 7.38 (t, ArH, 1H, J = 7.2 Hz), 7.28 (t, ArH, 1H, J = 7.8 Hz), 7.18 – 7.06 (m, ArH, 12H), 4.56 (m, C*H*NH, 1H), 4.45 (s, OCH_2, 2H), 4.40 (m, C*H*NH, 1H), 2.87 (m, C*H*$_2$Ph, 4H) ppm.

2-(2-(2-(1-Bromonaphthalen-2-yloxy)acetamido)-3-methylbutanamido)acetic acid **(1BrNapVG)** ^{1}H NMR (d_6-DMSO) – 81 % yield: 8.47 (t, ArH, 1H, J = 5.8 Hz), 8.10 (d, ArH, 1H, J = 8.6 Hz), 7.98 (d, NH, 1H, J = 9.0 Hz), 7.94 (d, NH, 1H, J = 10.0 Hz), 7.88 (d, ArH, 1H, J = 7.2 Hz), 7.65 (dt, ArH, 1H, J = 7.2, J = 1.0 Hz), 7.49 – 7.38 (m, ArH, 2H), 4.84 (d, OCH_2, 2H, J = 7.0 Hz), 4.33 (dd, C*H*$_2$NH, 2H, J = 9.0, J = 5.8 Hz), 2.05 (m, C*H*$(CH_3)_2$, 1H), 0.89 (d, CH(C*H*$_3)_2$, 6H, J = 6.8 Hz) ppm.

2.3 LMWG Sample Preparation

2.3.1 Solvent-Triggered Gelation

Stock solutions of gelator were prepared by dissolving in DMSO (or other solvents) and upon complete dissolution of gelator, distilled water was added to make up to a final volume of 2 mL to form a gel for analysis. The volume of DMSO and water added varied depending on the desired Φ_{DMSO}. No post-water mixing was required. Samples were left to stand overnight before any analyses of the gels formed were

carried out. When gelled, complete immobilisation of the solvent occurred and gels had a final gelator concentration of 0.5 wt% (5 mg/mL) unless otherwise stated.

2.3.2 pH-Triggered Gelation

A 0.5 wt% stock solution of dipeptide material at approximately pH 9 – 11 was prepared by adding dilute sodium hydroxide solution (1 molar equivalent of a 0.1 M solution) with stirring until fully dissolved.

For UV gelation (Chapter 4)
The photoacid generator (PAG) (1 molar equivalent) was added to this solution before leaving to stir overnight for the viscous solutions (7MeOFF, CNNapFF and 2NapFF) and less than 1 hour stirring was needed for complete dissolution in the other gelator solutions. Gels were formed using the method described below in Section 2.10.

For electrochemical gelation (Chapter 5)
Upon full dissolution, the pH was lowered to ~ pH 8 using 1 M hydrochloric acid (HCl). Hydroquinone was added before beginning experiments (final concentration of 0.065 M). Solutions were also prepared by replacing water with Dulbecco's Modified Eagle's Medium (DMEM) for certain samples used in the DMEM stability and cell culture studies. Gels were formed using the method described below in Section 2.14.

For gelation with glucono-δ-lactone (GdL) (Chapter 6)
The gelator stock solution was added to a weighed amount of GdL and gently shaken to dissolve GdL. The sample was then left to stand to allow gelation to occur over several hours. When preparing composite hydrogels: dextran (6000 g/mol) was dissolved in water (to the desired concentration) and added to the water component when preparing the gelator stock solution.

2.4 UV/Vis Absorption Spectroscopy

UV-Vis absorption data was collected using a Thermo Scientific Nanodrop 2000/2000c spectrophotometer. Samples were prepared, as described above (Section 2.3), in 1.0 cm pathlength PMMA cuvettes.

2.4.1 Turbidity Measurements (Chapter 2)

Gels samples were prepared *in situ* and monitored over time *via* sequential UV/vis measurements at 600 nm as soon as water was added to the gelator stock solution. Measurements were taken every 5 seconds for 600 seconds. Single scans from 200 to 800 nm were also measured on gels samples.

2.4.2 Dye Release *via* UV/vis Spectroscopy (Chapter 5)

Gels were prepared using the potentiometric method described below, where a three-electrode system containing a glassy carbon working electrode was utilised. 100 μL of dye (5 mg/mL) per 1 mL of gelator solution was added to gelator solutions prior to gelation. Gels were prepared by an applied current of 30 μA for 1000 s. Gels were then removed from the electrode using a microspatula and placed in a vial containing pH 4 water. Release of the dye into the surrounding solution was measured every 5 minutes for the first 60 minutes and then every 30 min thereafter. Measurements were taken at wavelengths of 426 nm, 482 nm and 556 nm for Naphthol Yellow S, Sunset Yellow and Rhodamine B, respectively.

2.4.3 Turbidity Measurements (Chapter 6)

UV measurements at 600 nm were taken immediately after adding gelator solution to GdL. Measurements were taken every minute for one hour and then every 30 min for 18 hours.

2.5 Fourier Transform Infrared (FT-IR) Spectroscopy

IR spectra were collected using a Bruker Tensor 27 spectrometer at 2 cm^{-1} resolution, averaging over 64 scans from 4000 cm^{-1} to 800 cm^{-1}. The gels were prepared as described above but water was replaced with D_2O. An aliquot of sample (around 2 mg) was transferred onto a CaF_2 liquid-cell window using a microspatula. A second

CaF_2 window was then placed on top of the gel.

2.6 Rheological Measurements

Rheology can be defined, in its simplest terms, as the study of the deformation and flow (viscosity) of matter. In practice, rheology is principally concerned with extending the "classical" disciplines of elasticity and (Newtonian) fluid mechanics to materials whose mechanical behaviour cannot be described with the classical theories.[4] Rheological studies are carried out on materials with complex structures – polymers, bodily fluids and hydrogels. These materials behave not as an ideal solid, where the stress of the material is proportional to the strain applied; nor do they behave as an ideal liquid, which displays a stress which is proportional to the strain rate applied (Figure 1).

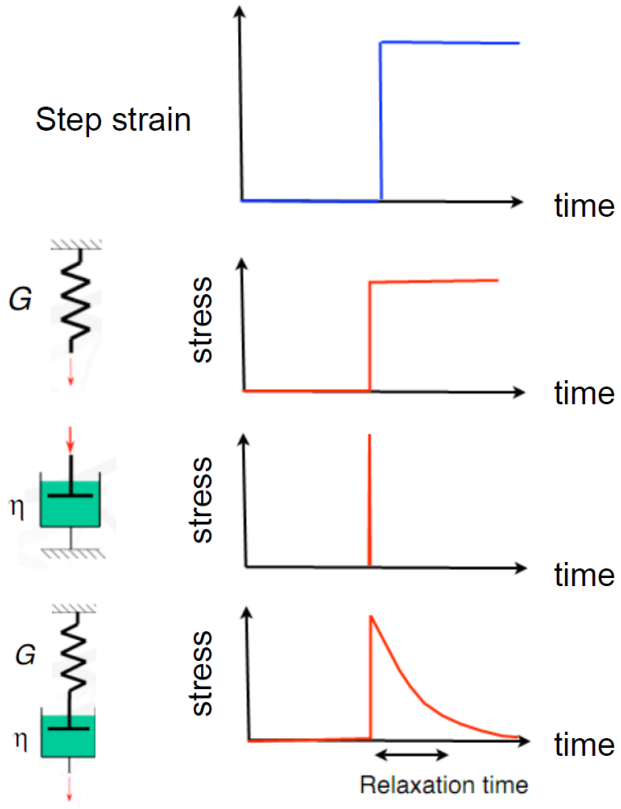

Figure 1 Classical responses of a Hookean solid, Newtonian Liquid and a viscoelastic material (top to bottom) to an applied strain step

In oscillatory shear measurements; where the viscoelastic material is subjected to a sinusoidal strain (γ) at an angular frequency of ω, the material will respond with a sinusoidal stress (σ) where:

$$\sigma = \gamma_0 (G'(\omega) \sin(\omega t) + G''(\omega) \cos(\omega t)) \quad (1)$$

From this measurement, the mechanical response of a viscoelastic material can be determined. The "solid-like" component of the material can be defined by the shear storage modulus (G'), which represents the in-phase (elastic) component of oscillatory flow. The "liquid-like" portion of the material is represented by the shear loss modulus (G'') which is the out of phase (viscous) component of oscillatory flow (Figure 2).[5]

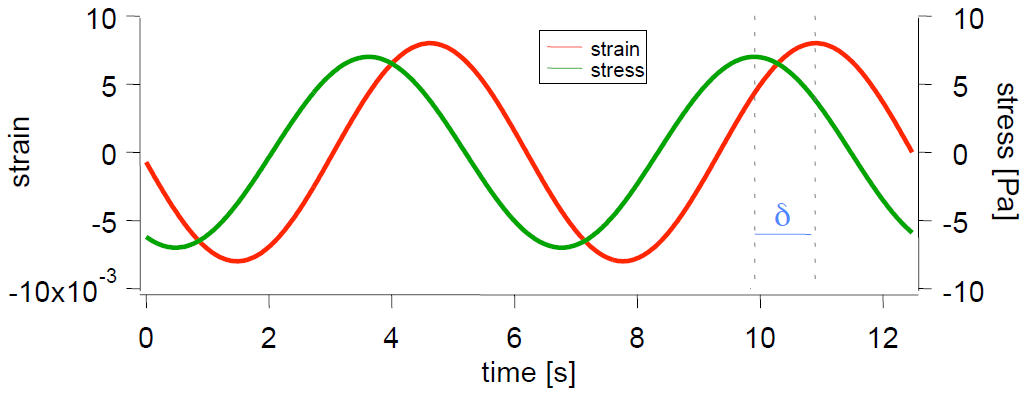

Figure 2 Sinusoidal response of a viscoelastic material

Both components can be determined from oscillatory experiments using the following equations (2 and 3):

$$G' = \sigma/\gamma \cos\delta \quad (2) \qquad G'' = \sigma/\gamma \sin\delta \quad (3)$$

For soft materials such as hydrogels, if the elastic component (G') dominates, a material is thought to therefore possess more solid-like qualities and can be considered a hydrogel. Conversely, if the viscous component (G'') dominates, then

the material is considered a liquid-like material and would not be deemed a hydrogel.[6-8]

Rheological measurements were carried out using an Anton Paar Physica MCR101 rheometer. A cup and vane system (Figure 3) was used which allowed the direct measurement of the gels formed in the 7 mL Sterilin cups. Chapter 5 and 6 used a parallel plates geometry (Figure 3) consisting of a 25 mm sandblasted plate and the gels were removed from the FTO-coated slide and transferred directly onto the plate using a microspatula.

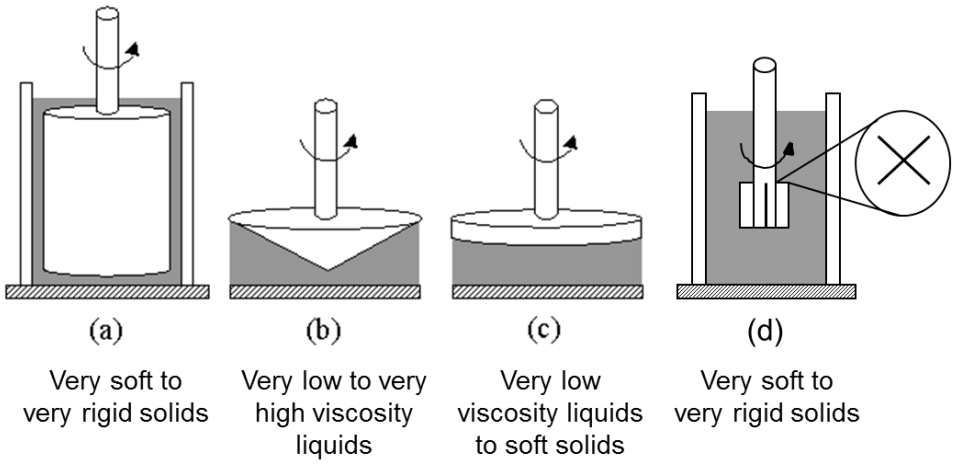

Figure 3 Measuring systems used to measure the mechanical properties of various materials. a) Couette geometry, b) cone and plate geometry, c) parallel plates geometry and d) vane cup geometry. The latter two are used throughout this thesis

2.6.1 Frequency Sweeps

Frequency scans were performed from 1 rad/s to 100 rad/s at a strain of 0.5 %. The shear moduli (storage modulus G' and loss modulus G'') were measured at a frequency of 10 rad/s. All shear moduli measured were within the linear viscoelastic (LVE) region for the gels measured.

2.6.2 Strain Sweeps

Strain scans were performed from 0.1 % to 100 % at a frequency of 10 rad/s. The critical strain was quoted as the point that *G′* starts to deviate from linearity and ultimately cross over the *G″*, resulting in gel breakdown. This method ensured that 0.5 % strain was in the viscoelastic region required for measuring the frequency sweep.

2.6.3 Recovery Tests

For the recovery test experiments, a constant frequency of 10 rad/s and strain of 0.5 % was first performed for 200 seconds, followed by higher strain of 300 % for 60 seconds to totally destroy the gel to a liquid state. Restoration of gel was monitored in the subsequent time sweep (with the frequency of 10 rad/s and strain of 0.5 %) for 200 seconds again. The shear-recovery cycles were performed for 5 times for the same sample to check the reproducibility. The recovery ratios were calculated by the ratios of the average storage modulus (*G′*) after restoration with the original storage modulus obtained in the first step of time sweep. Repeat measurements on fresh samples were also carried out to ensure reproducibility between samples.

2.6.4 Time Sweeps

Time sweep measurements were performed at a constant frequency of 10 rad/s and a strain of 0.5 % at 25 °C. *G′* and *G″* were measured over time for ~ 20 hours. All hydrogel systems used a 25 mm sandblasted plate, except for the gelator BrNapAV, where a 50 mm sandblasted plate was used to minimise slippage.

2.6.5 Viscosity Measurements

A 75 mm cone and plate system was used to measure the viscosities of gelator solutions at high pH. The gap distance between two plates used was 0.05 mm. 2 mL dipeptide solutions were transferred onto the plate for measurement. The viscosity of each solution was recorded under the rotation shear rate varying from 1 to 100/s. All experiments were conducted at 25 °C.

2.7 Confocal Microscopy

Confocal microscopy images were taken using a Zeiss LSM710 microscope with a 100X 1.45 NA alpha plan-fluor objective using a pinhole diameter of 1 airy unit. Fluorescence from Thioflavin T was excited using a 458 nm argon laser and emission was detected above 465 nm. Fluorescence from Nile blue was excited using a 633 nm helium neon laser and emission was detected above 650 nm. Gels were prepared *in situ*, using the same methodology as described above. Gels were prepared in MatTek dishes (10 mm diameter glass coverslip) made of uncoated borosilicate glass. Samples were analysed by Dr Yann Cesbron (Centre for Cell Imaging, Institute of Integrative Biology, University of Liverpool).

2.8 Hydrogel Washings

DMSO:water gels were prepared as previously described but with water being replaced with D_2O for FT-IR measurements. D_2O (5 mL) was added on top of the gels and left for 4 hours before replacing with more D_2O (5 mL) for each washing. The DMSO content of the gels was then measured using FT-IR (see FT-IR section for experimental details).

2.9 pH Measurements

A calibrated FC200 pH probe (HANNA instruments) with a (6 mm x 10 mm) conical tip was used for the pH measurements and pK_a titrations. The stated accuracy of the pH measurements is ± 0.1. The pK_a values of the dipeptide solutions were determined by titration at 25 °C *via* the addition of aliquots of a 0.1 M hydrochloric acid solution. To prevent gelation of the stock solution, gentle stirring was applied throughout.

2.10 UV Irradiation

To form gels, samples were irradiated with UV light from a 40 W Spectroline X-series UV lamp (wavelength 254 nm). 2 mL of stock solution was placed in a 7 mL Sterilin cup and UV light was irradiated from above with the lid off the cup.

2.11 Scanning Electron Microscopy (SEM)

Scanning electron microscopy images were recorded using a Hitachi S-4800 FE-SEM at 3 kV. Glass coverslips were stuck onto aluminium SEM stubs using carbon sticky tabs (Agar Scientific) and an aliquot of gel sample was then placed onto the surface of the glass (using a microspatula) and left to dry overnight. The samples were gold coated for 3 minutes at 15 μA using a sputter-coater (EMITECH K550X) prior to imaging. Samples were analysed by Dr Tom O. McDonald (Centre for Materials Discovery, University of Liverpool).

2.12 Hydrogel Patterning

For UV Gelation (Chapter 3)

Gelator solutions with PAG were prepared as described above. Samples were then placed in quartz glass cuvettes. Part of the cuvette was covered with card stuck onto the cuvette to act as a UV mask. The sample was then irradiated using 2 half cylinder arrangements of 6 x 8 W Coast Wave backlit UV lamps for 3 – 4 hours. Once removed, the gel was photographed and the pH measured.

2.13 Cyclic Voltammetry (CV)

All experiments were run using a Dropsens Potentiostat and a three-electrode system: the working electrode was a glassy carbon electrode; a platinum wire counter and a calomel reference electrode. Cyclic voltammetric (CV) measurements were carried out within a potential range of - 0.2 to 1 V vs a saturated calomel electrode at a scan rate of 40 mV/s. Each CV measurement consisted of one scan. For experiments using glass slides, the slides acted as the working electrode (fluorine-doped tin oxide (FTO) coated slides) and a printed electrode containing both the reference and counter electrodes completed the three-electrode system.

2.14 Potentiometry

For potentiometric experiments, 10 mL LMWG solutions containing HQ (0.065 M) were used, with either of the three-electrode systems mentioned above. The desired current was set and was run for 1000 s, unless stated otherwise. For the glassy carbon

electrode set-up, gel growth was monitored by taking images in 10 second increments (of the 1000 s period) using an Infinity 2-1C colour USB2 camera. The electrochemical cell and camera were mounted using clamps and backlit using LED torches. The images collected were processed using custom written Labview code (by Dr Jonathan R. Howse, Department of Chemical and Biological Engineering, University of Sheffield) capable of processing a series of images in batch mode. Essentially, the gel area was enhanced through subtraction of a background image and the resulting image subjected to a threshold procedure. Horizontal slices of the gel (1 pixel high) were taken and approximated as disc of gel. The sum of all slices of the visible gel is taken as the volume of the gel. Images were calibrated using the width of electrode. For pK_a vs lag time experiments, images were taken every 1 s and were manually analysed to pinpoint the time at which gelation began.

2.15 Surface Plasmon Resonance (SPR) Spectroscopy

Surface plasmon enhanced fluorescence spectroscopy (SPR) was measured in the Kretschmann attenuated total internal reflection configuration on a home-built set-up. Laser (Uniphase, HeNe λ=632.8 nm) light was passed through a chopper and two polarizers before being incident on one face of a LaSFN9 prism (Schott Glass). The first polarizer adjusted the intensity of the light and the second polarizer allowed only p-polarized light to reach the sample. The chopper modulated the light at 431Hz and provided a reference signal for the lock-in amplifier. The hydrogel film (prepared as described above in Section 2.14) was formed on top of a ~45 nm gold film evaporated on a LaSFN9 glass slide (Schott Glass). To improve its optical properties the gold film was annealed at 500 °C for 90 seconds. The gold coated LaSFN9 slide was separated from the back of the LaSFN9 prism by a thin layer of index matching fluid (Cargille Laboratories Inc., n = 1.700 ± 0.0002). The sample and the prism were mounted on a computer operated goniometer, which was used to control the precise angle of incidence of the light. The reflected light beam was focused through a collecting lens onto a silicon photodiode. Computer software was used to measure the magnitude of reflected light reaching the photodiode as a function of the incident angle controlled by the goniometer. Gels were formed in a Teflon electrochemical flow cell where the gold coated LaSFN9 and a microscope

slide were used as the two walls of the flow cell. Substrates for SPR were made as follows: a 50 nm layer of 99.99 % Au was evaporated onto LaSFN9 glass slides (Emitech Ltd. K975) and annealed for 90 s at 500 °C. Data was fitted using WINSPALL software (REStek GmbH) which uses the Fresnel equations to model the behaviour of light in a layered system. Samples were measured by Dr Petra J Cameron (Department of Chemistry, University of Bath).

2.16 Powder X-Ray Diffraction

Powder X-ray diffraction data were collected on a PANalytical X'pert pro multipurpose diffractometer (MPD) in transmission Debye−Scherrer geometry operating with a Cu anode at 40 kV and 40 mA. Gels were dried overnight and samples were ground and mounted as a loose powder onto a transparent film and spun at 2 s/rotation. PXRD patterns were collected in 4 Å~ 1 h scans with a step size of 0.013° 2θ and a scan time of 115 s step over 5−50° 2θ. The incident X-ray beam was conditioned with 0.04 rad Soller slits and an antiscattering slit of 0.5°. The diffracted beam passed through 0.04 rad Soller slits before being processed by the PIXcel2 detector operating in scanning mode.

2.17 Gelation Study *via* Nuclear Magnetic Resonance (NMR) Spectroscopy

LMWG solutions were prepared as previously described but using D_2O, NaOD and DCl in place of water, NaOH and HCl, respectively. Gels were prepared using potentiometric methods on FTO-coated glass slides before being transferred to NMR tubes. Gels were stirred to form a liquid before being pipetted into an NMR tube. An ethanol standard (2 μL per 1 mL of sample) was added. NMR spectra were recorded using a Bruker DPX-400 spectrometer operating at 400 MHz for ^1H.

2.18 Freeze-Drying

Hydrogel samples were prepared as described above and frozen with liquid nitrogen *in situ* before freeze-drying in a VIRTIS Advantage Freeze dryer. The condenser temperature was set at -80 °C and had a shelf temperature 10 °C.

2.19 Hydrogel Stability in Dulbecco's Modified Eagle's Medium (DMEM)

Gels were prepared on FTO-coated glass slides as described previously. Gels were then fully immersed in DMEM for desired time periods. The slides containing the gels were then removed from the medium and analysed.

2.20 Cell Culture Study

D1 murine mesenchymal stem cells (mMSCs) (ATCC®) were cultured in Dulbecco's Modified Eagle medium (DMEM) (Sigma-Aldrich) containing 10 % (v/v) foetal bovine serum (Gibco), non-essential amino acids (Sigma-Aldrich), 50 µg/mL penicillin-streptomycin (Gibco), 2 mM L-glutamine (Gibco) and 55 µM 2-mercaptoethanol (Gibco). Cells were maintained in a humidified atmosphere with 5 % CO_2 at 37 °C. Hydrogels were prepared using the galvanostatic gelation trigger described above (in Section 2.14) and sterilised by UV irradiation for 20 min and incubated in phosphate buffered saline (PBS) (Sigma-Aldrich) for 5 days at 37 °C with regular changes until no colour change from leached hydroquinone was observed. Prior to cell seeding, hydrogels were incubated in DMEM for 12 hours at 37 °C. MSCs were seeded at 2.5 X 10^5 cells per gel and cultured for up to 1 week. Phase contrast images were obtained with a Leica DM IL microscope (Leica Microsystems GmbH, Wetzlar, Germany). To investigate the cellular architecture of aggregates, cells were stained for F-actin using Alexa Fluor® 488 phalloidin (Invitrogen) and counterstained with 4',6-diamidion-2-phenylindole (DAPI) (Invitrogen) as follows; cells were fixed with 4 % (w/v) paraformaldehyde for 20 min at room temperature and washed 3 times with PBS. DAPI and phalloidin staining procedures were according to the manufacturer's protocol and images were obtained with a Leica DM2500 microscope. Samples were measured by Christopher Hill (Institute of Translational Medicine, University of Liverpool).

2.21 Fluorescence Spectroscopy

Fluorescence spectra were obtained on a PerkinElmer Luminescence spectrometer LS55. Gels were formed *in situ* as described above in 1.0 cm path-length PMMA

cuvettes. Emission spectra were recorded with a scan rate of 100 nm/min, with sequential scans every minute for one hour and then every 30 min for 18 hours. For each of the dyes tested, the following parameters were used:

Dye	Concentration Added to 2 mL Gelator Solution	Excitation Wavelength (λ_{ex}) (nm)	Emission Wavelength (λ_{ex}) (nm)	Slit Widths (nm)
Thioflavin T	100 µL of 5 µM	455	475	2.5 and 2.5
9-(2,2-Dicyanovinyl)julolidine (DCVJ)	100 µL of 5 µM	470	485	2.5 and 2.5
9-(2-Carboxy-2-cyanovinyl)julolidine (CCVJ)	100 µL of 5 µM	460	485	5 and 5
Nile Blue	40 µL of 0.1 µM	630	660	10 and 5

Single scans were also measured of hydrogels containing the dyes using the same parameters.

2.22 References

1. D. J. Adams, M. F. Butler, W. J. Frith, M. Kirkland, L. Mullen and P. Sanderson, *Soft Matter*, 2009, **5**, 1856-1862.
2. L. Chen, S. Revel, K. Morris, L. C. Serpell and D. J. Adams, *Langmuir*, 2010, **26**, 13466-13471.
3. J. Raeburn, T. O. McDonald and D. J. Adams, *Chem. Commun.*, 2012, **48**, 9355-9357.
4. M. A. Rao, *Rheology of Fluid and Semisolid Foods: Principles and Applications*, 2 edn., Springer, New York, 2007.
5. A. Y. Malkin, *Rheology Fundamentals*, ChemTec Publishing, 1994.
6. L. Chen, J. Raeburn, S. Sutton, D. G. Spiller, J. Williams, J. S. Sharp, P. C. Griffiths, R. K. Heenan, S. M. King, A. Paul, S. Furzeland, D. Atkins and D. J. Adams, *Soft Matter*, 2011, **7**, 9721-9727.
7. C. Tang, A. M. Smith, R. F. Collins, R. V. Ulijn and A. Saiani, *Langmuir*, 2009, **25**, 9447-9453.
8. W. J. F. Marco Berta, M. Kirkland, R. Holman, P. Schuetz, *Ann. T. Nordic Rheo. Soc.*, 2013, **21**, 273-280.

CHAPTER 3

Tunable Mechanical Properties in Fmoc-Protected Low Molecular Weight Hydrogels

3.1 Introduction

Functionalised dipeptide gelators have emerged as a promising class of low molecular weight gelators (LMWG). More specifically, dipeptides functionalised with aromatic groups at the N-terminus are being commonly reported in the literature.[1, 2] Perhaps the most reported LMWG of this class consists of the aromatic group fluorenylmethoxycarbonyl (Fmoc) attached to diphenylalanine (FF) to give FmocFF.[3-7] Particular interest in this gelator stems from its ability to form gels at physiological pH, making it potentially useful for biomedical applications.[4] FmocFF gels have reportedly been used for a variety of applications such as cell culturing,[3, 4, 8] controlled drug release[6] and biosensing applications.[9] Furthermore, FmocFF can form gels *via* a range of different triggers of self-assembly. Uljin and his group have reported FmocFF gels prepared *via* a pH switch, with slight variations in the method reportedly all successfully forming gels.[3, 8, 10-12] Many reported methods of pH switch have utilised changes in temperature, rate of pH decrease, final pH value and even mixing conditions[13] to afford gels of FmocFF. Our group has devised a different method of pH switch, which employs the slow hydrolysis of glucono-δ-lactone (GdL) to gluconic acid in water to give a homogeneous pH drop throughout the solution.[5, 14] Switching from using a mineral acid to GdL to initiate the drop in pH required for gelation resulted in an improvement in the final mechanical properties of the gels – both in terms of mechanical strength and reproducibility.[7]

Another reported method of producing reproducibly rigid gels is the "solvent switch" method. Here, the gelator is dissolved in an organic solvent before being diluted by the addition of water to produce a gel. FmocFF gels prepared from dimethylsulfoxide (DMSO) in water and hexafluoroisopropanol (HFIP) in water have been reported by Gazit and his group.[6, 15] Reports of these types of FmocFF gels contain slight variations in the concentrations and solvent compositions. Again, the final mechanical properties of these gels differ from the FmocFF gels prepared using the previously mentioned pH switch methods. Through judicious choice of the self-assembly trigger, the mechanical properties can be tuned. This is of promise for

biomedical applications where specific mechanical properties have been shown to affect cell attachment and growth.[16] It is clear that the mechanical properties are affected by not only the method used to trigger self-assembly, but by subtle differences in the conditions of a particular trigger which also seemingly having an effect. This Chapter studies the tunability of the final gel properties of FmocFF gels prepared *via* the solvent switch method and compares these properties to similar Fmoc-dipeptide gelators.

3.2 Results and Discussion

3.2.1 Preparation of DMSO/Water Hydrogels

LMWG that form hydrogels contain two specific moieties: a hydrophilic and hydrophobic region. The former is a necessity for compatibility with water, whereas the latter is responsible for driving the self-assembly of the LMWG. Despite these design rules being known, there is no scope beyond these rules that are currently known to decisively play a role in the gelation of LMWG.[2, 17] For example, molecules that contain both hydrophobic and hydrophilic moieties that form gels are very similar in structure to molecules that do not form gels. The difference can be as simple as order or conformation of amino acids in the peptide chain.[3, 18, 19] To try to understand the parameters required to design a successful LMWG, molecular libraries are commonly produced.[3, 17, 20, 21] One of the most commonly reported LMWG is FmocFF (Scheme 1a).

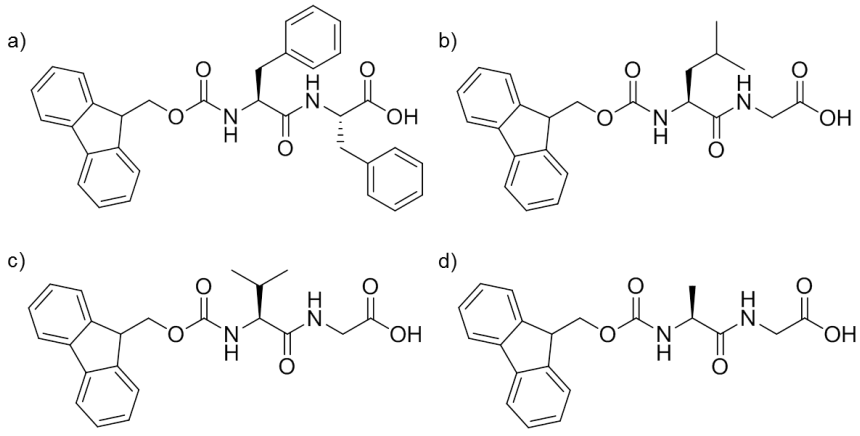

Scheme 1 Structures of a) FmocFF, b) FmocLG and c) FmocVG and d) FmocAG

Here, this Chapter will focus mainly on describing a solvent-mediated method utilising DMSO as the solvent. FmocFF is insoluble in water (unless at basic pH[11]). To prepare solvent-triggered gels, FmocFF is first dissolved in DMSO before adding water to dilute the solvent and initiate gelation. Different final volume fractions of DMSO (Φ_{DMSO}) can successfully produce hydrogels of FmocFF. Figure 1 shows gels with different volume fractions of DMSO. Hydrogels throughout this Chapter were prepared at a final gelator concentration of 0.5 wt% unless otherwise stated. This concentration is commonly used in our group, as it has been known to form homogenous, transparent hydrogels for similar materials. [14, 20, 22]

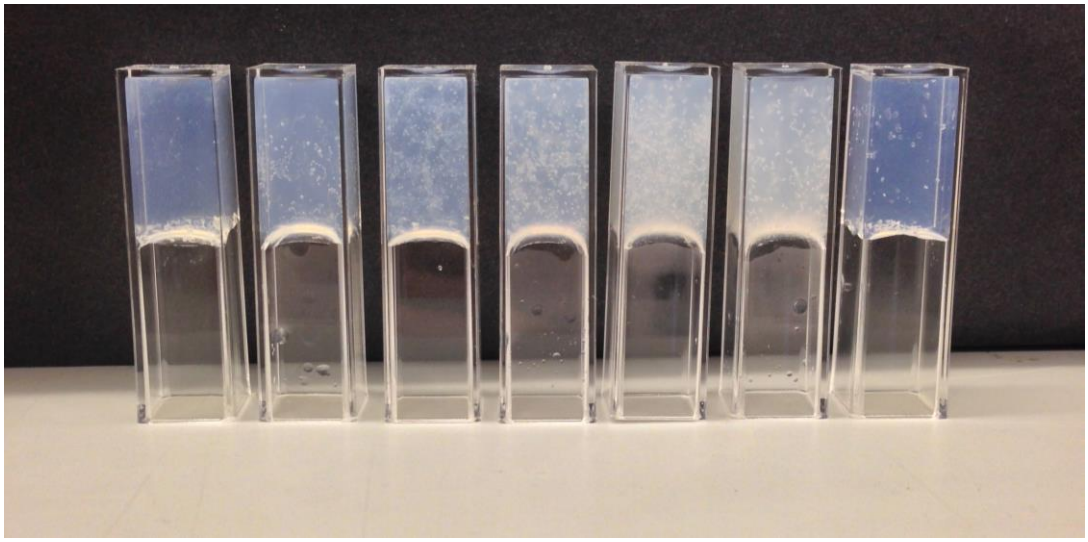

Figure 1 5 mg/mL FmocFF hydrogels with Φ_{DMSO} of (from left to right) 0.05, 0.1, 0.2, 0.3, 0.4, 0.5 and 0.6

When water is added to a gelator/DMSO solution, an increase in turbidity ensues before the turbidity clears within ~ two minutes (for a Φ_{DMSO} of 0.1) to give a transparent hydrogel. Gazit's group have also exhibited transparent hydrogels of FmocFF using a DMSO/water system.[6] The turbidity events described here are dependent on the Φ_{DMSO} of the hydrogel system. Using UV/vis spectroscopy, the duration of these events could be monitored. Figures 2a and 3a show that after adding water to the aliquot of DMSO (containing FmocFF), turbidity increased before decreasing again, within minutes (or seconds). The duration of the turbidity event was deemed as the time from addition of water (and onset of turbidity event), until the absorbance decreased to a plateau. FmocFF gels with Φ_{DMSO} of 0.6, showed no increase in turbidity upon the addition of the water component. The duration of

the turbidity event decreased as the Φ_{DMSO} increased up to a Φ_{DMSO} of 0.4, before increasing again (Figure 2a). The opposite trend was observed for the final turbidities of these gels. The final turbidity increased from a Φ_{DMSO} of 0.05 to 0.4 and then decreased. Hence, the shorter turbidity events gave more turbid gels when the Φ_{DMSO} is between 0.05 and 0.4. A visual observation of these gels also shows this turbidity trend (Figure 1).

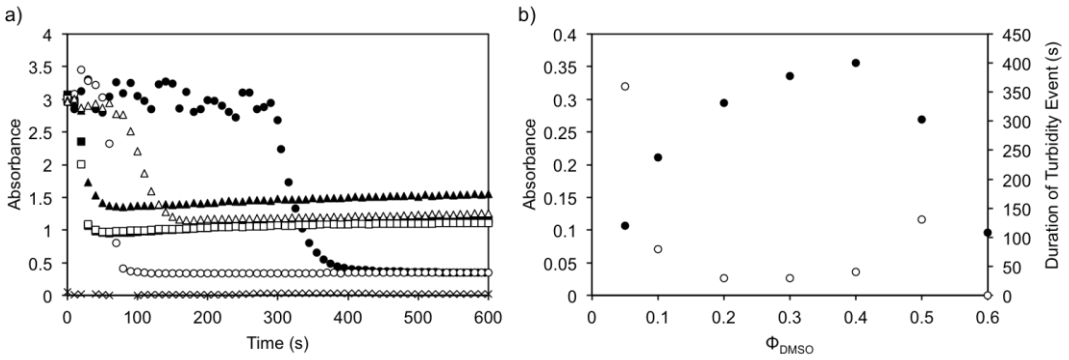

Figure 2 Turbidity changes with time for FmocFF gels after water component is added. FmocFF gels with different Φ_{DMSO} (all 5mg/mL gelator concentration) a) 0.05 (●), 0.1 (○), 0.2 (■), 0.3 (□), 0.4 (▲), 0.5 (△) and 0.6 (x). b) Final gel turbidities (●) and duration of turbidity events (○). Measured by UV/vis spectroscopy (600 nm)

Changes in turbidity events were also noted for FmocFF gels with different gelator concentrations (Figure 3). These gels had a constant Φ_{DMSO} of 0.1. Here, the duration of the turbidity event decreased below 5 mg/mL and increased for 5 mg/mL and above. Gels with higher final FmocFF concentrations produced more turbid gels. Notably, the kinetics of turbidity change (Figure 3a) shows a plateau in the turbidity after the turbidity decreases. This value does not correspond to the final turbidity observed. Turbidity must, therefore, slowly decrease beyond the time of the kinetic experiments. Previous reports for similar FmocLG (structure shown in Scheme 1b) gels have attributed turbidity profiles, akin to those observed here, as being linked to phase separation events.[22] Phase separation events then lead to the formation of spherical structures, followed by the nucleation and growth process of the self-assembled gelator molecules. Confocal microscopy showed that the nucleation and fibril growth did not spawn from these spherulitic sites.[22] Huang *et al.* have noted similar network formation for their organogels.[23] Visual phase separation is not a required factor for hydrogelation as FmocLG gels with 0.3 Φ_{DMSO} or more, had no changes in turbidity but still formed gels.[22] Orbach *et al.* have shown similar

FmocFF gels prepared from the addition of water to a DMSO/FmocFF solution (as used here) and noted changes in turbidity as gelation occurred.[19] Turbidity also cleared to afford transparent gels – as seen in this Chapter. Transitions from turbidity to transparency are not noted for FmocFF gels formed *via* a pH switch method,[7] suggesting that kinetic process must differ between methods of trigger. A change in turbidity suggests a formation of aggregated structures upon the addition of water. Orbach *et al.* attributed the changes in turbidity observed in their FmocFF hydrogel systems to such aggregated structures, and further suggested that irregular aggregates form initially upon self-assembly followed by a transition to a highly ordered structures.[19] Highly ordered, fibrous networks are reminiscent of the hydrogels commonly reported for these materials.

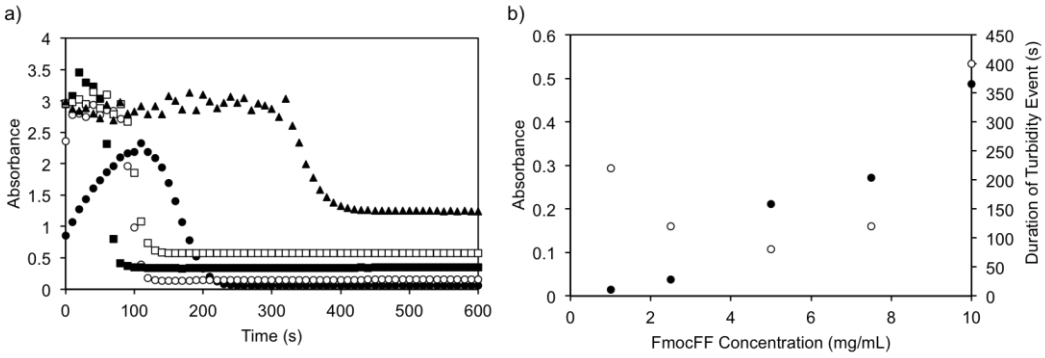

Figure 3 Turbidity changes with time for FmocFF gels after water component is added. a) FmocFF gels with final gelator concentrations of 1 (●), 2.5 (○), 5 (■), 7.5 (□) and 10 mg/mL (▲). b) Final gel turbidities (●) and duration of turbidity events (○).All gels have a Φ_{DMSO} of 0.1. Measured by UV/vis spectroscopy (600 nm)

Along with changes in turbidity as gelation ensues, an exotherm is also apparent. When DMSO is diluted in water, an exothermic reaction occurs due to fluctuation in H-bonding between water and DMSO[24, 25] – both of which have the ability to H-bond. This exotherm seems to be unaffected by the presence of FmocFF (data not shown). For 5 mg/mL FmocFF gels, an increase in temperature ranging from 2 – 19 °C (Table 1) is observed. The exotherm noted increased as the Φ_{DMSO} increased – similar to that of the final turbidity. A slightly lower exotherm was observed for gels with Φ_{DMSO} of 0.6. Gels with Φ_{DMSO} of 0.6 also did not follow the turbidity profile trend. The increase in temperature was immediate upon addition of water to DMSO and lasted seconds before returning to room temperature. Samples were then left to

stand and allow gelation to occur. No further mixing occurred. Due to the weak acidity of FmocFF, all gels prepared had a final pH value of ~ 4. Gels were left to stand overnight before any analysis was carried out.

Φ_{DMSO}	Exotherm (No Gelator) (°C)	Exotherm (Gelator Present) (°C)
0.6	19	18
0.5	18	19
0.4	16	16
0.3	13	12
0.2	8	8
0.1	4	4
0.05	2	2

Table 1 Temperature increase upon addition of water in FmocFF gels with different Φ_{DMSO}

From both visual analysis and measuring of the turbidity profiles of the gels upon hydrogelation (Figures 2 and 3), there must be distinct differences in the fibrillar structures that constitute the gel matrices with varying Φ_{DMSO}. Some of the gels are clearly scattering more light than others as a result of the presence of larger structures within the gels. It is unclear from these analyses as to where these differences have arisen from. To probe the packing of the fibres at the molecular level, FT-IR spectra were collected. Samples were prepared with increasing Φ_{DMSO} until no gelation occurred (at a gelator concentration of 5 mg/mL). Above a Φ_{DMSO} of 0.1, increments of 0.1 were screened. A Φ_{DMSO} of 0.7 was found not to form gels at 5 mg/mL gelator concentration, therefore Φ_{DMSO} increments of 0.02 were screened between 0.6 and 0.7 to find the gelation threshold. FT-IR spectra were collected for all gels and for the sample with a Φ_{DMSO} just above the highest Φ_{DMSO} that successfully form a gel. FT-IR spectra of FmocFF gels showed peaks in the amide I region at 1640 cm^{-1}, 1690 cm^{-1} and 1740 cm^{-1}. The peak at 1740 cm^{-1} can be ascribed to the carboxylic acid end group of the gelator molecules. The peak at 1690 cm^{-1} is attributed to the carbamate linker of the gelator[26], whereas the peak at 1640 cm^{-1} has been assigned as an indication of β-sheet formation.[26, 27] All three of these peaks are

present in every FmocFF gel measured, regardless of the Φ_{DMSO} of the gel. It is clear from these spectra that the packing of gelator at the molecular level is the same and therefore independent of the Φ_{DMSO} of the gel. Hence, any differences between gels must occur from assembly of the gelator molecules at a longer length scale. Figure 4 shows FT-IR spectra of FmocFF samples around the critical gelation point. A gel with a Φ_{DMSO} of 0.62 shows the presence of the three peaks in the amide I region, however a sample with a Φ_{DMSO} of 0.64 shows no peaks in this region. The FmocFF sample with a Φ_{DMSO} of 0.64 did not form a gel. No assembly of the gelator molecules under these conditions, therefore there is no indication of secondary peptidic structure.[28] Orbach *et al.* also found similar spectral data for Fmoc di- and tri-peptide gelators that did not form gels.[19] The spectrum for FmocFF with a Φ_{DMSO} of 0.64 also showed no sign of a carboxylic acid peak in this region.

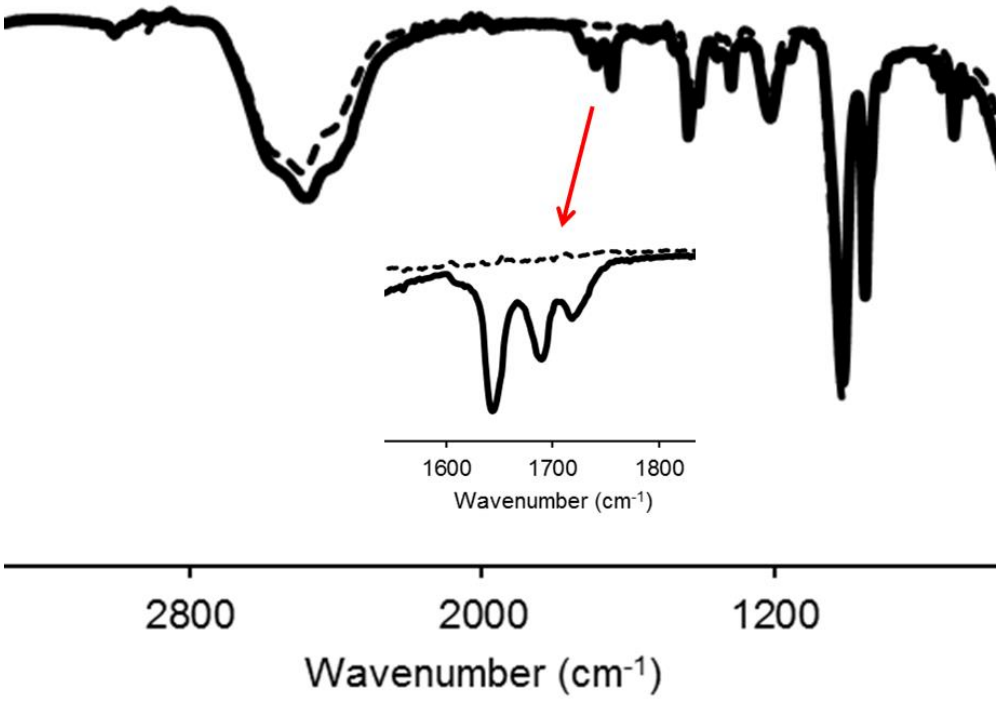

Figure 4 FT-IR spectra of FmocFF samples with Φ_{DMSO} around the critical point of gelation. An FmocFF sample with a Φ_{DMSO} of 0.64 (– –) does not form a gel and a sample with a Φ_{DMSO} of 0.62 (—) can form a gel. Partial spectra of amide I region shown inset

3.2.2 Relationship Between Hydrophobicity and Gelation

As mentioned previously, FmocFF can form gels (with a final gelator concentration of 5 mg/mL) across a range of Φ_{DMSO} values. When preparing these gels, the range of Φ_{DMSO} values screened was increased until no gelation occurred. This threshold for FmocFF was found to be at a Φ_{DMSO} of 0.62. All Φ_{DMSO} below this value could successfully form gels at this concentration – down to a Φ_{DMSO} of 0.05. Gelation was deemed successful upon a simple vial inversion test.[29] When the vial was inverted and no flow of material occurred, gelation was confirmed as successful. The bulk mechanical properties of these gels were then measured using rheology.

On comparison with other Fmoc dipeptides, the gelation range differs between gelators. From the literature, FmocLG is known to form gels (at the same concentration) in a slightly smaller Φ_{DMSO} window than that observed for FmocFF. FmocLG can form gels from Φ_{DMSO} ranging from 0.5 down to 0.05.[22] The same range was observed for FmocVG (Table 2). Another gelator tested (Table 2) was FmocAG. This gelator had an even smaller window for successful gelation. At a final gelator concentration of 5 mg/mL, FmocAG can form solvent-mediated gels with a Φ_{DMSO} of between 0.2 and 0.05. The gelation range appears to be correlated to the hydrophobicity of the gelator. Table 2 shows that FmocFF, FmocLG, FmocVG and FmocAG have *log P* values (calculated as *clogP* by an online prediction program[30]) of 5.6, 4.2, 3.6 and 2.9, respectively. Therefore, with increased hydrophobicity, a larger gelation range with respect to the Φ_{DMSO} of the gels is noted. FmocLG and FmocVG had the most similar *log P* values and were found to successfully form hydrogels at a final gelator concentration of 5 mg/mL across the same range of Φ_{DMSO}.

Gelator	Log P	Gelation Range (Φ_{DMSO})	G' Range (kPa)	Hydrogel Recovery (%)
FmocFF	5.6	0.62 – 0.05	10 - 28	~ 85 ($\leq$ 0.35 Φ_{DMSO}) < 60 ($\geq$ 0.4 Φ_{DMSO})
FmocLG[a]	4.2	0.5 – 0.05	< 10	~ 80 ($\leq$ 0.2 Φ_{DMSO}) ~ 30 - 40 % (> 0.2 Φ_{DMSO})
FmocVG	3.6	0.5 – 0.05	< 10	-[b]
FmocAG	2.9	0.2 – 0.05	< 8	~ 70 - 80

Table 2 Relationship between hydrophobicity and final mechanical properties of Fmoc dipeptide gelators (gelator concentration of 5 mg/ml). [a]Data taken from reference 1. [b]Not measured. Log P values were calculated using an online prediction program[30]. Hydrogel recovery data discussed in Section 3.2.5

Such a trend may be expected as hydrophobicity ultimately drives self-assembly which precedes gelation. Further relationships between bulk gel properties and hydrophobicity are observed. Across the gelation ranges of these gelators, stronger mechanical properties were measured for the most hydrophobic gelator i.e. FmocFF. Gels prepared from FmocFF had measured *G'* values of between 10 and 28 kPa – with gels of this mechanical strength being amongst the highest quoted in the literature for this type of material.[6, 10, 12, 13] FmocLG and FmocVG gels produced gels of mechanical strengths below 10 kPa and gels formed from the most hydrophilic gelator of the four (FmocAG) were weaker still, with *G'* values measured to be lower than 8 kPa. Table 2 also shows that the ability of the gels to recover from high shear differs between gelators. This will be discussed further below in Section 3.2.5.

3.2.3 Mechanical Properties of FmocFF Hydrogels

Once gelation had occurred, the mechanical properties were tested. Both strain (Figure 5) and frequency (Figure 6) sweeps were measured. Figure 6 shows the frequency sweep measurements collected for FmocFF gels with different Φ_{DMSO}. The gels measured had a final gelator concentration of 5 mg/mL. The frequency sweep measurements were run at a constant strain of 0.5 % and within the linear viscoelastic region of the materials (see below in Figure 5); determined by strain amplitude sweeps (summarised in Table 3 and shown in Figure 5). This ensured that

the storage moduli (*G'*) and loss moduli (*G''*) measured for these materials were independent of the strain amplitude.

Φ_{DMSO} (5 mg/mL Final FmocFF concentration)	% Strain Upon Hydrogel Breakdown	FmocFF Concentration (mg/mL) 0.1 Φ_{DMSO}	% Strain Upon Hydrogel Breakdown
0.05	6.3	1	12.6
0.1	15.8	2.5	6.3
0.2	15.9	5	15.8
0.3	8.0	7.5	5.1
0.4	6.3	10	5.1
0.5	4.0		
0.6	3.2		

Table 3 Summary of the strains at which various FmocFF hydrogels break down and revert from gel to solution

Strain sweep measurements were run on the gels samples at a constant frequency of 10 rad/s and measured the strain at which the hydrogel breaks down and reverts from a gel to a liquid (Figure 5 and Table 3). Gels with a Φ_{DMSO} of 0.1 or 0.2 broke down at the highest strain (~ 16 %) and the strain at which gel breakdown occurs decreased on either side of these Φ_{DMSO} values – with the lowest recorded strain at gel breakdown being measured for FmocFF gels with a Φ_{DMSO} of 0.6. As this is close to the critical gelation point, weaker and more brittle gels could be expected. Strains of gelation breakdown are noted at the point at which *G'* deviates from linearity and could be considered slightly subjective, meaning that slight variability in the exact strain at which a particular gel breaks down. However, as frequency sweep measurements were carried out at a constant strain of 0.5 %, it was clear that all gels studied were not broken down to liquids at this strain and were, therefore, in the linear viscoelastic region of the gelator material and were permanent networks throughout the measurements. The same was observed when the concentration of gelator was varied in FmocFF gels with a Φ_{DMSO} of 0.1. The strains at which gels broke down for gels with final concentrations ranging from 1 mg/ml to 10 mg/ml, were all in the range observed for 5 mg/mL gels with varying Φ_{DMSO} (Table 3).

Therefore, it could be confirmed that gels were in the linear viscoelastic region of the material when the mechanical properties were measured.

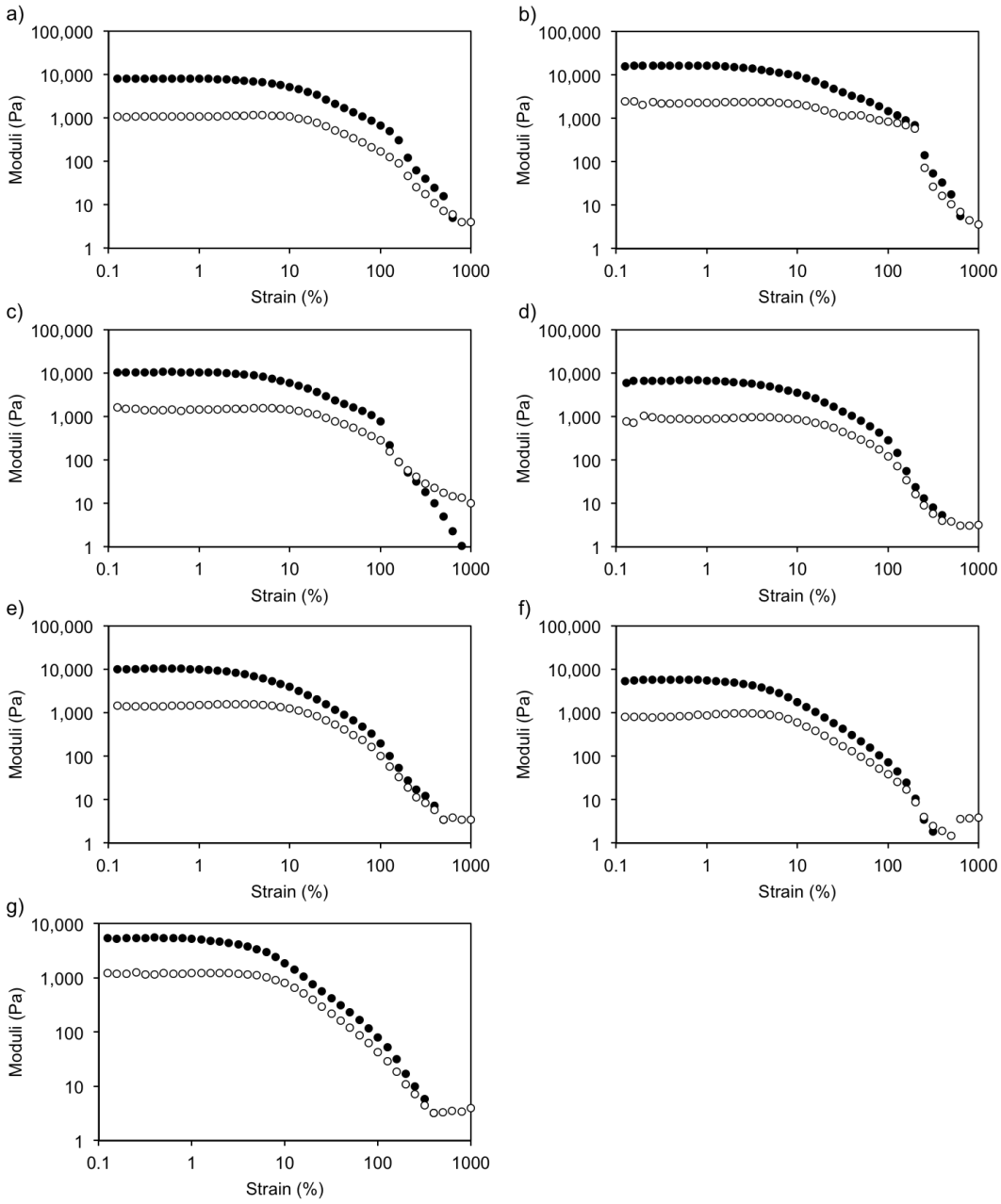

Figure 5 Strain sweep measurements of FmocFF (5 mg/mL) hydrogels with different Φ_{DMSO}: a) 0.05 b) 0.1 c) 0.2 d) 0.3 e) 0.4 f) 0.5 and g) 0.6. ● represent *G'* and ○ represent *G''*

Figure 6 and Table 4 show that all gels produced were mechanically strong and produced *G'* values above 10 kPa. The storage moduli (*G'*) measured were an order of magnitude higher than the loss moduli (*G''*) measured, which is indicative of a rigid hydrogel structure.[10, 20, 31] In addition, gels showed no frequency dependence, as is common for this kind of gel.[6, 10, 22] Mechanical properties for FmocFF gels of the same concentration but with hexafluoroisopropanol (HFIP) as the solvent entity are reported to have a storage modulus of 20 kPa[6] and hence, similar to that observed here for DMSO gels.

The amount of DMSO in the gel affects the final gel properties. Furthermore, data collected by Liebmann *et al.*[4] and by previous work in our group has shown that the final pH of the gel also affects the final properties. Through the use of buffers in place of the water portion of the gel, gels with different pH values could be prepared.[4, 7] Significantly stiffer gels were recorded when the final pH was below 5 – as seen here. FmocFF gels were weaker when the pH was around physiological pH – achieved using varying buffers. As gelation is reported to occur below the pK_a of a gelator (for LMWG), it can be expected that mechanical strength increases as the pH decreases further below the pK_a and be non-existent above the pK_a for pH and solvent-mediated methods.[14, 32-35] The gels reported in this Chapter have final pH values below 4.

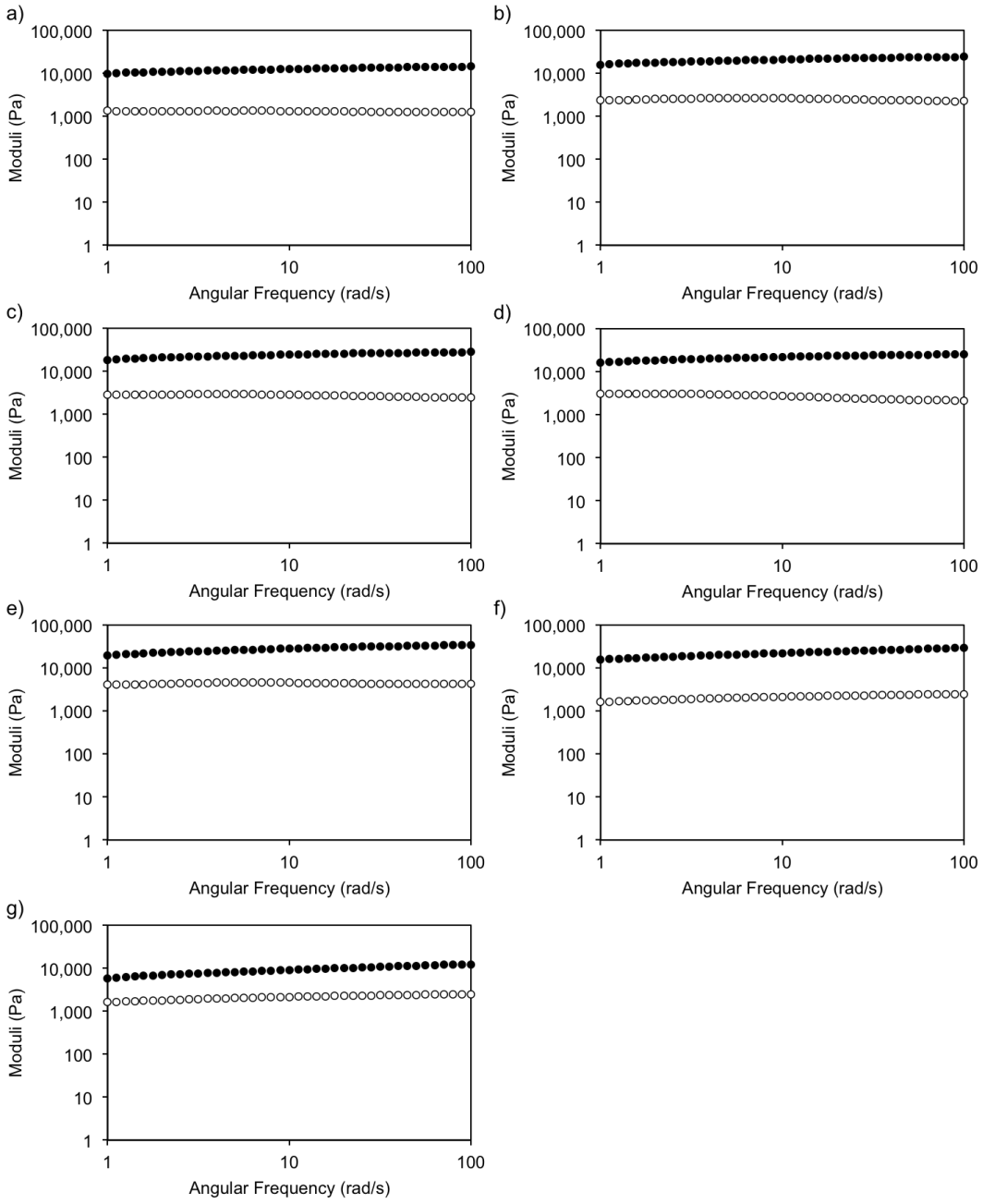

Figure 6 Frequency sweep measurements of FmocFF (5 mg/mL) hydrogels with different Φ_{DMSO}: a) 0.05 b) 0.1 c) 0.2 d) 0.3 e) 0.4 f) 0.5 and g) 0.6. ● represent *G'* and ○ represent *G''*

Table 4 summarises the mechanical properties of FmocFF gels with both varying Φ_{DMSO} and final gelator concentration. For gels of varying Φ_{DMSO}, a general increase in mechanical strength is observed with increasing Φ_{DMSO} up until a Φ_{DMSO} of 0.4. Above a Φ_{DMSO} of 0.4, mechanical strength decreases. No gelation occurs above a Φ_{DMSO} of 0.62 and hence, no measurable rheological properties are reported.

Dudukovic *et al.* also observed a decrease in mechanical strength when the Φ_{DMSO} increases.[36] The trend in mechanical strength observed here in this Chapter mirrors that of the final turbidity of these gels. Although the changes in final turbidity are not substantial, these subtle differences suggest that larger fibril structures within the hydrogel matrix increase mechanical strength of the bulk. Table 4 also summarises the rheological properties of FmocFF gels prepared with varied final gelator concentrations with a constant Φ_{DMSO} of 0.1. As expected, mechanical strength is increased with increased concentration. Gels with storage moduli (G') of over 60 kPa were recorded for gels with a final FmocFF concentration of 10 mg/mL.

Φ_{DMSO} (5 mg/mL Final FmocFF Conc.)	G' (Pa)	G" (Pa)	Final Turbidity (A at 600 nm)	FmocFF Conc. (mg/mL) (0.1 Φ_{DMSO})	G' (Pa)	G" (Pa)	Final Turbidity (A at 600 nm)
0.05	17600	1300	0.11	1	170	20	0.02
0.1	19700	2600	0.21	2.5	3600	380	0.04
0.2	23300	2800	0.30	5	19700	2600	0.21
0.3	21100	2700	0.34	7.5	45900	5500	0.27
0.4	25200	4500	0.36	10	62100	8900	0.49
0.5	19500	2200	0.27				
0.6	10700	2200	0.10				

Table 4 Summary of the rheological properties and turbidities (measured *via* UV/vis spectroscopy) of FmocFF gels prepared from various and Φ_{DMSO} and final gelator concentration

Confocal microscopy images demonstrate the differences in fibril networks between gels with different Φ_{DMSO}. Confocal microscopy allows the gels to be imaged in the 'wet' state and could therefore be considered as a truer representation of the hydrogel structure than a xerogel equivalent required for other microscopy methods such as SEM. However, confocal microscopy requires the loading of a fluorescent dye into the fibrous network, meaning that only wherever the dye incorporates into the network will be stained and hence, visible. Fibres were stained by adding the hydrophobic dye Nile Blue to the water component when preparing the gels. Chapter 6 also demonstrates that Nile Blue is an effective stain for similar gelator materials.

Confocal images of FmocFF gels containing Φ_{DMSO} of 0.05 and 0.4 and FmocFF gels prepared from GdL and HCl with the same final pH were analysed for comparison. Figure 7a shows that an FmocFF gel with a Φ_{DMSO} of 0.05 consists of spherulitic domains of densely packed fibres, connected *via* sparsely packed fibres – appearing much different in network to that of a corresponding gel with a Φ_{DMSO} of 0.4 (Figure 7b). Structures such as these are evidence of a nucleation and growth preceded by a phase separation event.[22] Phase separation is also suggested by the turbidity changes upon the addition of water, Figures 2 and 3).[22] However, there are turbidity changes for all Φ_{DMSO} (except a Φ_{DMSO} of 0.6) but clearly there are distinct differences between the final microstructure of the gels shown in Figures 7a and 7b. For gels with a Φ_{DMSO} of 0.4 (Figure 7b), the fibres appear much more abundant; appearing thicker and more densely packed throughout. This gel also has greater mechanical strength. Therefore, FmocFF gels with a Φ_{DMSO} of 0.4 are the most turbid and mechanically strong gels, with both effects arising from a more densely packed fibril network than the other gels studied. Inherently, this shows that the final properties of an FmocFF hydrogel can be tuned by varying the Φ_{DMSO}. The same such properties are reminiscent in FmocLG gels at both high Φ_{DMSO} and low Φ_{DMSO}.[22]

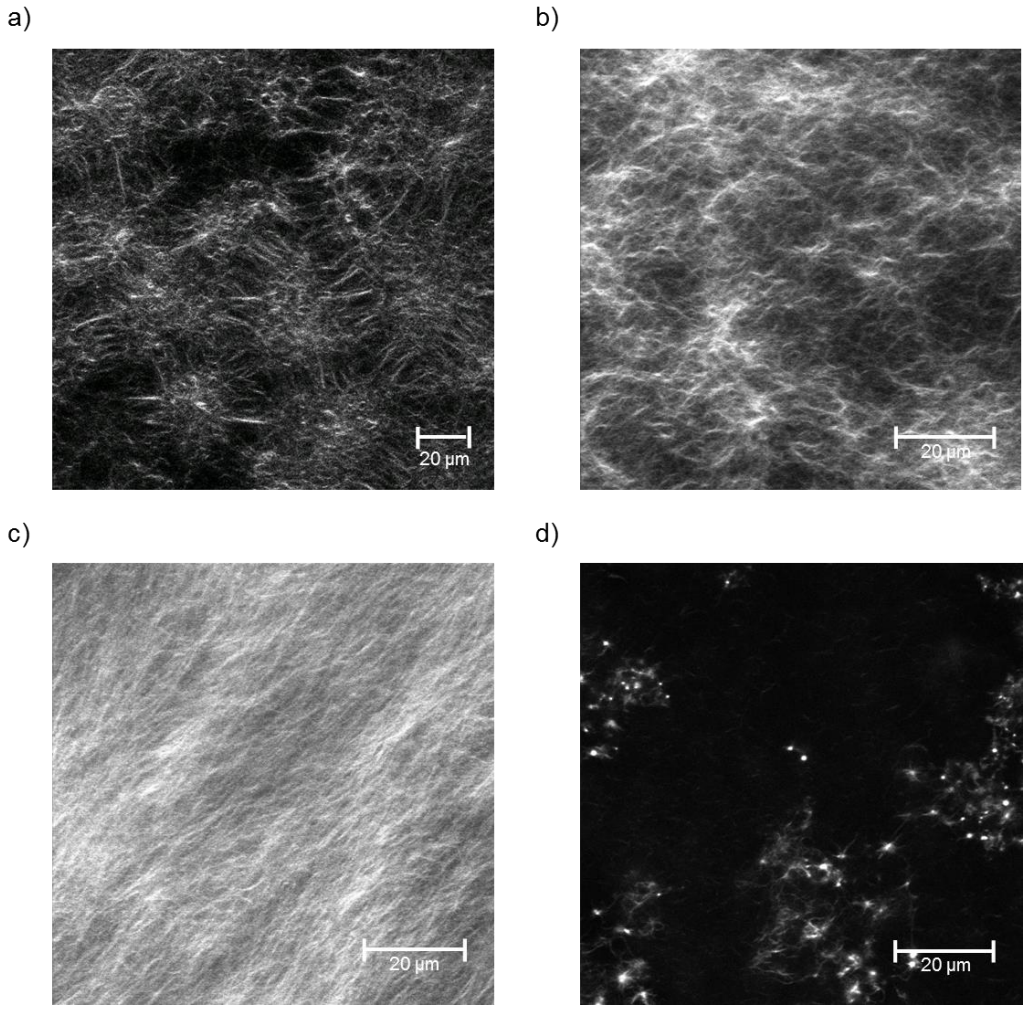

Figure 7 Confocal microscopy images of FmocFF gels prepared *via* different methods: a) 0.05 Φ_{DMSO}, b) 0.4 Φ_{DMSO}, c) GdL and d) HCl. All gels were stained with 0.1 wt% Nile Blue and had final pH values of ~ 4

Furthermore, these gels also differ in network properties to FmocFF gels prepared by other methods of trigger. Gels prepared at the same concentration and final pH *via* pH triggers using GdL and HCl were analysed. The confocal images are shown in Figures 7c and 7d. GdL is known to produce transparent, homogenous gels for FmocFF and other similar Fmoc gelators[5] and it appears to have a very different fibril network to the corresponding DMSO gels. Although it is very densely packed (similar to 0.4 Φ_{DMSO} gels), the fibres appear longer and less entangled than for DMSO gels. Using HCl to trigger gelation, however, has been shown to produce heterogeneous gels[5]. This is evident in the confocal microscopy image of an FmocFF gel prepared from HCl shown in Figure 7d. Nile Blue appears to accumulate only in certain regions, which could be indicative of randomly gelled regions, rather than

homogenous, complete gelation of the bulk solution. Gels with more densely packed networks have been demonstrated for gels prepared from HCl, but they had different final pH and/or preparation methods to that shown here. Those gels from the literature that displayed fibrous networks were imaged using SEM and TEM methods, and not confocal microscopy.[3, 6]

3.2.4 Comparison of FmocFF to other Fmoc Hydrogel Systems

Along with FmocFF, the rheological properties of both FmocVG and FmocAG were also measured for comparison. FmocVG is more hydrophilic than FmocFF (see Table 2, above) and the gelation range for gels of FmocVG at a final gelator concentration of 5 mg/mL is slightly smaller than for FmocFF. FmocVG successfully forms gels over the same range of Φ_{DMSO} as that of FmocLG (Table 2).[22] Both gelators are similar in hydrophobicity. FmocFF is the most hydrophobic of the gelators studied in this Chapter and therefore the most insoluble in water, aiding in the self-assembly of FmocFF over a larger range of Φ_{DMSO}. Over the range of Φ_{DMSO} that gelation occurred for FmocVG (Table 5), the *G′* was generally similar for gels with Φ_{DMSO} of 0.05 or 0.1 at ~ 4000 Pa – this is significantly weaker than FmocFF and FmocLG gels with the same Φ_{DMSO}. At Φ_{DMSO} of 0.05 and 0.1, *G′* values of 17600 and 19700 Pa for FmocFF gels and ~ 9000 Pa for FmocLG gels[22], respectively. Although, the gelation range is the same for both FmocVG and FmocLG, the mechanical properties are not. FmocLG produces gels with *G′* values of ~ 8500 - 10000 Pa for Φ_{DMSO} of 0.05 – 0.3 and the *G′* decreases above this range. A Φ_{DMSO} of 0.35 contains "intermediate" mechanical properties with a *G′* value of ~ 5000 Pa being recorded. Above this Φ_{DMSO} *G′* decreases to give *G′* values ranging from ~ 4000 – 2000 Pa for Φ_{DMSO} of 0.4 – 0.5. There appears to be a transition between mechanically rigid gels with low Φ_{DMSO} to mechanically weaker gels (but still strong gels in their own right) at higher Φ_{DMSO} – a Φ_{DMSO} of 0.35 being the point of inflection in this transition. This transition is further demonstrated by study of the hydrogel microstructure *via* confocal microscopy. A hydrogel network consisting of spherulitic domains was shown for gels with low $\Phi_{DMSO,}$ whereas at higher Φ_{DMSO}, homogeneous and densely packed fibril networks are observed.[22] These networks are reminiscent of that observed for FmocFF gels shown in Figures 7a and 7b. FmocVG gels show no such transition as the aforementioned Fmoc gelator systems. FmocVG

gels with a Φ_{DMSO} of 0.2 have the greatest mechanical strength across the range of Φ_{DMSO}. Above this Φ_{DMSO}, *G'* values sharply decrease to lower (3600 – 2500 Pa) than those observed at Φ_{DMSO} of 0.05 and 0.1. Above Φ_{DMSO} of 0.2, the *G'* values are comparable with FmocLG gels but are considerably weaker than FmocFF gels across the range of Φ_{DMSO} studied. FmocVG gels with varying final gelator concentrations (and constant Φ_{DMSO} of 0.1) were also measured (Table 5). Again, the gelation range was smaller than that of the more hydrophobic FmocFF. At a Φ_{DMSO} of 0.1, successful gelation was observed for gels with concentrations ranging from 5 – 10 mg/mL. If no flow of gelator material was observed upon vial inversion, rheological measurements were carried out. As expected, increasing concentration would lead to more fibre production and therefore provide increased mechanical strength. Gels of FmocVG were still weaker than FmocFF gels of the same concentration.

Φ_{DMSO} (5 mg/mL Final FmocVG concentration)	G' (Pa)	G" (Pa)	FmocVG Concentration (mg/mL) (0.1 Φ_{DMSO})	G' (Pa)	G" (Pa)
0.05	4100	660	2.5	1100	220
0.1	3800	670	5	3800	670
0.2	11500	2300	7.5	12600	2400
0.3	3600	530	10	24300	4600
0.4	2700	500			
0.5	2500	470			

Table 5 Summary of the rheological properties of FmocVG gels prepared from various concentrations and Φ_{DMSO}

The same gelation study was also repeated on the most hydrophilic gelator of the four: FmocAG (Table 6). As expected, the gelation at a final gelator concentration of 5 mg/mL occurs over a much smaller range of Φ_{DMSO}. In this case, gelation was only proved successful at Φ_{DMSO} of 0.05, 0.1 and 0.2. Gels were weaker as the Φ_{DMSO} increased. Again, gels were weaker than FmocFF and FmocLG gels but were mechanically stronger than FmocVG gels at Φ_{DMSO} of 0.05 and 0.1 only. Similar to the other gelator systems, *G'* increased as the final gelator concentration increased (at a constant Φ_{DMSO} of 0.1).

Φ_{DMSO} (5 mg/mL Final FmocAG concentration)	G' (Pa)	G" (Pa)	Recovery Ratio	FmocAG Concentration (mg/mL) (0.1 Φ_{DMSO})	G' (Pa)	G" (Pa)
0.05	7200	950	0.73	2.5	600	80
0.1	5200	660	0.69	5	5200	660
0.2	1100	130	0.82	7.5	9500	1500
				10	17700	3400

Table 6 Summary of the rheological properties of FmocAG gels prepared from various concentrations and Φ_{DMSO}

FmocVG gels are slightly weaker at the various concentrations measured. The maximum concentration studied was a final gelator concentration of 10 mg/mL and *G'* values of 62100 Pa, 24300 Pa and 17700 Pa were recorded for FmocFF, FmocVG and FmocAG, respectively. The mechanical strengths of FmocFF, FmocVG and FmocAG are compared in Figure 8. Here, the gels were prepared at range of concentrations at a constant Φ_{DMSO} of 0.1. Clearly, the FmocFF gels were significantly stronger than the other two gelators. The other two have similar rheological properties under the conditions studied. Gelation of FmocLG at concentrations other than 5 mg/mL was not studied.

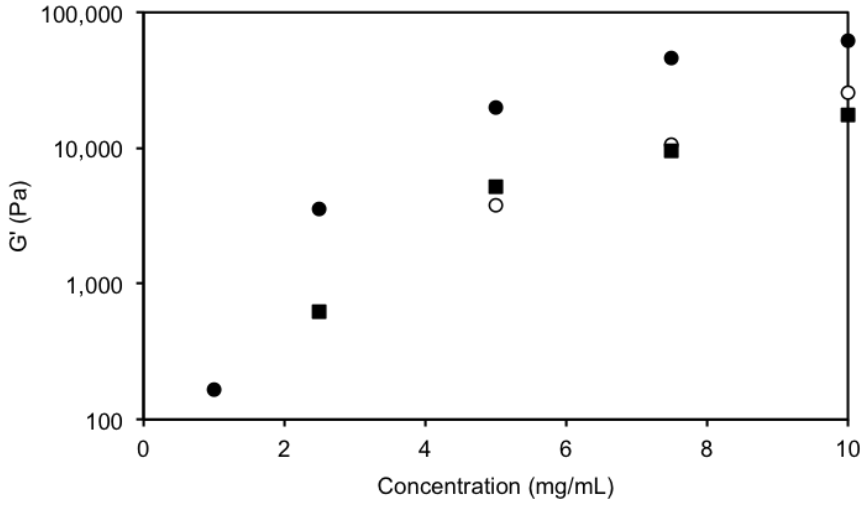

Figure 8 Comparison of rheological properties of FmocFF (●), FmocVG (○) and FmocAG (■) gels at different concentrations - all with Φ_{DMSO} of 0.1

3.2.5 Characterisation of the Microstructure of FmocFF Hydrogels

It is clear that judicious choice of not only gelator, but the final concentration and Φ_{DMSO} of the gel can all be vital to tuning the final mechanical properties of a gel for a desired application. Varying these properties appears to have no effect on the packing of gelator molecules at a molecular level, as previously mentioned in Section 3.2.1. However, the bulk rheological properties appear to be affected by fluctuations at a higher length scale. Confocal microscopy (Figure 7, and other microscopy techniques[6]) has indicated differences in the fibrillar networks of the gel matrices of FmocFF gels (and FmocLG gels[22]). Differences in the microstructure between gels with different Φ_{DMSO} could be investigated further by probing the recovery of the mechanical properties after shear. To do so, a constant shear rate was applied to disrupt the equilibrated state of the gel and hence, break the hydrogel network, resulting in a solid-liquid transition. Upon cessation of shear, *G′* and *G″* were measured with time. This group previously reported that FmocLG gels with Φ_{DMSO} lower than 0.25 had spherulitic microstructures which displayed the ability to recover from shear, however above this Φ_{DMSO}, a densely packed fibrous network was noted.[22] These did not recover from shear. The uniform fibrous networks of these gels broke down when exposed to high shear and the crosslinks were permanently broken and therefore unable to re-heal.[22] The recovery properties were measured for FmocFF gels (5 mg/mL) with a Φ_{DMSO} from 0.05 – 0.6. Gazit has previously demonstrated that FmocFF gels are injectable and hence recoverable from high shear.[6] Figure 9 shows the recovery tests for a gel with a Φ_{DMSO} of 0.1 and a gel with a Φ_{DMSO} of 0.6. These show five cycles of constant shear/shear cessation, with *G′* and *G″* measured at all times. It can be seen that when the steady shear is applied, *G′* and *G″* cross over and samples are no longer gels - *G″* is higher than *G′*. After this steady shear is ceased, *G′* and *G″* cross over again and *G′* becomes higher than *G″*, meaning a solid-like (gel) state has been restored.

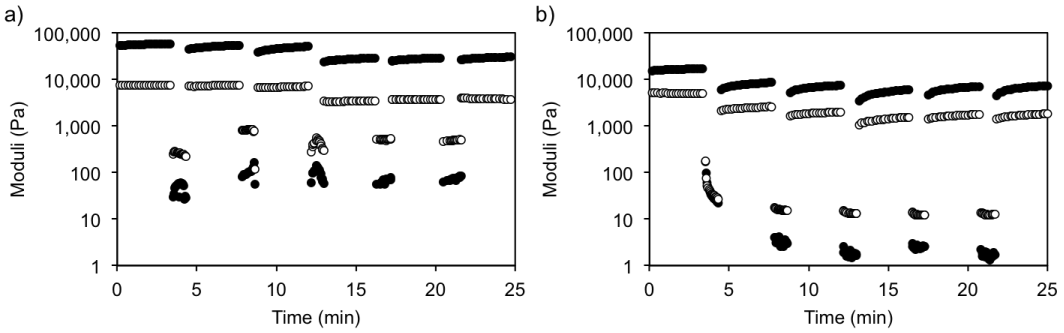

Figure 9 Rheological measurements showing recovery after shear of FmocFF gels with Φ_{DMSO} of a) 0.1 and b) 0.6. ● represents *G'* and ○ represents *G''*

Upon comparison of the recovery of the mechanical properties across the range of Φ_{DMSO} studied, there is a clear correlation between the bulk mechanical properties and the ability for the hydrogel network to recover from breakdown by application of steady shear (Figure 10). Where the mechanical properties increase with increased Φ_{DMSO} up until a Φ_{DMSO} of 0.4, the gels' ability to recover to its original *G'* also increased, with gels displaying the ability to recover to ~ 75 – 100 % of their original *G'* values. However, where the mechanical properties showed a decrease above a Φ_{DMSO} of 0.4, the recovery properties began to deteriorate beyond a Φ_{DMSO} of 0.35. For the gels with higher DMSO content and hence lower values of *G'*, the ability to recover upon cessation of shear was poorer, with less than ~ 60 % of the original *G'* being recovered. Around a Φ_{DMSO} of 0.5 displayed the poorest recovery as only ~ 20 % of the original mechanical properties being recovered.

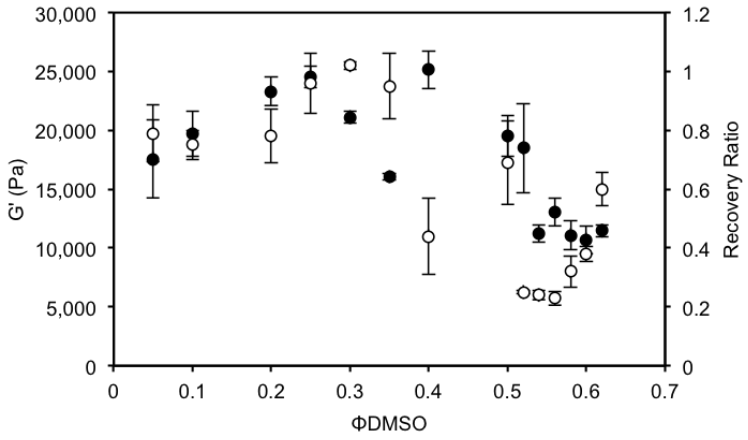

Figure 10 *G'* for FmocFF gels (final concentration of 5 mg/mL) at different Φ_{DMSO} (●) and the corresponding recovery ratios for these gels (○)

Much like FmocFF, FmocLG experienced a transition in the network and mechanical properties by changing the Φ_{DMSO}.[22] FmocLG gels with lower Φ_{DMSO} could recover to ~ 80 % of their original *G'* and at higher Φ_{DMSO}; where the gels displayed weaker mechanical properties, the ability to recover from shear was lowered to ~ 20 – 30 % of their original *G'* values. Again, this transitional period slightly differed between the bulk mechanical properties (transition at a Φ_{DMSO} of 0.35) and the recovery properties (transition at a Φ_{DMSO} of 0.2) of the gels.[22] FmocAG showed 69 – 80 % recovery of gels with Φ_{DMSO} ranging from 0.05 to 0.2 (Table 6).

It is clear that in the case of FmocFF (and FmocLG), that the fibril network properties have an effect on not only the mechanical properties but the ability to recovery these properties after disruption of the networks. The ability to recover the mechanical properties was better in stronger gels with lower Φ_{DMSO}. These gels showed spherulitic domains of fibres much like that observed in low Φ_{DMSO} FmocLG gels.[22] Gels with higher Φ_{DMSO}, appear to consist of thicker and more densely packed fibres across the entire region of the matrix. However these fibres must be more brittle than those produced in lower Φ_{DMSO} due to their inability to recover their mechanical properties as well.

3.2.6 Relationship Between Gelator Concentration, Mechanical Properties and Type of Fibrous Network

To better understand the tuning of the mechanical properties in these DMSO:water gels, a more profound understanding of the networks that constitute the gels is needed. From the literature, researchers have drawn a scaling relationship between the concentration of the gelator and the final mechanical properties i.e. *G'* of the gel. Semiflexible network elasticity theories can be used to rationalise this relationship.[37, 38] Most of the gels shown in this Chapter demonstrate storage moduli (*G'*) approximately an order of magnitude higher than their corresponding loss moduli (*G''*) - behaviour which has been predicted by Mackintosh *et al.*[37] Pochan and his group have shown the same behaviour for their β-hairpin gels.[39] Additionally Pochan's gels also showed an increase in strain required for gel breakdown with increased gelator concentration. This was in agreement with the behaviour predicted by Mackintosh *et al.*[37] However, the gels described in this Chapter showed no such

trend. Mackintosh (and Pochan) attributed such rheological behaviour to the crosslinking properties within the gels.[37, 39] Here the crosslinks are described as permanent junction points rather than mere entanglements between fibres. It is important to note that in the case of Pochan's β-hairpin gels and the gels described in this Chapter, the aforementioned crosslinks are physical crosslinks formed during the self-assembly process and not chemical crosslinks. However, these assembled, crosslinked fibres are attributes of a semiflexible network and therefore allow theories derived on the basis of a semiflexible network of a model biopolymer system to be exploited here. Furthermore, the homogeneity of the gels discussed in this Chapter provides further basis to allow correlation with natural systems.

Figure 11 shows the scaling relationship between G' and concentration for FmocFF gels with varying Φ_{DMSO}. The Φ_{DMSO} within the gel has an effect on the relationship between G' and the final gelation concentration and inherently, the network properties within the gel. The exponents of the graphs differ between Φ_{DMSO}. A Φ_{DMSO} of 0.05 (Figure 11a) gives the highest exponent of 3.0 ($G' \propto C^{2.9}$), with the exponent decreasing down to a Φ_{DMSO} of 0.3, having a value of 1.8 (Figure 11d). There appears to be no correlation between the final turbidities of the gels (Figure 2) and the exponents at each Φ_{DMSO}. For example, gels with a Φ_{DMSO} of 0.05 have an exponent of 3.0 and, from UV/vis measurements, show a similar final turbidity (Figure 2) to gels with a Φ_{DMSO} of 0.6 (at a final gelator concentration of 5 mg/mL), which have an exponent of 1.8. This may suggest that the gels are similar in the bulk but they consist of different fibrous networks. Gels prepared with a Φ_{DMSO} of 0.6 also show no increase in turbidity, thus hinting at a different assembly pathway to gels with a Φ_{DMSO} of 0.05 (or the other Φ_{DMSO} studied), which would support the idea of different networks perhaps being formed for these two particular Φ_{DMSO}. The scaling relationships proposed here are similar and in agreement with Mackintosh theory (Equation 1).[37]

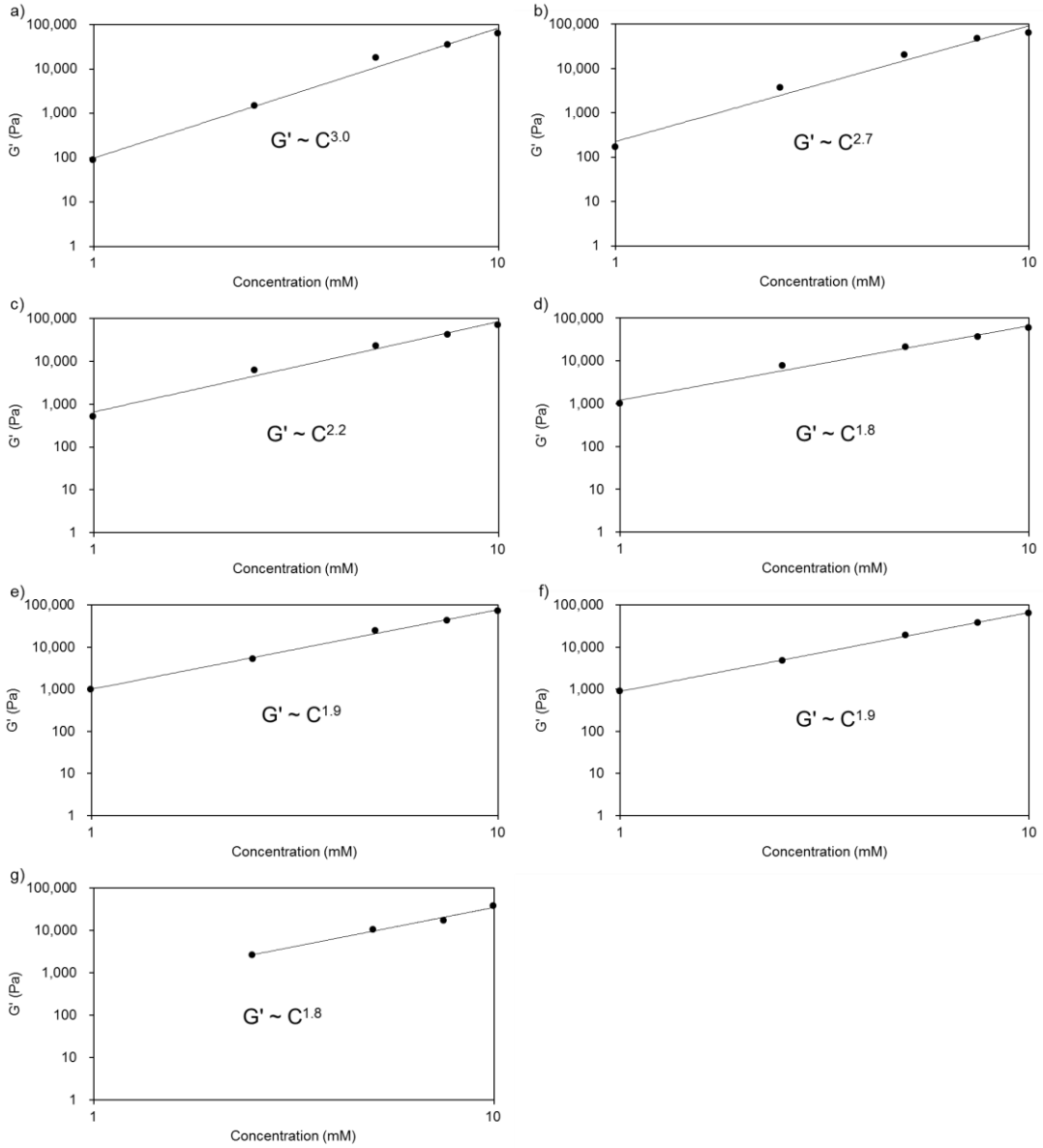

Figure 11 The relationship between *G'* and final gelator concentration for FmocFF gels with different Φ_{DMSO}: a) 0.05, b) 0.1, c) 0.2, d) 0.3, e) 0.4, f) 0.5 and g) 0.6

Mackintosh *et al.* devised a theory[37] based on F-actin to describe densely crosslinked polymer networks where *G'* is defined as

$$G' \sim \kappa^2/kT\,(ac)^{5/2} \tag{1}$$

where κ is the semiflexible chain bending modulus, a is the monomer size and c is the concentration. On the basis of this theory, the graph of F-actin concentration versus *G'* shows an exponent of 2.5. Rammensee *et al.* prepared both crosslinked and

non-crosslinked synthetic spider silk C_{16} gels which showed scaling relationships in agreement with Mackintosh theory, indicating both networks resemble crosslinked networks.[40] The exponents derived from the scaling relationships of gels with Φ_{DMSO} of 0.05 – 0.2, show similar or greater concentration dependence to that of F-actin. Thus, it could be suggested that these FmocFF gels consist of densely crosslinked networks. The exponent for FmocFF gels with a Φ_{DMSO} above 0.2 shows a weaker concentration dependence than that proposed by the Mackintosh theory. Above a Φ_{DMSO} of 0.4, the exponents of the graphs are virtually the same as one another (1.9). The lower concentration dependence of these systems is in agreement with an alternative semiflexible network elasticity theory proposed by Isambert and Maggs[41] and Morse (Equation 2).[38] They derived the relationship between *G'* and concentration as

$$G' \sim kT/l_e\xi^2 \qquad (2)$$

where l_e is the entanglement length and ξ is the mesh size. Here, the basis of their work looked at relatively dilute F-actin concentrations, which formed entangled chain networks rather than densely crosslinked networks seen by Mackintosh *et al.* They proposed an exponent of 1.4 for F-actin gels. Schmidt *et al.* also prepared entangled networks of bacteriophage fd which they found to be in agreement with the theory of Morse rather Mackintosh.[42]

Although the absolute values are not identical to those proposed for the actin networks, there is a clear change in the exponent for FmocFF gels with different Φ_{DMSO}. Ultimately, with consideration of both theories, the network changes in these systems. It appears that for FmocFF gels with lower $\Phi_{DMSO,}$ the fibrous network resembles that of a densely crosslinked system on the basis of their rheological behaviour. A transitional period between densely crosslinked networks and the proposed entangled networks at higher Φ_{DMSO} seems apparent for gels with a Φ_{DMSO} of 0.3. This is in agreement with the rheological properties collected for these gels at concentration of 5 mg/mL. Figure 5, Table 4 and Figure 10 show that the change between mechanically strong gels with the ability to recover from high shear to

weaker gels with the inability to get close to full recovery upon shear cessation occurs around gels with Φ_{DMSO} of 0.3 – 0.4. Therefore, it is clear that there is a change in network of some capacity between these Φ_{DMSO} ranges. Confocal microscopy images (Figure 7) also indicate a clear difference between these networks. Clearly, subtle differences in hydrogel composition result in changes to the network and resulting bulk properties of that network. It is worth noting that this correlation is on the basis of hydrogels with final gelator concentrations of 5 mg/mL.

Analysis of the rheological data collected for the more hydrophilic FmocAG gels show that the exponents exhibit a strong concentration dependence, much like that of FmocFF gels with Φ_{DMSO} between 0.05 and 0.2. Again, these exponents measured for FmocAG gels (Figure 12) could be correlated to that observed for F-actin gels in agreement with Mackintosh theory. The concentration dependence of the exponents weakened with increasing $\Phi_{DMSO,}$ much like the *G'* values of the gels (at 5mg/mL gelator concentration). FmocFF and FmocAG gels at these Φ_{DMSO} have similar ability to recover from shear but the FmocAG gels are weaker than FmocFF gels with the same Φ_{DMSO}. The proposed differences in network between gelators could be attributed to the crosslink densities in the gels. FmocAG gels may have more uniform, densely crosslinked networks that could be more similar in structure to FmocFF (and FmocLG) gels with higher $\Phi_{DMSO.}$ What distinguishes FmocAG gels from these higher Φ_{DMSO} gels of FmocFF is that they can recover from shear and their scaling relationship is more in agreement with Mackintosh theory[37], thus suggesting that although FmocAG gels are densely crosslinked, these crosslinks are not permanently broken upon shear. The reason that the FmocAG gels are mechanically weaker than FmocFF gels with the same Φ_{DMSO} could be assigned to the fact that FmocFF gels contain spherulitic domains of fibres (with slightly lower crosslink densities than FmocAG networks), which could affect the bulk properties between the two gelators; much in the same as between high and low Φ_{DMSO} in FmocFF (and FmocLG[22]).

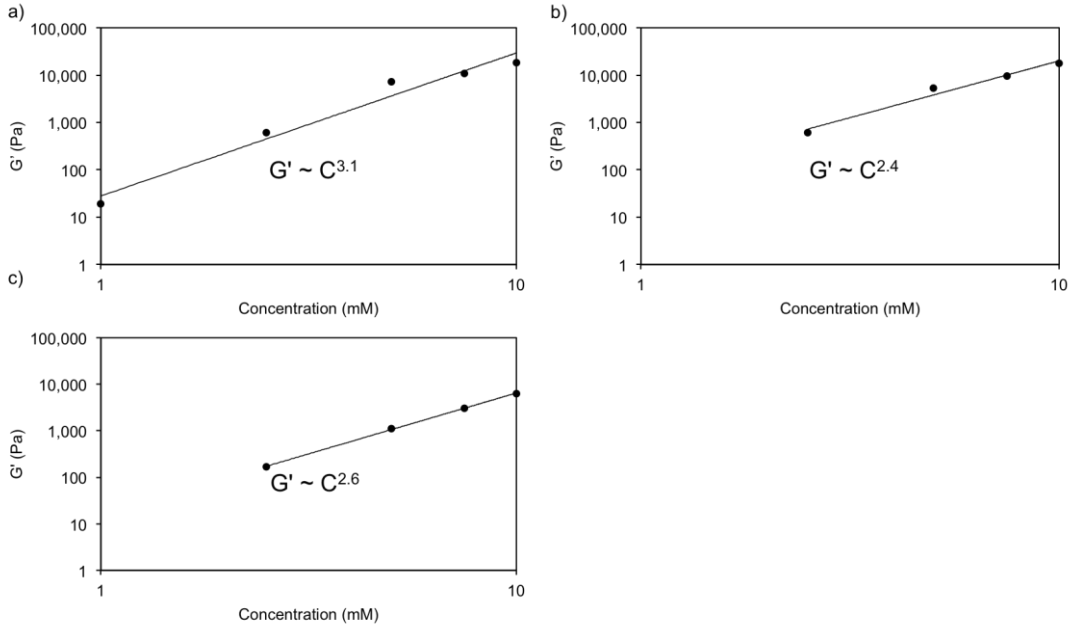

Figure 12 The relationship between *G'* and final gelator concentration for FmocAG gels with different Φ_{DMSO}: a) 0.05, b) 0.1 and c) 0.2

3.2.7 Removal of DMSO from FmocFF Hydrogel Network

FmocFF hydrogels have been shown in this Chapter (and in the literature[7, 10, 36, 43]) to be desirably rigid and healable after shear, making them of potential use for drug delivery and tissue engineering applications.[44] To increase potential cell viability and biocompatibility by increasing the percentage of water that constitutes the gel matrix, there is the possibility to remove the solvent from the hydrogel network. FmocFF gels were prepared as before, utilising a final gelator concentration of 5 mg/mL and a Φ_{DMSO} of 0.4. Water was, however, replaced with D_2O for analysis of DMSO removal. Gels were again left overnight to fully form before any experiments were carried out. To the vial containing the gel, a volume of water was added on top of the gel and left for 4 hours before replacing with another equal volume of D_2O. This was repeated for subsequent washings. After washing with D_2O, the gels were then analysed using FT-IR. Fresh gels were prepared for analysis of each number of washing. By monitoring the sulfoxide peak at 1020 cm^{-1}, the removal of DMSO *via* washing of the gels could be quantified. FT-IR spectra showed that after just one washing, the Φ_{DMSO} of the gel had decreased from a Φ_{DMSO} of 0.4 to 0.3 (Figure 13). Each subsequent washing further removed DMSO, with each washing removing less

DMSO than the preceding washing. After four washings, the Φ_{DMSO} of the gel was 0.15.

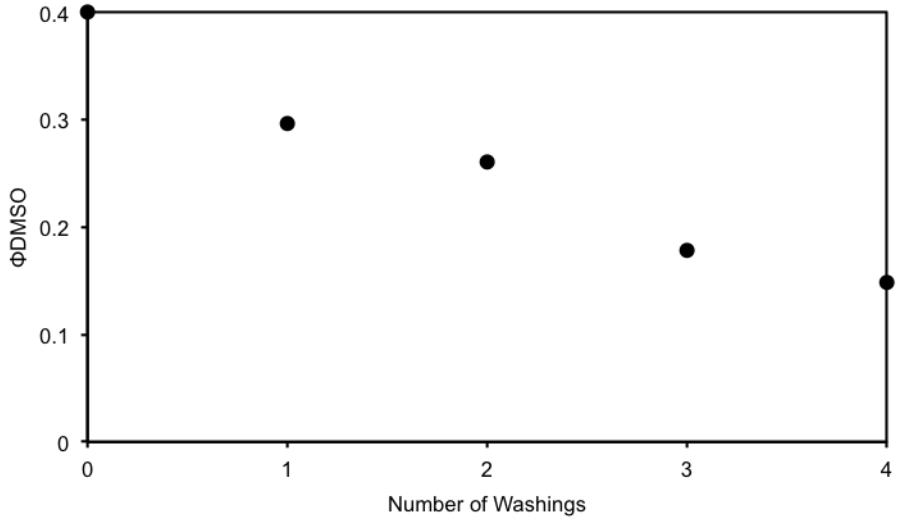

Figure 13 DMSO is removed from FmocFF gels (5 mg/ml gelator concentration, 0.4 Φ_{DMSO}) upon washing with water

Successful removal of DMSO by washing demonstrates that DMSO is not non-covalently bonded to the fibres (or incorporated in each individual fibre). Rather, it went from being free flowing in solution before gelation to being physically embedded in the fibrous matrix of the FmocFF gels. FT-IR spectra also showed that after washing, the molecular packing of the gels remained unchanged as the amide I region showed no differences between gels (Figure 14).

Figure 14 Partial FT-IR spectra of FmocFF gel samples (from top to bottom) before washing, after 1, 2, 3 and 4 washings, respectively

Although the molecular packing appeared to be unaffected by the removal of solvent from the hydrogel matrix of FmocFF gels, the effects on the fibril network on higher length scales required probing. After all washings, the rheological properties were measured to assess any potential detriment to the bulk properties of the gels. Table 7 summarises the rheological properties of the gels after washing. Frequency sweep measurements show that the mechanical properties show no significant difference after one washing, with a G' value of 25000 Pa measured for gels before and after one washing. Interestingly, after one washing the Φ_{DMSO} of the gel is 0.3 and a gel prepared with an original Φ_{DMSO} of 0.3 has a G' of 21100 Pa (Figure 15a and Table 4). Therefore, the bulk network is unchanged upon washing and is reminiscent of a

gel with a Φ_{DMSO} of 0.4, rather than a gel with a Φ_{DMSO} of 0.3. Further washings also show no correlation between gels prepared with the corresponding Φ_{DMSO} to that of the "washed" gels (Figure 15). The *G'* did decrease slightly after two or more washings but not significantly. After four washings the *G'* recorded is 23000 Pa and has a Φ_{DMSO} of 0.15. Strain amplitude sweeps also indicate that the bulk properties of the gels are unaffected by the removal of DMSO. All gels tested showed breakdown of the hydrogel network at a strain of 6.3 %. Again, no correlations could be drawn between the washed gels and those gels with corresponding Φ_{DMSO}.

Number of Washings	G' (Pa)	G" (Pa)	% Strain at Hydrogel Breakdown	Recovery Ratio	Final Φ_{DMSO} of Gel
0	25000	4500	6.3	0.44	0.40
1	25000	3800	6.3	0.29	0.30
2	23000	3400	6.3	0.10	0.26
3	23000	3700	6.3	0.09	0.18
4	25000	3700	6.3	0.14	0.15

Table 7 Summary of rheological properties and Φ_{DMSO} of FmocFF gels (5 mg/ml gelator concentration, 0.4 Φ_{DMSO}) before and after washing with water

Despite the bulk properties appearing unaffected by the removal of DMSO from within the gel network, the ability of the gels to recover their rheological properties upon cessation of a steady shear deteriorated (Table 7 and Figure 15b). An FmocFF gel with a Φ_{DMSO} of 0.4, before washing, could recover to 44 % of its original *G'* value. After washing, gels could only recover between ~ 10 and 30 % of their original *G'* values. A more brittle fibril network is apparent upon the removal of some of the DMSO from between the fibres. Again, these properties are very different from gels with the same Φ_{DMSO}. Figure 15b shows that gels with a Φ_{DMSO} below 0.4 (without washing) can recover at least 60 % of their original *G'* values.

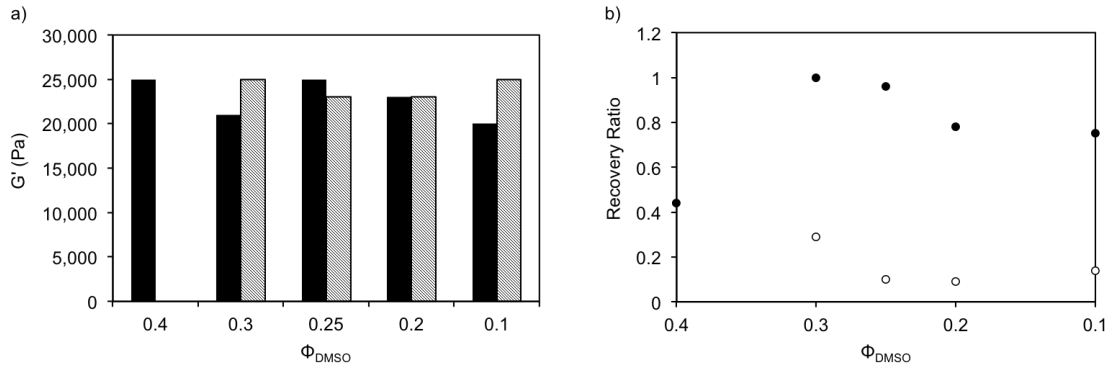

Figure 15 Comparison of rheological properties between 'unwashed' and 'washed' gels: a) *G'* of FmocFF gels with different Φ_{DMSO} (black) and gels with different Φ_{DMSO} as DMSO has been washed out (grey). b) Recovery ratios of these 'unwashed' (●) and 'washed' (○) gels. The Φ_{DMSO} of the washed gels are rounded to the nearest Φ_{DMSO} of the gels prepared at different Φ_{DMSO}

3.2.8 FmocFF Hydrogels Prepared from other Solvents

Tunability of FmocFF hydrogels produced *via* a solvent switch method has been shown throughout this Chapter to be controlled by altering the gelator concentration or quantity of solvent in the solvent/water mixture of which the hydrogel is composed. Another aspect of the FmocFF hydrogel composition that can be manipulated to tune the final mechanical properties is the type of solvent. Hydrogels of FmocFF produced by way of solvent-mediated methods, which utilise solvents other than DMSO, do exist in the literature. Specifically, Mahler *et al.* have produced FmocFF hydrogels which use hexafluoroisopropanol (HFIP) as the solvent portion of the hydrogel.[6] They have demonstrated that these gels are as mechanically strong as gels produced from DMSO/water, however it is unclear which Φ_{HFIP} they have used in their gels. In this Chapter, FmocFF hydrogels were prepared from ethanol, acetone and HFIP and their rheological properties measured, as for the DMSO gels described above. All of these solvents are polar solvents that are miscible in water.

Addition of water to FmocFF dissolved in each of the solvents afforded transparent gels, with the turbidity (visually) generally increasing with both increasing $\Phi_{solvent}$ and gelator concentration. The same has been noted above for DMSO gels up until a Φ_{DMSO} of 0.5. The type of solvent has an effect on the hydrogel formation. As mentioned previously in this Chapter, at a final gelator concentration of 5 mg/mL,

FmocFF gels made using DMSO can successfully be prepared across a range of Φ_{DMSO}; from 0.05 to 0.6. At this concentration of gelator, the gelation range is slightly varied for the other solvents tested (Table 8). To try to rationalise these differences in gelation ability between solvents, several standard solvent properties were compared and are shown in Table 8. The dipole moment; a measure of the magnitude of charge between the distance of partial negative and positive charges on a molecule (the overall polarity), does not appear to play a significant role in gelation ability. Inherently, more polar solvents could be expected to elicit better hydrogen bonding ability with both gelator and water, which would allow more gelator to be dissolved across a larger range of $\Phi_{solvent}$, ultimately leading to gelation over a wider range of $\Phi_{solvent}$. However, gelation with ethanol occurs across a wider range of $\Phi_{solvent}$ than that for acetone. Ethanolic solutions required gentle heating to dissolve FmocFF, which could have aided in allowing FmocFF to be solubilised and in turn gelled across a slightly wider range of $\Phi_{solvent}$. Another indicator of solvent polarity, dielectric constant; which measures the ability of a molecule to stabilise charge, also does not appear to have a profound effect on the gelation ability in the different solvents. From consideration of these values, DMSO would appear to be the most polar and possess the greatest ability to hydrogen bond to the gelator (Table 8). Hence, it can form gels across a wider range of Φ_{DMSO}, as demonstrated in this Chapter. The other three solvents have more similar values to one another. However, HFIP, which is a polar protic solvent, shows the same gelation range to DMSO. FmocFF gels can be prepared from HFIP with Φ_{HFIP} ranging from 0.05 to 0.6. Acetone is slightly less polar than DMSO (both are aprotic), but it shows a gelation range more similar to ethanol (a polar protic solvent).

Solvent	Gelation Range ($\Phi_{solvent}$)	Melting Point (°C)	Boiling Point (°C)	Dipole Moment, μ (D)	Dielectric Constant, ε
DMSO	0.05 – 0.6	19	189	4.1	46.7
Ethanol	0.1 – 0.6	-114	79	1.7	22.4
Acetone	0.1 – 0.5	-95	56	2.7	20.7
HFIP	0.05 – 0.6	-4	59	~ 2	< 16

Table 8 Ranges of successful hydrogelation using different solvents and general solvent properties.[45] All gels have a final gelator concentration of 5 mg/mL. Values taken from literature[46, 47]

For gels formed under the solvent compositions described in Table 8, the rheological properties were measured. Figure 16a compares the *G′* measured for gels of all solvents (including DMSO) and across the range of $\Phi_{solvent}$. For gels prepared using DMSO, ethanol, or acetone, higher mechanical properties were recorded between ~ $\phi_{solvent}$ of 0.2 and 0.4, with the mechanical properties slightly lower for gels prepared at a $\phi_{solvent}$ on either side of this range (Figure 16a). However, for HFIP, all ϕ_{HFIP} resulted in storage moduli (G') < 10 kPa; except for a ϕ_{HFIP} of 0.05 which resulting in significantly mechanical stronger gels with a *G′* of ~ 26 kPa. All four solvents have different dipole moments and dielectric constants (Table 8) and therefore have different abilities to donate and accept hydrogen bonds. This could attribute to the differences in final rheological properties between solvents. Along with differences in *G′* between solvents, the ability of gels to recover after high shear does not correlate either. As all solvents could form gels with a $\Phi_{solvent}$ of 0.3, the recovery of these gels could be compared between solvents (Figure 16b). It could be seen that not only do DMSO and HFIP form gels over a wider range of $\Phi_{solvent}$, but they also produce gels that can regain > 95 % of their mechanical properties upon shear cessation. Ethanol and acetone can only recover 26 and 30 % of their *G′* values, respectively. Despite HFIP gels being weaker than ethanol and acetone at a $\Phi_{solvent}$ of 0.3, they have a better ability to recover from shear.

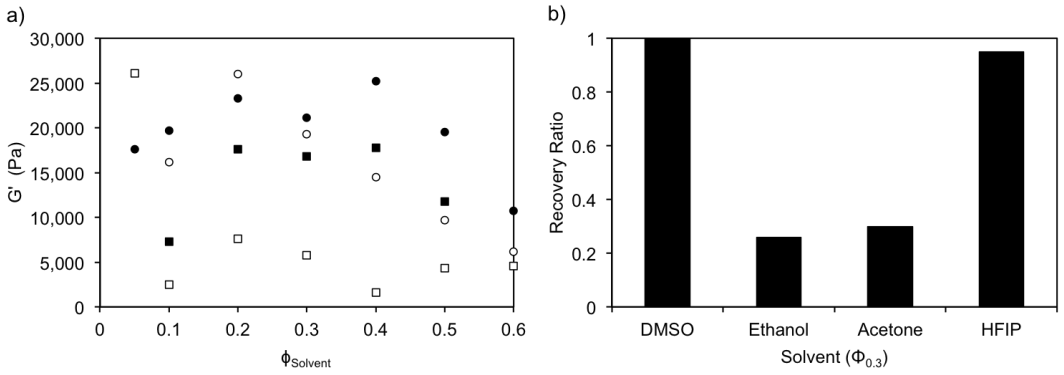

Figure 16 Comparison of the rheological properties of FmocFF gels prepared from different solvents. a) *G'* of gels prepared using DMSO (●), ethanol (○), acetone (■) and HFIP (□) with different $\Phi_{solvent}$ and b) shows the recovery ratios of gels prepared with a $\Phi_{solvent}$ of 0.3 using the solvents DMSO, acetone, ethanol and HFIP. All gels have a final gelator concentration of 5 mg/mL

From the comparison of the mechanical properties of the FmocFF gels with different solvents, it is clear that solvent choice and composition has an effect on the final hydrogel properties. Hence, on the bulk scale, there are differences between the gels. By utilising the scaling relationship between *G'* and gelator concentration, comparisons of the fibrillar matrices of the gels with different solvents can be drawn (Figure 17). The exponents depend on the solvent, which again shows that the network is tuneable by solvent. In all cases, the exponents are much lower than predicted by Mackintosh theory. This suggests that, over the concentration range studied here, the networks observed are more reminiscent of relatively dilute F-actin systems, which formed entangled chain networks rather than densely crosslinked networks.[38, 41] We previously found similar values for Fmoc-dipeptide gels formed using a pH switch.[48]

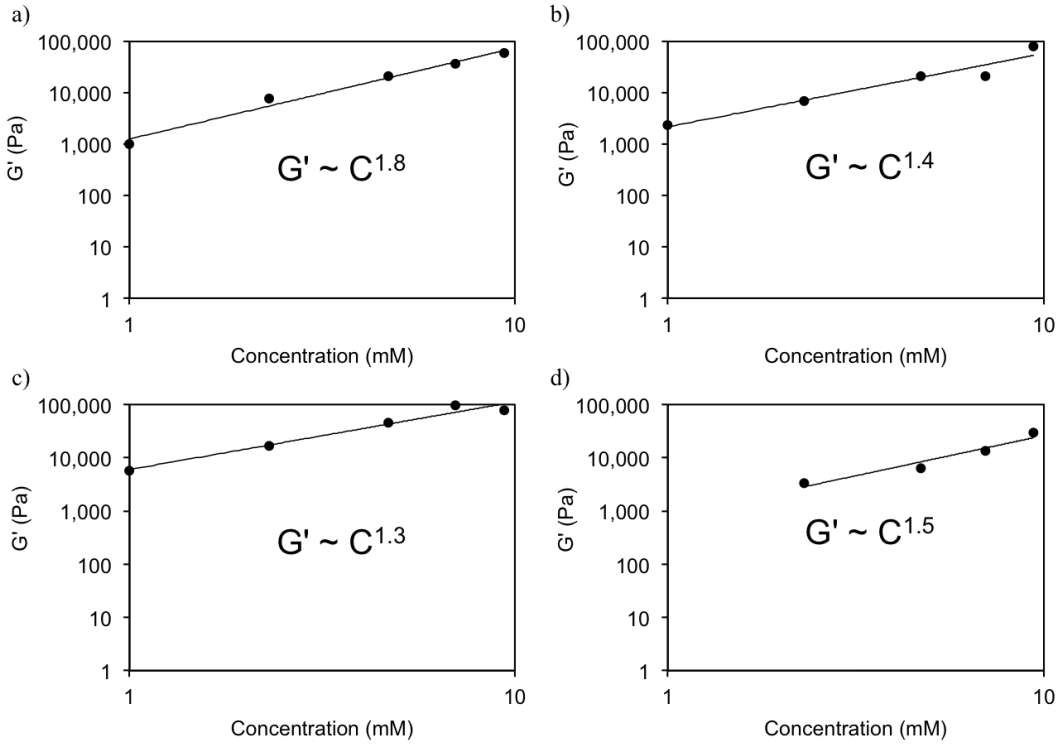

Figure 17 Comparison of relationships between *G'* and gelator concentration for FmocFF gels prepared using a) DMSO b) ethanol c) acetone and HFIP. All gels have a final gelator concentration of 5 mg/mL and a $\Phi_{solvent}$ of 0.3

3.3 Conclusion

FmocFF is an extensively studied and reported gelator, which produces homogenous, transparent and mechanically strong gels, making them attractive for many applications. Although, mechanically strong gels have been reported, there is extensive variability in the final mechanical properties between methods of preparing these gels, which is largely unexplained. Here it has been demonstrated that judicious choice of concentration and solvent conditions can be utilised to tune the mechanical properties. When preparing these gels with DMSO, a turbidity increase ensues before clearing to produce a gel, thus suggesting the assembly of larger structures that reorganise to produce smaller structures that make up the hydrogel network. This can be extended to other Fmoc-dipeptide gelators; where the hydrophobicity of the gelator is shown to play a vital role in the range of solution conditions that gelation can occur. More hydrophobic gelators such as FmocFF can successfully form hydrogels under a wider range of $\Phi_{solvent}$ than Fmoc-dipeptides that are more

hydrophilic. It is clear that the process of gelation is affected by these attributes, leading to different bulk properties. Along with systematic changes in the hydrogel composition, including concentration of gelator and solvent composition, changing the solvent itself can affect the mechanosensitivity of the gels. Altering the experimental protocols of gelation allows the mechanical properties to be tuned for solvent-mediated hydrogels. Manipulation of such protocols impacts the process of gelation and through consideration of several theories composed to characterise crosslinked and semi-flexible networks, tuning the process impacts the hydrogel network. Fine tunability of these materials is a very attractive quality, however the pH of these gels would eliminate the possibility for use in cell culturing, where many others have applied pH-triggered FmocFF gels - which can form gels at physiological pH.

3.4 References

1. D. J. Adams and P. D. Topham, *Soft Matter*, 2010, **6**, 3707-3721.
2. D. J. Adams, *Macromol. Biosci.*, 2011, **11**, 160-173.
3. V. Jayawarna, M. Ali, T. A. Jowitt, A. F. Miller, A. Saiani, J. E. Gough and R. V. Ulijn, *Adv. Mater.*, 2006, **18**, 611-614.
4. T. Liebmann, S. Rydholm, V. Akpe and H. Brismar, *BMC Biotechnol.*, 2007, **7**, 88-98.
5. D. J. Adams, M. F. Butler, W. J. Frith, M. Kirkland, L. Mullen and P. Sanderson, *Soft Matter*, 2009, **5**, 1856-1862.
6. A. Mahler, M. Reches, M. Rechter, S. Cohen and E. Gazit, *Adv. Mater.*, 2006, **18**, 1365-1370.
7. J. Raeburn, G. Pont, L. Chen, Y. Cesbron, R. Levy and D. J. Adams, *Soft Matter*, 2012, **8**, 1168-1174.
8. V. Jayawarna, S. M. Richardson, A. R. Hirst, N. W. Hodson, A. Saiani, J. E. Gough and R. V. Ulijn, *Acta Biomater.*, 2009, **5**, 934-943.
9. J. Ryu, S. W. Kim, K. Kang and C. B. Park, *Adv. Mater.*, 2010, **22**, 5537-5541.
10. A. M. Smith, R. J. Williams, C. Tang, P. Coppo, R. F. Collins, M. L. Turner, A. Saiani and R. V. Ulijn, *Adv. Mater.*, 2008, **20**, 37-41.
11. C. Tang, A. M. Smith, R. F. Collins, R. V. Ulijn and A. Saiani, *Langmuir*, 2009, **25**, 9447-9453.
12. M. Zhou, A. M. Smith, A. K. Das, N. W. Hodson, R. F. Collins, R. V. Ulijn and J. E. Gough, *Biomaterials*, 2009, **30**, 2523-2530.
13. W. Helen, P. de Leonardis, R. V. Ulijn, J. Gough and N. Tirelli, *Soft Matter*, 2011, **7**, 1732-1740.
14. L. Chen, K. Morris, A. Laybourn, D. Elias, M. R. Hicks, A. Rodger, L. Serpell and D. J. Adams, *Langmuir*, 2010, **26**, 5232-5242.
15. N. Amdursky, R. Orbach, E. Gazit and D. Huppert, *J. Phys. Chem. C*, 2009, **113**, 19500-19505.
16. A. J. Engler, S. Sen, H. L. Sweeney and D. E. Discher, *Cell*, 2006, **126**, 677-689.
17. J. H. van Esch, *Langmuir*, 2009, **25**, 8392-8394.
18. Y. Zhang, H. W. Gu, Z. M. Yang and B. Xu, *J. Am. Chem. Soc.*, 2003, **125**, 13680-13681.
19. R. Orbach, L. Adler-Abramovich, S. Zigerson, I. Mironi-Harpaz, D. Seliktar and E. Gazit, *Biomacromolecules*, 2009, **10**, 2646-2651.
20. L. Chen, S. Revel, K. Morris, L. C. Serpell and D. J. Adams, *Langmuir*, 2010, **26**, 13466-13471.
21. L. Chen, T. O. McDonald and D. J. Adams, *RSC Adv.*, 2013, **3**, 8714-8720.
22. L. Chen, J. Raeburn, S. Sutton, D. G. Spiller, J. Williams, J. S. Sharp, P. C. Griffiths, R. K. Heenan, S. M. King, A. Paul, S. Furzeland, D. Atkins and D. J. Adams, *Soft Matter*, 2011, **7**, 9721-9727.
23. X. Huang, S. R. Raghavan, P. Terech and R. G. Weiss, *J. Am. Chem. Soc.*, 2006, **128**, 15341-15352.
24. D. B. Wong, K. P. Sokolowsky, M. I. El-Barghouthi, E. E. Fenn, C. H. Giammanco, A. L. Sturlaugson and M. D. Fayer, *J. Phys. Chem. B*, 2012, **116**, 5479-5490.
25. J. Catalán, C. Díaz and F. García-Blanco, *J. Org. Chem.*, 2001, **66**, 5846-5852.
26. S. Fleming, P. W. J. M. Frederix, I. Ramos Sasselli, N. T. Hunt, R. V. Ulijn and T. Tuttle, *Langmuir*, 2013, **29**, 9510-9515.

27. A. Aggeli, I. A. Nyrkova, M. Bell, R. Harding, L. Carrick, T. C. B. McLeish, A. N. Semenov and N. Boden, *Proc. Nat. Acad. Sci.*, 2001, **98**, 11857-11862.
28. J. Kong and S. Yu, *Acta Biochim.*, 2007, **39**, 549-559.
29. R. G. Weiss, Terech, P., *Molecular Gels and Fibrillar networks – A Comprehensive Guide to Experiment and Theory*, Springer, Dordrecht, The Netherlands, 2006.
30. http://www.molinspiration.com/cgi-bin/properties
31. Z. Yang, G. Liang, M. Ma, Y. Gao and B. Xu, *J. Mater. Chem.*, 2007, **17**, 850-854.
32. J. Raeburn, B. Alston, J. Kroeger, T. O. McDonald, J. R. Howse, P. J. Cameron and D. J. Adams, *Mater. Horiz.*, 2014, **1**, 241-246.
33. J. Raeburn, A. Zamith Cardoso and D. J. Adams, *Chem. Soc. Rev.*, 2013, **42**, 5143-5156.
34. K. L. Morris, L. Chen, J. Raeburn, O. R. Sellick, P. Cotanda, A. Paul, P. C. Griffiths, S. M. King, R. K. O'Reilly, L. C. Serpell and D. J. Adams, *Nat. Commun.*, 2013, **4**, 1480-1485.
35. J. Raeburn, T. O. McDonald and D. J. Adams, *Chem. Commun.*, 2012, **48**, 9355-9357.
36. N. A. Dudukovic and C. F. Zukoski, *Langmuir*, 2014, **30**, 4493-4500.
37. F. C. Mackintosh, J. Kas and P. A. Janmey, *Phys. Rev. Lett.*, 1995, **75**, 4425-4428.
38. D. C. Morse, *Macromolecules*, 1998, **31**, 7030-7043.
39. B. Ozbas, K. Rajagopal, J. P. Schneider and D. J. Pochan, *Phys. Rev. Lett.*, 2004, **93**, 28106-28109.
40. S. Rammensee, D. Huemmerich, K. D. Hermanson, T. Scheibel and A. R. Bausch, *Appl. Phys. A*, 2006, **82**, 261-264.
41. H. Isambert and A. C. Maggs, *Macromolecules*, 1996, **29**, 1036-1040.
42. F. G. Schmidt, B. Hinner, E. Sackmann and J. X. Tang, *Phys. Rev. E*, 2000, **62**, 5509-5517.
43. R. Orbach, I. Mironi-Harpaz, L. Adler-Abramovich, E. Mossou, E. P. Mitchell, V. T. Forsyth, E. Gazit and D. Seliktar, *Langmuir*, 2012, **28**, 2015-2022.
44. C. Yan, A. Altunbas, T. Yucel, R. P. Nagarkar, J. P. Schneider and D. J. Pochan, *Soft Matter*, 2010, **6**, 5143-5156.
45. I. M. Smallwood, *Handbook of Organic Solvent Properties*, Butterworth-Heinemann, Oxford, 1996.
46. F. A. Carey, Sundberg, Richard J., *Advanced Organic Chemistry Part A: Structure and Mechanisms*, 5 edn., Springer Science & Business Media, New York, USA, 2007.
47. A. Berkessel, J. A. Adrio, D. Hüttenhain and J. M. Neudörfl, *J. Am. Chem. Soc.*, 2006, **128**, 8421-8426.
48. D. J. Adams, L. M. Mullen, M. Berta, L. Chen and W. J. Frith, *Soft Matter*, 2010, **6**, 1971-1980.

CHAPTER 4

Hydrogelation Triggered *via* Ultraviolet Light

4.1 Introduction

UV light can be used to tune the properties of some materials. More specifically, UV light can be used to trigger self-assembly of certain molecules. For many polymeric materials, UV light can trigger crosslinking to induce polymer hydrogelation.[1, 2] Hydrogels formed by this method will be mechanically strong and irreversible. For instance, Lee *et al*. used UV light to polymerise poly(acrylic acid) (PAAc) to give a crosslinked PAAc network within linear chitosan chains. The resulting hydrogels are mechanically strong, with storage moduli (*G'*) measured in the MPa range.[1] Hydrogels of gelatin have also been reported, where the network formation occurs from UV-initiated radical polymerisation of derivatives of chitosan. The chitosan derivatives were crosslinked *via* methacrylamide side groups to produce gels with controllable mechanical properties based on the storage temperature before photoinitiation.[2] UV-initiated hydrogelation of polymer materials is distinctly different from self-assembled hydrogels – the former are covalently bonded and can be extensively crosslinked and irreversible, whereas the latter are bonded by weaker, non-covalent interactions, allowing reversibility of the self-assembled hydrogel state.[3-5] For self-assembled molecules, UV-initiated crosslinking does not occur. Li *et al*. have shown how UV light can be used to change the phase of gel to solution – where the UV exposure changes the conformation of the gelator from *trans* to *cis* (in this case).[5] When in the *cis* conformation, the individual azobenzene molecules are bent and unable to stack, inhibiting the stability of the network. A gel-sol transition is therefore observed. Stupp's group have shown the activation of a pro-gelator by photo-cleavage of a nitrobenzyl group.[6] This precedes gelation in the presence of $CaCl_2$. Raghavan and co-workers have demonstrated that UV light can be used to tune the rheological properties of a dispersion containing laponite, a poly(ethylene oxide)-poly(propylene oxide)-poly(ethylene oxide) triblock copolymer and a photoacid generator (PAG).[7] PAGs are a class of molecule that can be photolysed by UV light to produce an acid. In this case, the photolysis of the PAG induced aggregation in the laponite/polymer suspension, increasing viscosity. Raghavan has also shown photogelation of alginate can occur by the addition of a PAG.[8] The PAG was added to a solution of alginate along with a calcium salt. When irradiated with

UV light, the PAG released protons that reacted with the calcium salt to produce Ca^{2+} ions, which acted as crosslinks by bridging between adjacent alginate molecules to form gels by an "egg-box" based model.

Light as a self-assembly trigger has clear advantages over other stimuli as light can be focused to a particular area, allowing for targeted gelation rather than gelation of a bulk solution.[9, 10] This enables patterned hydrogel surfaces to be produced, where the topography of the hydrogel can be tuned to control cell proliferation. For example, Tamaki *et al*. have demonstrated the formation of hydrogels consisting of siloxane oligomers, where the combination of a PAG and photolithography, allowed hydrogel line patterns to be made. These hydrogel lines were confirmed using SEM.[11] Stupp *et al.* have shown peptide amphiphile (PA) patterned surfaces, consisting of the sequence arginine-glycine-aspartic acid-serine (RGDS), which showed effects on the growth and characteristics of human mesenchymal stem cells (hMSCs) due to the hydrogel pattern.[12] Although examples of light stimuli-activated gelation of polymers exist in the literature,[8, 11] to the best of our knowledge, there is no data showing hydrogels formed from LMWGs *via* UV-triggered gelation. We report here the UV-triggered gelation of a number of dipeptide conjugates using a PAG. The PAG is used to lower the pH of a gelator solution below the apparent pK_a of the gelator, resulting in gelation.

4.2 Results and Discussion

4.2.1 Photoacid Generators (PAGs)

Four PAGs were investigated (Scheme 1): diphenyliodonium nitrate (DPIN); diphenyliodonium carboxylate monohydrate (DPIC); 8-hydroxypyrene-1,3,6-trisulfonic acid (HPTS) and dipotassium 2-naphthol-6,8-disulfonate hydrate (DPNDS).

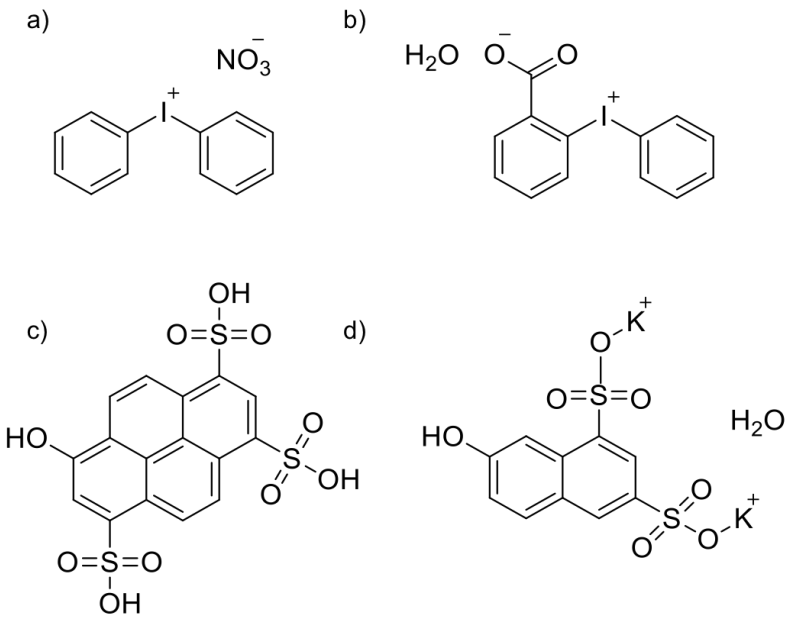

Scheme 1 Structures of photoacid generators (PAGs) a) DPIN b) DPIC c) HPTS and d) DPNDS

DPIN has been successfully demonstrated as a PAG which can induce hydrogelation upon UV irradiation. As previously mentioned in Section 3.1, DPIN causes alginate and pectin hydrogelation *via* the reaction of its resulting protons (upon UV irradiation) with calcium salt in the alginate or pectin solution.[8] DPIC has previously been used in the gelation of photorheological fluids, where UV irradiation results in the breakdown of DPIC to benzoic acid and iodobenzene, affording a drop in overall pH of solution. This allowed gelation of laponite nanoparticle/triblock copolymer (Pluronic F127) suspensions, where the kinetics of gelation were tunable upon alteration of concentrations of components and UV light intensity.[7, 13] HPTS, also known as pyranine, is a fluorescent dye used as a proton (or deuteron) producing, water-soluble reaction marker[14] or membrane-impermeant model drug molecule.[15-17] It has been effectively used to monitor the reaction dynamics of carbonic acid through the time-dependent decay of the photoacid and subsequent production of photobase *via* the IR markers produced from this reaction.[18] Along with HPTS, DPNDS is a hydrophilic photoacid generator that has also been used in the study of the reaction of carbonic acid in aqueous conditions due to its ability to rapidly transfer a single proton to HCO_3^-.[18]

Figure 1 shows the UV/vis spectra of the PAGs in pH 10 water. The λ_{max} of the DPIN is 284 nm; the wavelength of the lamp for irradiation of the PAG was 254 nm. Based on the available wavelengths of the lamp used and the concentrations of PAG added, no gelation occurred for samples containing HPTS or DPNDS when irradiated under UV light for the time required to successfully trigger gelation in samples containing DPIN (~14 hours). Irradiation times were also extended to 21 hours, however, successful gelation was still not achieved. Notably, HPTS contained a λ_{max} value at a much higher wavelength than that of the UV lamp. It is important to note that both DPNDS and HPTS were significantly diluted to measure the UV/vis spectra in water, compared to the concentration present in the gelation experiments. Both PAGs do show adsorption in the region close to the wavelength of the UV lamp, along with other adsorption peaks at higher wavelengths. These higher wavelength peaks could possibly be attributed to J-aggregates of the PAG molecules[19-21], which could be magnified at higher concentrations. In the case of HPTS however, this is deprotonated under alkaline conditions, affording the peak at 452 nm.[22]

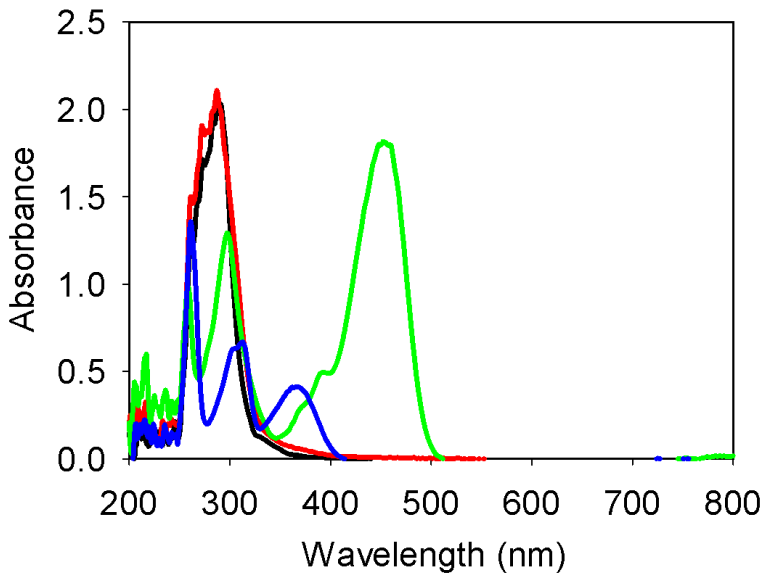

Figure 1 UV/vis spectra of the 4 PAGs in pH 10 water: DPIN (black), DPIC (red), HPTS (green) and DPNDS (blue). Both HPTS and DPNDS were diluted by a factor of 80 to measure UV spectra

These aggregated states perhaps hinder proton production under UV light resulting in a smaller drop in pH when compared to that produced by DPIN or DPIC.

Conversely, the intense peak at 452 nm in the spectrum of HPTS could also suggest that the mechanism by which HPTS generates protons must be reliant on visible light absorption at this wavelength, and not at 260 or 290 nm, where the other peaks are present.

Table 1 compares the pH values measured before and after UV irradiation for the different PAGs in BrNapAV (Scheme 2) solutions. Despite being similar in structure to DPIN, DPIC did not induce gelation. The reason for this is not known, but interaction between DPIC and gelator molecules may have inhibited the breakdown of the PAG to produce protons. DPIC was also not as soluble in water or gelator solution, which would have likely contributed to the problem.

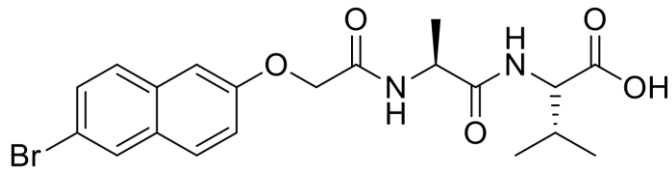

Scheme 2 Structure of the gelator BrNapAV

Table 1 shows the pH values measured for BrNapAV (Scheme 2) solutions irradiated with UV light for the same time period. A slight buffering effect was observed as the pH of each solution slightly dropped (~ 0.3 pH units) on addition of DPIN (Table 1). The drop in pH was more significant in gelator solutions containing HPTS and DPNDS, where the decrease in pH was more than 1 or 2 pH units from the original gelator solution (Table 1). Only DPIN provides a sufficient pH drop for self-assembly to occur.[23] Solutions containing the other PAGs were further irradiated, past the time taken for gelation to occur with DPIN, still with no successful gelation observed. In particular, the pH of BrNapAV containing HPTS remained constant even after 21 hours of UV irradiation. This could be expected based on the UV spectra (Figure 1), as previously mentioned. Only BrNapAV was screened here as our group has previously shown its proficiency to form transparent, homogeneous hydrogels by a variety of other self-assembly triggers.[24, 25] On the basis of the data presented above, the entirety of the remainder of this Chapter will focus on gels formed using DPIN.

PAG (1 equivalent)	Initial pH	pH After Addition of PAG	Solution	pH After UV Irradiation	Gel
DPIN	9.4	9.1	Transparent	5.4	Y
DPIC	9.4	8.9	Transparent	5.9	N
HPTS	11.5	7.9	Fluorescent yellow/green transparent	7.9	N
DPNDS	11.5	9.1	Transparent	7.5	N

Table 1 pH values of BrNapAV solutions before and after being irradiated with UV light (~ 14 hours for DPIN and ~21 hours for other PAGs) in the presence of various PAGs

From the literature[26], a suggested mechanism for the production of protons by DPIN describes the direct photolysis of DPIN by it absorbing a photon, which leads to an excited state. Heterolysis could next occur to give iodobenzene and a phenyl cation as the major products, or homolysis to afford an iodobenzene radical cation and phenyl radical as products, or intersystem crossing to the triplet state (Scheme 3). Homolysis could also take place here to give an iodobenzene radical cation and phenyl radical – both triplet state radicals. Recombination of iodobenzene-phenyl pairs could form a cyclohexadienyl cation (along with the possibility of the starting material), leading to the eventual formation of iodobiphenyls and the desired protons.[26] The anion counter to the diphenyliodonium salt is found to have no effect on the product distribution, suggesting the same photolysis mechanism for both DPIN and DPIC.

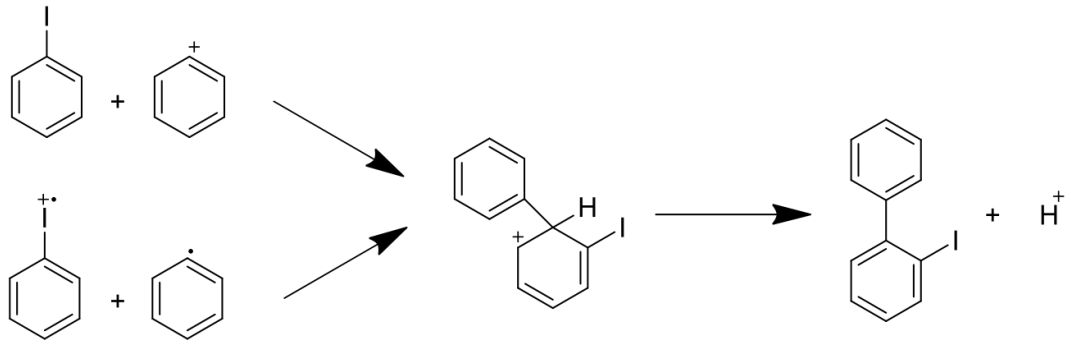

Scheme 3 Proposed mechanism for the photolysis of DPIN[26]

4.2.2 Hydrogel Preparation

Stock solutions at a concentration of 5 mg/mL were prepared for a range of gelators shown in Schemes 2 and 4. All of these gelators can form gels by using the GdL method[23, 25, 27] and their apparent pK_a values range from 5.5 – 7[23, 28] (Table 2). CNNapFF, 7MeONapFF and 2NapFF produced quite viscous solutions (as previously reported[29]), CNNapFF also formed a turbid solution. BrNapAV, 2NapAA, 2NapFF and FmocLG produced transparent solutions. When preparing the FmocLG solution, after dissolving at high pH (~ pH 10) the solution was lowered to around pH 7 – 8 (before adding the PAG) to avoid deprotection of the Fmoc group.[30] After dissolving the gelators in solution at pH 10, one molar equivalent of PAG was added to the solution and left to stir for up to an hour, until the PAG fully dissolved.

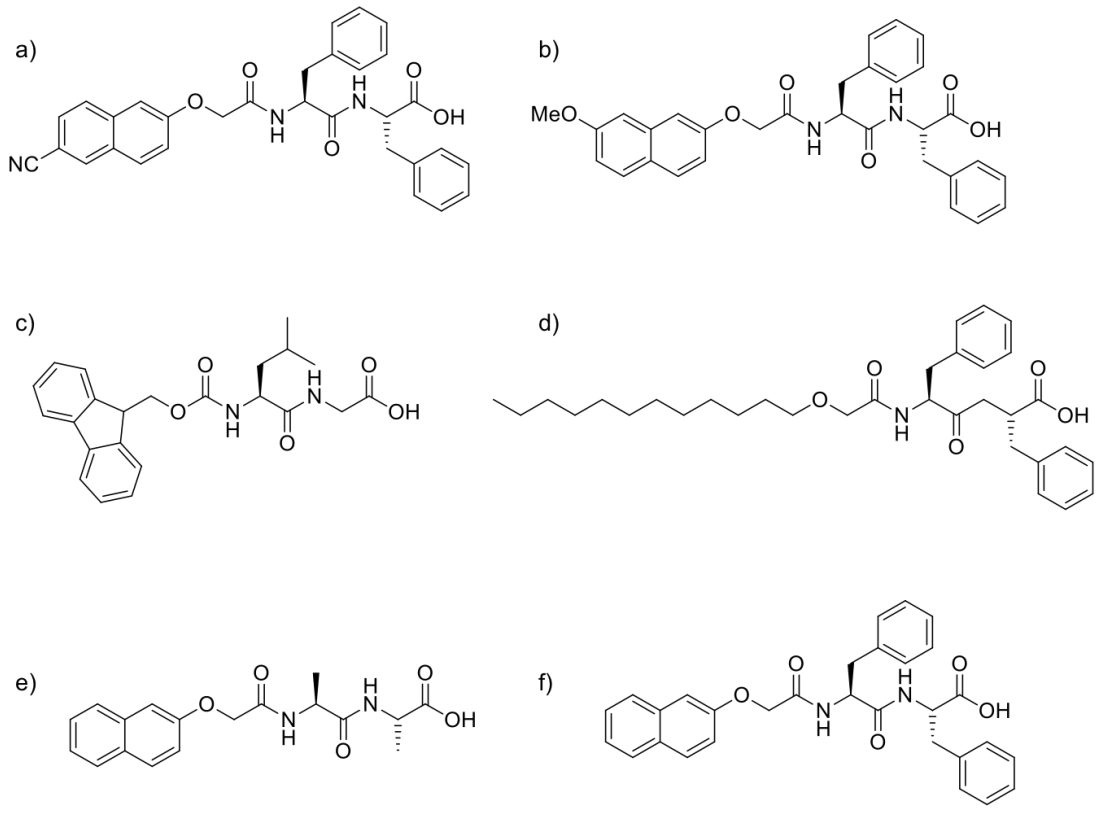

Scheme 4 Structures of the gelators a) CNNapFF b) 7MeONapFF c) FmocLG d) C12FF e) 2NapAA and f) 2NapFF

After PAG dissolution, each solution was still above the apparent pK_a of the gelator. After the addition of DPIN, turbid solutions were formed for all gelators except BrNapAV, FmocLG, 2NapAA and BrNapAG. The solutions were then irradiated for approximately 14 hours.

Gelator	pK_a	Initial pH	pH After Addition of PAG	Solution	pH After UV Irradiation	Gel
BrNapAV	5.8	9.4	9.1	Transparent	5.4	Yellow, transparent
CNNapFF	6.6	10.0	9.6	Turbid	6	Slightly turbid, yellow
7MeONapFF	7.0	9.7	9.4	Transparent, viscous	6.3	Very slightly turbid, yellow
FmocLG	5.5	7.4	6.8	Transparent	5	Very slightly turbid, yellow
C12FF	6.6	9.8	9.4	Turbid	6.2	Turbid, yellow
2NapAA	5.1	10.0	9.7	Transparent	4.7	Precipitate
2NapFF	6.0	10.4	9.9	Transparent, viscous	5.5	Precipitate
PAG Only	n/a	10.6	10.4	Transparent	3.1	n/a

Table 2 Physical properties of gels formed and the pH changes observed before/upon UV irradiation

No gelation (probed by inverting the vial[31] - where gelation was confirmed by a free-standing material which did not flow) was observed for shorter irradiation times. When DPIN was placed in water only and irradiated with UV light, a much lower final pH value (3.1) was achieved with the same irradiation time. Figure 2 shows that the kinetics of the pH change is much slower for DPIN in a solution of gelator than in solution alone.

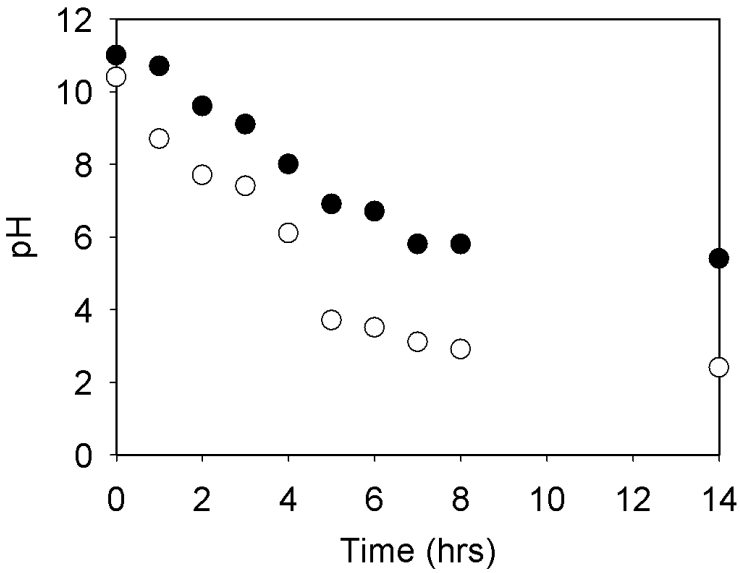

Figure 2 pH kinetics of BrNapAV with DPIN (•) and DPIN alone (○) when irradiated with UV light over time

Buffering effects of the gelator in the PAG solution are apparent. The pH kinetics displays a constant decrease in pH before becoming fairly constant around the pK_a (5.8) of BrNapAV. After 14 hours, the pK_a is just bypassed, leading to gelation. When there is no gelator present in the PAG solution, the pK_a of BrNapAV is reached and subsequently drops below this pH in under 4 hours. After irradiation, the gels appeared to have a slight orange colour (Figure 3), which was not apparent in gels prepared using GdL (Figure 3e). Such an evolution in colour could be attributed UV-initiated breakdown of the PAG to form another aromatic species.

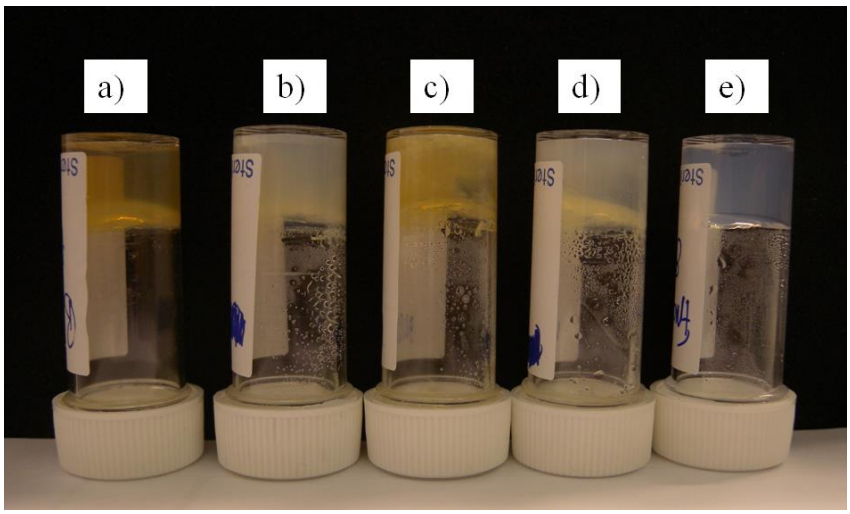

Figure 3 UV triggered gels of BrNapAV, CNNapFF, 7MeONapFF and FmocLG, respectively. e) FmocLG gel prepared using GdL

Figure 4 shows that upon UV irradiation of DPIN, the NMR spectrum shows the appearance of new peaks in the aromatic region of the spectrum. The original DPIN peaks are all still present. It is unclear as to what these new peaks could be attributed to exactly, but could possibly be the presence of the iodobiphenyl product suggested in the mechanism for the irradiation of DPIN (Scheme 3). This may attribute to the colour change observed upon irradiation. The colour is much more pronounced in the presence of gelator.

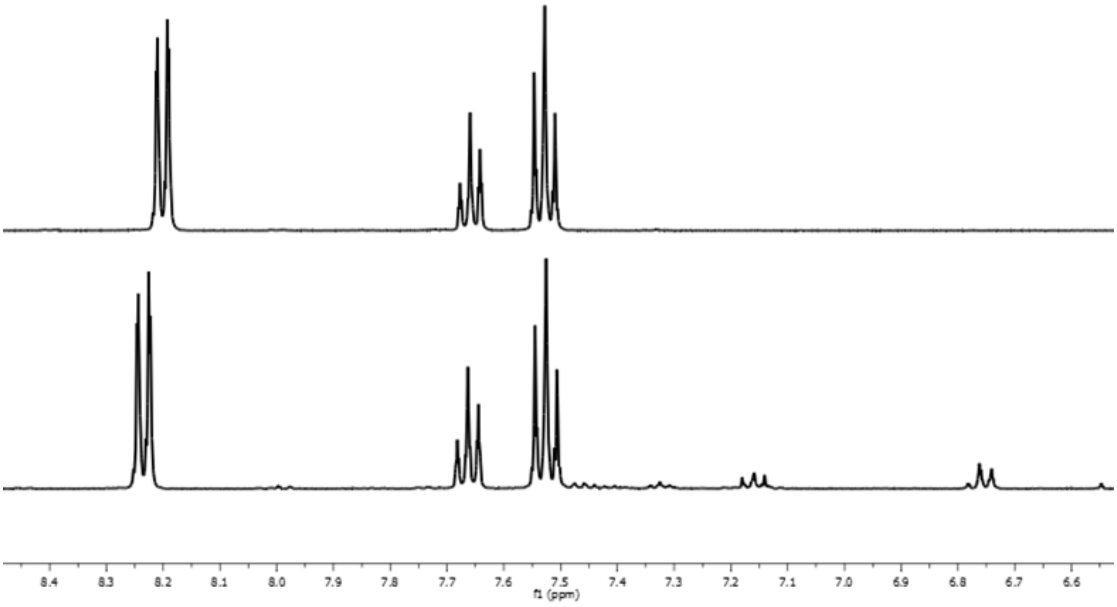

Figure 4 NMR Spectra of DPIN before UV irradiation (top) and after UV irradiation (bottom)

Once samples had been irradiated, the pH was measured again and those that formed gels were found to be at a pH below the apparent pK_a of that gelator. Conversely, those that did not form gels were found to be at a pH above their pK_a (Table 2).

Of the gelators that formed gels using one molar equivalent of DPIN, in solution, the pH reached was lower than the pK_a of the gelator (after the 14 hours irradiation time). In an attempt to achieve lower final pH values, higher molar equivalents of PAG were tried but solubility was an issue in these cases, with heterogeneous suspensions of the PAG and gelator being produced even after overnight stirring. The reason that pH values below the pK_a of some gelators are reached and not in all those gelators tested is not understood. The presence of gelator in solution has an effect on the proton generation as the final pH of the gels/solutions differs between

gelators which have been irradiated with UV light and ultimately differs from that of DPIN irradiated alone. In cases where self-assembled aggregates are already present at high pH (7MeONapFF and 2NapFF), where the DPIN is added, any inhibition could be heightened. Under the conditions studied, no gels are formed for gelators possessing a pK_a below 5.5. Interestingly, both 7MeONapFF and 2NapFF were also found to form gels in the presence of DPIN and the absence of UV light. 7MeONapFF and 2NapFF form gels *via* the GdL method[23] and *via* the addition of salts.[29, 32] The diphenylalanine chain of these gelator makes them quite hydrophobic dipeptide gelators[32, 33], with *log P* values of 2.79 and 2.76, respectively, resulting in the formation of worm-like micelles at high pH.[32] The cationic nature of DPIN may interact with 7MeOFF and 2NapFF such as in salt-triggered gelation[29], but the cation has much more steric bulk than a Ca^{2+} or Na^{+} in this case. Gelation occurs when the gelator solutions containing DPIN are left to stand and are not irradiated with UV light. This is not seen for the other gelators studied.

4.2.3 Hydrogel Characterisation

Rheological measurements were carried out to characterise those gelators that did produce hydrogels upon UV irradiation. The storage modulus (*G'*) measured was approximately an order of magnitude higher than the loss modulus (*G''*), which is indicative of a rigid hydrogel[23, 34-37] (Figure 5, 6 and Table 3).

	UV Gels			GdL Gels			Salt Gels		
Gelator	G' (Pa)	G'' (Pa)	pH	G' (Pa)	G'' (Pa)	pH	G' (Pa)	G'' (Pa)	pH
BrNapAV	6000	600	5.4	1300	100	5.3	-[b]	-[b]	-[b]
CNNapFF	2500	300	6.0	-[a]	-[a]	6.0	620	100	9.7
7MeONapFF	3100	200	6.3	150	50	6.2	3200	500	9.4
FmocLG	6100	900	5.0	1200	170	5.0	-[b]	-[b]	-[b]
C12FF	2200	400	7.7	620	140	7.5	-[c]	-[c]	-[c]
2NapFF	1700	200	5.5	1300	170	5.2	1400	200	9.9

Table 3 Rheological properties of gels formed *via* UV irradiation and using GdL and a salt-induced gelation, where DPIN is added and samples were left on the bench overnight (no UV irradiation) [a]gel too weak to be measured [b]no gelation occurred [c]crystallised

Notably, the *G'* values were much higher than the corresponding *G'* values of gels

produced by the GdL method (Table 3), with gels formed from CNNapFF using GdL being too weak to measure the rheological properties. The latter was considered to be a gel on the basis of the vial inversion test. This supports the argument that the self-assembly trigger affects the final gel properties.[38, 39] Stronger gels have been produced using the GdL method but these gels have much lower final pH values, giving rise to higher *G'* values i.e. the pH values of these gels are more significantly lower than the pK_a in comparison. Chen *et al.* have shown gels of BrNapAV and CNNapFF, prepared using GdL, with *G'* values of 25000 Pa and 15000 Pa, respectively, and final pH values of 3.4 ±0.2 for both. These gels are much stronger than BrNapAV (6000 Pa) and CNNapFF (2500 Pa) UV-triggered gels with the same final pH.[23]

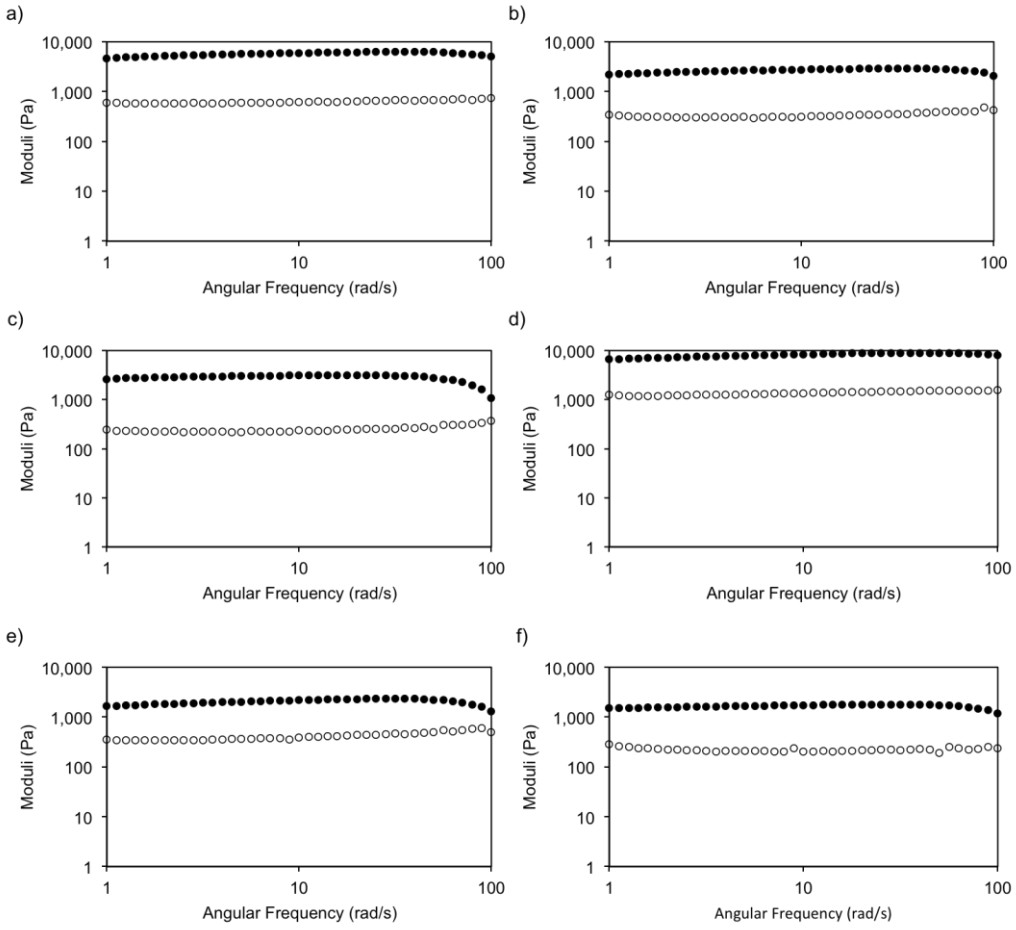

Figure 5 Frequency sweep measurements of hydrogels of a) BrNapAV b) CNNapFF c) 7MeNapOFF and d) FmocLG e) C12FF and f) 2NapFF (*G'* = ●, *G''* = ○)

Electrochemically-induced gelation (Chapter 5) of BrNapAV also shows different rheological properties still, with a *G'* of 5200 Pa measured for gels at pH 4. Adams *et al.* have previously reported FmocLG gels with substantially stronger rheological

properties than that of the UV-triggered FmocLG gels. The FmocLG gels produced using GdL were at pH 4 and had a *G'* of 196 kPa[40] – an order of magnitude higher than the UV-triggered equivalent (Figure 5 and Table 3). FmocLG gels produced by self-assembly triggered by changes in solvent (Chapter 3), in this case DMSO, give further variability in the rheological properties that can be produced by an individual gelator. These gels show *G'* values ranging from ~ 2000 to 10000 Pa; values differed depending on the volume fraction of DMSO in the hydrogel.[41] Clearly, the self-assembly process plays an important role in the final gel properties.[38, 39] Figure 6 shows the strain amplitude sweeps measured for the UV-triggered gels. These show the point at which the *G'* and *G''* deviate from linearity and hence, break down and become free-flowing liquids. All of the gels measured break down at approximately 10 % strain. This is similar behaviour to these gels of these gelators with other triggers.[25, 32, 41]

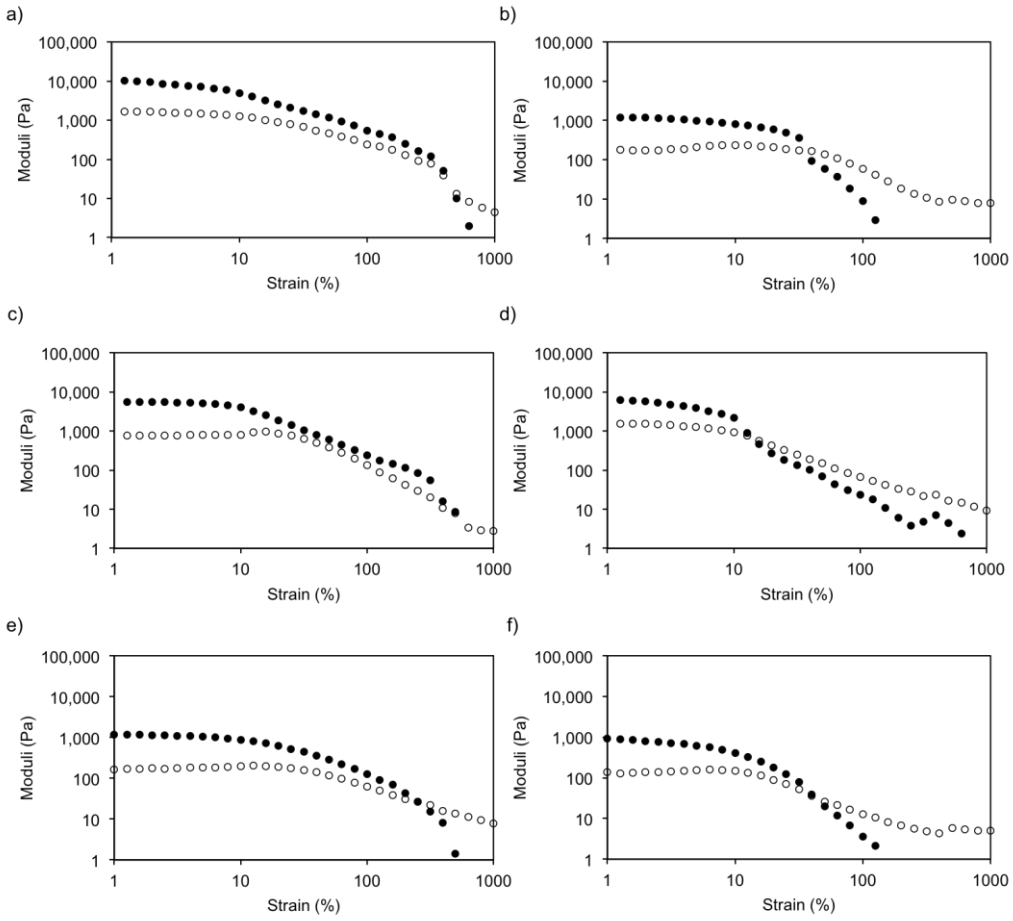

Figure 6 Strain sweep measurements of hydrogels of a) BrNapAV b) CNNapFF c) 7MeNapOFF and d) FmocLG e) C12FF and f) 2NapFF (*G'* = ●, *G''* = ○)

Figure 7 shows SEM images (collected by Dr Tom O. McDonald) of the four gels

formed *via* the UV trigger, with BrNapAV and 7MeONapFF showing dense fibrous networks with fibres measuring ~ 20 nm and ~ 10 nm in width, respectively. Despite these comparable fibril networks from SEM, BrNapAV gels produce a much higher *G'* than 7MeONapFF (6000 and 2200 Pa, respectively). BrNapAV gels formed using GdL have shown smaller fibril widths from TEM, where the widths measured were ~ 10 nm.[25] CNNapFF and FmocLG showed much wider fibres, measuring ~ 70 nm in width, giving the gels a turbid appearance in the bulk. Again, FmocLG produces much stronger gels than that of CNNapFF despite appearing to have a similar network from SEM. By inference of this data, there is no correlation between fibril width and rheological properties of the bulk gel for this set of gelators. These SEM images are of xerogel (dried in air) equivalents of the hydrogels and may, therefore, not be representative of the true hydrogel structure.

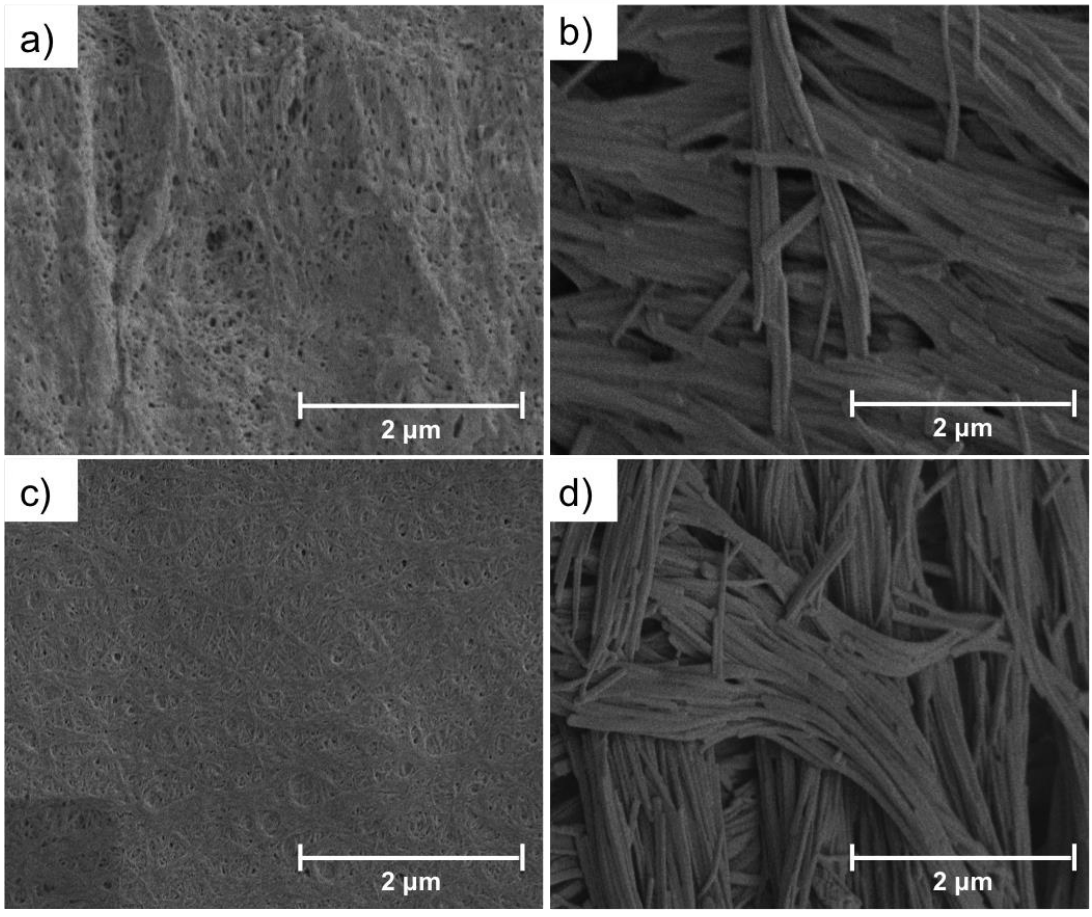

Figure 7 SEM images of a) BrNapAV b) CNNapFF c) 7MeONapFF and d) FmocLG hydrogels. Gels were dried in air overnight before imaging

Although the purpose of using DPIN was to produce hydrogels through the means of

a photoacid generator to produce protons, much like a pH trigger such as GdL or HCl, DPIN was also able to produce gels similar to that of salt-induced gelation.[29, 32] After adding DPIN to 7MeONapFF and 2NapFF solutions and leaving them to stand overnight, self-supporting gels were produced. As mentioned in section 4.2.2, these gelators form worm-like micelles at high pH and can form gels with divalent salts to produce gels with *G'* values in the kPa range.[29, 32]

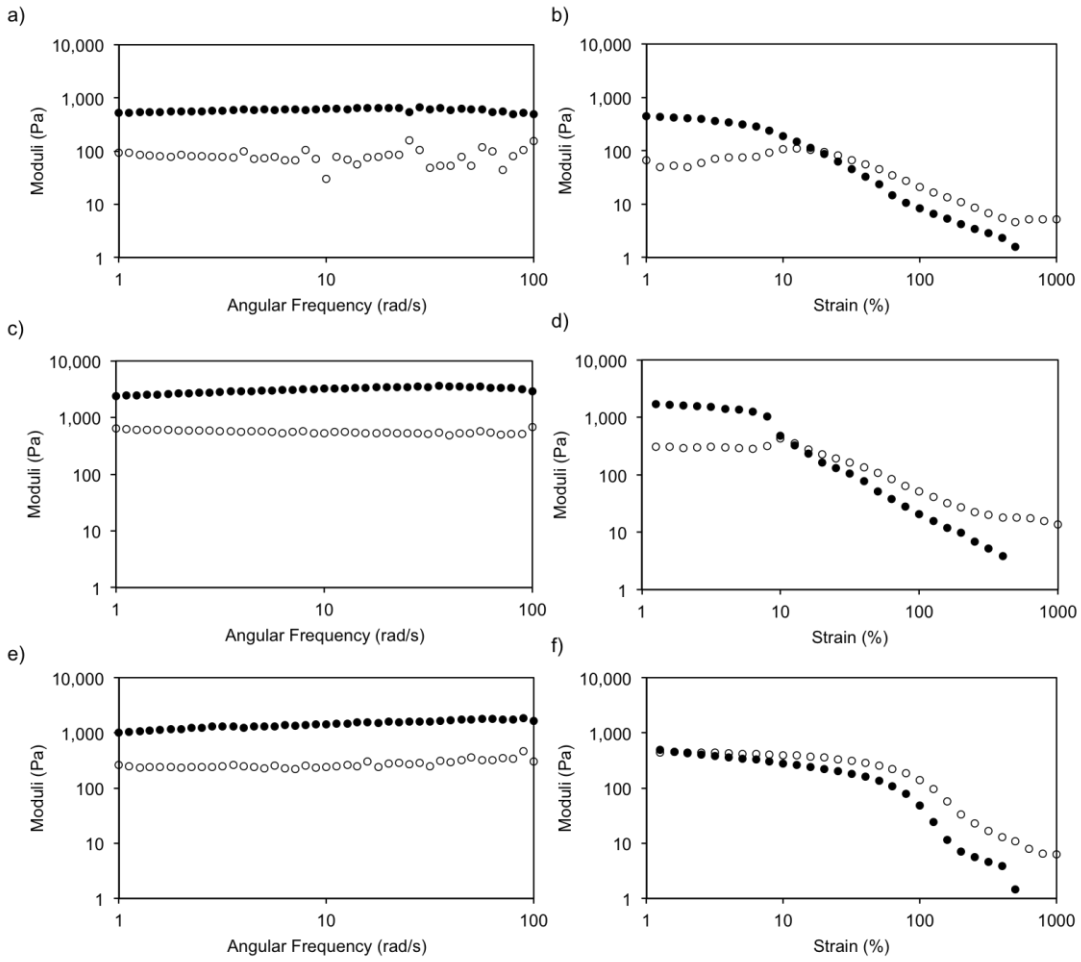

Figure 8 Rheological properties of gels produced *via* the addition of DPIN with no UV irradiation. 7MeONapFF: a) frequency sweep and b) strain sweep. 2NapFF: c) frequency sweep and d) strain sweep. CNNapFF: e) frequency sweep and f) strain sweep. (*G'* = ●, *G"* = ○)

Figure 8 shows the rheological properties of the gels produced with DPIN and no UV irradiation. The gels are weaker than UV-irradiated gels (Figure 5 and Table 3) and previously reported salt-induced gels, where CNNapFF and 2NapFF can produce gels at pH 11 with *G'* values of up to 23000 Pa and 95000 Pa, respectively, when the salt used is $Ca(NO_3)_2$.[29, 32] Chen *et al.* have also reported values for GdL gels of

CNNapFF and 2NapFF. The pH of these gels were 3.4±0.2 and the gels were found to be mechanically stronger in the case of CNNapFF but were conversely found to be weaker for 2NapFF gels.[23] The gels prepared from DPIN (and no UV irradiation) are also less rigid, with *G'* being less than an order of magnitude higher than *G"*, which is typical for gels produced by all other methods (as previously mentioned). The strain amplitude sweeps measured for both CNNapFF (Figure 8b) and 7MeONapFF (Figure 8d) show gelation breakdown at ~ 10 % strain, which is comparable to that of their counterpart gels prepared *via* UV irradiation of DPIN (Figure 6c). However, 2NapFF (Figure 8f) appears to break down at a much lower strain (~ 1 %) than that observed for 2NapFF gels (Figure 6f) prepared using UV irradiation (~ 10 %). Interestingly, the UV-initiated gels studied in this Chapter must go through a transition from a salt-induced hydrogel to a UV-triggered hydrogel. Although in the case of 7MeONapFF and 2NapFF, the storage moduli are very similar to the storage moduli after being irradiated with UV light, the loss moduli is slightly lower in salt-induced 7MeONapFF gels and the pH is significantly lower in both 7MeONapFF and 2NapFF UV-triggered gels.. Therefore a change in the hydrogel environment is apparent. In 2NapFF gels prepared using $Ca(NO_3)_2$, the transition from a high pH gel (salt-triggered) to a lower pH gel (GdL) results in increased mechanical strength, which is not seen here for 2NapFF gels (or 7MeONapFF).[29] This was observed for CNNapFF gels in this Chapter. The salt-induced gels (Figure 8) have final pH values akin to that of the solutions before UV-irradiation (9.7, 9.4 and 9.9, respectively), above their apparent pK_a values, but the UV-initiated gels have final pH values much lower (6, 6.3 and 5.5, respectively), below their apparent pK_a values. Therefore, a transition from that of a weak gel (Figure 8) to a mechanically rigid gel (Figure 5) is observed as the pH is lowered by the UV-irradiated breakdown of the PAG for CNNapFF only.

4.2.4 Photomask

A potential application for this assembly-method was suggested by demonstrating a photolithographic technique in which simple hydrogel patterning is employed by means of a photomask.

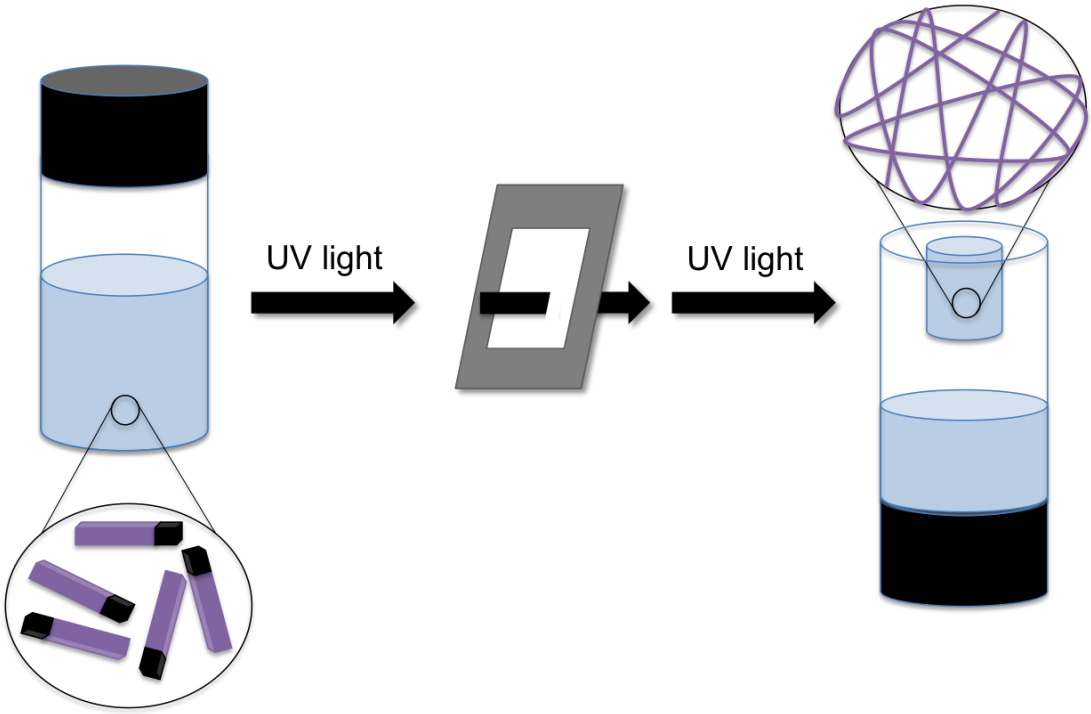

Figure 9 Schematic showing the self-assembly of a gelator, where self-assembly only occurs in the region that is exposed to UV light. This leads to a fibrous network and hydrogelation in the exposed region, while the region covered by the photomask remains as a solution

This opens up the possibility of using such materials in the future to make patterned channels of gels for use in microfluidics[42] and for use in biosensors[43] and synthetic biomaterials.[12] To demonstrate this, 7MeONapFF was chosen due to its higher pK_a, meaning shorter irradiation times would be required for gelation. A higher power (96 W) UV lamp was used to lower the irradiation time required for gelation to occur. Longer irradiation times may allow pH equilibration of the masked and non-masked regions, leading to bulk gelation. Firstly, gelation under the high power lamp was tested in the absence of a photomask. Hydrogelation was successful. Table 4 shows that the pH of the gel was just below the pK_a of the gelator, as seen with the lower power lamp (40 W). Gelation had occurred after ~ 3 hours, with slightly yellow, turbid gels produced. The UV light was then passed through a specific region of the solution of gelator/PAG, with the rest being covered by a photomask (Figures 9 and 10). The solution was irradiated for ~ 3 hours. Despite the mechanical properties being constant between both the salt triggered and UV-triggered phases of 7MeONapFF, spatially resolved gelation with a UV mask was possible, indicating that there must be a distinction between the UV-triggered and salt-induced self-assembly processes to allow the UV-triggered process to dominate here.

Gelator	pK_a	Initial pH	pH After 1 hr	pH After 2 hrs	pH After 3 hrs	Gel
7MeONapFF	7.0	10.0	8.9	7.3	6.3	Turbid

Table 4 Gelator properties and pH changes with time of a 7MeONapFF gelator solution (containing DPIN) irradiated using a higher power lamp

Some shrinkage of the gel phase was observed, ascribed to syneresis - as noted elsewhere for some dipeptide gelators.[40] Gelation only occurred in the region exposed to the UV light. The pH of the gel phase and solution phase were both measured. The pH of the gel phase (6.3) was below the pK_a of the gelator. The solution pH was also lower (~ 6.9 – 7) than the initial state (presumably due to diffusion), but not below the pK_a of the gelator.

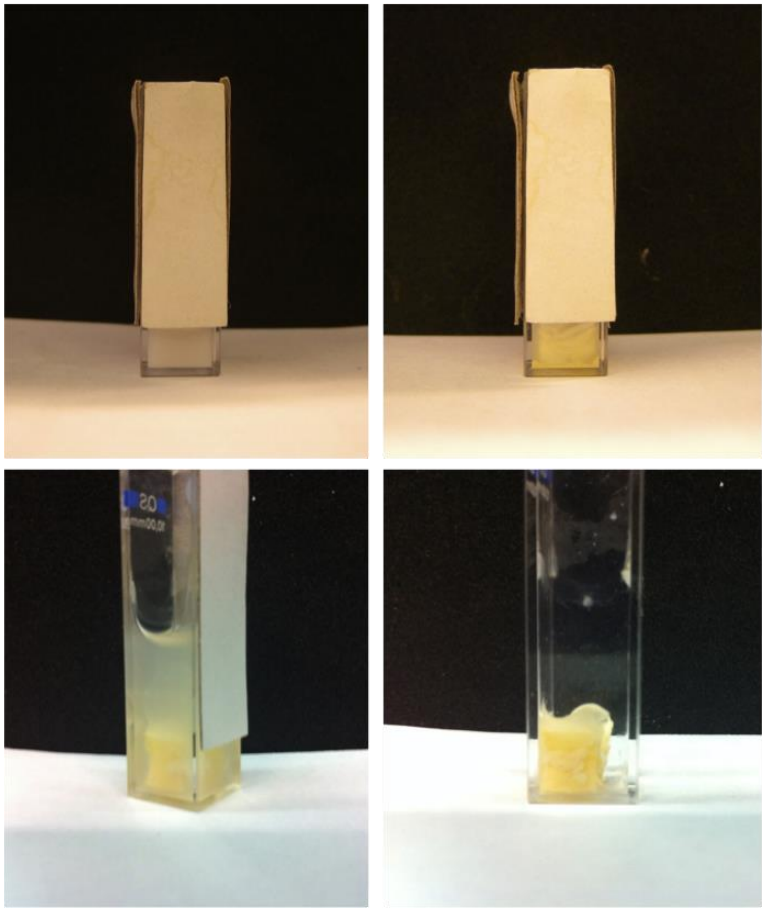

Figure 10 Stages of gel formation in the presence of UV mask. From top left to right – Solution of 7MeONapFF and PAG before UV irradiation; after UV irradiation; removal of mask shows only gelation of the exposed region occurs; liquid removed – slight syneresis of gel.

4.3 Conclusion

It has been demonstrated that rigid hydrogels can be formed for a number of dipeptide derivatives by utilising a PAG coupled with UV irradiation. This method provides a new approach to lowering the pH of the solution of these materials below their apparent pK_a to induce self-assembly into fibrous networks and produce a hydrogel. Hydrogels produced by this method displayed bulk properties comparable to similar hydrogel materials made by adopting other self-assembly triggers. We have also shown that photopatterning of such materials is possible by adopting simple photolithography to produce region-specific gelation. It would be valid to anticipate that this will be of use in the generation of patterned surfaces and thin films, for example, for use in microfluidic bioanalysis such as to operate as valves within a microfluidic channel to create autonomous "lab-on-a-chip" systems[44] or in the production of complex, patterned hydrogel surfaces with topographies and multiple gel properties tunable to suit cell attachment and proliferation.[12]

4.4 References

1. J. W. Lee, S. Y. Kim, S. S. Kim, Y. M. Lee, K. H. Lee and S. J. Kim, *J. Appl. Polym. Sci.*, 1999, **73**, 113-120.
2. A. I. Van Den Bulcke, B. Bogdanov, N. De Rooze, E. H. Schacht, M. Cornelissen and H. Berghmans, *Biomacromolecules*, 2000, **1**, 31-38.
3. W. A. Petka, J. L. Harden, K. P. McGrath, D. Wirtz and D. A. Tirrell, *Science*, 1998, **281**, 389-392.
4. J. P. Schneider, D. J. Pochan, B. Ozbas, K. Rajagopal, L. Pakstis and J. Kretsinger, *J. Am. Chem. Soc.*, 2002, **124**, 15030-15037.
5. X. Li, Y. Gao, Y. Kuang and B. Xu, *Chem. Commun.*, 2010, **46**, 5364-5366.
6. T. Muraoka, C.-Y. Koh, H. Cui and S. I. Stupp, *Angew. Chem. Int. Ed.*, 2009, **48**, 5946-5949.
7. K. Sun, R. Kumar, D. E. Falvey and S. R. Raghavan, *J. Am. Chem. Soc.*, 2009, **131**, 7135-7141.
8. V. Javvaji, A. G. Baradwaj, G. F. Payne and S. R. Raghavan, *Langmuir*, 2011, **27**, 12591-12596.
9. V. Liu and S. Bhatia, *Biomed. Microdevices*, 2002, **4**, 257-266.
10. A. Revzin, R. G. Tompkins and M. Toner, *Langmuir*, 2003, **19**, 9855-9862.
11. K. Tamaki, T. Utaka, H. Takase, Y. Eriyama and T. Ukachi, *J. Photopolym. Sci.* 2002, **15**, 103-108.
12. A. Mata, L. Hsu, R. Capito, C. Aparicio, K. Henrikson and S. I. Stupp, *Soft Matter*, 2009, **5**, 1228-1236.
13. K. A. Juggernauth, A. E. Gros, N. A. K. Meznarich and B. J. Love, *Soft Matter*, 2011, **7**, 10108-10115.
14. M. Rini, D. Pines, B.-Z. Magnes, E. Pines and E. T. J. Nibbering, *J. Chem. Phys.*, 2004, **121**, 9593-9610.
15. Y. Nagai, L. D. Unsworth, S. Koutsopoulos and S. Zhang, *J. Control. Release*, 2006, **115**, 18-25.
16. J.-C. Leroux, E. Roux, D. Le Garrec, K. Hong and D. C. Drummond, *J. Control. Release*, 2001, **72**, 71-84.
17. K. E. Beauregard, K.-D. Lee, R. J. Collier and J. A. Swanson, *J. Exp. Med.*, 1997, **186**, 1159-1163.
18. K. Adamczyk, M. Prémont-Schwarz, D. Pines, E. Pines and E. T. J. Nibbering, *Science*, 2009, **326**, 1690-1694.
19. M. Reers, T. W. Smith and L. B. Chen, *Biochemistry*, 1991, **30**, 4480-4486.
20. E. E. Jelley, *Nature* 1936, **138**, 1009-1010.
21. R. Alicante, Springer, Berlin Heidelberg, 2013.
22. G. Velásquez, M. S. Ureta-Zañartu, C. López-Alarcón and A. Aspée, *J. Phys. Chem. B*, 2011, **115**, 6661-6667.
23. L. Chen, S. Revel, K. Morris, L. C. Serpell and D. J. Adams, *Langmuir*, 2010, **26**, 13466-13471.
24. K. L. Morris, L. Chen, J. Raeburn, O. R. Sellick, P. Cotanda, A. Paul, P. C. Griffiths, S. M. King, R. K. O'Reilly, L. C. Serpell and D. J. Adams, *Nat. Commun.*, 2013, **4**, 1480-1485.
25. L. Chen, K. Morris, A. Laybourn, D. Elias, M. R. Hicks, A. Rodger, L. Serpell and D. J. Adams, *Langmuir*, 2010, **26**, 5232-5242.
26. J. L. Dektar and N. P. Hacker, *J. Org. Chem.*, 1990, **55**, 639-647.
27. D. J. Adams, M. F. Butler, W. J. Frith, M. Kirkland, L. Mullen and P. Sanderson, *Soft Matter*, 2009, **5**, 1856-1862.
28. J. Raeburn, T. O. McDonald and D. J. Adams, *Chem. Commun.*, 2012, **48**, 9355-9357.
29. L. Chen, G. Pont, K. Morris, G. Lotze, A. Squires, L. C. Serpell and D. J. Adams, *Chem. Commun.*, 2011, **47**, 12071-12073.

30. A. K. Tickler, C. J. Barrow and J. D. Wade, *J. Pept. Sci.*, 2001, **7**, 488-494.
31. R. G. Weiss, Terech, P., *Molecular Gels and Fibrillar networks – A Comprehensive Guide to Experiment and Theory*, Springer, Dordrecht, The Netherlands, 2006.
32. L. Chen, T. O. McDonald and D. J. Adams, *RSC Adv.*, 2013, **3**, 8714-8720.
33. C. Tang, A. M. Smith, R. F. Collins, R. V. Ulijn and A. Saiani, *Langmuir*, 2009, **25**, 9447-9453.
34. Z. Yang, G. Liang, M. Ma, Y. Gao and B. Xu, *J. Mater. Chem.*, 2007, **17**, 850-854.
35. S. Sutton, N. L. Campbell, A. I. Cooper, M. Kirkland, W. J. Frith and D. J. Adams, *Langmuir*, 2009, **25**, 10285-10291.
36. A. M. Smith, R. J. Williams, C. Tang, P. Coppo, R. F. Collins, M. L. Turner, A. Saiani and R. V. Ulijn, *Adv. Mater.*, 2008, **20**, 37-41.
37. A. Mahler, M. Reches, M. Rechter, S. Cohen and E. Gazit, *Adv. Mater.*, 2006, **18**, 1365-1370.
38. J. Raeburn, G. Pont, L. Chen, Y. Cesbron, R. Levy and D. J. Adams, *Soft Matter*, 2012, **8**, 1168-1174.
39. J. Raeburn, A. Zamith Cardoso and D. J. Adams, *Chem. Soc. Rev.*, 2013, **42**, 5143-5156.
40. D. J. Adams, L. M. Mullen, M. Berta, L. Chen and W. J. Frith, *Soft Matter*, 2010, **6**, 1971-1980.
41. L. Chen, J. Raeburn, S. Sutton, D. G. Spiller, J. Williams, J. S. Sharp, P. C. Griffiths, R. K. Heenan, S. M. King, A. Paul, S. Furzeland, D. Atkins and D. J. Adams, *Soft Matter*, 2011, **7**, 9721-9727.
42. M. Backer, M. Raue, S. Schusser, C. Jeitner, L. Breuer, P. Wagner, A. Poghossian, A. Forster, T. Mang and M. J. Schoning, *Phys. Status Solidi. A-Appl. Mat.*, 2012, **209**, 839-845.
43. O. Andersson, A. Larsson, T. Ekblad and B. Liedberg, *Biomacromolecules*, 2009, **10**, 142-148.
44. L. Dong and H. Jiang, *Soft Matter*, 2007, **3**, 1223-1230.

CHAPTER 5

Electrochemically-Triggered Spatially and Temporally-Resolved Multi-Component Hydrogels

5.1 Introduction

Hydrogelation of low molecular weight gelators (LMWG) can be triggered by many stimuli.[1-4] In the majority of cases, gelation occurs upon the addition of the trigger and occurs homogeneously throughout the solution. Hence, temporal control is possible (i.e. by when the trigger is applied), but spatial control is often difficult due to thermal and chemical diffusion. Previously, gelation has been triggered in specific locations within a solution of LMWG using a photoacid and an optical mask (Chapter 4).[5] Similarly, masks have been used to photodegrade specific regions within a gel,[6] making use of the reversibility of the network. Lithographic approaches have also been used to generate patterned areas of gel on a surface.[7] Immobilisation of an enzyme on a surface can be used to spatially gel some LMWG; gelation only occurs where the enzyme is located.[8] One method which demonstrates through use of a high molecular weight gelator, spatial control over the formation of biopolymer gels is electrodeposition, where a pH gradient is generated electrochemically relative to the electrode surface.[9-16] Biopolymers such as chitosan that respond to a change in pH then assemble locally, forming a gelled region on the electrode. The majority of the biopolymer remains free in solution. In 2010, Johnson *et al.* showed that a similar approach could be used to locally form very thin gel layers (on the order of tens of nanometres) on an electrode surface using a dipeptide-based LMWG *via* a pH trigger.[17] Liu *et al.* showed similar results for an amino acid-based LMWG.[10, 18] This approach is very appealing in that it allows both spatial and temporal control over the gelation of LMWG. Such control is a desirable prospect as patterned hydrogel surfaces can be used to manipulate cell growth, making them an important and emerging area in biomaterials research.[19, 20] An electrodepositioning approach can be advanced for the preparation of spatially-resolved dipeptide hydrogels on a larger scale than previously reported by Johnson *et al.*[17] In the majority of cases, LMWGs are studied as single components and are assumed to be homogeneously distributed throughout the solvent. There are few examples describing the mixing of two LMWG[21] (although there are specific systems which only form a gel when two components are present[22-24]). For the first time, fine

control over the chemical composition of the gels is displayed, allowing access to uniquely controlled gel structures. Here, gelation utilises an electrochemically-induced pH drop to assemble the LMWG at the electrode surface.

5.2 Results and Discussion

A number of functionalised naphthalene-based dipeptide LMWG have been shown to form gels at a concentration of 5 mg/mL when the pH of the solution is lowered below the apparent pK_a of the C-terminus.[2, 5, 25] This pH decrease has been demonstrated previously using glucono-δ-lactone (GdL) to induce gelation by yielding gluconic acid from the hydrolysis of GdL in water.[26] This method led to gelation of the bulk solution – with homogeneous gels produced due to the slow hydrolysis of GdL. Here, it is demonstrated that gelator solutions containing NaCl and hydroquinone (HQ) (0.1 M and 0.065 M, respectively) can lead to localised gel formation by way of electrochemical oxidation of hydroquinone at an electrode surface. Johnson *et al.* have previously shown that hydroquinone can be used to produce thin membrane hydrogels of FmocLG.[17] HQ is oxidised to 1,4-benzoquinone and two protons, leading to surface-induced gelation *via* a pH switch. The LMWG is solubilised at high pH and upon oxidation of HQ, the pH is lowered at the surface of the electrode where gel growth occurs when the pH is lowered below the pK_a. The gelators studied in this chapter have apparent pK_a values ranging from 5 – 7.

5.2.1 Cyclic Voltammetry (CV)

As mentioned above, HQ is oxidised to liberate protons (forming benzoquinone), resulting in gelation of the LMWG. Cyclic voltammetry was used to demonstrate that under the conditions used to produce hydrogels, HQ is the only material in solution being oxidised within the potential range observed. Throughout this chapter, a conventional three-electrode system was used for all electrochemical experiments, where the working electrode (where gelation occurred) was either a glassy carbon electrode or fluorine-doped tin oxide-coated (FTO) glass slide (discussed in Section 5.2.6 onwards). Voltammetric measurements were run for solutions of HQ (and NaCl) only and gelator plus HQ (and NaCl). These measurements were also repeated

in the absence of NaCl as a control. Figures 1a shows a cyclic voltammogram (CV) of HQ in the presence of NaCl, with a distinct oxidation peak at 0.75 V (versus a standard calomel electrode) for the oxidation of HQ in water (containing NaCl) and the subsequent two-electron reduction wave on the reverse sweep after the oxidation of HQ. Cycles of this measurement showed no new or diminished redox peaks, demonstrating that the oxidation product of HQ (i.e. *p*-benzoquinone) can combine with the protons in solution within the time limits of the experiment.[27] An excess of HQ molecules in solution compared to the number of molecules used up in cyclic voltammetry means that the bulk HQ concentration will hardly change after many CV cycles; giving rise to the consistent voltammograms. Figure 1b shows a CV of a gelator solution (BrNapFV – structure shown in Scheme 1j) containing HQ but no NaCl. A negligible current is produced with no distinct peak observed, compared to that of the CV of HQ in Figure 1a. Figure 1c shows a voltammogram of a BrNapFV solution containing HQ and NaCl. Figure 1c shows a voltammogram similar to that in 1a – where the oxidation peak of HQ is clearly visible in the presence of gelator, with the gelator appearing to have little to no effect on the oxidation of HQ. On this basis, it can be deduced that the LMWG is not oxidised under the conditions tested. This would suggest that LMWG gelator remains in its unchanged, deprotonated state, meaning that protonation of the carboxylate group is possible (upon HQ oxidation); which is a necessity for self-assembly of the LMWG. The oxidation peak of HQ has slightly shifted to 0.82 V in the presence of gelator, however, this is likely due to slight variability in the pH between solutions.[28]

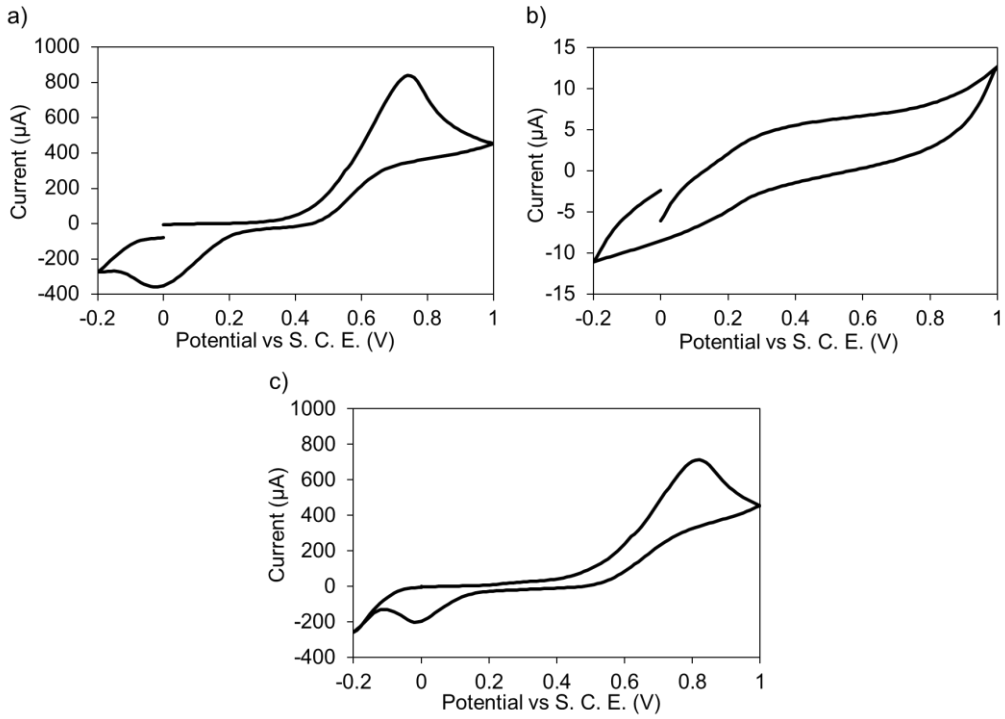

Figure 1 Cyclic voltammograms of a) HQ and NaCl solution b) BrNapFV solution containing NaCl and c) BrNapFV solution containing both NaCl and HQ. Measured using glassy carbon as the working electrode All CVs were measured at a scan rate of 40 mV/s

This is supported by the CVs in Figure 2. These show that for BrNapFV, when the pH of solution is changed, the oxidation peak of HQ shifts. When the stock solution pH is 7, the oxidation peak occurs at 0.77 V, the peak then shifts to 0.82 V for a pH 8 stock solution (all solutions throughout this chapter are at pH 8) and for a stock solution at pH 9, the oxidation peak slightly shifts to 0.91 V.

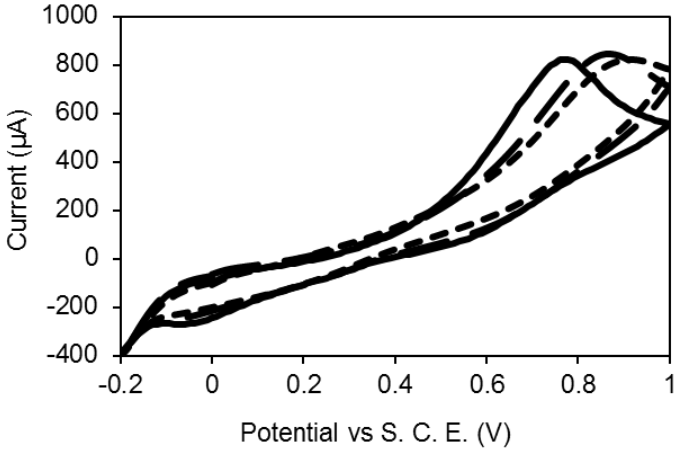

Figure 2 CVs of BrNapFV at pH 7 (—), pH 8 (– –) and pH 9 (- -)

CV measurements were run on a small library of functionalised dipeptides to investigate the relationship (if any) between the gelator and hydroquinone. More specifically, we investigated if the HQ oxidation peak shifts or disappears in the presence of specific gelators or if HQ is oxidised and produces the same CV profile regardless of the gelator used. The structures of all of the gelators studied throughout this Chapter are shown in Scheme 1.

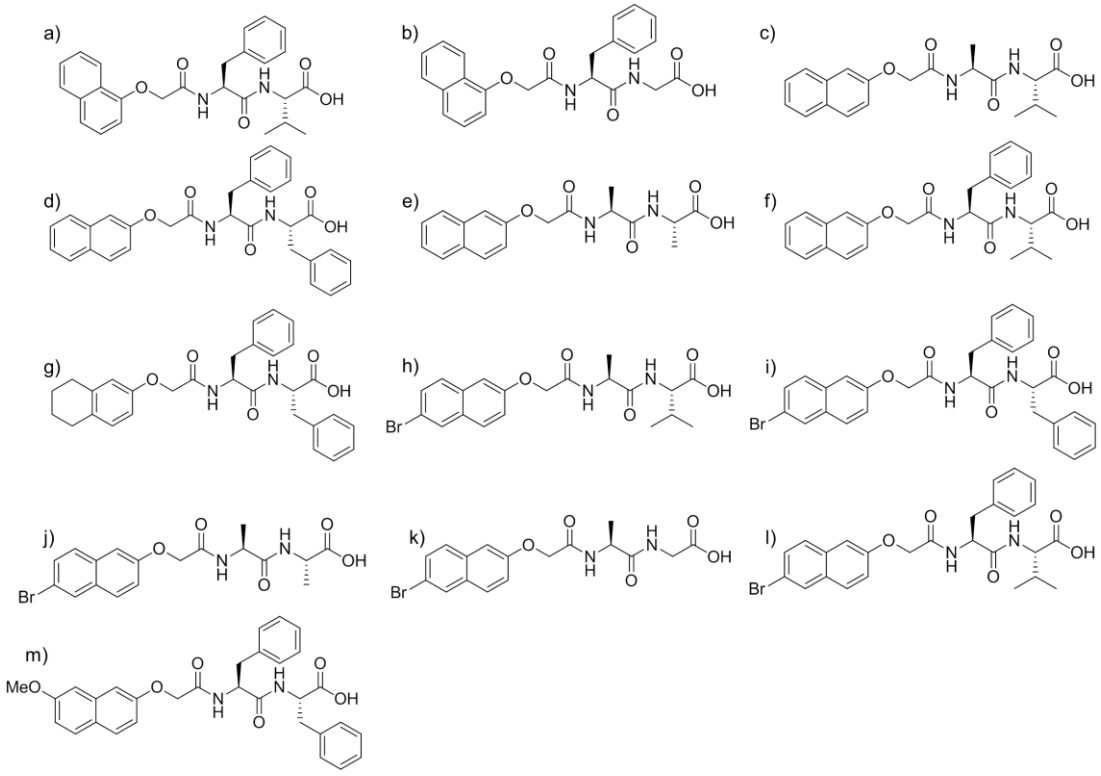

Scheme 1 Chemical structures of a) 1NapFV b) 1NapFG c) 2NapAV d) 2NapFF e) 2NapAA f) 2NapFV g) ArFF h) BrNapAV i) BrNapFF j) BrNapAA k) BrNapAG l) BrNapFV and m) 7MeONapFF

Functionalised dipeptides that formed gels upon application of a current (with HQ) could also form gels using GdL to lower the pH. The CVs of those gelators that formed gels all displayed a CV profile and resulting oxidation peak concordant with that observed for the oxidation of HQ in water (Figure 1a) - such as that in Figure 1c. The oxidation peak of HQ shifted slightly between 0.72 V and 0.95 V in those samples that formed gels, likely due to slight variability between the gelator stock solutions when the pH of each solution was manually adjusted to pH 8 (shown in Figure 2). Table 1 shows that of all the gelators tested, there is a correlation between gelation *via* GdL and electrochemical methods. Of the materials tested that did not

form gels, this 'negative' result was apparent for both electrochemical and GdL methods, except for 2NapAV. However, electrochemically produced 2NapAV gels were unstable and irreproducible. 2NapFV does not form gels by either of the aforementioned methods. The reason why these two materials do not produce gels by these methods is not currently understood. The CVs show oxidation peaks with currents of up to 1000 μA produced. Throughout the rest of this Chapter, only those materials which could form gels upon application of a current were studied further.

Gelator	Oxidation Peak (V)	Current Produced upon Oxidation (μA)	Gel	Gel (using GdL)
1NapFV	0.72	850	Y	Y[b]
2NapAV	0.52	18	Y[a]	N[b]
2NapFF	0.81	290	Y	Y[b]
2NapAA	0.95	590	Y	Y[b]
2NapFV	0.41	5.4	N	N[b]
ArFF	0.80	330	Y	Y[c]
BrNapFV	0.82	710	Y	Y[b]
BrNapAG	0.93	690	Y	Y[b]

Table 1 CV properties of a subset of gelators and comparison between gelation *via* electrochemical or GdL methods. Measured using glassy carbon as the working electrode. [a]2NapAV produced irreproducible, unstable gels. [b]Rheological properties measured previously[2, 25, 29] [c]ArFF was defined as a gel *via* a positive vial inversion test[30]

5.2.2 Hydrogelation using a Glassy Carbon Working Electrode

As previously mentioned, the formation of electrochemically-induced hydrogels utilises a three-electrode system. Here, the glassy carbon working electrode provides a surface for spatially-resolved gel formation. HQ is oxidised at the surface of the

glassy carbon electrode and, given the rate of formation of protons at the electrode surface and diffusion coefficient of the free protons, a localised pH drop at the electrode surface is produced.[17] For other pH triggered methods, using these types of materials, gelation does not occur until the pH drops below the pK_a of the LMWG.[5, 25, 26, 31] Here, when the local pH drops, a gel forms at the surface of the electrode. This process is shown schematically in Figure 2a.

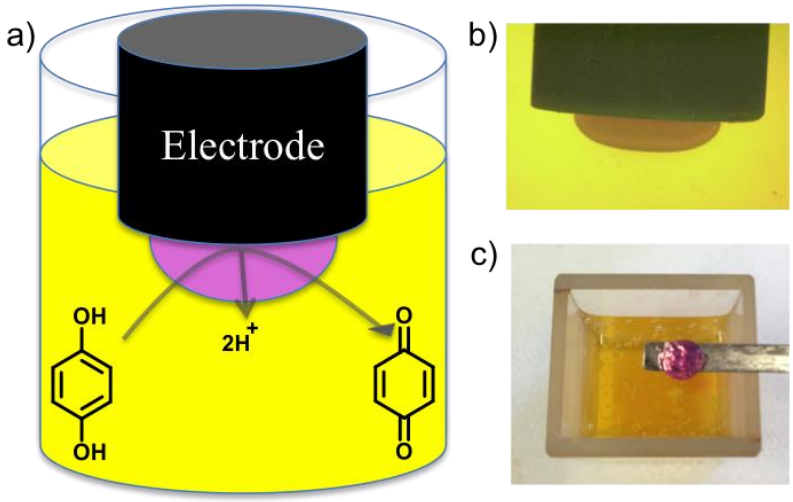

Figure 2 Schematic showing hydrogelation at a glassy carbon electrode surface as a consequence of hydroquinone oxidation. b) Adding Methyl Red allows visualisation of the gel (low pH, pink) from bulk solution (high pH, yellow) and c) shows the gel removed from the electrode using a spatula

It is important to note that bulk gelation does not occur, and that a gelling front is seen to move away from the electrode surface. To visualise the localised pH change in solution, Methyl Red (pK_a ~ 5.0[32]) was added as an indicator. The bulk solution was yellow in colour indicative of pH = 8, whilst on the application of a current, the gel turned pink (Figure 2a - c) indicating that in this specific case, the pH of the gel was lower than ~ pH 4.4 (confirmed on larger samples using a pH probe). The LMWG used here all have apparent pK_a values higher than 4.4 and hence form gels. No gradient in colour was observed, suggesting that the pH within the gel is uniform. This is similar to the sharp pH interface observed in electrodeposited chitosan gels, where a distinct region of pH 10 electrodeposited gel was observed to be well-defined from the surrounding pH 5.3 solution.[33]

It is possible to more finely control the gelation process. Using a galvanostatic measurement approach (i.e. constant current for a set time), the final gel volume could be controlled. As the current supplied is increased, the faster the HQ oxidation occurs and therefore the supply of protons at the electrode surface is both increased and produced more quickly. Ultimately, the gelation kinetics can be controlled. To demonstrate this, two gelators were chosen based on their significantly different apparent pK_a values (Scheme 1). However, it is important to note that this methodology is not restricted to these gelators, but can be applied to all gelators displayed in Table 1 that were shown to form gels. BrNapFV has a pK_a of 6.6 and 2NapAA has a pK_a of 5.0. For BrNapFV, using currents from 5 to 100 μA (current densities of 0.7 to 14.2 A/m^2 respectively) for a set duration of 1000 s, it can be seen that gelation occurred across all of these currents (Figure 3), with increased volumes of gel formed at the higher currents. Clearly, the increase in current results in increased proton concentration, leading to more hydrogel being formed.

Figure 3 Photographs of gels of BrNapFV grown on glassy carbon electrodes at different currents: (from left to right) 5 μA, 20 μA, 40 μA, 60 μA, 80 μA. All gels were grown for 1000 s. The scale bar applies to all images shown

Figure 4 shows the parallel growth of two gels formed from BrNapFV, where the size difference in gels produced by different currents is more easily visualised. Hence, by using multiple electrodes in the same gel solution, it is possible to spatially position different regions of gel, if required, with different sizes and properties.

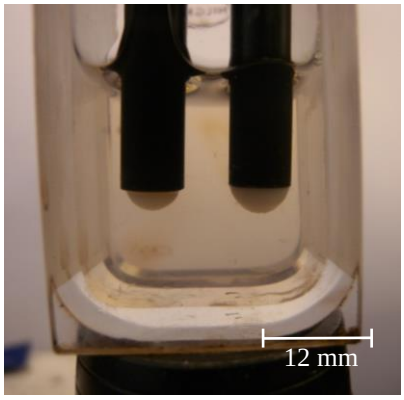

Figure 4 Two BrNapFV gels grown in parallel on two electrodes with different currents applied

Experiments were also carried out using the more hydrophilic 2NapAA. For this gelator it was evident that no gelation occurred when the current was set to 5 or 10 μA for 1000 s. From the BrNapFV potentiometric data it was clear that these currents were sufficient for the oxidation of HQ. Hence, the number of protons produced at these currents must not be sufficient enough to reach a pH below the apparent pK_a of 2NapAA. Figure 5 shows the hydrogels of 2NapAA grown from different currents. By visual comparison of the gel images in Figures 3 and 5, the hydrogels of 2NapAA are notably smaller than that of the corresponding BrNapFV gels.

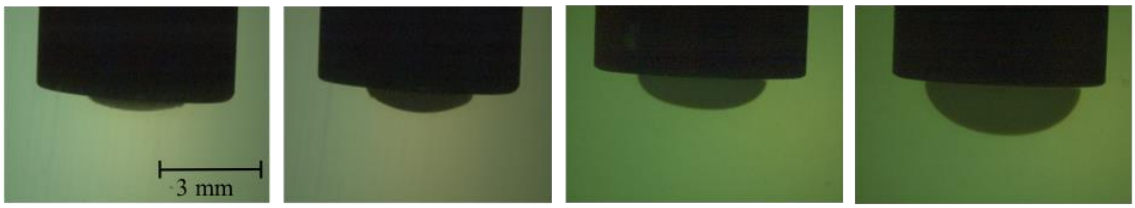

Figure 5 Photographs of gels of 2NapAA grown on glassy carbon electrodes at different currents: (from left to right) 20 μA, 40 μA, 60 μA, 80 μA. All gels were grown for 1000 s. The scale bar applies to all images shown

5.2.3 Quantitative Hydrogel Analysis *via* an Automated Gel Measuring Program

Dynamic gel growth was monitored and the sequential images analysed, allowing quantitative measurements of the gels with respect to the current applied. A program devised by Dr Jon Howse (University of Sheffield) made this possible. The program,

firstly, required the dimensions of the electrode and final gel size to be marked out by uploading the series of images collected (Figure 6a). The program was set up to monitor gels grown in a hemispherical shape analogous to that observed experimentally.

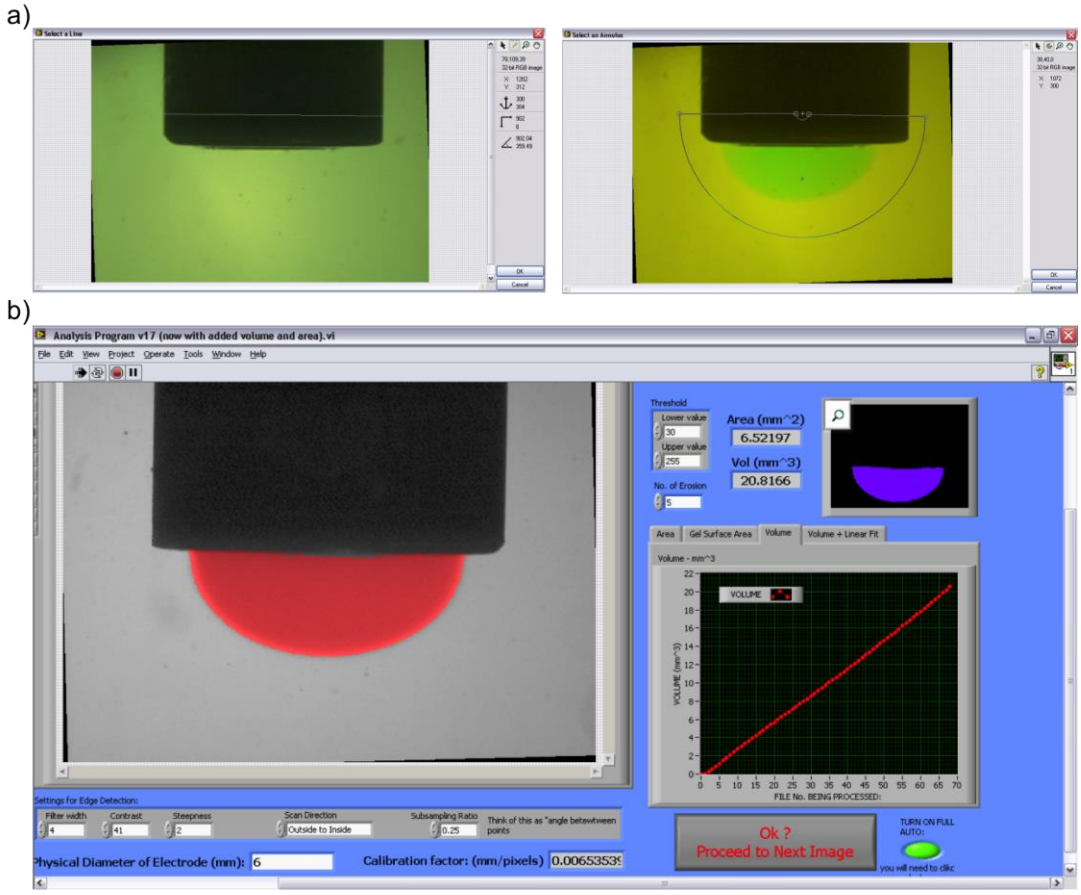

Figure 6 Screenshots of the gel analysis program used to measure the volume of hydrogel produced a) shows the marking out of the dimensions of the electrode and gel to be analysed and b) shows the part of the photograph being classed as the hydrogel portion of the photograph (highlighted in red by the program) and used to determine the volume of the gel

After uploading the photos to be analysed and marking out the required parameters, the images could then be sequentially monitored. The program uses the contrast between the background solution and gel produced. Stringent conditions were needed for appropriate analysis and representative results. The hydrogels have to be sufficiently turbid to be in contrast with the stock solution to make it measurable by the program. Figure 6b shows an image of a gel under analysis, the program highlights in red the area that is being used to measure the volume of gel produced.

Any part of the gel that has not been recognised/analysed by the program will not be shaded in red, allowing it easy to identify the accuracy of the data being collected.

Figure 7 Shows the limitations of the gel analysis program a) shows a BrNapAV gel which is too transparent to be analysed b) shows a 2NapFF in its solution which is too viscous to allow the gel to be monitored and c) shows a BrNapFV before filtering, where there dust particles in solution which affect the analysis and subsequent gel volume data produced by the program

Figure 7 demonstrates some of the limitations of the analysis program. If the hydrogel produced is very transparent and hence there is little to no contrast between the gel itself and the gelator solution from which it was produced, the program will not be able to identify the presence of the gel in the photograph. For hydrogels where this was the case, the program could not be used to give quantitative data. This was the case for a BrNapAV hydrogel for example (Figure 7a). Another limitation was the need for gelator solutions to be of a viscosity similar to that of water. Many of the hydrophobic gelators studied by this group tend to be quite viscous[5, 25, 34, 35] and some of these also produce quite transparent hydrogels. This combination makes them impossible to analyse under the current setup. Figure 7b shows a 2NapFF hydrogel in its solution. The solution is clearly inhibiting the observation of the gel, despite being transparent. There are bubbles visible and the gel is barely visible due to the viscous nature of 2NapFF solutions. By the scrutiny of many gels and their solutions, the conclusion was that transparent solutions with near-transparent to turbid/opaque gels were the optimum samples for quantitative analysis. However, even after this realisation, a further limitation was realised which was, fortunately, easily rectified. Due to the method by which the program measured the volume of gel in each picture - contrast - any particles in solutions would also be considered by the program to be gel. Figure 7c shows a BrNapFV solution with dust particles visible in solution. Filtering of gelator solutions before use, allowed this problem to be eradicated (Figures 3 and 5). On the basis of this, BrNapFV and 2NapAA were not only chosen

for their significantly differing pK_a values, but they also provided viably measurable hydrogels from transparent solutions.

The previous section (5.2.2) shows that the gels are visibly different sizes when the current is varied. Quantitative analysis supports this observation. As the current was increased, and hence production of protons increased, the gel volume produced for a given time period increased (Figures 8a, 10a and 11a). BrNapFV gels could be produced for all currents tested (5 – 1000 µA) for 1000 s, with linear gel growth observed (Figure 8a). As the current was kept constant for each experiment, the corresponding potential required was monitored with time. Figure 8b shows that the potential required increased as the current applied increased. When a gel forms, it partially blocks the electrode surface and to keep the current constant, the potentiostat will increase the driving force (potential) to ensure that the current remains the same. The current measured is directly proportional to electrode area, therefore if the area decreases, an inherent decrease in current follows. As a result, potential will increase to drive more current.

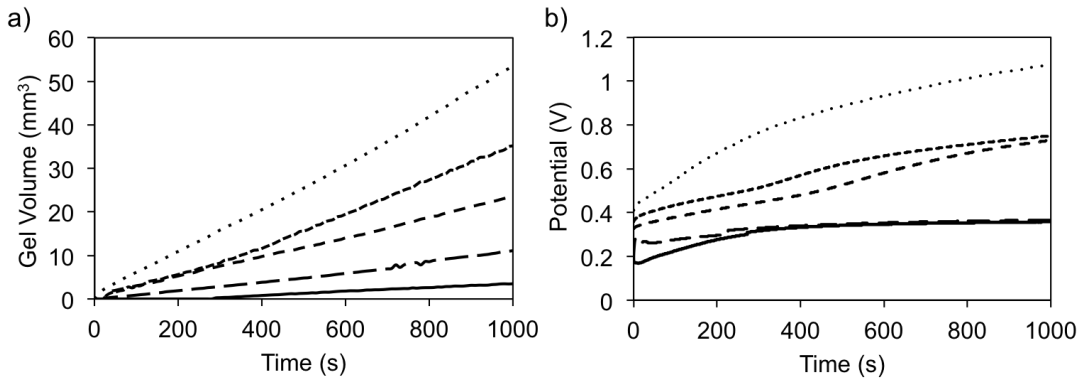

Figure 8 a) Volume of gel produced from BrNapFV at different currents for 1000 s. Only 5 µA, 20 µA, 40 µA, 60 µA and 80 µA are shown (top to bottom). b) Potential produced over time for the growth of the gels in a). Symbols represent the same currents in both figures

Higher currents/time periods were also attempted to search for a plateau in the gel volume, however, gel growth continued until the gel was not only too large to be quantitatively analysed by the program, but began to touch the sides of the cell (Figure 9).

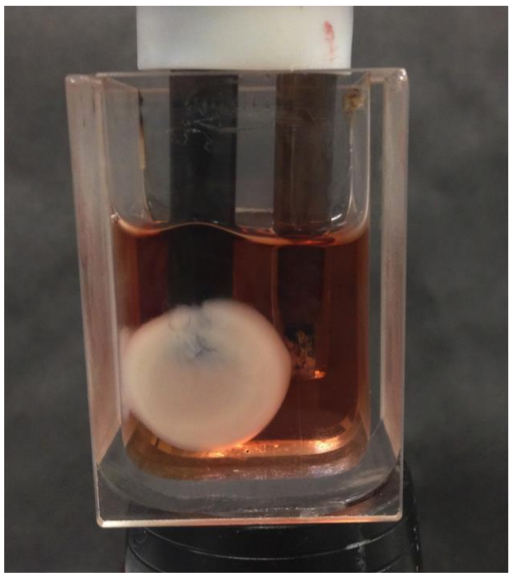

Figure 9 BrNapFV gel grown at a current of 100 µA until the gel began to touch the sides of the cell

As mentioned in Section 5.2.2, the gel growth experiments were repeated for 2NapAA. With 2NapAA having the lower pK_a of the two gelators, the gels produced were visibly smaller than gels of BrNapFV grown from the same current over the same time period. Figure 10 shows the gel volumes measured and corresponding potentials produced for 2NapAA gels at different currents. Notably, the growth of 2NapAA gels appears non-linear as opposed to BrNapFV. Also, a smaller range of currents produced gels from 2NapAA after 1000 s. From the data collected for BrNapFV gels (Figure 8), it was clear that a current of 5 µA (0.7 A/m^2) or 10 µA (1.4 A/m^2) (for 1000 s) was sufficient for the oxidation of HQ. No gels were produced from 2NapAA under these conditions; hence, the number of protons produced at these currents must not be sufficient enough to reach below the apparent pK_a of 2NapAA. Notably, the potential produced over time for each set current is similar for both gelators (Figures 8b and 10b), even applying the lower currents (5 and 10 µA (latter not shown)) where 2NapAA does not form a gel after 1000 s. In the case of 2NapAA, under all currents tested, the potential produced reached a plateau after approximately 100 s and remained constant for the remainder of the 1000 s.

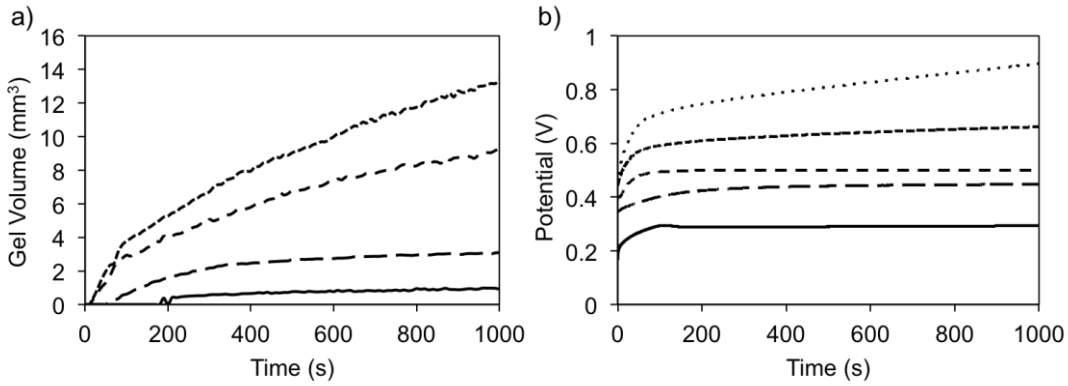

Figure 10 a) Volume of gel produced from 2NapAA at different currents for 1000 s. Only 20 μA, 40 μA, 60 μA and 80 μA are shown (top to bottom). b) Potential produced over time for the growth of the gels in a). Symbols represent the same currents in both figures

Comparison of the final sizes of gels produced from currents of 20 μA to 100 μA (2.8 – 14.1 A/m^2) for BrNapFV and 2NapAA showed significant differences in gel size. For example, at 50 μA, BrNapFV produced a gel with a volume of 31.7 mm^3 whereas 2NapAA produced a considerably smaller gel with a volume of 6.7 mm^3 at this current after 1000 s (Figure 10a). Interestingly, the amount of current supplied to the system can also control the gelation lag time in these gelators. For instance, both BrNapFV and 2NapAA can form gels when the current is set to 20 μA (2.8 A/m^2) for 1000 s (Figures 3, 5, 8a, 10a and 11a). Not only do they produce different sized gels but gelation begins much quicker for the higher pK_a gelator i.e. BrNapFV. BrNapFV began to form a gel after 30 s and 2NapAA did not start to form a gel under these conditions for the first 190 s (Figure 11b). This is demonstrated in Figure 11a where it is evident that the lag time for gelation decreases as the current increases i.e. the supply of protons at the electrode surface is increased. Furthermore, the apparent pK_a of the gelator is an intrinsic factor in the gelation lag time variability. The higher the pK_a of the gelator, the lower the gelation lag time (Figure 11c). As gelation does not occur until the pK_a of the gelator is reached, higher pK_a gelators will require fewer protons to be reached than that of a lower pK_a, leading to shorter lag times (if any quantifiable lag time at all).

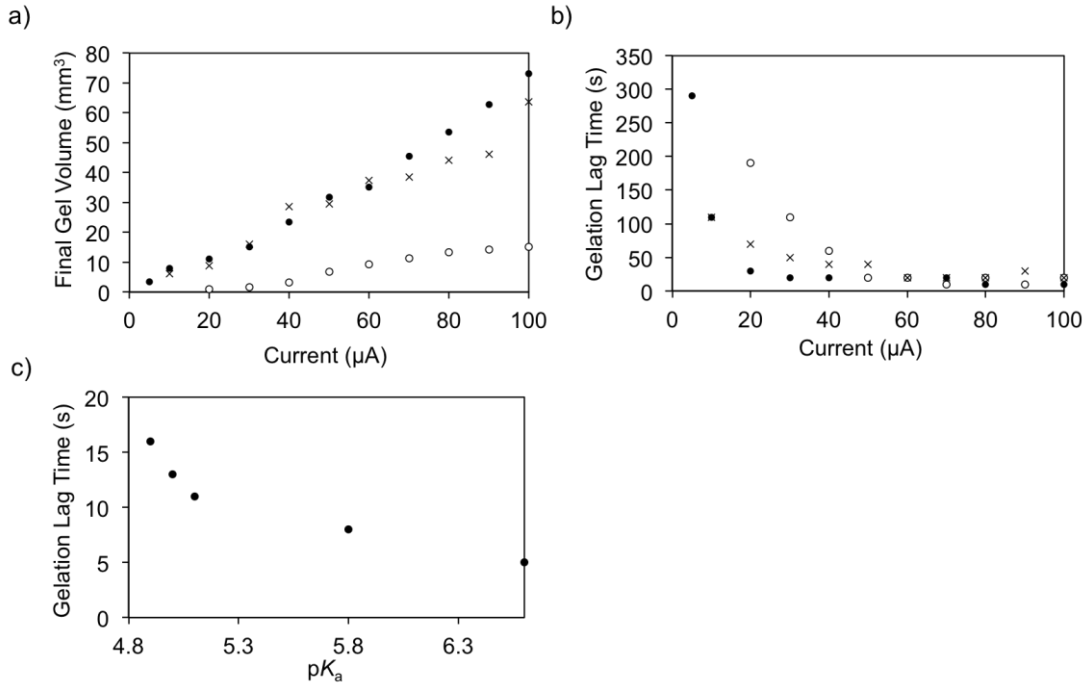

Figure 11 a) Final volume of gels grown at currents from 5 – 100 μA for BrNapFV (●), 2NapAA (○) and 1:1 BrNapFV:2NapAA (x). No gels were observed for 2NapAA at 5 and 10 μA b) lag time observed for gels grown from BrNapFV (●), 2NapAA (○) and 1:1 BrNapFV:2NapAA (x) and c) relationship between lag time of gelation and pK_a for the gelators BrNapAA, BrNapAG, 2NapAA, BrNapAV and BrNapFV, respectively

Figures 12a and b also demonstrate the relationship between pH, pK_a and the gel formed. Here, instead of the pH of all stock solutions starting off at pH 8; meaning that higher pK_a gelators will require fewer protons to trigger gelation and vice versa for lower pK_a gelators, the pH difference (ΔpH) between the pK_a of the gelator and its stock solution. Inherently, the required protons by each gelator should be the same. In doing so, it can be seen that by increasing the pH of a BrNapFV solution to pH 9.6 (the same ΔpH as 2NapAA at pH 8), there are slight differences in the growth of gel (Figure 12a), with the final gel volume being approximately 2 mm^3 more than the gel grown from a pH stock solution as normal. However, the growth of gel from a pH 9.6 solution does appear relatively linear and therefore similar to all the other gel growth data collected for BrNapFV (Figure 8a). Despite this, a 2NapAA gel produced from a solution with a starting pH of 6.4 (same ΔpH as a pH 8 solution of BrNapFV), linear growth was not observed (Figure 12b). Growth appeared to slow at later timepoints which was observed for all 2NapAA gels measured. The lower ΔpH than normally used in this Chapter for 2NapAA, resulted in a larger volume of gel

grown and a shorter gelation lag time (as expected). The 2NapAA gel grown from a smaller ΔpH solution was still significantly smaller than any BrNapFV gel grown under the same conditions.

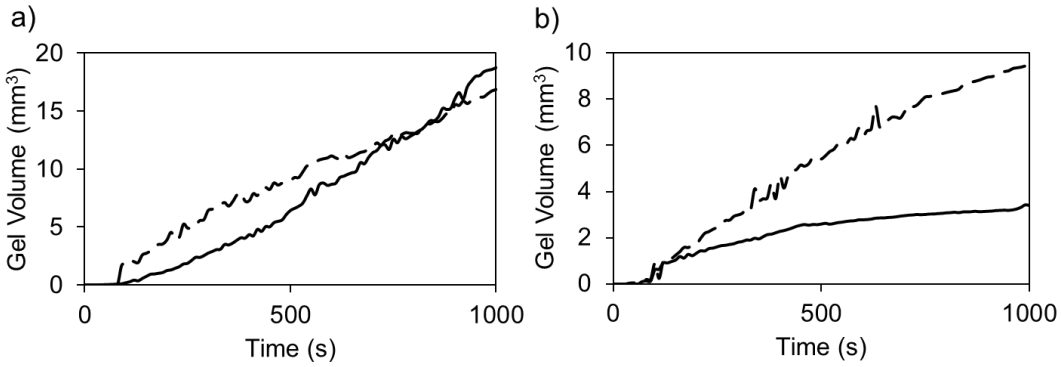

Figure 12 a) Volume of gel produced from BrNapFV with different pH values of starting solutions. Stock solution of pH 8 (—) and pH 9.6 (– –). b) Volume of gel produced from 2NapAA with different pH values of starting solutions. Stock solution of pH 8 (—) and pH 6.4 (– –)

We also demonstrate the potential to form more complex multi-component LMWGs with a fine degree of control over LMWG composition. We have previously shown that bulk gels can be formed from self-sorted multi-component LMWG systems.[36] By slowly adjusting the pH, two LMWG with different pK_a values can independently self-assemble; the slow pH change means that the pH reaches the pK_a of one LMWG before that of the other. Hence, the first LMWG self-assembles, with the other gelator remaining in solution until the pH decreases further to the second pK_a.[37] Here, by using the electrochemical oxidation of HQ as the means of lowering the pH, we are able to finely control the composition of a spatially resolved gel in a mixture of multiple LMWG. On the basis of this concept, the gel growth experiments were carried out on a 1:1 concentration of BrNapFV:2NapAA and compared to that of the gelators individually. From the data collected, the higher pK_a BrNapFV appears to dominate the gelation. Figure 11a shows that final gel volumes measured for the mixed gel system is comparatively similar despite the presence of 2NapAA. The gelation lag times are slightly slower (at lower currents) than BrNapFV gels alone but are considerably quicker than 2NapAA gels grown under the same conditions (Figure 11b). It is interesting to note that the growth of the mixed gels also mimic BrNapFV gels in that the gelation is linear with time (Figure 13a). Here, the potential

produced over 100 s is very slightly lower than those observed for the gelators individually at the set currents measured. Consideration of the data collected for these gels suggests that the BrNapFV would begin to self-assemble and gel at the electrode surface first (as expected in individual systems) – due to its pK_a, causing it to dominate gelation behaviour over 2NapAA. The ability of the mixed system to form gels at both 5 µA and 10 µA further supports this.

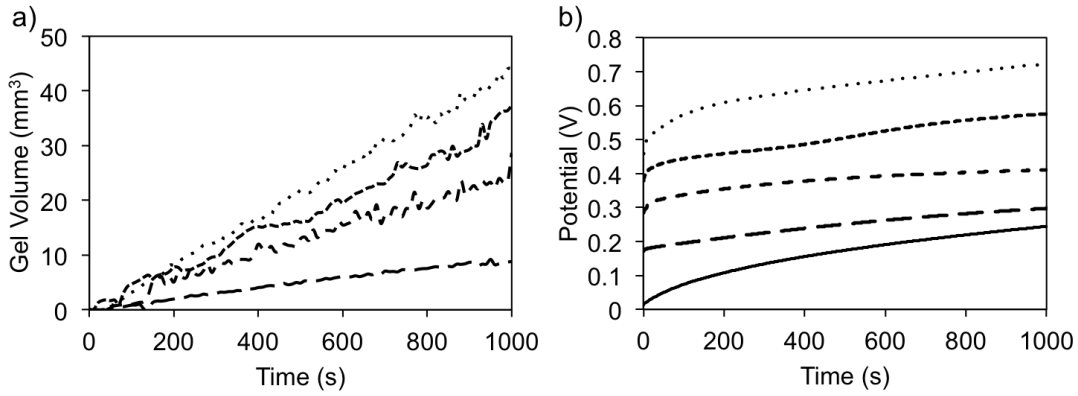

Figure 13 a) Volume of gel produced from 1:1 BrNapFV:2NapAA at different currents for 1000 s. Only 5 µA, 20 µA, 40 µA, 60 µA and 80 µA are shown (top to bottom). b) Potential produced over time for the growth of the gels in a)

5.2.4 Multilayered Hydrogel Systems

The aforementioned methodology can be further extended to grow multilayer gels. This is done by removing the electrode from one solution and placing in another. Layers can be formed from either the same LMWG or from different LMWG if the solution is changed. Using either BrNapFV and/or 2NapAA, visibly distinct hemispherical layers could readily be grown. The first gel layer was grown as described in the previous section, where a current was applied to trigger the growth of the gel. To make it easier to visualise the layers, the first gel of the multilayered system was stained with Direct Red as it was found not to diffuse out of the preceding gel into the following layer (seen in Figure 14).

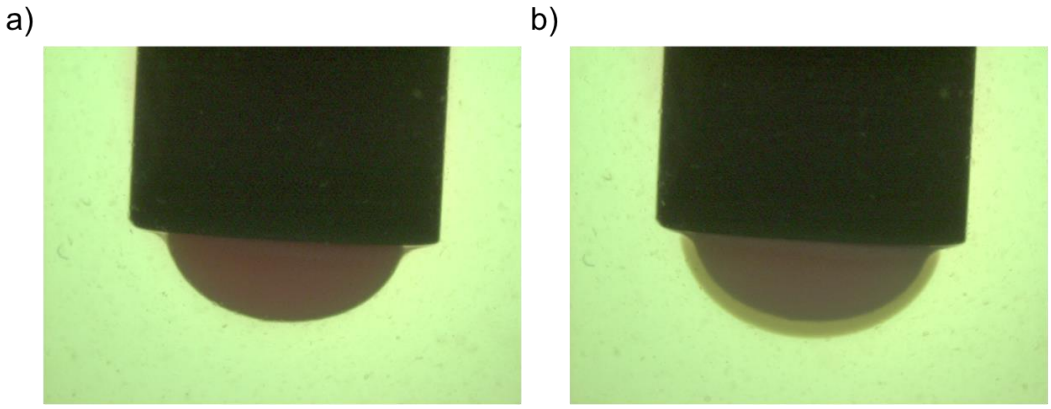

Figure 14 a) BrNapFV gel containing to Direct Red dye. b) A layer of a BrNapFV gel grown on the pre-existing gel layer

Once the first gel had grown on the electrode surface, the electrode was placed into another solution (either containing the same or different gelator from the initial layer) and the current was applied again. It is important to note that gelation does not ensue when the current is switched off which was previously observed for thin hydrogel films made by Cameron's group.[38] They reported that a "seeding layer" of a hydrogel of a related material, FmocLG, present on the electrode surface before cessation of current acted as a nucleation surface for spontaneous hydrogel growth after the current application ceased.[38] However, our current analytical methodology could not discount continual growth, *via* passive diffusion, on the nanometre level after the current ceases. When the current was applied, gels grew outward from the surface of the existing gel. Gelation is the result of protonation of the LMWG and hence protons produced at the electrode surface diffuse through a "proton-loaded" gel structure which then diffuses to the gel-solution interface. Gel growth is determined by whichever LMWG is present in solution at the gel/solution interface, allowing for variable gel-on-gel layers to be formed. Even growth of the second gel layer over a pre-existing gel is observed.

5.2.4.1 Surface Plasmon Resonance Spectroscopy

Multilayered hydrogels could also be demonstrated on nanometre thick films of BrNapFV and/or 2NapAA. Multiple layers were grown in the same way as described above but the glassy carbon working electrode was replaced with a planar gold electrode.[17] With hydrogels of a thickness < 200 nm, surface plasmon resonance

(SPR) spectroscopy could be used to demonstrate not only the control over the growth of the layers, but give an inclination of the thickness of film grown on the gold electrode.[17] SPR excites surface plasmons (an oscillation of electrons) in the gold film by way of laser light, with the surface plasmonic tails being sensitive to changes in dielectric constant within close proximity to the surface of the gold. This means that the decaying tail (in close proximity to the gold surface) is surrounded by the dielectric medium - in this case, the gel or solution if no gelation occurs. Hydrogelation on the gold surface would ultimately alter the refractive index measured close to the gold surface and such changes in dielectric constant indicate this change in mass on the gold surface. Due to the length scale of the surface plasmon tail, only thicknesses of up to approximately 200 nm are measurable.[39] Therefore, it is important to note that the thickness values of any gel growth that occurs outwith the evanescent tail of the plasmon is immeasurable unless optical waveguide modes are observed. Only bulk refractive index changes can be measured out of this range. Figure 13 shows surface plasmon resonance spectra for a gold film in a solution of BrNapFV and a corresponding BrNapFV gel (~ 200 nm) grown on the gold film from this solution. The sharp dips observed in both spectra are due to excitation of surface plasmons in the gold film. From Figure 15 it can be seen that there is a shift in spectra when a gel is present on the gold surface. Changes in critical angle and reflectivity minimum are indicative of the dielectric properties of layers present on the gold surface.[40] The critical angle measured for the BrNapFV stock solution was 47.5° and the angle at the reflectivity minimum was 51.9°. Upon gelation of BrNapFV on the gold surface, the critical angle and angle at the reflectivity minimum were shifted to 59.0° and 65.7°, respectively. The dielectric constants of the films were obtained by carrying out Fresnel fitting of the SPR curves (carried out by Dr. Petra Cameron, University of Bath). A Fresnel model used to describe nanometer dimensions of poly(hydroxyethyl methacrylate) hydrogels was a good approximation for hydrogel films of the materials described in this Chapter.[41] A four-layer model of glass/gold/hydrogel/water (or air) was used. Fresnel modeling allowed an approximate film thickness to be extracted for the thinnest hydrogel films. This model can be used to calculate layer thickness only when the hydrogel film is <200 nm thick (i.e., it is thinner than the evanescently decaying surface plasmon tail).

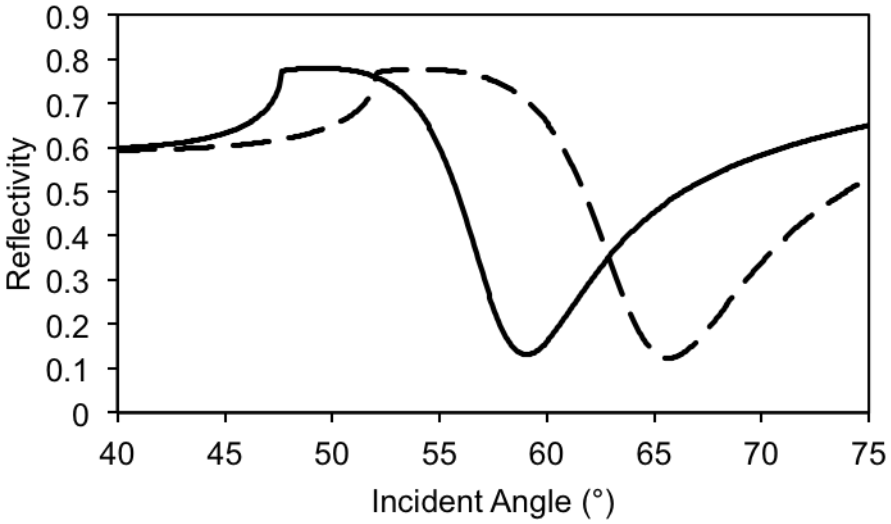

Figure 15 Surface plasmon resonance (SPR) spectra showing the intensity of reflected light as a function of the incident angle. The SPR spectra show that the critical angle shifts when the BrNapFV solution on the gold surface (—) forms a gel on the gold surface (−−)

Gels were grown by applying a current of 10 μA in pulses for 10 s, with 10 s rest periods between each pulse. Figure 16a shows the fine control over the growth of hydrogel layers by controlling the current applied. Firstly, a layer of 2NapAA was grown on the gold surface – eleven pulses of current produced a gel film with an approximate film thickness of 120 nm (Figure 16b). This stock solution was then replaced with a stock solution of BrNapFV and current pulses were applied again. Due to the relatively thin film of 2NapAA present on the surface and the pH 8 stock solution of gelator surrounding the gel, some of the gel dissolved back into the stock solution as a result. This is evident from the slight decrease in film thickness observed before BrNapFV growth begins (Figure 16b). Therefore a layer of 2NapAA with a thickness of ~ 60 nm was present on the surface of the gold before the BrNapFV gel film was grown on top. Eleven pulses of current were applied to produce the BrNapFV layer. The BrNapFV gel layer was calculated to be approximately 140 nm, giving a total gel film thickness of ~ 200 nm. However, as seen in Figure 16a, the reflectivity plateaus when the BrNapFV layer (2^{nd} layer) is grown on top due to the restriction of the technique to only have the capability of measuring a film thickness of ~ 200 nm. From the angle scan collected after both layers had grown (such as that shown in Figure 15), the real film thickness is calculated to more likely be around 700 nm. Despite the reflectivity being restricted and therefore reaching a plateau, the gel will continue to grow as more current is

applied, thus leading to a continued increase in film thickness. Although the thickness values shown are approximate values, the use of SPR spectroscopy demonstrates further evidence that multi-layered hydrogel systems is possible.

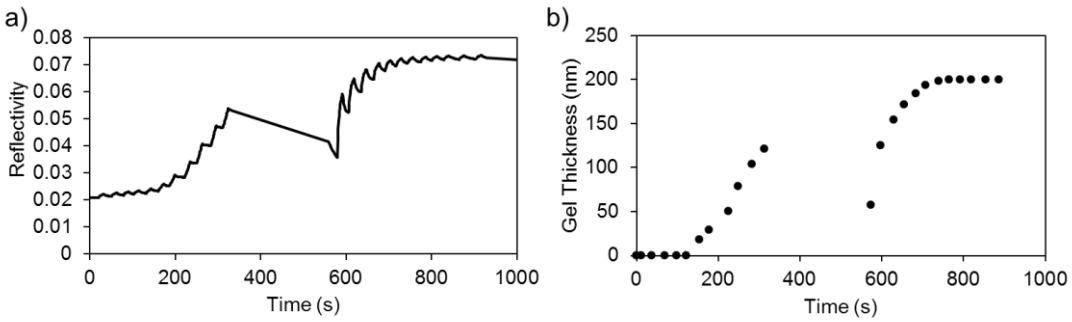

Figure 16 a) Stepwise growth of a multi-layered hydrogel system where pulses of 10 µA for 10 s (and intervals of 10 s between pulses) were applied to give a 2NapAA gel with a BrNapFV gel grown on top. b) The approximate hydrogel film thickness calculated after each pulse of current

5.2.5 Release of Dyes from Electrochemically-Induced Hydrogels

Release of model drug molecules from hydrogel scaffolds has been extensively reported in the literature, with the extensive fibrillar network being an effective temporary scaffold for the entrapment of small molecules.[42-45] Model drug molecules, due to their size, are able to be entrapped in the entangled network of the hydrogel before diffusing out of the hydrogel into the surrounding medium.[42, 44, 45] Dye molecules are commonly used as model drug molecules to allow the release from hydrogel to be monitored *via* UV/vis spectroscopy or other methods. Zhang and his group have previously shown the diffusion of various dyes from peptide hydrogels, in this case - RADA16 hydrogels.[42] Their experiments showed that the diffusion rates differ between dyes and this is a factor of not only the size of the entrapped molecule but of the interaction between the dye molecules and the fibrous matrix of the gel itself.[42] In this Chapter, three dye molecules are investigated: Naphthol Yellow S, Sunset Yellow and Rhodamine B. They are all well characterised dyes which are used as a protein stain (Naphthol Yellow S)[46]; a food additive that has been found to non-covalently bind to DNA molecules (Sunset Yellow)[47] and as a hydrophobic stain (Rhodamine B)[48], respectively. Monitoring the release of several different dyes from the hydrogel matrix may aid in probing the fibrous network that

constitutes the matrix, as the fibrous network has been known to affect release rates of common dyes and drug molecules.[49, 50]

To measure the controlled release of these three dyes from electrochemically-induced hydrogels, the dye was added to the gelator solution and then gelation was induced. The dye was trapped in the gel as it grew outward from the surface of the electrode. An aliquot of 5 mg/mL dye solution was added to the solution of the gelator ArFF (shown in Scheme 1g) and gelation was induced using the electrochemical methodology described previously in this Chapter. Gels were all grown for 1000 s with an applied current of 30 μA (4.2 A/m^2). Gels grown were approximately 19.8 mm^3 in volume. Due to the nature of the gel growth from the surface of the electrode and entrapment of the dye present in the vicinity of the electrode surface, it was unclear how much of the dye had become entrapped and therefore what concentration of dye had been loaded into the gel. Naphthol Yellow S (Figure 17a) is the smallest of the three dye molecules investigated. When entrapped in the ArFF gel, a bright yellow, transparent hydrogel was observed. Figure 18b shows the gel before and after release of Naphthol Yellow S. The image on the left shows the yellow gel immersed in pH 4 water – this was used as the gel would dissolve at higher pH values. The image on the right, taken after the release of the dye, shows the gel is now transparent and not yellow. Conversely, the surrounding solution is now yellow as the dye has dispersed throughout. Figure 17c shows the release data collected for the ArFF gel containing Naphthol Yellow S. The concentration of Naphthol Yellow S in the initial LMWG solution (from which the gel was made) was 0.7 mM but it was unclear of the exact amount entrapped in the gel. Therefore, it was not possible to know if all of the dye loaded was released. Despite this, Figure 17c shows a steady increase in dye released before reaching a plateau after 200 min. The assumption that all of the dye entrapped had been released could perhaps be drawn here. The steady release shown here is on a similar timescale to similar FmocF and FmocY gels prepared using GdL.[51] A slightly lower concentration of Naphthol Yellow was entrapped in these gels than shown to be released in the gels described in this Chapter. Naphthol Yellow S is hydrophilic and a quicker release from the hydrophobic ArFF gel would be expected.

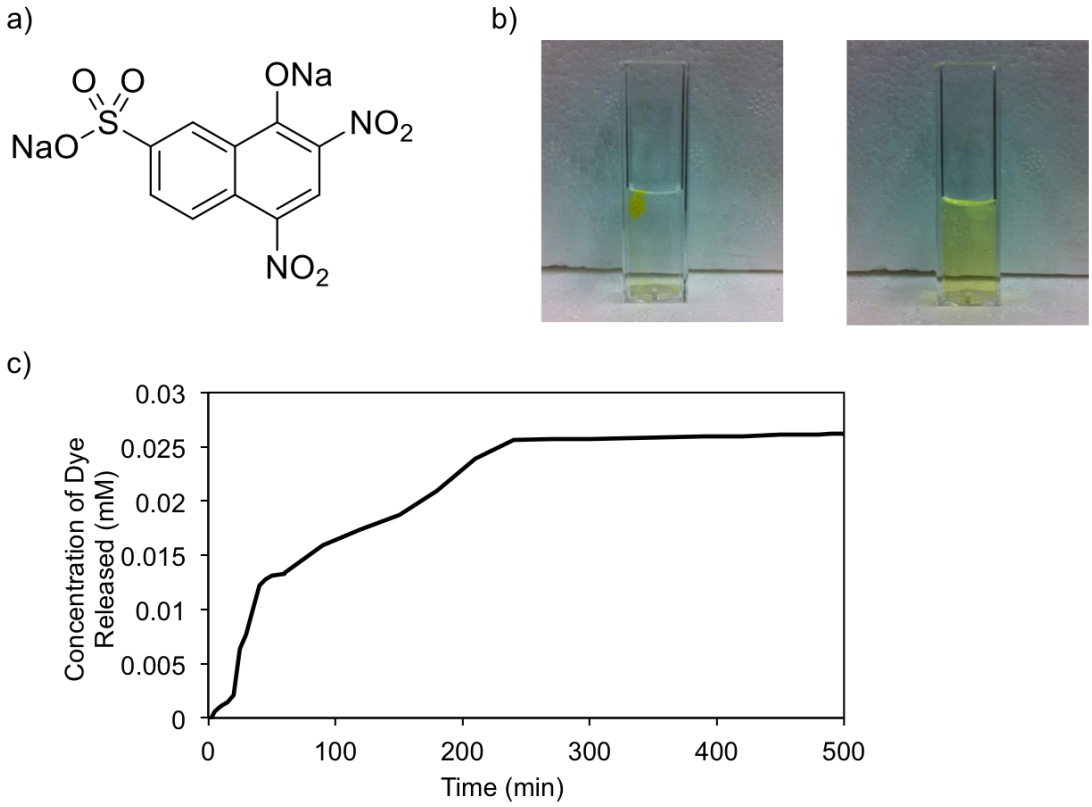

Figure 17 a) Structure of Naphthol Yellow S b) ArFF gel containing Naphthol Yellow S before (left) and after (right) release of Naphthol Yellow S and c) concentration of Naphthol Yellow S dye released over time

The same was also observed for Sunset Yellow. Sunset Yellow (structure shown in Figure 18a) could be successfully entrapped and released from an ArFF gel. The gel containing Sunset Yellow was an orange colour (Figure 18b), which visually appeared to completely be released and therefore afforded a colourless, transparent gel surrounded by an orange/yellow solution. The release monitored by UV also appeared to indicate that the entire payload of dye was released from the gel. Figure 18c shows a sharp increase in dye release before a plateau is reached after ~ 100 min. Both Naphthol Yellow S and Sunset Yellow are hydrophilic and therefore interaction with the gel matrix will not be favourable. Diffusion of the dye molecules through the gel matrix can, however, be paramount. Wallace *et al.* have shown that the mesh size of 2NapFF hydrogels can be probed by the entrapment of various dextran molecules over a range of different molecular weights.[52] They have shown that smaller molecules can move freely through the hydrogel matrix and conversely, larger molecules are more restricted and diffusion becomes limited.

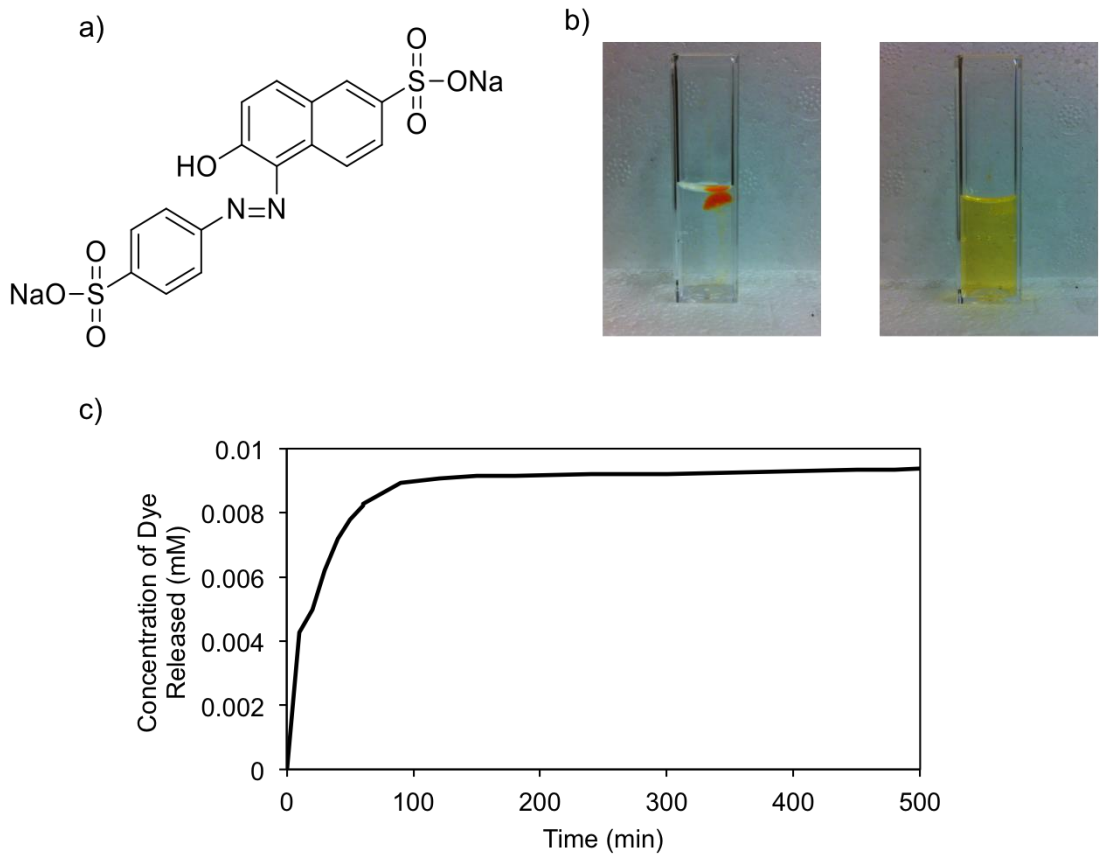

Figure 18 a) Structure of Sunset Yellow b) ArFF gel containing Sunset Yellow before (left) and after (right) release of Sunset Yellow – gel just seen in top right corner of solution and c) concentration of Sunset Yellow dye released over time

Rhodamine B (Figure 19a) is the bulkiest molecule of the three dyes studied, but it is also a hydrophobic dye known to adhere to hydrophobic fibres of hydrogels. Rhodamine B is significantly more hydrophobic than both Naphthol Yellow S and Sunset Yellow, with the *log P* values being 2.7, -1.1 and -0.3 for the three dyes, respectively. This could explain why the release of Rhodamine B is not only much slower than both Naphthol Yellow S and Sunset Yellow but also why the full payload of Rhodamine B entrapped is not released. Again, the exact concentration loaded into the gel is unknown. The LMWG stock solution contained 0.5 mM of Rhodamine B (same as for Sunset Yellow) and the release data shown in Figure 19c does not reach a plateau within the time examined. Thus, suggesting that Rhodamine B is still slowly being released over this time period.

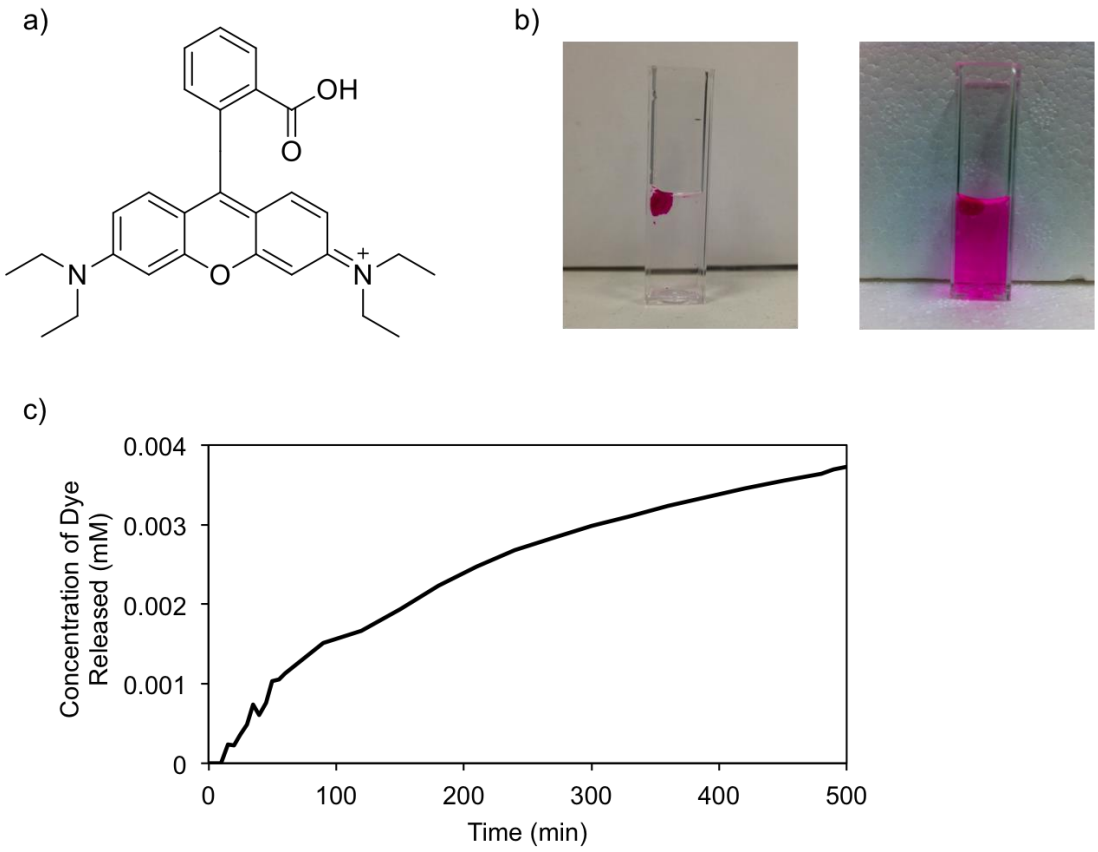

Figure 19 a) Structure of Rhodamine B b) ArFF gel containing Rhodamine B before (left) and after (right) release of Rhodamine B and c) concentration of Rhodamine B dye released over time

Banerjee's group have previously shown the strong adsorption of Rhodamine B (when compared to the other dyes in their study) to the fibres of tripeptide gels.[48] They have also attributed the retention of the dye to its hydrophobic nature. There is also the possibility of hydrogen bonding interactions between Rhodamine B and the peptidic moieties of the fibres. Both Naphthol Yellow S and Sunset Yellow FCF could also exhibit hydrogen bonding interactions between gelator and dye, however. To the best of our knowledge, this is the first electrochemically-induced hydrogels shown to successfully entrap model drug molecules and demonstrate steady release into a medium. In doing so has shown the ability to probe the network of the gel matrix. Probing further with larger molecules such as dye-containing dextrans like fluorescein isothiocyanate-dextran (FITC-dextran) could give more comprehensive information on the mesh size of the ArFF network.

5.2.6 Hydrogelation using a Fluorine-Doped Tin Oxide Coated Glass Slide

The technique used to electrochemically induce hydrogelation can be applied to any conductive surface, allowing for scale-up and extension to complex structures and topographies. For example, fluorine-doped tin oxide (FTO) glass slides can be used to provide a larger surface area for HQ oxidation and subsequent hydrogel formation to occur, demonstrated here using a three-electrode system, with the FTO glass slide acting as the working electrode in the system. Homogeneous gel growth occurred across all the exposed conductive areas of the slide immersed in the LMWG solution (Figures 20a and b) when current is applied. Here, the hemispherical shape is not observed, making them unable to be analysed by the current setup of the hydrogel analysis program to gain quantitative data regarding the gel volume.

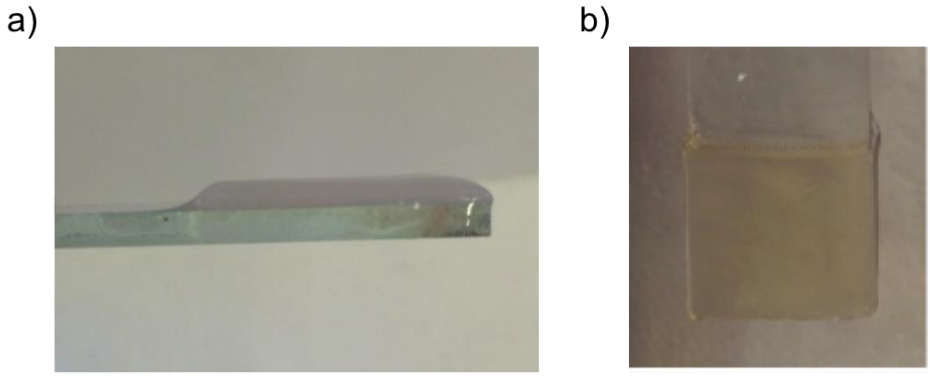

Figure 20 a) BrNapFV gel grown on an FTO coated glass slide. Gel growth occurs across region of slide that is immersed in solution. b) Top view of a)

Gels with thicknesses in the millimetre range could readily be produced from a 10 mL solution (at a concentration of LMWG of 0.5 wt%) of the LMWG at currents of 800 to 2000 μA, equivalent to current densities of 1.7 to 4.4 A/m^2, respectively. These current densities are comparable to those found for the glass carbon electrode studies reported earlier when the current applied was between ~ 10 and 40 μA. Hydrogels of BrNapFV and 2NapAA, produced using this method, were found to have the same concentration as the stock solution from which they were formed. These gels were freeze-dried after gelation, and the lypholised material remaining as a result of the freeze-drying process was analysed *via* nuclear magnetic resonance spectroscopy (NMR) to obtain the spectral information about the gelator. The material was found to be at a concentration of 0.5 wt% with approximately 2 – 3

times more HQ present (data not shown).

5.2.7 Rheological Properties of Hydrogels Prepared on FTO Slides

Using the galvanostatic method as described similarly above on a series of gelators with ranging pK_a values, where, in this case, the current applied was 1000 μA (2.2 A/m^2) for a period of 1000 s was found to produce a sufficient volume of gel (in all cases) to enable rheological analysis. Along with BrNapFV and 2NapAA, the gelators which were known to form gels by this method (Table 1) had their rheological properties measured, with their structures shown in Scheme 1. Figures 21 and 22 show the frequency and corresponding strain sweeps for all of the gelators studied, respectively. The only omission is BrNapAA, as the gels were too weak to be successfully removed from the FTO slide and transferred to the plate of the rheometer – a requirement for the use of the parallel plates geometry. Such weak gels are consistent with BrNapAA gels produced using GdL, where BrNapAA produced considerably weaker gels than the other gelators measured.[25] All hydrogels prepared using the methodology described throughout this Chapter give storage moduli (*G'*) in the kPa region and corresponding loss moduli (*G''*) approximately an order of magnitude lower than *G'* which is indicative of a rigid hydrogel structure (Figure 21).[25, 53, 54] Chapter 4 demonstrated BrNapAV UV-induced gels with similar rheological properties to that of BrNapAV gels described here. The UV-induced BrNapAV gels have a higher final pH than the BrNapAV gel in Figure 21d (and in Table 2) and may be expected to therefore have weaker mechanical properties.[2, 5] However, the gels described in Chapter 4 were formed in the bulk and measurements could be performed *in situ* using a vane and cup measuring system (see Experimental Chapter), whereas the gels described here had to be removed from the conductive slide and their rheological properties measured using a parallel plates measuring system. Different measuring systems can give varied results for the same sample.[55] The *G'* values are, however, comparable to gels prepared *via* other pH triggered methods for the same gelators.[2, 5, 25, 35]

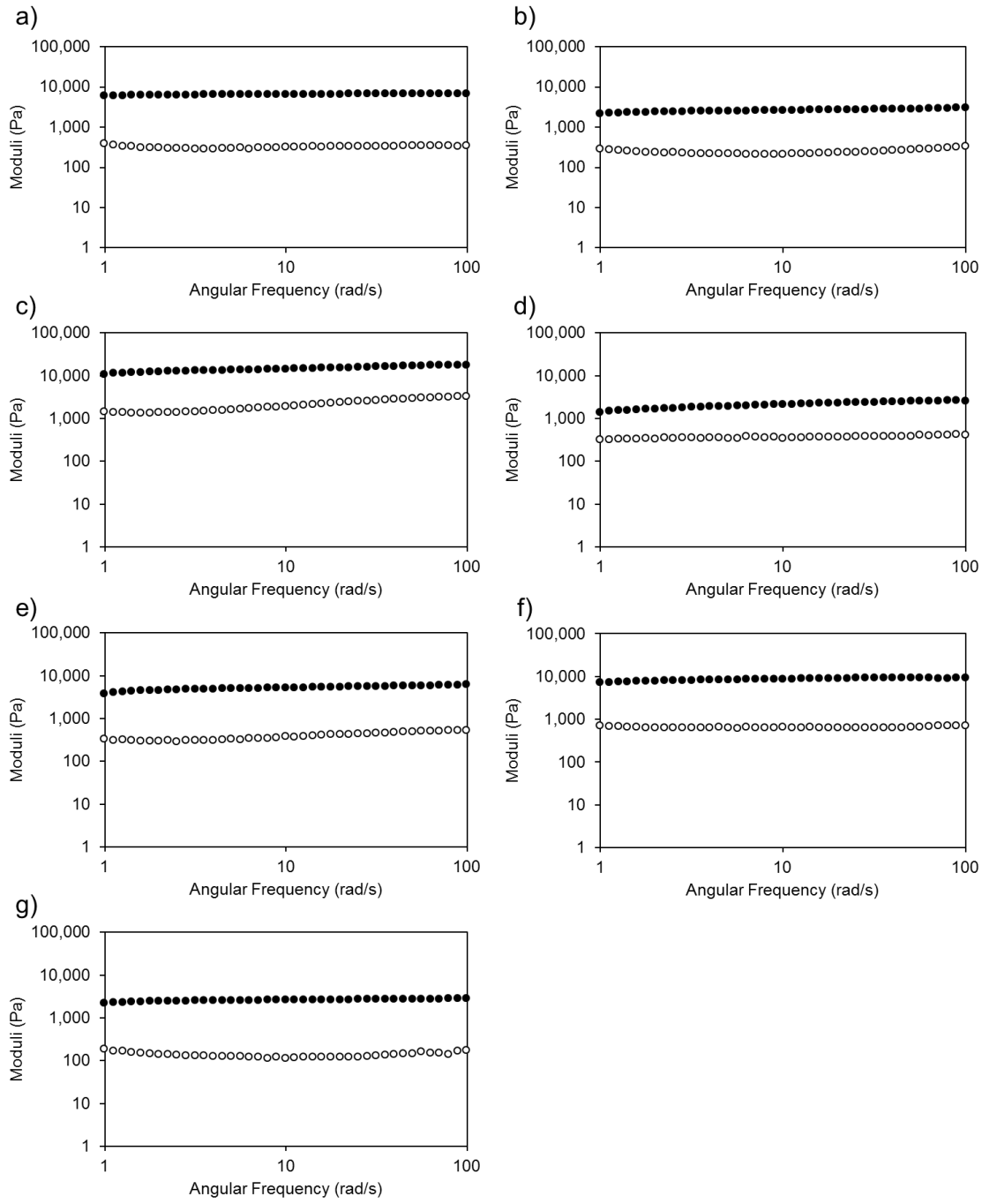

Figure 21 Frequency sweep measurements of a) BrNapFV b) 2NapAA c) ArFF d) BrNapAG e) BrNapAV e) BrNapFF and f) 1NapFG. *G′* is represented by ● and *G″* by ○

Along with the frequency sweeps, which ultimately measure the mechanical strength of the hydrogels, the strain sweeps were also measured. These measurements indicate the strain at which the hydrogel breaks down and reverts back to a liquid. It also ensures that the frequency sweep measurements were carried out in the linear viscoelastic region of the material i.e. the storage and loss moduli measured were

independent of the frequency. Again, similar to gels prepared *via* other methods of trigger, the strain at which all of the gels measured broke down was approximately at a strain of between 5 and 10 % (Figure 22).[2, 35]

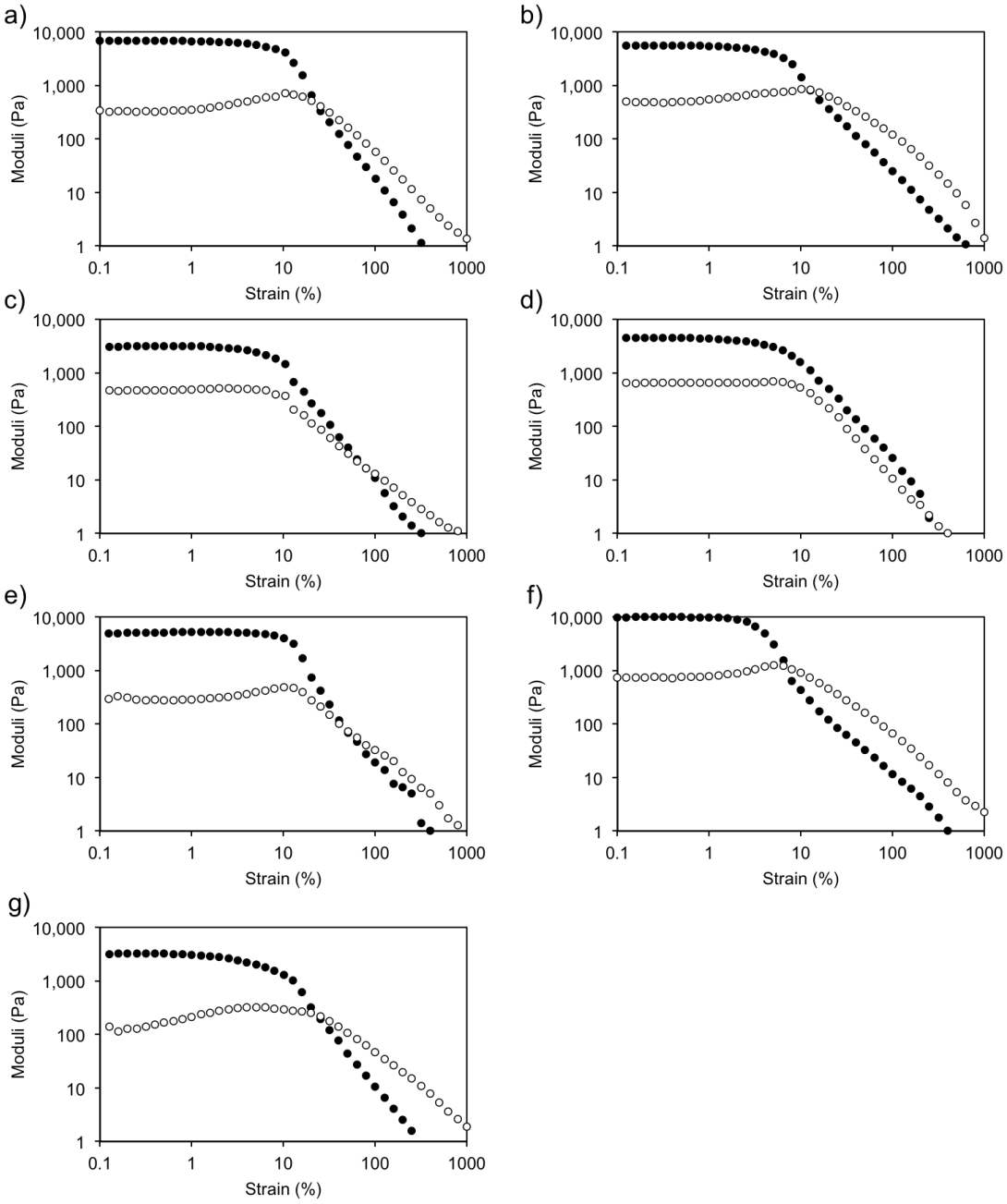

Figure 22 Strain sweep measurements of a) BrNapFV b) 2NapAA c) ArFF d) BrNapAG e) BrNapAV e) BrNapFF and f) 1NapFG. *G′* is represented by ● and *G″* by ○

Table 2 comparatively summarises the rheological properties of hydrogels prepared using the electrochemical method described here and shows that the strain at which gel breakdown occurs differs slightly between the gelators measured, with the strains ranging from 2 – 8 %. Despite these differences, the frequency sweep measurements were run at a constant strain of 0.5 % and therefore in the linear viscoelastic region of all of the materials analysed.

	Electrochemical Gels			
Gelator	G' (Pa)	G" (Pa)	Strain at Gel Breakdown (%)	Final pH
BrNapFV	6800	330	8.2	3.8
2NapAA	2600	200	4.0	3.2
ArFF	14000	1800	6.5	4.4
BrNapAG	2800	400	5.0	3.2
BrNapAV	5200	340	8.0	4.0
BrNapFF	9000	720	2.0	3.2
1NapFG	2900	130	3.2	4.8

Table 2 Rheological properties (and corresponding final pH values) for gels prepared *via* the electrochemical method

It is interesting to note that the kinetics of self-assembly (to afford a hydrogel) does appear to have an effect on the final gel bulk rheological properties. Previous data reported for BrNapAG by Cardoso *et al.* showed kinetic data whereby the final mechanical properties (in the bulk) were the same, regardless of the kinetic pathway taken upon self-assembly.[56] When a BrNapFV gel was grown by applying a range of currents, the rheological properties were increased as the current applied was also increased. Table 3 summarises the frequency sweep data collected for gels (FTO slides) produced by applying currents which correspond to the same current densities as produced when currents of 10, 20 and 30 µA were applied using the glassy carbon electrode. This allowed the kinetic data from the glassy carbon gel growths to be

correlated with the rheological properties, which can only be measured from gels grown on the FTO slides. Data described in Section 5.2.3 of this Chapter show that as the current is increased, so does the rate of gelation. We attributed the increase in gelation kinetics with higher current to faster proton liberation. Table 3 shows that *G'* values also increase as the current applied is increased. Notably, the hydrogels in Table 3 were grown to the same thickness. Furthermore, the pH values are also decreased as the current applied is increased; hence it is unclear as to whether or not the differences in rheological properties are a result of the inherent kinetics of gel formation or differences in the final pH.

Current (μA)	Time (s)	G' (Pa)	G" (Pa)	Final pH
644	1000	4600	300	3.9
1288	800	6500	500	3.2
1932	800	8000	600	2.9

Table 3 Rheological properties (and corresponding final pH values) for BrNapFV gels prepared on FTO glass slides

5.2.8 Scanning Electron Microscopy (SEM) of Hydrogels Prepared on FTO Slides

Along with the bulk properties of the hydrogels produced electrochemically being comparable to other methods of triggering self-assembly, the gels appear to be ultimately similar on the nanometre and micron length scales to gels prepared using other pH trigger methods.[2, 5, 25, 35] All gels imaged were prepared from a current of 2000 μA (4.4 A/m^2) applied for 1000 s and the resulting gels were dried down in air overnight and their xerogel counterparts were then analysed to give the fibrous images shown. Figure 23 shows SEM images collected for BrNapFV (xero)gels. These images show a very densely packed fibrillar network with fibre widths in the nanometre region.

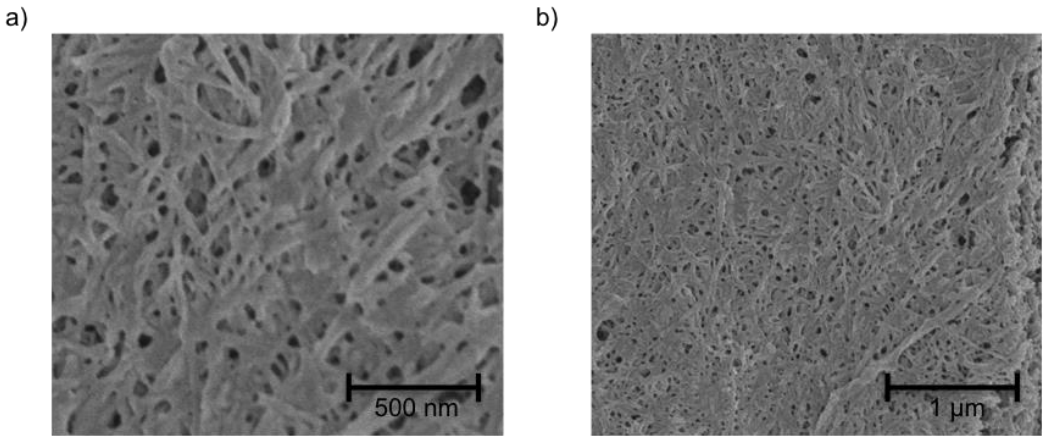

Figure 23 SEM images of BrNapFV at two magnifications

Figure 24 displays the SEM images of 2NapAA gels. These images did not show the expected fibrous network. However, 2NapAA has been known to crystallise under certain conditions[29] and as a result of the drying process required for SEM, crystallisation of the gels may have occurred.

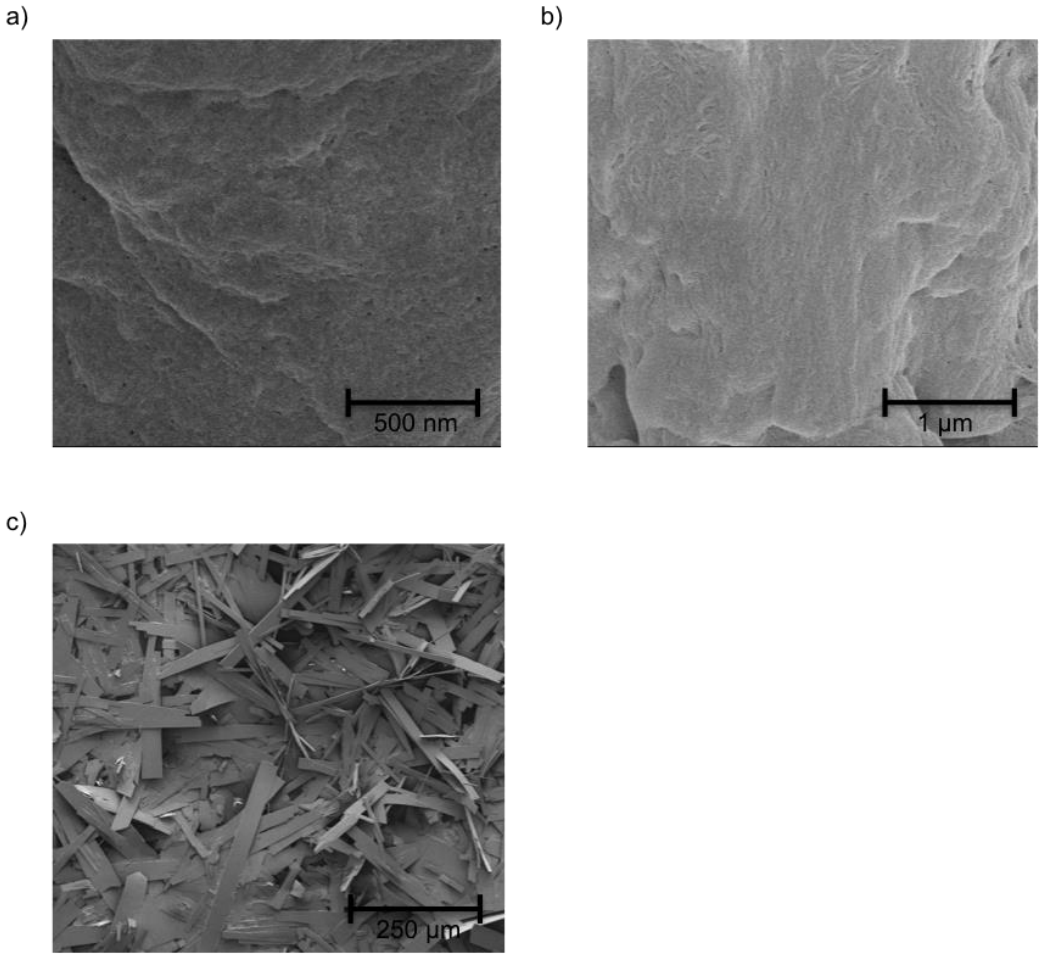

Figure 24 SEM images of 2NapAA at three magnifications

Figure 24a and b do not have clear fibres visible, perhaps 2NapAA consists of much smaller, thinner fibres which are very densely packed – compared to that of BrNapFV (Figure 23) which may make them more difficult to visualise. Other, lower magnification images of 2NapAA gels (Figure 24c) show much larger crystal-like material, further supporting the idea that 2NapAA crystallised upon drying. Figure 25 shows that a dried down 2NapAA gels prepared electrochemically are in agreement with previously measured pXRD data collected for crystals grown from the gel phase and the dried down state of a 2NapAA gel prepared using GdL.[29] The dried down gel prepared electrochemically also shows the presence of NaCl and HQ crystals (Figure 25).

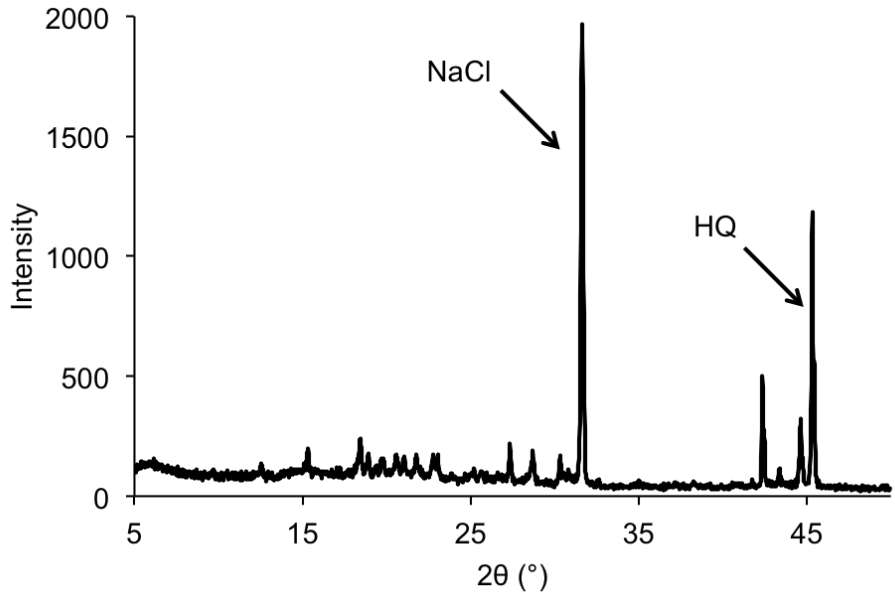

Figure 25 pXRD of a dried down 2NapAA gel

5.2.9 Multi-Component and Patterned Hydrogels on FTO Glass Slides

Section 5.2.4 demonstrates that complex, multilayer structures can be produced on a single electrode surface, which is of interest as it gives the potential ability to incorporate multiple component systems. By scaling up onto the surface of an FTO slide, complexity of the hydrogel produced can be extended further. As gelation occurs homogeneously across the whole section of FTO glass slide that is immersed in the gelator solution, there is the opportunity to manipulate where the gel grows. Thus, hydrogel patterning is possible. A methodology relatively similar in principle

to lithographic techniques previously used to grow patterns of gels is demonstrated here. Where previous techniques use a mask and UV light to create a patterned surface,[57] here, a mask is incorporated onto the surface of the conductive slide to inhibit HQ from oxidising to benzoquinone and liberate protons needed to induce hydrogelation. Figure 26 demonstrates a simple technique to create a patterned surface. Four plastic circles were glued to the surface of the FTO-coated slide to 'remove' the conductivity in the sections underneath these circles (Figure 26a). When gelation was induced by applying a current (as before), gelation only occurred where the conductive regions were exposed. Using ArFF, a transparent homogeneous hydrogel could be formed on the slide, with four voids produced in the non-conductive regions (Figure 26b and 26c). Not only does this demonstrate the ability to pattern hydrogels on a surface, it interestingly provided these cavities which could be utilised. When the slide containing the gel was removed from the gelator solution, the gel remained intact and adhered to the slide; another gelator solution could then be added to the cavities. To do so, another solution of ArFF containing GdL was added to the voids using a pipette and allowed to gel over time within the voids. This is demonstrated in Figure 26d. Direct Red was added to help the gels in the voids be visualised more easily. Once gelled, a gel-in-gel layer was made which gave different rheological properties and ultimately more than one type of fibrous network within one layer. Having different rheological properties within a layer could be of potential use as a matrix for cell culturing where the rheological properties are known to affect the differentiation and proliferation of stem cells.[58, 59] Hydrogels of collagen I-coated polyacrylamide can influence the differentiation of human mesenchymal stem cells (MSCs) based on the respective elasticities of the gels. 2D cell culture of human MSCs demonstrated that for soft (1 kPa), intermediate (11 kPa) and stiff (34 kPa) gels; neuronal, myogenic and osteoblastic differentiation occurs, respectively.[58] Therefore, multiple rheological properties in one surface may encourage differentiation into different cell types in one matrix.

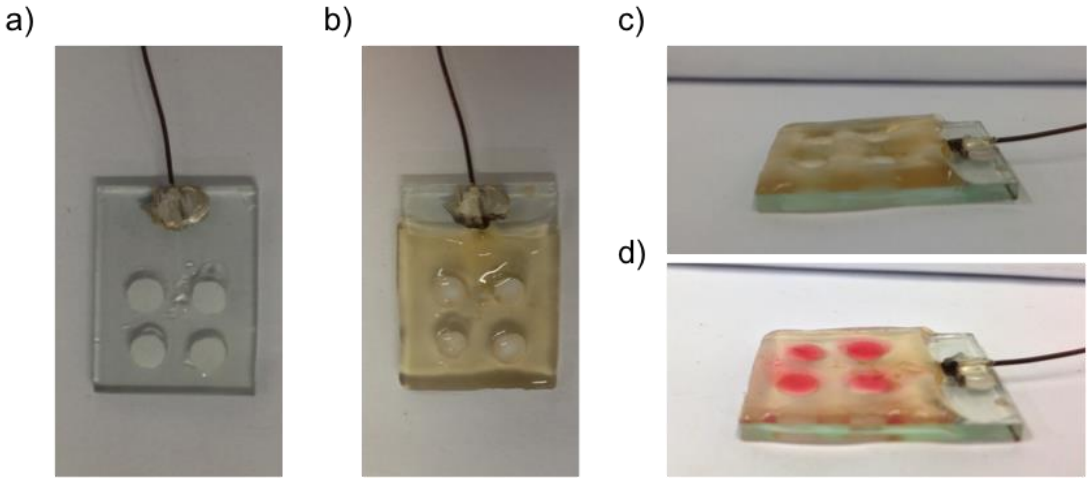

Figure 26 a) FTO glass slide with four circular conductive areas removed with masks b) and c) gel of ArFF grown on the masked slide. d) A second ArFF gel dyed with Direct Red and formed using GdL inside the voids left by the mask

Another simple example of gel-in-gel hydrogel systems is shown in Figure 27. Here, the conductivity is inhibited by painting transparent varnish over a region of the slide. By doing so, the region where conductivity has been inhibited is invisible. Figure 27a and 27b show that conductivity has been removed down the centre of the slide to give electrochemically-induced gel with a small channel down the centre. Using the same approach to the gels shown in Figure 26, the channel was filled with ArFF containing GdL (and Direct Red) and therefore this demonstrated another example of a gel-in-gel layer. Potentially, this technique could be refined to give a micron-sized channel for a possible application in microfluidics.[60]

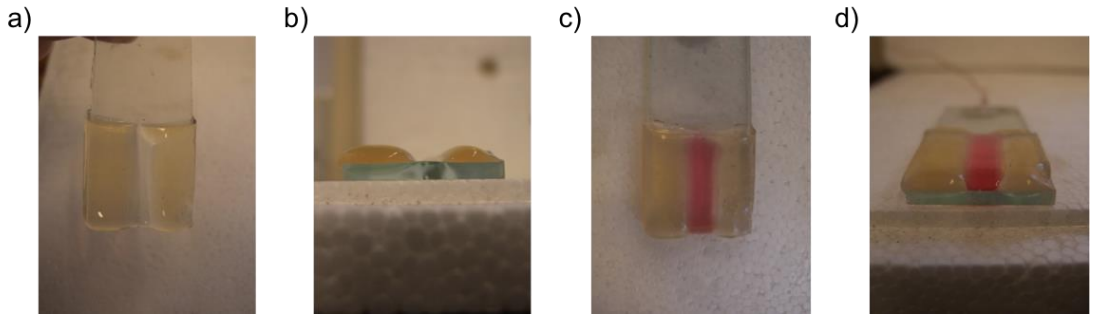

Figure 27 a) and b) FTO- glass slide with a channel of conductivity removed from the centre of the slide and ArFF gel grown on either side of the channel. c) and d) a second ArFF gel dyed with Direct Red and formed using GdL inside the channel

The previous examples are promising demonstrations of the gel patterning possibilities of electrochemically-induced hydrogels. Further and more complex gel layers can be prepared. The previous examples shown in Figures 25 and 26

manipulated the electrode surface to create complex, patterned gel layers but by capitalising on this idea further, the composition and topography of the gel layer could be tuned. Instead of creating patterns from a single electrode, the FTO slide could be etched to remove two linear lines of conductivity to create multiple electrodes on a single surface (Figure 28a). In doing so, multiple currents could be applied in parallel to a single surface. In turn, this could produce multiple gels on a single surface. As seen from the gel-in-gel approach, multiple rheological properties can be produced on a single surface. With the multiple electrodes, this could be replicated but from a single gelator solution and from electrochemically-induced gels only.

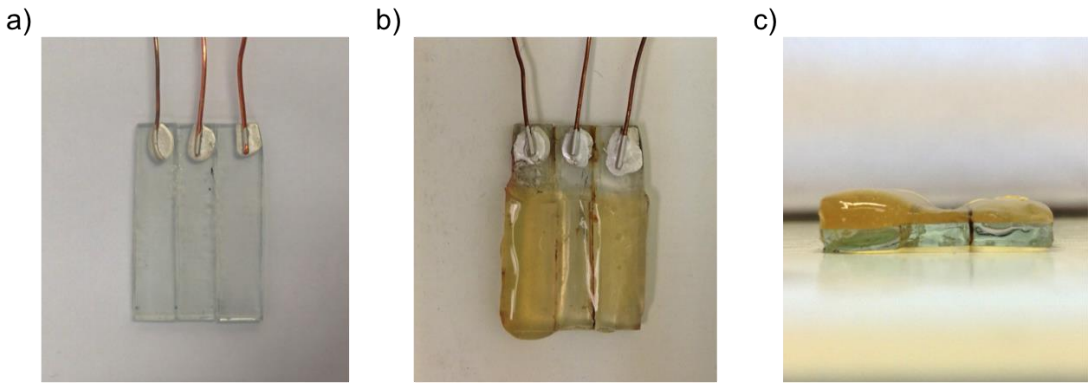

Figure 28 a) FTO slide which has been etched to remove conductivity along two lines to create three parallel electrodes. b) Three gels grown on the three parallel electrodes and c) shows a side view of the three gels grown on the parallel electrodes (from left to right) for 2000 µA, 500 µA and 1000 µA for 500 s

From an ArFF solution, each electrode had a different current applied and three gels were grown. As described in Section 5.2.3, the current applied has an effect on the final gel volume produced. Therefore, when different currents are applied to the three electrodes of the slide, gels of different size are produced. Figure 28c shows the different thicknesses of the gels of ArFF grown on a glass slide. Three different hydrogel thicknesses (grown from three different currents applied) are clearly visible. Enabling the surface roughness to be altered by simply controlling the current applied potentially desirable for cell culturing. The topography of a hydrogel matrix can influence cell proliferation and growth[61], meaning that this method may be optimised to suit specific cell lines and applications. Complexity can be further enhanced by having the "strips" of gels being produced from different gelators.

Using the same slide shown in Figure 28a, a layer of gel with multiple rheological and chemical properties could be produced. This is reminiscent of the gel-in-gel "striped" system consisting of both an electrochemical and GdL gel shown in Figure 27a but consists of electrochemically-induced hydrogels only. This has the advantage over the former in that the gels could be grown in 1000 s or less whereas the former would require the GdL gel to form over a longer time period.

5.2.10 Fine Control over Multi-Component Gelation using Nuclear Magnetic Resonance Spectroscopy (NMR)

We also demonstrate the potential to form more complex multi-component LMWGs with a fine degree of control over LMWG composition. This allowed the possibility for more complex gel systems to be made. Sections 5.2.3, 5.2.8 and 5.2.9 discuss the successful gelation of multi-component systems, where the properties are similar to that of single component hydrogel systems. Previously, it has been reported that self-sorted multi-component gelator systems are possible.[37] By slowly lowering the pH, two gelators in the same solution (with different pK_a values) can independently self-assemble when the pH of the system reaches the pK_a of one gelator before that of the other. Hence, the first gelator will begin to self-assemble, while the other gelator remains in solution until the pH is lowered further and the second pK_a is reached. This is schematically demonstrated in Figure 29.

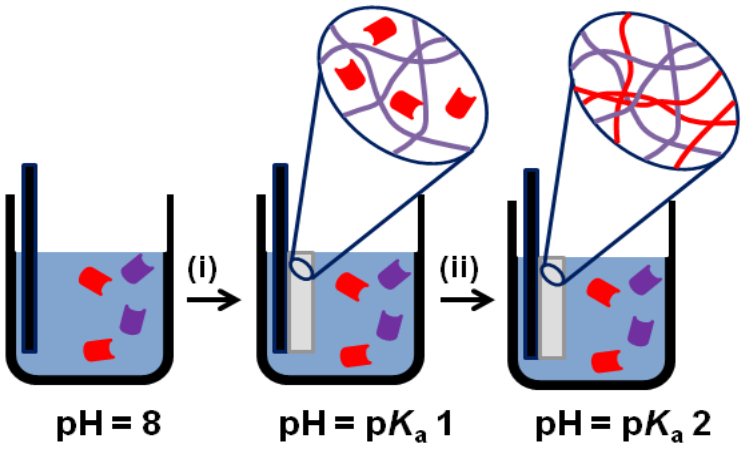

Figure 29 Schematic showing the sequential assembly of two LMWG in a multi-component system

Using the electrochemical oxidation of HQ as the means of lowering the pH, we are able to finely control the composition of a spatially resolved gel in a mixture of multiple gelators. To exemplify this, a solution containing both BrNapFV and 2NapAA (both 5 mg/mL) was used with the FTO glass slide setup to prepare gels. By mixing 1:1 concentrations (both 5 mg/mL) of BrNapFV and 2NapAA, it can be seen that the network observed by SEM (Figure 30) appears the same as for BrNapFV alone (Figure 23). Section 5.2.3 demonstrates that the gelation kinetics and final gel volumes of the gel mixtures closely emulate that of BrNapFV alone. It seems clear that BrNapFV dominates assembly and gelation kinetics.

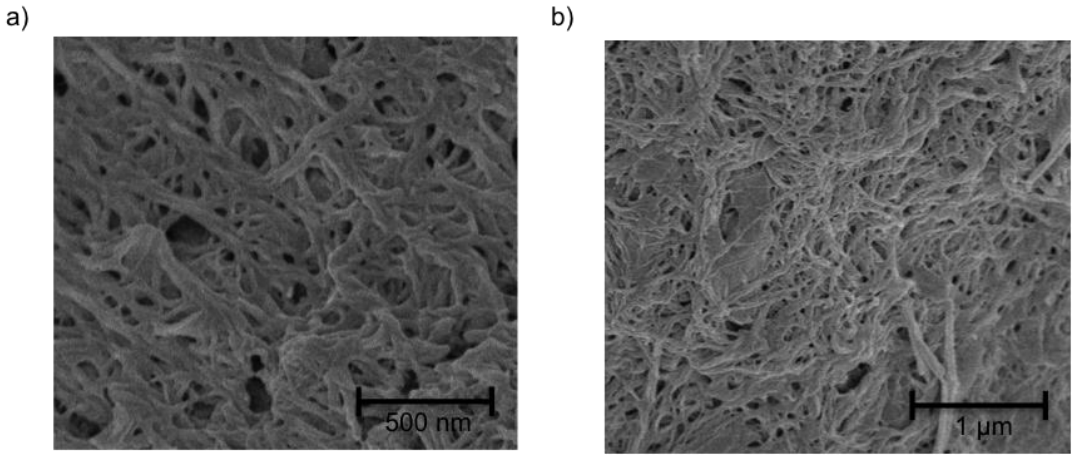

Figure 30 SEM images of 1:1 mixtures of BrNapFV and 2NapAA at two magnifications

NMR spectroscopy was used to probe gelation. When the gelator molecules are self-assembled into fibres, they are NMR invisible.[62, 63] Therefore, NMR spectroscopy could be used to determine the amount of gelator that has assembled. Due to the higher concentration of HQ in solution compared to that of gelator, the NMR spectra had to be magnified to make the peaks of the gelators more visible and able to be integrated properly. LMWG solutions were also prepared using D_2O and NaOD instead of H_2O and NaOH. A galvanostatic method was used to grow gels with a set current and time as described previously in this Chapter. It was identified that after a set current of 800 µA (1.74 A/m^2) has been applied for 100 s (Figure 31), BrNapFV is not visible in the NMR spectrum of the gel formed. The NMR spectrum of this gel shows 100 % of the expected amount of 2NapAA if no assembly of this material had occurred. Hence, under these conditions, the gel formed consisted of a network formed from BrNapFV only and 2NapAA remained in the solution surrounding the

fibres (shown schematically in Figure 29). The solution containing BrNapFV and 2NapAA from which gelation occurs shows the presence of both gelators.

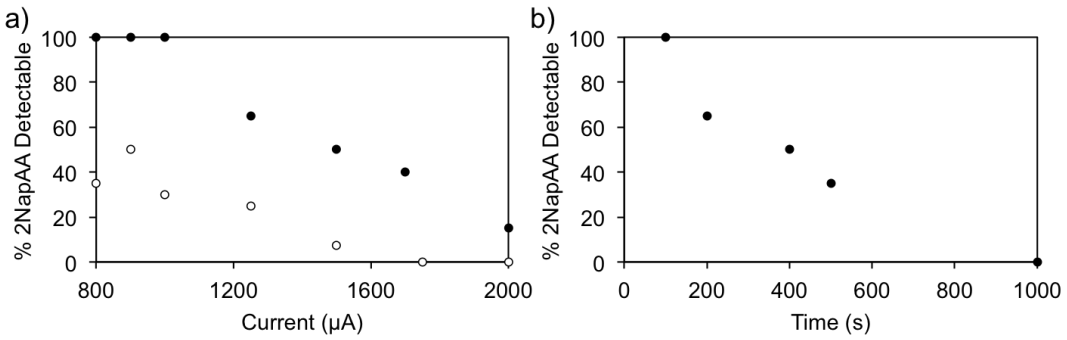

Figure 31 a) Percentage of 2NapAA detectable in the NMR spectrum of a gelled 1:1mixture of BrNapFV and 2NapAA; gels formed at different currents for times of 100 s (●) and 300 s (○). b) Percentage of 2NapAA detectable in the NMR spectrum of a gelled 1:1 mixture of BrNapFV and 2NapAA; gels formed at a current of 800 μA for different times

At a higher current of 1750 μA (3.80 A/m^2) for a fixed time of 300 s and above, both gelators are self-assembled and NMR-invisible (Figure 31a). Figure 31a shows that, as the current applied was increased (for a constant time), the percentage of 2NapAA detectable by NMR spectroscopy decreased – BrNapFV remained invisible throughout. By using the same currents but for a fixed time of 300s, showed a more rapid decrease in the concentration of 2NapAA remaining in solution as compared to a fixed time of 100 s (Figure 31a). Figure 31b shows that for a fixed current (800 μA shown), the amount of 2NapAA remaining in solution is controlled by the time used to form the gel. This further demonstrates the concept that current applied affects both the value and rate of decrease in pH. Hence, we are able to both temporally and spatially gel different LMWG from a multi-component mixture. To exemplify this, two FTO slides were placed within a solution containing both BrNapFV and 2NapAA. Gels were grown in parallel, one at a current of 1250 μA for 100 s and the second at 2000 μA for 300 s (Figure 32).

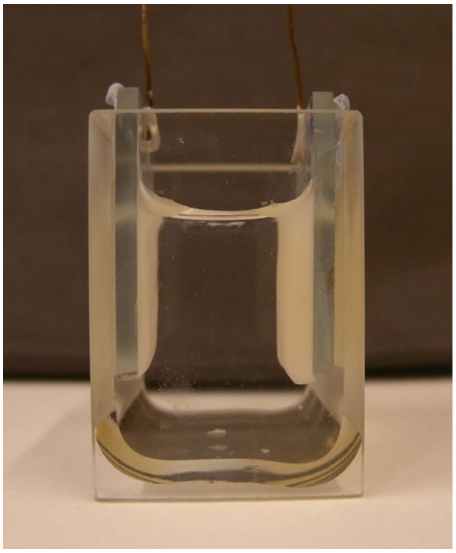

Figure 32 Two gels of different thickness grown in parallel on two FTO glass slides at (left) 1250 for 100 s and (right) 2000 μA for 300 s from a 1:1 mixture of BrNapFV and 2NapAA

As expected from the data shown in Figure 31, the NMR spectrum of the gel grown at 1250 μA for 100 s showed only the presence of 2NapAA, demonstrating that the network comprised only of BrNapFV, whilst the gel grown at 2000 μA for 300 s showed the presence of neither gelator, showing that both gelator had assembled in this case. Figure 33 shows partial NMR spectra of the solution containing both BrNapFV and 2NapAA, where both gelators are in solution and NMR-invisible; partial NMRs of the gel grown at 1250 μA for 100 s where only BrNapFV was assembled and had gelled and the gel grown at 2000 μA for 300 s consisting of fibres of BrNapFV and 2NapAA – both LMWG were assembled and NMR-invisible. To the best of our knowledge, this is the only example where such control over both the time of assembly and gel composition has been demonstrated for these low molecular weight gelators.

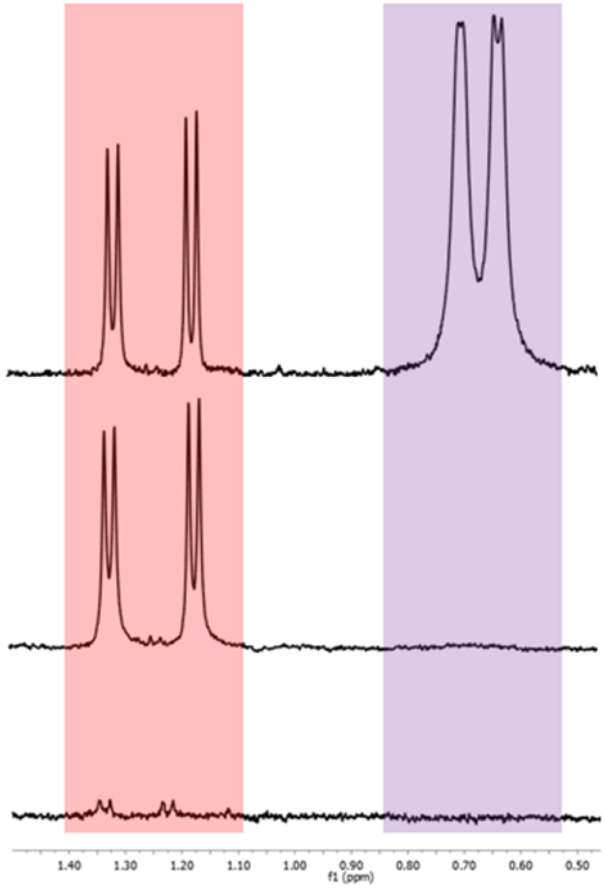

Figure 33 Partial NMR spectra for (top) stock solution of BrNapFV and 2NapAA, each at a concentration of 0.5 wt% at pD 8 in D_2O – the purple peaks are from the valine methyl peaks of BrNapFV and the red peaks are from the alanine methyl groups on 2NapAA; (middle) application of a current of 1250 μA for 100 s results in loss of the peaks from BrNapFV whilst 2NapAA remains in solution; (bottom) application of a current of 2000 μA for 300 s results in the loss of peaks from both BrNapFV and 2NapAA, showing that both have gelled

5.2.11 Stability of Electrochemically-Induced Hydrogels in Cell Culture Medium

The fine control that can be achieved *via* electrochemically triggering the formation of hydrogels makes it easy to envisage the adaptation of this methodology for the growth of cells in culture. This has been alluded to in previous sections in this Chapter. Not only can these gels provide spatially controlled cell entrapment and growth[64] but they can also provide a tailored roughness and shape to suit specific conditions needed for successful cell attachment and proliferation. Before these hydrogels can be used as a scaffold for cell attachment and growth, it is important to ensure that the hydrogel themselves are chemically viable for the particular application. Cell proliferation and growth occurs in cell culture medium under

physiological conditions. Cell culture media contain many components. The cell culture medium used in this Chapter is Dulbecco's Modified Eagle's Medium (DMEM), which contains mainly sugars, several amino acids, salts, vitamins and the dye Phenol Red. This has been optimised to include the constituents required by proliferating cells; however, additives may affect the hydrogel structure.[65, 66] Of equal importance, the hydrogels used must also be stable under physiological conditions and for the desired time period. From the library of LMWG studied in this Chapter, several LMWG were considered potentially suitable for use in cell culturing as they had pK_a values close to physiological pH. All of the LMWG in this Chapter have a pK_a between ~ 5 and 7. BrNapFV, BrNapFF and 7MeNapOFF were chosen as they possessed apparent pKa values of 6.6, 6.8 and 7.0, respectively[5, 25]. Hydrogels were grown on FTO-coated glass slides as before (1000 µA for 1000 s) and the slides were then removed from the LMWG solution and placed into DMEM, ensuring that the gel formed on the slide was fully immersed in the medium. Gels were left in solution for 7 days and the rheological properties were measured before and after immersion in DMEM (Table 4). The rheological properties were measured at 37 ºC. Along with single component gels of BrNapFV, BrNapFF and 7MeONapFF – all of which give storage moduli in the kPa range and corresponding loss moduli over an order of magnitude less than the storage moduli, multi-component gels were also tested. As the apparent pK_a of 2NapAA is 5.1, 2NapAA gels were found to be unstable and dissolve into the medium at physiological pH. Notably, this pK_a value has been measured at 25 ºC and due to temperature effects, physiological temperature will results in an even lower pK_a value for 2NapAA (and other gelators), making it even more susceptible to dissolution in the medium.[25] Despite this, multi-component gels consisting of BrNapFV/2NapAA, BrNapFF/2NapAA and 7MeONapFF/2NapAA were all prepared and immersed in the medium. As 2NapAA would always have the lower pK_a value of the two gelators in each multi-component system, the assumption that the other gelator in the system would grow first and in the case of BrNapFF/2NapAA and 7MeONapFF/2NapAA, the higher pK_a gelator would dominate the kinetics of gelation such as the case for BrNapFV/2NapAA gels. The inclusion of another gelator constituting the fibres of the gel network with 2NapAA could perhaps ensure a better stability of the gel at physiological pH.

Gelator	G' (Pa)	G" (Pa)	G' (Pa) After 7 Days	G" (Pa) After 7 Days	pH Before Immersion in Medium	pH After 7 Days
BrNapFV	6600	400	-[a]	/	3.8	/
BrNapFF	8200	400	740	110	3.7	7.3
7MeNapOFF	9800	1100	160	30	4.3	7.6
BrNapFF:2NapAA	6400	600	680	120	-[b]	-[b]
7MeNapOFF:2NapAA	3000	300	160	30	-[b]	-[b]
BrNapFV in DMEM	500	100	-[a]	/	-[b]	-[b]
BrNapFV:2NapAA in DMEM	220	20	-[a]	/	-[b]	-[b]

Table 4 Rheological properties of gels before and after being immersed in DMEM. [a]Gel had dissolved. [b]Not measured

Of all the gels screened (both single and multi-component), no gels containing BrNapFV were intact after seven days of immersion in DMEM. For gels containing BrNapFF or 7MeONapFF, gels remained intact after seven days of immersion in DMEM and rheological properties could be recorded. However, some gels were visibly thinner after seven days and were dark brown in colour (Figure 34), the latter inherently being due to HQ oxidation over time. The DMEM became darker in colour too as a result of diffusion of the oxidised product into the medium. The former suggests that HQ has diffused out of the gelator or some gelator may have dissolved over time which is entirely plausible due to the close proximity of the pK_a values of the gelators and physiological pH. Ulijn's group also experienced thinning of their FmocFF/RGD hydrogels after 3 days of immersion in DMEM.[1] The rheological properties for those gels in Table 4 that remained after seven days in medium show that the gels are significantly weaker than before. Again, this indicates a loss of gelator into the surrounding medium over time. All gels studied showed an order of magnitude loss in *G'* and *G"* after seven days.

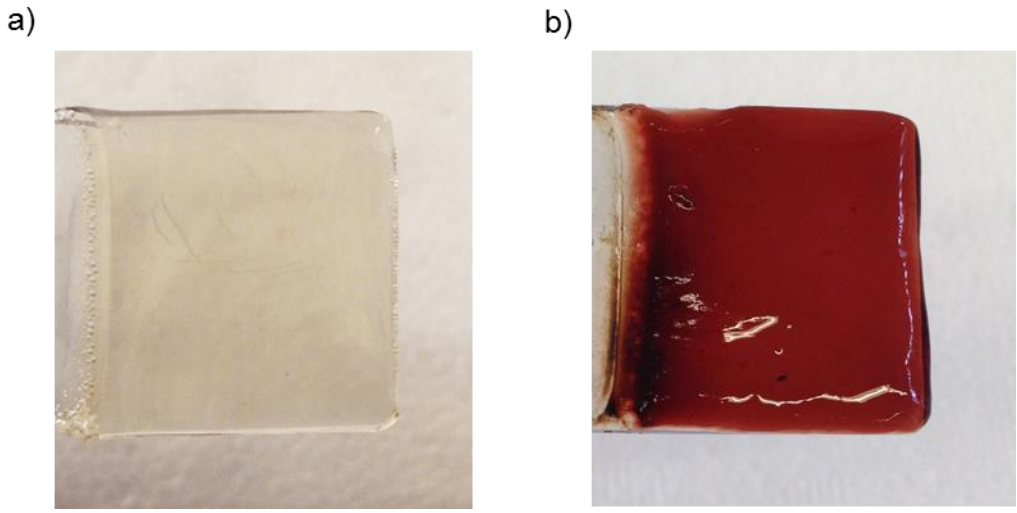

Figure 34 a) BrNapFF gel on FTO-coated glass slide b) BrNapFF gel after being immersed in DMEM for seven days

It is interesting to note that the final rheological properties after seven days are the same for the 7MeONapFF gel and the multi-component 7MeONapFF/2NapAA gel (Table 4). Before the immersion in media, 7MeONapFF gave a *G′* of 9800 Pa, whereas the multi-component gel was weaker, with a *G′* value of 3000 recorded. After seven days both gels gave a *G′* of 160 Pa and were therefore significantly weakened by being in the presence of DMEM. Having equal rheological properties would indicate that 2NapAA has become unassembled (as seen in single component, 2NapAA gels) in the multi-component gel, leaving only 7MeONapFF assembled and now virtually the same gel as the single component, 7MeONapFF gel. The same was observed for BrNapFF and BrNapFF/2NapAA gels after seven days. The pH of the gels were also measured before and after seven days in the presence in medium for BrNapFF and 7MeONapFF. Before immersion in the medium the pH values noted for BrNapFF and 7MeONapFF gels prepared were pH 3.7 and 4.3, respectively. After being removed from the DMEM after seven days, the pH values recorded for BrNapFF and 7MeONapFF were 7.3 and 7.6, respectively. DMEM had diffused into the hydrogel matrix, causing an increase in pH, but due to the substantially weaker gels after one week it is likely that some dissolution of gelator has occurred, leading to the increase in pH of the gels. After one week, both BrNapFF and 7MeONapFF were above their pK_a values and would be expected to be unassembled. However, these gels can form salt-induced gels from divalent salts such as Ca_2NO_3 and the salt-

containing DMEM could therefore be positively influencing the gelation stability of these materials.[34, 35] Despite being weakened, the gels could still be considered as "soft" gels after seven days, making it possible to carry out cell culturing experiments using these gels. Soft gels are classified as having *G'* values of ~ 100 – 1000 Pa - an elasticity similar to that of brain tissue.[58]

Firstly, cell growth was examined, and as stem cells have been known to differentiate into different lineages of cells depending on the "stiffness" of the gel matrix in which they are cultured, stem cells were used.[58] [59] More specifically, mouse mesenchymal stem cells (MSCs) were used. Hydrogels were prepared as described previously in this section but they then had to be placed under UV light for ~ 20 – 30 min before immersing in DMEM to ensure that the glass slide and gel were sterile. Seeding of cells and subsequent culturing and analysis was carried out by Christopher Hill (Institute of Translational Medicine, University of Liverpool). 5 x 10^4 mouse MSCs were seeded onto the surface of gels and allowed to attach and proliferate for one week at 37°C before analysis. However, it was found that cell death occurred within 24 hours of being seeded in the gels. As similar hydrogel materials have previously been demonstrated as suitable matrices for cell culture,[53] it was possible that the presence of HQ within the gel matrix was causing cell death. Gels of BrNapFF and 7MeONapFF were freeze-dried and NMR spectra of the remaining lipholised material were collected (Figure 35). Consequently, by comparison of gels before and after immersion in medium for seven days, it was found that virtually all of the HQ had diffused from the gels after seven days in DMEM (Figure 35). Gels were placed in DMEM for seven days before repeating any cell culturing experiments.

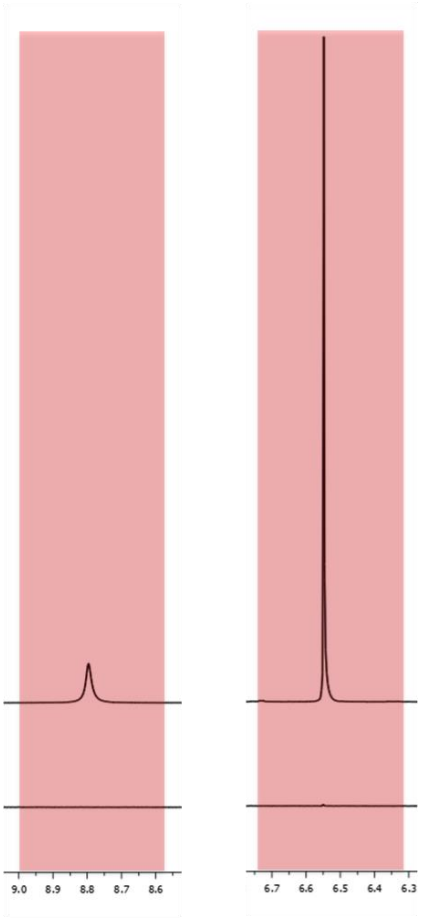

Figure 35 Partial NMR spectra for freeze-dried BrNapFF gels before (top) and after (bottom) immersion in DMEM, showing the presence of HQ peaks which diminish after seven days of immersion in DMEM

Seeding the same cell line as before, with the HQ now removed from the gel matrix showed an improvement in the environment for the cells. After seven days, cells were alive and some attachment to the gels and proliferation was visible (Figure 36).

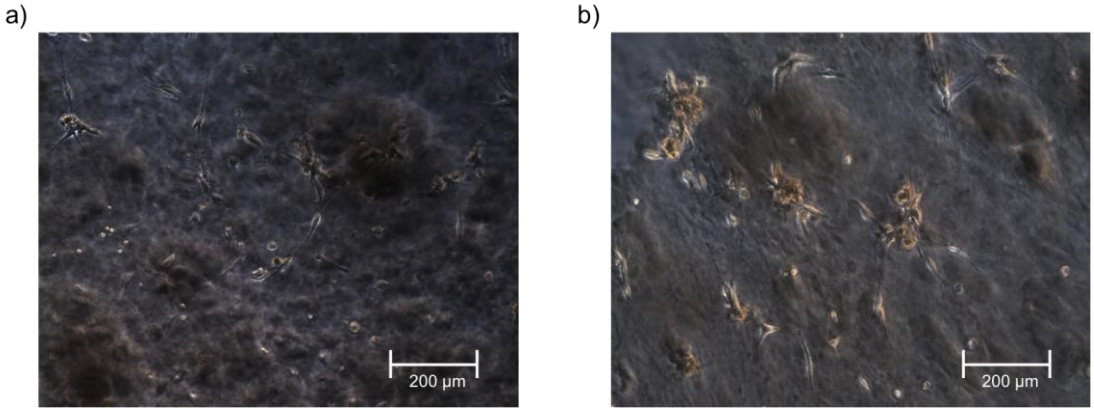

Figure 36 a) and b) show the attachment of some MSCs to a 7MeONapFF gel

Unfortunately, cell attachment to the hydrogels was sparse and strangely, cell attachment to the FTO-coated glass surface was more apparent. However Lakard *et al.* found that there was some affinity of a rat neuronal cell line to an FTO-coated glass slide. They observed attachment and cell growth of the rat neuronal cells on the FTO surface but this was not as abundant as on polyethyleneimide (PEI) and polypropyleneimine (PPI) gels grown on the FTO-coated slides.[67] Figure 37 shows the attachment and proliferation of MSCs to the surface of the FTO-coated slide. Here, formation of cell spheres was observed and staining for nuclear and cytoskeletal markers highlighted the cell-based architecture of these structures. As MSCs typically grow in a monolayer in culture, it is possible that this effect is due to the presence of soluble hydrogel components in the medium which are affecting cell behaviour. Alternatively, cells which had previously adhered to the gel surface and become detached may have been influenced by the nanotopography/chemical composition to differentiate.

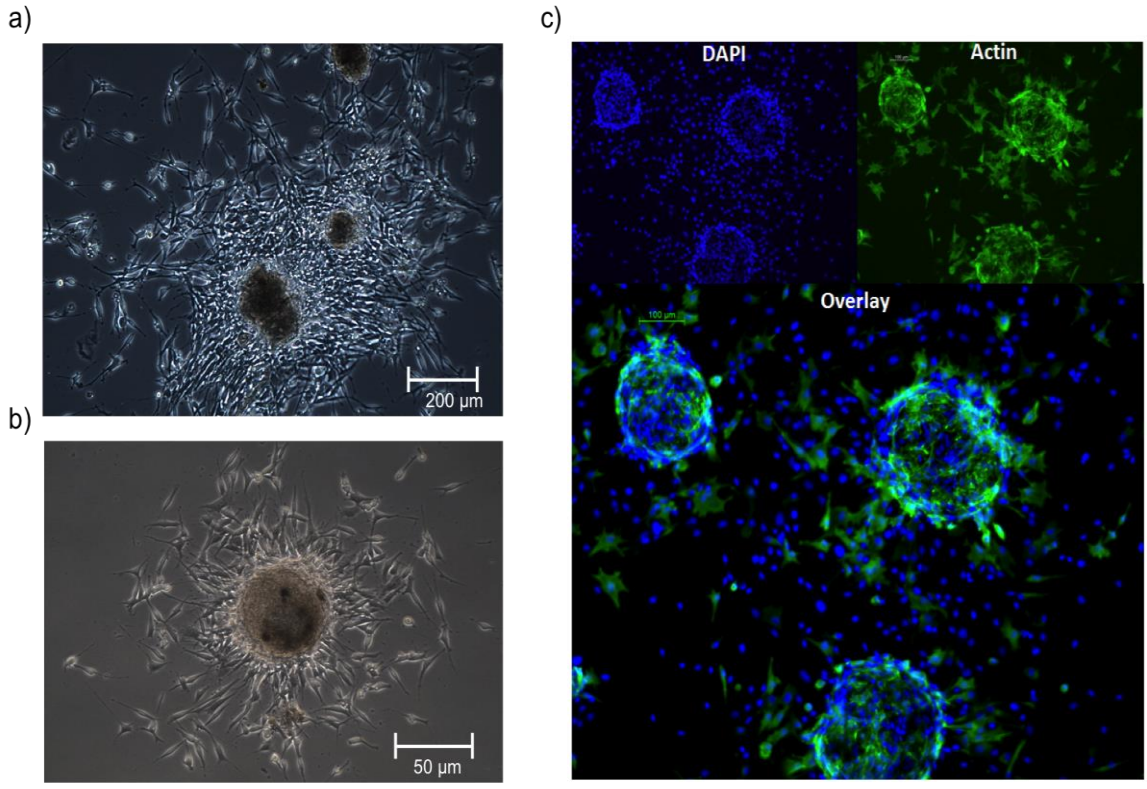

Figure 37 a) and b) show the formation of cell spheres on the surface of an FTO-coated slide at different magnifications and c) shows fluorescently stained cell spheres (nuclear stain DAPI (blue) and cytoskeletal stain F-actin (green))

5.3 Conclusion

It has been demonstrated that a galvanostatic approach can be used to electrochemically trigger gelation in some LMWG on a relatively large scale (and on multiple surfaces). By utilising the oxidation of HQ to lower the pH at an electrode surface, hydrogelation can be spatiotemporally controlled through prudent choice of gelator and current applied. The onset of gelation has been shown to be related to the pK_a of the gelator, along with final gel volume. Such profound control over gel properties has allowed for complex multiple layer and multi-component gels. This is of potential importance for use in cell culturing, where hydrogels with multiple fibrous matrices and more complex information content could influence the attachment and growth of cells. Patterned hydrogels can also be prepared from these materials which provide further complexity, with the potential to prepare topographies with a roughness suitable for influencing cell differentiation for example. These gelators also have the ability to form gels directly in cell culture medium, aiding in the significant potential of this methodology. However, there is some issue with stability under physiological conditions which must be rectified to optimise the promise of these materials.

5.4 References

1. M. Zhou, A. M. Smith, A. K. Das, N. W. Hodson, R. F. Collins, R. V. Ulijn and J. E. Gough, *Biomaterials*, 2009, **30**, 2523-2530.
2. L. Chen, K. Morris, A. Laybourn, D. Elias, M. R. Hicks, A. Rodger, L. Serpell and D. J. Adams, *Langmuir*, 2010, **26**, 5232-5242.
3. R. Orbach, L. Adler-Abramovich, S. Zigerson, I. Mironi-Harpaz, D. Seliktar and E. Gazit, *Biomacromolecules*, 2009, **10**, 2646-2651.
4. R. Vegners, I. Shestakova, I. Kalvinsh, R. M. Ezzell and P. A. Janmey, *J Pept Sci*, 1995, **1**, 371-378.
5. J. Raeburn, T. O. McDonald and D. J. Adams, *Chem. Commun.*, 2012, **48**, 9355-9357.
6. T. J. Measey, B. N. Markiewicz and F. Gai, *Chem. Phys. Lett.*, 2013, **580**, 135-140.
7. A. Mata, L. Hsu, R. Capito, C. Aparicio, K. Henrikson and S. I. Stupp, *Soft Matter*, 2009, **5**, 1228-1236.
8. R. J. Williams, A. M. Smith, R. Collins, N. Hodson, A. K. Das and R. V. Ulijn, *Nat. Nanotech.*, 2009, **4**, 19-24.
9. Y. F. Wang, Y. Liu, Y. Cheng, E. Kim, G. W. Rubloff, W. E. Bentley and G. F. Payne, *Adv. Mater.*, 2011, **23**, 5817-5821.
10. Y. Liu, Y. Cheng, H. C. Wu, E. Kim, R. V. Ulijn, G. W. Rubloff, W. E. Bentley and G. F. Payne, *Langmuir*, 2011, **27**, 7380-7384.
11. K. M. Gray, B. D. Liba, Y. F. Wang, Y. Cheng, G. W. Rubloff, W. E. Bentley, A. Montembault, I. Royaud, L. David and G. F. Payne, *Biomacromolecules*, 2012, **13**, 1181-1189.
12. J. L. Terrell, T. Gordonov, Y. Cheng, H. C. Wu, D. Sampey, X. L. Luo, C. Y. Tsao, R. Ghodssi, G. W. Rubloff, G. F. Payne and W. E. Bentley, *Biotechnol. J.*, 2012, **7**, 428-439.
13. Y. Cheng, C. Y. Tsao, H. C. Wu, X. L. Luo, J. L. Terrell, J. Betz, G. F. Payne, W. E. Bentley and G. W. Rubloff, *Adv. Funct. Mater.*, 2012, **22**, 519-528.
14. J. Redepenning, G. Venkataraman, J. Chen and N. Stafford, *J. Biomed. Mater. Res. Part A*, 2003, **66A**, 411-416.
15. X. L. Luo, J. J. Xu, Y. Du and H. Y. Chen, *Anal. Biochem.*, 2004, **334**, 284-289.
16. R. Fernandes, L. Q. Wu, T. H. Chen, H. M. Yi, G. W. Rubloff, R. Ghodssi, W. E. Bentley and G. F. Payne, *Langmuir*, 2003, **19**, 4058-4062.
17. E. K. Johnson, D. J. Adams and P. J. Cameron, *J. Am. Chem. Soc.*, 2010, **132**, 5130-5136.
18. Y. Liu, E. Kim, R. V. Ulijn, W. E. Bentley and G. F. Payne, *Adv. Funct. Mater.*, 2011, **21**, 1575-1580.
19. H. Aubin, J. W. Nichol, C. B. Hutson, H. Bae, A. L. Sieminski, D. M. Cropek, P. Akhyari and A. Khademhosseini, *Biomaterials*, 2010, **31**, 6941-6951.
20. J. L. Charest, M. T. Eliason, A. J. Garcia and W. P. King, *Biomaterials*, 2006, **27**, 2487-2494.
21. L. E. Buerkle and S. J. Rowan, *Chem. Soc. Rev.*, 2012, **41**, 6089-6102.
22. J. R. Moffat and D. K. Smith, *Chem. Commun.*, 2009, 316-318.
23. A. R. Hirst, J. E. Miravet, B. Escuder, L. Noirez, V. Castelletto, I. W. Hamley and D. K. Smith, *Chem. Eur. J.*, 2009, **15**, 372-379.
24. W. Edwards and D. K. Smith, *J. Am. Chem. Soc.*, 2013, **135**, 5911-5920.

25. L. Chen, S. Revel, K. Morris, L. C. Serpell and D. J. Adams, *Langmuir*, 2010, **26**, 13466-13471.
26. D. J. Adams, M. F. Butler, W. J. Frith, M. Kirkland, L. Mullen and P. Sanderson, *Soft Matter*, 2009, **5**, 1856-1862.
27. X. Ji, C. E. Banks, D. S. Silvester, A. J. Wain and R. G. Compton, *J. Phys. Chem. C*, 2006, **111**, 1496-1504.
28. M. Quan, D. Sanchez, M. F. Wasylkiw and D. K. Smith, *J. Am. Chem. Soc.*, 2007, **129**, 12847-12856.
29. K. A. Houton, K. L. Morris, L. Chen, M. Schmidtmann, J. T. A. Jones, L. C. Serpell, G. O. Lloyd and D. J. Adams, *Langmuir*, 2012, **28**, 9797-9806.
30. R. G. Weiss, Terech, P., *Molecular Gels and Fibrillar networks – A Comprehensive Guide to Experiment and Theory*, Springer, Dordrecht, The Netherlands, 2006.
31. C. Tang, A. M. Smith, R. F. Collins, R. V. Ulijn and A. Saiani, *Langmuir*, 2009, **25**, 9447-9453.
32. S. W. Tobey, *J. Chem. Educ.*, 1958, **35**, 514-515.
33. Y. Cheng, X. Luo, J. Betz, S. Buckhout-White, O. Bekdash, G. F. Payne, W. E. Bentley and G. W. Rubloff, *Soft Matter*, 2010, **6**, 3177-3183.
34. L. Chen, G. Pont, K. Morris, G. Lotze, A. Squires, L. C. Serpell and D. J. Adams, *Chem. Commun.*, 2011, **47**, 12071-12073.
35. L. Chen, T. O. McDonald and D. J. Adams, *RSC Adv.*, 2013, **3**, 8714-8720.
36. K. L. Morris, L. Chen, J. Raeburn, O. R. Sellick, P. Cotanda, A. Paul, P. C. Griffiths, S. M. King, R. K. O'Reilly, L. C. Serpell and D. J. Adams, *Nat. Commun.*, 2013, **4**, 1480-1485.
37. K. L. Morris, L. Chen, J. Raeburn, O. R. Sellick, P. Cotanda, A. Paul, P. C. Griffiths, S. M. King, R. K. O'Reilly, L. C. Serpell and D. J. Adams, *Nat. Commun.*, 2013, **4**, 1480-1485.
38. E. K. Johnson, L. Chen, P. S. Kubiak, S. F. McDonald, D. J. Adams and P. J. Cameron, *Chem. Commun.*, 2013, **49**, 8698-8700.
39. J. Dostalek, Y. Wang, A. Brunsen, F. Yu, A. Kasry and W. Knoll, *J. Nonlinear Opt. Phys.*, 2008, **17**, 121-129.
40. W. Knoll, *Annu. Rev. Phys. Chem.*, 1998, **49**, 569-638.
41. I. S. Lokuge and P. W. Bohn, *Langmuir*, 2005, **21**, 1979-1985.
42. Y. Nagai, L. D. Unsworth, S. Koutsopoulos and S. Zhang, *J. Control. Release*, 2006, **115**, 18-25.
43. C. W. Ou, H. M. Wang, Z. M. Yang and M. S. Chen, *Chin. J. Chem.*, 2012, **30**, 1781-1787.
44. Q. G. David, B. N. Zorraquin-Cornejo, A. Ganem-Rondero, E. Pinon-Segundo, M. G. Nava-Arzaluz and J. M. Cornejo-Bravo, *J. Mex. Chem. Soc.*, 2008, **52**, 272-278.
45. A. Mahler, M. Reches, M. Rechter, S. Cohen and E. Gazit, *Adv. Mater.* 2006, **18**, 1365-1370.
46. J. Tas, P. Oud and J. James, *Histochemistry*, 1974, **40**, 231-240.
47. S. Kashanian, S. Heidary Zeidali, K. Omidfar and N. Shahabadi, *Mol. Biol. Rep.*, 2012, **39**, 10045-10051.
48. B. Adhikari, G. Palui and A. Banerjee, *Soft Matter*, 2009, **5**, 3452-3460.
49. B. B. Mandal, S. Kapoor and S. C. Kundu, *Biomaterials*, 2009, **30**, 2826-2836.
50. N. B. Graham and M. E. McNeill, *Biomaterials*, 1984, **5**, 27-36.
51. S. Sutton, N. L. Campbell, A. I. Cooper, M. Kirkland, W. J. Frith and D. J. Adams, *Langmuir*, 2009, **25**, 10285-10291.
52. M. Wallace, D. J. Adams and J. A. Iggo, *Soft Matter*, 2013, **9**, 5483-5491.
53. Z. Yang, G. Liang, M. Ma, Y. Gao and B. Xu, *J. Mater. Chem.*, 2007, **17**, 850-854.
54. A. M. Smith, R. J. Williams, C. Tang, P. Coppo, R. F. Collins, M. L. Turner, A. Saiani and R. V. Ulijn, *Adv. Mater.*, 2008, **20**, 37-41.

55. M. Djalili-Moghaddam, R. Ebrahimzedah, S. Toll, *Annu. T. Nordic Rheo. Soc.* 2002, **10**, 139-145.
56. A. Z. Cardoso, A. E. Alvarez Alvarez, B. N. Cattoz, P. C. Griffiths, S. M. King, W. J. Frith and D. J. Adams, *Faraday Discuss.*, 2013, **166**, 101-116.
57. R. Fernandes, L.-Q. Wu, T. Chen, H. Yi, G. W. Rubloff, R. Ghodssi, W. E. Bentley and G. F. Payne, *Langmuir*, 2003, **19**, 4058-4062.
58. A. J. Engler, S. Sen, H. L. Sweeney and D. E. Discher, *Cell*, 2006, **126**, 677-689.
59. J. Nam, J. Johnson, J. J. Lannutti and S. Agarwal, *Acta Biomater.*, 2011, **7**, 1516-1524.
60. L. Dong and H. Jiang, *Soft Matter*, 2007, **3**, 1223-1230.
61. S. M. DePorter, I. Lui and B. R. McNaughton, *Soft Matter*, 2012, **8**, 10403-10408.
62. D. C. Duncan and D. G. Whitten, *Langmuir*, 2000, **16**, 6445-6452.
63. B. Escuder, M. Llusar and J. F. Miravet, *J. Org. Chem.*, 2006, **71**, 7747-7752.
64. J. F. Betz, Y. Cheng, C. Y. Tsao, A. Zargar, H. C. Wu, X. Luo, G. F. Payne, W. E. Bentley and G. W. Rubloff, *Lab Chip*, 2013, **13**, 1854-1858.
65. G. Pont, L. Chen, D. G. Spiller and D. J. Adams, *Soft Matter*, 2012, **8**, 7797-7802.
66. R. Huang, W. Qi, L. Feng, R. Su and Z. He, *Soft Matter*, 2011, **7**, 6222-6230.
67. S. Lakard, G. Herlem, A. Propper, A. Kastner, G. Michel, N. Vallès-Villarreal, T. Gharbi and B. Fahys, *Bioelectrochemistry*, 2004, **62**, 19-27.

CHAPTER 6

The Use of Molecular Rotors to Probe the Kinetics of Assembly in Low Molecular Weight Hydrogels

6.1 Introduction

Several classes of low molecular weight gelators (LMWG) have been demonstrated in the literature to form hydrogels that are tunable by altering the parameters that trigger gelation.[1-4] Along with changes in the self-assembly trigger, the introduction of additives[5-10] and salts[11-14] can have an influence on the final behaviour and attributes of a gel. It is clear that even subtle changes in the gelation conditions can affect the final gel properties.[15] Despite knowing that tunability of the final properties of these materials is possible, there is less known about the process by which these gels form.[16] If the self-assembly process could be better understood, the possibility to specifically tune materials to possess desired properties for a particular application is one that could be of paramount importance. When a gel forms, the gelator molecules in solution must firstly self-assemble – triggered by a change in solution conditions, before the assembled fibrils continue to grow, entangle and form a network capable entrapping the solvent (water) and affording a gel.[17-19] This increase in structure in solution ultimately leads to an increase in viscosity as the transition from a solution to a gel ensues.

Fluorescent probes have been frequently used in assembled materials to monitor the formation and/or presence of micellar structures.[20, 21] For example, pyrene is known to bind and fluoresce in the presence of poly(styrene)-poly(ethylene oxide) block copolymer micelles, showing an increase in fluorescence upon transition from aqueous environment in solution to a hydrophobic micellar environment.[20] The fluorescent data can be interpreted to give an indication of the critical micelle concentration of the material. Similar studies can also be demonstrated with the dye 8-anilino-1-naphthalenesulfonic acid (ANS)[21]; as this dye also shows sensitivity to hydrophobic environments associated with micelles. ANS can probe the micelle production of peptide amphiphilic gelators[21] – similar materials to that studied in this Chapter (and Thesis). In recent years, a class of fluorescent materials known as molecular rotors have been used as non-mechanical viscosity sensors in some bio- and polymeric materials.[22-24] These materials differ from fluorescent probes such as

pyrene and ANS as they are sensitive to changes in viscosity and therefore sensitive to structural changes within close proximity to the rotor structure itself. These molecules are characterised by a viscosity-dependent fluorescent quantum yield which has a relationship with viscosity (Equation 1), as described by the Förster-Hoffman equation[25, 26]:

$$\log I = C + x \log \eta \qquad (1)$$

I = fluorescent intensity
C = conc. and temp. constant
x = dye-dependent constant
η = viscosity

Fluorescent molecular rotors are flexible molecules which undergo an intramolecular twisting motion upon photo-excitation.[26-28] This twisting episode leads to a return to the ground state of the molecule *via* non-radiative emission or by red-shifted emission (dependent on molecular structure). The fluorescent activity is therefore dependent on local viscosity.[27] A typical molecular rotor consists of three components: an electron donor unit, an acceptor unit and an electron-rich spacer unit. The latter brings the other two components together in conjugation, allowing movement of electrons. When the molecule is in a planar configuration, an intramolecular twisting motion of the sub-groups is induced by electrostatic forces which causes the molecule to enter a non-planar configuration. This state has a lower excited-state energy and the molecule fluoresces from this state.[28] Steric hindrance of the twisted state caused by increases in local viscosity is known to increase the energy gap between the planar locally excited and the twisted state emission bands. The emission therefore shifts in favour of the planar emission band.[28] Structural differences between rotors may afford more sensitivity. Wang *et al.* demonstrated that strong electron donor groups on phenyl rings of rotors increases sensitivity in ethylene glycol/water mixtures.[29] Molecular rotors have become increasingly popular due to their high sensitivity and ability to compare the results to mechanical data collected using expensive rheometers.[24] The data collected by these rheometers provide information regarding the evolution of structure during the assembly and hydrogelation process. Molecular rotors have the potential to provide information that can correlate with this rheological data.[24]

Perhaps the most commonly studied molecular rotor is 9-(2,2-dicyanovinyl)julolidine (DCVJ).[26, 30] This class of molecule has been known to be particularly sensitive in a variety of solvents[31], in organized assemblies[20, 32] (micelles, cells) and in polymers[22, 23] (solutions and solid matrices). Loutfy and Teegarden demonstrated an increase in fluorescent intensity of DCVJ was dependent on tacticity of PMMA.[33] Here in this Chapter, the kinetics of gelation is probed using known molecular rotors DCVJ and 9-(2-carboxy-2-cyanovinyl)julolidine (CCVJ) but the study of Thioflavin T (ThT) is also investigated here. ThT is widely regarded as a stain for β-amyloid structures[34, 35], with further reports showing that the binding of ThT to this type of structure is affected by the cavity size, which in turn, affects the fluorescence.[36] Despite this, it has been suggested that ThT could in fact be a molecular rotor. Stsiapura *et al.* showed that fluorescent intensity of ThT increased in the presence of glycerol/water mixtures with increasing viscosity.[37] They hypothesised that ThT does indeed bind to β-amyloid structures but the increase in fluorescence intensity is determined by the rigidity of the local environment in which ThT is located i.e. the local viscosity affects the ability of the benzathiole ring to rotate relative to the aminobenzene ring in the excited state.[37] Thus, ThT appears to be behaving as a molecular rotor. This Chapter will investigate whether or not ThT behaves as a molecular rotor when probing the self-assembly and hydrogelation kinetics of several LMWG. This group has previously demonstrated the use of ThT to probe the gelation process of the gelator BrNapAV[38], which will also be further investigated in this Chapter.

6.2 Results and Discussion

6.2.1 pH-Triggered Hydrogelation using Glucono-δ-lactone (GdL)

In the previous Chapters, various types of trigger have been shown to induce self-assembly and hence gelation of several gelators. The gelation times of these gels vary depending on the trigger and the conditions of that trigger. Chapter 4 discussed UV-triggered gels where a slow pH drop allowed for gelation to progress over ~ 14 hours. In this Chapter, a pH trigger is adopted which itself allows a slow liberation of

protons to give a decrease in pH slowly with time. This pH trigger utilises the hydrolysis of glucono-δ-lactone (GdL) to gluconic acid in water (Scheme 1).[39] GdL hydrolyses slowly in water, with the dissolution of GdL in water being much quicker than the hydrolysis, enabling a homogeneous pH drop throughout the solution.[40]

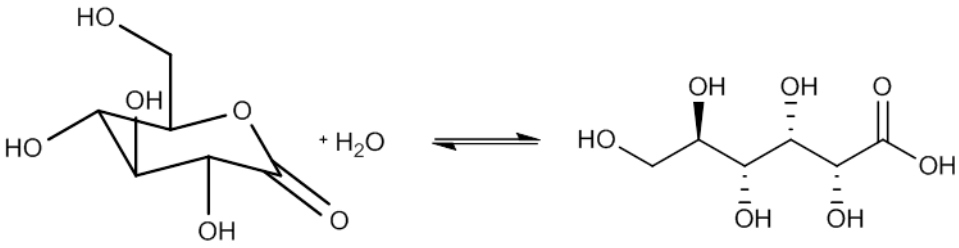

Scheme 1 Hydrolysis of glucono-δ-lactone (GdL) to gluconic acid

To probe the kinetics of gelation, a GdL trigger is capable of causing a pH decrease slow enough to sufficiently monitor the kinetics of the gelation process.[40] Solvent mediated methods such as that discussed in Chapter 3 induced gelation over a much shorter time period, rendering the kinetic process of gelation difficult to monitor. In this Chapter, various naphthalene-based dipeptide gelators (Scheme 2) were used to study the kinetics of gelation. All gelator samples were prepared at concentration of 5 mg/mL (unless stated otherwise) by dissolving the gelator in water with one molar equivalent of sodium hydroxide (NaOH, 0.1 M). Once dissolved, a homogenous, transparent solution was formed for all gelators studied. 7MeONapFF, 1NapFF and 2NapFF were also viscous solutions, as previously reported.[13, 41, 42] A weighed amount of GdL was then placed in another vial to which a gelator solution was added. After adding the gelator solution, gentle manual mixing allowed the GdL to dissolve before the kinetics of gelation was monitored.

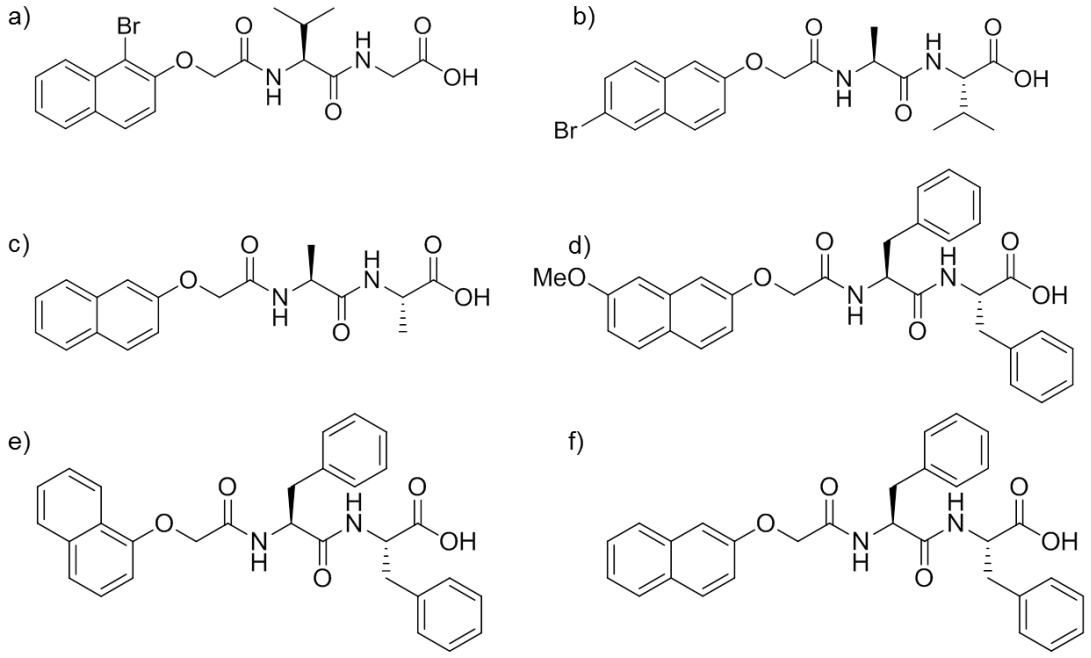

Scheme 2 Structures of the gelators a) 1BrNapVG b) BrNapAV c) 2NapAA d) 7MeONapFF e) 1NapFF and f) 2NapFF. The pK_a of 1BrNapVG was measured by adding GdL and recording the pH decrease. All other pK_a values have been measured previously[38, 41-43]

6.2.2 Kinetics of Hydrogelation of Various Gelators Monitored using Molecular Rotors

To probe the kinetics of gelation *via* spectroscopic methods, a molecular rotor was added to the gelator solution before gelation occurred. The molecular rotors studied in this Chapter are DCVJ, CCVJ and ThT (Scheme 3). The presence of these molecular rotors in the gelling solution allows the kinetic process to be probed. Despite the instability of ThT at high pH[44], the pH drop upon addition of GdL to the gelator solution, and prior to the addition of ThT, was sufficient enough to allow ThT fluorescence to be monitored during the gelation process.

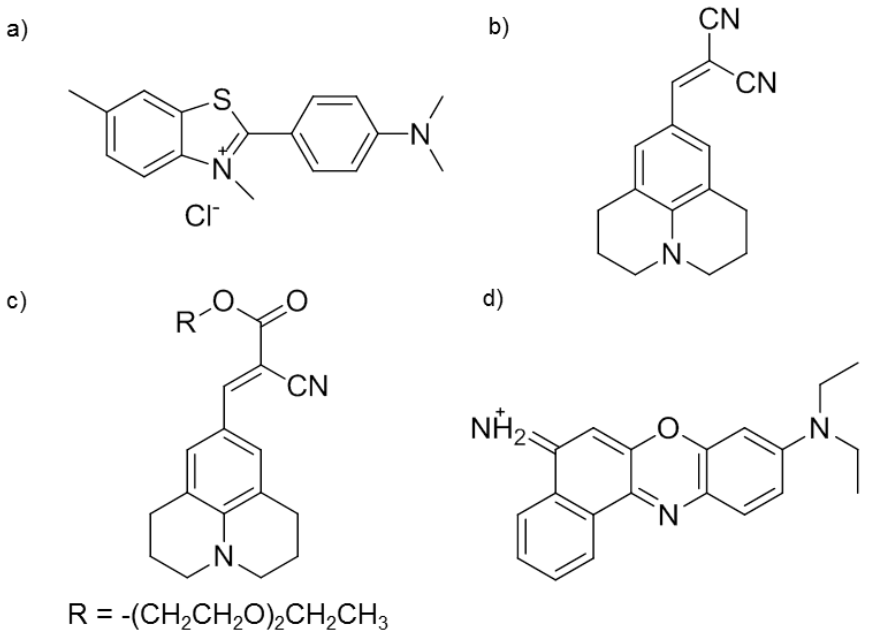

Scheme 3 Structures of the molecular rotors: a) Thioflavin T b) DCVJ c) CCVJ and d) the hydrophobic stain Nile Blue

Using real-time analysis to correlate the fluorescent and rheological properties can provide vital information about the gelation process.[38] As gelation ensues, fibril growth occurs. This growth leads to longer fibres and fibre entanglement, which entraps the solvent component of the hydrogel. In doing so, a transition from a liquid to viscoelastic material occurs. From a rheological standpoint, this leads to an increase in the storage modulus (*G'*) over the loss modulus (*G''*) i.e. the elastic properties take precedence over the liquid properties and a more 'solid-like' material is measured. This can be related to the information that a molecular rotor can provide, in that it can probe changes in local viscosity – a factor that ultimately coincides with the formation of structure and evolution of mechanical properties of a hydrogel. As viscosity increases with gelation, the fluorescence output increases when a molecular rotor is present.

6.2.2.1 1BrNapVG

Figure 1a shows the fluorescence data for the gelation of 1BrNapVG in the presence of ThT, DCVJ and Nile Blue. Nile Blue is a hydrophobic stain and is used as a negative control because although Nile Blue stains the fibres of the gel[40], it is not currently known to be viscosity-dependent and hence, behave as a molecular rotor.

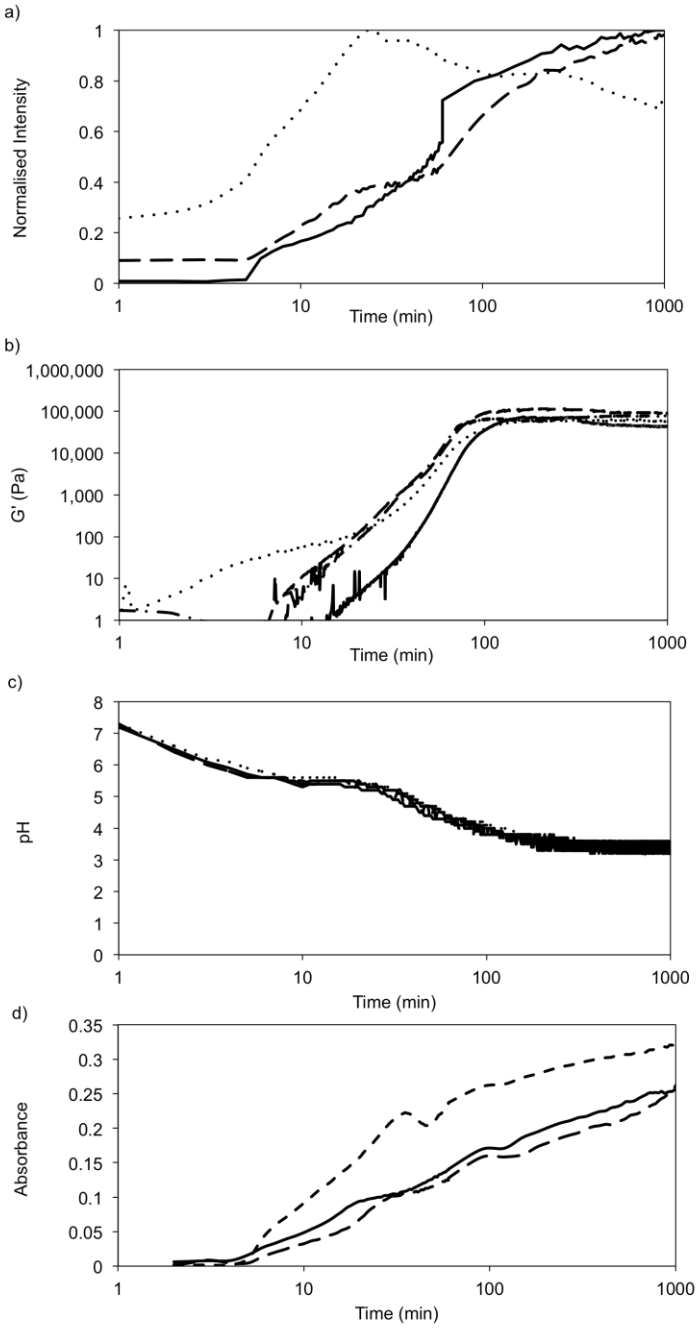

Figure 1 Kinetics of gelation of 1BrNapVG. a) Normalised changes in fluorescence of the dyes: Thioflavin T (—) at 475 nm (λex = 455 nm); DCVJ (– –), at 485 nm (λex = 470 nm) and Nile Blue (···) at 660 nm (λex = 630 nm) upon addition of 1BrNapVG solutions to GdL (8 mg/mL). b) Rheological properties during the kinetic process of gelation of 1BrVG (—) and in the presence of ThT (– –), DCVJ (- -) and Nile Blue (···). c) Changes in pH with time after GdL is added to 1BrVG (in the presence and absence of rotors) and gelation ensues and d) shows the changes in turbidity with time (measured by UV/vis spectroscopy at 600 nm) for 1BrVG in the absence of rotor (—), the presence of ThT (– –) and DCVJ (- -)

It can be seen that in the presence of Nile Blue, a fluorescence output is observed as soon as GdL is added to a 1BrVG solution. In the presence of Nile Blue, a maximum intensity is reached after just 22 minutes before steadily decreasing with time. Nile Blue fluorescence is pH dependent and so the decrease in fluorescence at longer times can be ascribed to the pH decreasing below a critical value.[45] At the point of maximum intensity little measurable G' (< 100 Pa) is observed from the rheology (Figure 1b), therefore the fluorescent behaviour shown by Nile Blue does not indicate a sensitivity to changes in local viscosity. Rather, its affinity for hydrophobic environments would suggest it becomes associated with the fibres of 1BrNapVG upon addition of GdL to the gelator solution and therefore, aggregation of the gelator molecules occurs even if a network is not being formed.

The fluorescence behaviour, however, is different in the presence of the proposed molecular rotor, ThT, and for DCVJ. The data for Nile Blue shows a sharper increase in intensity at the same time as the samples containing rotor. In the presence of ThT or DCVJ, there is no fluorescent signal for the first five minutes after the addition of GdL. After this time, there is a steady increase in the intensity – an analogous measurement of the pH decrease over time after the addition of GdL (Figure 1c) shows that the increase in intensity occurs when a pH of 5.7 is reached. The apparent pK_a of 1BrNapVG is 5.6. Hence, in common with other gelators, the initial changes in viscosity occur at approximately the pK_a of the gelator.[38] It is important to note that the kinetics of pH change and the pK_a of the gelator in solution is unaffected by the presence of either molecular rotor or Nile Blue (Figure 1c). As mentioned in previous Chapters and in the literature[38, 41, 42, 46], gelation occurs below the pK_a of these materials. It would appear from the fluorescence data collected that at the pK_a of 1BrNapVG, self-assembly occurs and fibrillar growth is significant enough to change the local viscosity in the environment surrounding the rotor. There also appears to be a two-stage fluorescent profile, which is reminiscent of the fluorescent data shown by Chen at al. for the gelation of BrNapAV in the presence of ThT.[38] The second stage increase occurs after ~ 50 min – at a pH of 4.5. Therefore the second stage occurs well below the pK_a of the gelator. These changes in fluorescence intensity and hence, inherent changes in viscosity correlate with the kinetics of rheology (Figure 1b). A measurable G' value occurs (i.e. $G' > 0$) a few minutes after

the first detected changes in viscosity from the fluorescent data. This may be expected as molecular rotors are sensitive to local changes in viscosity whereas rheological measurements are sensitive to changes in the bulk, which would not be apparent until more significant changes in structure are present. The initial evolution of *G'* occurs slightly below the pK_a of the gelator (or at the pK_a in the case of gelation in the presence of DCVJ), close to the initial changes in viscosity. A steady increase in the rheological properties, where *G'* becomes increasingly higher than *G"*, occurs as the pH becomes lower than the pK_a. Here, it can be expected that significant fibril growth has occurred, water is being entrapped and gelation is underway. Interestingly, the second stage in the fluorescence profile occurs (Figure 1a) during this. The times at which these processes occur differ slightly between the presence of rotors and the absence of any rotor but, crucially, the pH at which these processes occur remains relatively constant. When the pH reaches ~ 4, *G'* reaches a plateau. The presence of the molecular rotors appears to have an effect on the plateau modulus. Figure 1b shows that *G'* ranges from 58000 – 22000 Pa, depending on the rotor present (or lack thereof). Perhaps, these differences in final mechanical properties relate to the lateral association of the rotors within the fibres of the gel. Each gelator may bind or associate differently. The measured final rheological properties are in a range similar, if not at the higher end of the range to related LMWG prepared using GdL and other assembly methods.[17, 42, 47]

Clearly, the self-assembly process is unaffected by the presence of any rotor. Only the final properties appear affected. Figure 1d shows that UV turbidity measurements indicate minimal differences between gels and therefore there are no notable changes in the size range of the fibres – on a larger length scale at least. Differences on a nanometre scale would not be detectable from these measurements. 1BrNapVG gels containing Nile Blue were not measured as the λ_{max} of Nile Blue is in the same region as that monitored for turbidity (600 nm). No noteworthy differences in turbidity are observed for any of the gelators studied and therefore the data is not shown for other gelators discussed in this Chapter.

6.2.2.2 BrNapAV

The use of molecular rotors to study the kinetics of gelation is not restricted to a single gelator system. The two gelators: BrNapAV (previously studied with ThT[38]) and 2NapAA (structures shown in Scheme 2); similar in structure to 1BrNapVG were also studied. Figure 4 shows the kinetic fluorescence data collected for BrNapAV in the presence of ThT, DCVJ and Nile Blue. An additional molecular rotor, CCVJ was also studied here to gain further evidence that ThT correlates with the behaviour of molecular rotors. Figure 4 shows a clear correlation in behaviour between both DCVJ and CCVJ (known molecular rotors) and ThT. Although BrNapAV has previously been thought to form β-sheet structures in GdL gels[38], the behaviour of ThT essentially mirrors that of a molecular rotor, giving the same kinetic information as a molecular rotor and therefore does not appear to behave as a β-sheet stain (shown previously by this group[38]). In the presence of these rotors, no fluorescence is observed until the pH drops to around the pK_a (5.8) of BrNapAV.[38] At this point, the fluorescence intensity steadily increases before subtly undergoing a sharper increase in intensity (at pH ~ 4.3) leading to a plateau in intensity around pH 3.8. ThT has been previously reported by this group to probe the gelation process of BrNapAV but shows slightly different results from that reported in this Chapter. The data collected here shows that the initial increase in fluorescence (with ThT) occurs just above (pH 6.1) the pK_a of the gelator, whereas previous reports indicate that this initial increase occurs slightly below (5.4) the pK_a.[38] The reason for this could be due to an unintentional lag time between setting the pH and fluorescence measurements, leading to a slight offset in the times. Furthermore, the previous work used both lower concentration of ThT and GdL. The latter would result in a slower pH drop than shown in this Chapter which may suggest that the pH at which the fluorescence of ThT initially increases is more accurate in the previous report. Conversely, the lower ThT concentration could also play a role in the onset of fluorescence intensity.

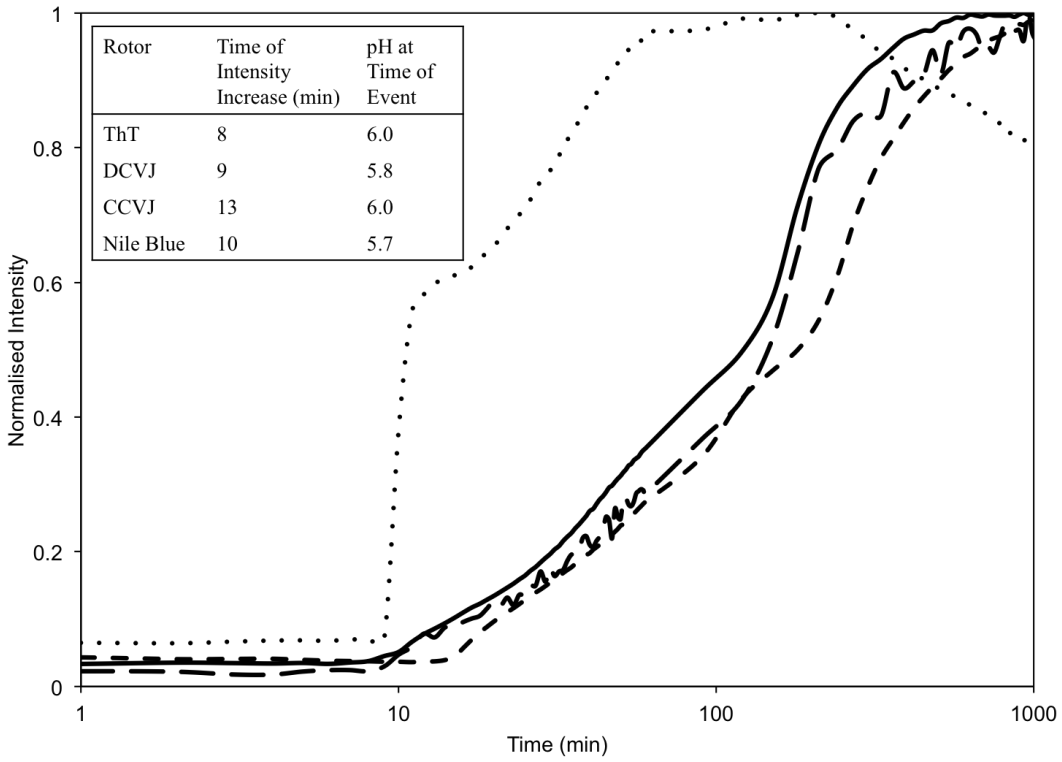

Figure 4 Normalised changes in fluorescence of the dyes: Thioflavin T (—) at 475 nm (λ_{ex} = 455 nm); DCVJ (– –) at 485 nm (λ_{ex} = 470 nm); CCVJ (- -) at 485 nm (λ_{ex} = 460 nm) and Nile Blue (···) at 660 nm (λ_{ex} = 630 nm) upon addition of BrNapAV solutions to GdL (8 mg/mL). Shown inset is a table of the times and pH values at which the fluorescent behaviour changes

The initial increase in fluorescence intensity shows a direct correlation with kinetic rheological properties (summarised in Table 2) as the initial measurable *G'* value and hence, initial indication of 'solid-like' structure within the material also occurs at approximately the pK_a of the gelator much like that observed for 1BrNapVG. Further correlation is noted in the points at which plateaus in the fluorescence intensity and *G'* are observed. For all rotors tested, the fluorescence intensity reached a plateau around pH 3.8, as did *G'*, thus suggesting that fibril growth and entanglement is extensive enough to fully immobilise the solvent and therefore bulk hydrogelation is complete at this point. No further changes in viscosity would be experienced in the vicinity of the molecular rotors and as such, the fluorescence intensity would not continue to increase. Similarly, once hydrogelation is complete no further changes would be noted on the bulk scale, leading to *G'* remaining constant after pH 3.8 (approximately) is reached.

Again, in the presence of Nile Blue different fluorescent behaviour is noted. The fluorescence intensity does not begin to increase until the pK_a of BrNapAV is reached, much in the same way as in the presence of the rotors, but a sharp increase in intensity is noted after this point before a plateau is reached at pH 5.2. From the rheological data, this plateau in fluorescence intensity occurs before gelation and does therefore give evidence of fibril growth before bulk gelation and Nile Blue association with the hydrophobic fibres of the gelator. The intensity does decrease slightly as lower pH values are reached due to the sensitivity of Nile Blue to changes in pH.[45] It is also notable that although the presence of molecular rotors allow the kinetic process of self-assembly and gelation of these materials to be monitored, it appears to have an adverse effect on the final bulk rheological properties of the gelator. The kinetic pathway to reach the final hydrogel appears the same, but hydrogels of BrNapAV show a plateau storage modulus of 38000 Pa in the absence of any rotor, which decreases to 11000 Pa in the presence of any of ThT, DCVJ, or CCVJ and significantly decreases to 2000 Pa in the presence of Nile Blue. These differences in *G'* are more pronounced in BrNapAV gels than in 1BrNapVG gels. Our group has previously shown that altering the gelation conditions affects the kinetics, but appears to have little to no effect on the final mechanical properties.[48] Conversely, the data shown in here in this Chapter shows that the kinetic behaviour correlates with the pH decrease during gelation in all cases, despite the kinetics of the pH change being affected by the presence of the dye, but the final mechanical properties are affected by changes in the gelation conditions. However, the previous work carried out by this group shows changes in gelation conditions by altering the temperature and/or GdL concentration whereas the data shown in this chapter alters the gelation conditions by way of an additive (a dye), which could rationally explain why the latter gels mechanically differ. The presence of an additive can affect the network formation, leading to changes in the bulk properties.[8, 49] Interactions between gelator and rotor and position of rotor molecules within the fibril matrix could contribute to the diminished rheological properties of gels containing a molecular rotor (or Nile Blue). Many researchers use molecular rotors to monitor the assembly of their materials but perhaps fail to check if the assembly is affected by the presence of the rotor itself. Despite the findings in this Chapter, there is also evidence of the inclusion of an additive being of no effect on the rheological

properties.[50] Previously, this group has added a dansyl derivative to solution of the gelator 2NapFF and added GdL to form a gel as described in this Chapter. Addition of a dansyl derivative did not affect the rheological properties.[50]

Rotor	Time when G' > 0 (min)	pH at Time of Event	Time of Sharp G' Increase (min)	pH at Time of Event	Time of G' Plateau (min)	pH at Time of Event
No Rotor	11	5.8	86	4.6	413 (38000 Pa)	3.5
ThT	7	6.1	70	5.2	363 (11000 Pa)	3.8
DCVJ	10	5.8	36	5.4	232 (11000 Pa)	4.0
CCVJ	7	6.1	33	5.7	205 (1000 Pa)	4.0
Nile Blue	7	5.8	33	5.5	205 (2000 Pa)	3.8

Table 2 Summary of the kinetic changes in the rheology of BrNapAV gelation in the presence (and absence) of various dyes

6.2.2.3 2NapAA

The gelation kinetics of 2NapAA showed similar behaviour to both 1BrNapVG and BrNapAV. In the presence of either ThT or DCVJ, the fluorescence data (Figure 5) shows an increase in intensity at approximately the pK_a of 2NapAA (5.1), where self-assembly begins and structure is of a size significant enough to induce changes in local viscosity. Again, this correlates with the rheological properties (Table 3) measured on the same time scale during the gelation process. A measurable *G'* value (evolution of 'solid-like' properties) occurs at the same point as initial detected changes in viscosity by the rotors. Despite these similarities being noted between the gelators tested, ThT and DCVJ fluorescence do not reach a distinct plateau in intensity, but *G'* does. From the fluorescence data, it would appear that the local viscosity is still increasing at 1000 min. However, the rheological properties do not change after ~ 200 - 300 min (pH 4.2 – 4.4). This may be because the sensitivity of both the molecular rotors to their environment and the fluorescence spectroscopy

technique itself elude to subtle changes in local viscosity at longer times that are not detectable at the bulk scale and hence, by rheology. As seen for the previous gelators tested, the presence of a molecular rotor in the gelator solution also has an effect on the final mechanical properties measured (Table 3), although the kinetics of gelation are unaffected. Notably, Nile Blue showed no fluorescent output upon addition to a 2NapAA solution with GdL, or throughout the gelation process. This could be attributed to the more hydrophilic nature of 2NapAA (*log P* = -0.16) when compared to the other gelators studied (*log P*[51] of 1BrNapVG, BrNapAV, 7MeONapFF, 1NapFF and 2NapFF calculated as 1.57, 1.40, 2.79, 2.74, and 2.76, respectively). Nile Blue stains hydrophobic materials and it is possible that 2NapAA is below the 'hydrophobicity threshold' and therefore the fibres of 2NapAA are not stained by Nile Blue. Nile Blue must merely remain in the surrounding solution and have no affiliation with fibrous matrix. It is important to note that ThT monitors the kinetic behaviour of 2NapAA during hydrogelation much in the same way as DCVJ and therefore appears to behave as a molecular rotor.

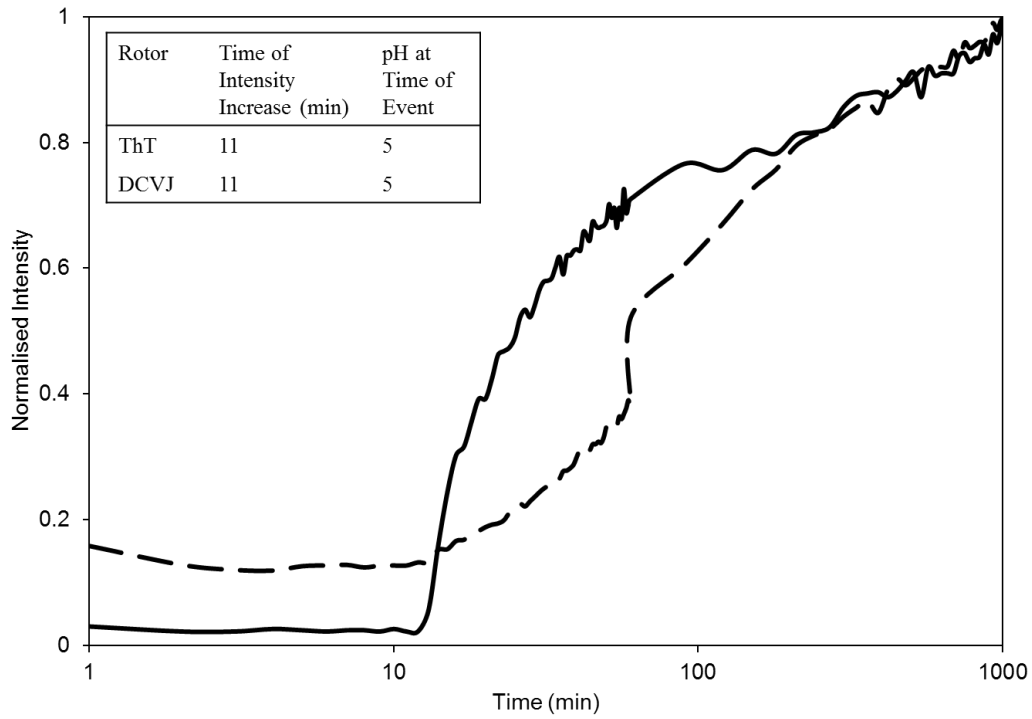

Figure 5 Normalised changes in fluorescence of the dyes: Thioflavin T (—) at 475 nm (λ_{ex} = 455 nm) and DCVJ (– –) at 485 nm (λ_{ex} = 470 nm) upon addition of 2NapAA solutions to GdL (8 mg/mL). Shown inset is a table of the times and pH values at which the fluorescent behaviour changes

Rotor	Time when G' > 0 (min)	pH at Time of Event	Time of Sharp G' Increase (min)	pH at Time of Event	Time of G' Plateau (min)	pH at Time of Event
No Rotor	15	5.0	47	4.9	268 (100000 Pa)	4.2
ThT	20	5.0	56	4.8	166 (48000 Pa)	4.4
DCVJ	17	5.0	49	4.9	166 (48000 Pa)	4.4

Table 3 Summary of the kinetic changes in the rheology of 2NapAA gelation in the presence (and absence) of various dyes

6.2.2.4 7MeONapFF

Although the gelators studied so far differ in chemical structure by the addition of substituents and the position of the dipeptide (and the amino acid composition) on the naphthalene ring, the solutions of these gelators all have a viscosity akin to that of water.[12] Therefore, the assumption that the changes in viscosity during the transition from solution to gel phase is not only distinct but significant can be made. Thus, allowing a clear evolution in fluorescent output to observed when a molecular rotor experiences changes in local viscosity. For gelators that form viscous solutions due to the formation of micellar structures at high pH, a locally viscous environment will already be apparent in the vicinity of the molecular rotor. A fluorescent signal would be expected before hydrogelation due to self-assembly of the gelator molecules to worm-like micelles before the addition of GdL. The combination of this increased initial viscosity and the tendency for more viscous gelators to be more hydrophobic with higher apparent pK_a values[13, 42, 46] could render the ability to monitor the kinetic process of gelation *via* the use of molecular more difficult. To test this, we examined the assembly of the gelator 7MeONapFF (Scheme 2), which has previously been shown to form transparent gels by other methods and also produces a viscous solution at high pH.[12, 13, 41] The kinetics of the gelation of 7MeONapFF was monitored using ThT and the known rotors DCVJ and CCVJ (Figure 6a).

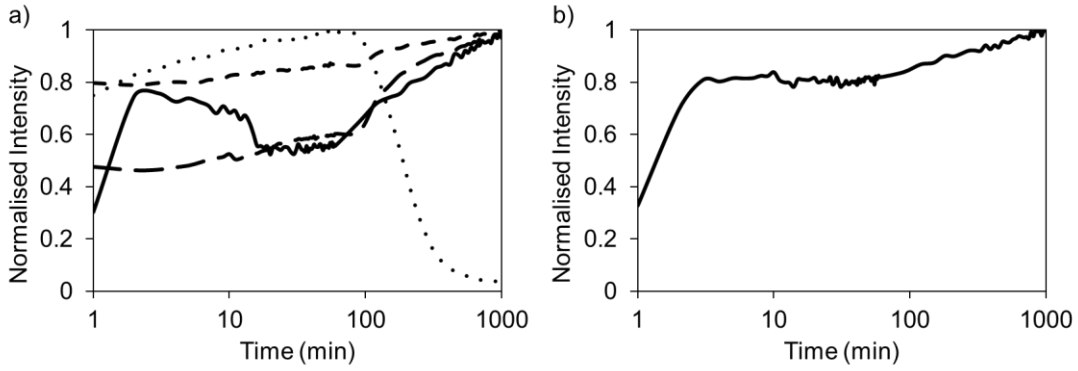

Figure 6 Normalised changes in fluorescence of the dyes: Thioflavin T (—) at 475 nm (λ_{ex} = 455 nm); DCVJ (— —) at 485nm (λ_{ex} =470 nm); CCVJ (- -) at 485 nm (λ_{ex} = 460 nm) and Nile Blue (···) at 660 nm (λ_{ex} = 630 nm) upon addition of a) 7MeONapFF and b) 1NapFF solutions to GdL (8 mg/mL)

All three rotors give a fluorescent signal immediately following the addition of GdL; as could be envisaged due to the viscous nature of the gelator samples. CCVJ gives a fairly constant fluorescence intensity throughout the time period of the experiment, however the other two rotors show slight deviations from this. Although the presence of ThT shows an immediate fluorescent signal, the intensity (data shown in Figure 6 is normalised) is much lower than for CCVJ, and shows an increase until the pH reaches 7.0 – the apparent pK_a of the gelator – after only 3 min. DCVJ does not show this trend. Rather it gives a constant intensity from the beginning of the measurements. This increased fluorescence within the first few minutes in the presence of ThT suggests that ThT probes a different environment to the other two rotors. There is also the possibility that, due to the presence of worm-like micelles at high pH[12] which give a viscous solution, there is a lag time associated with ThT incorporation into the local environment which elicits an increase in the fluorescent quantum yield. This may be a result of mixing the viscous gelator solution with the aliquot of ThT. An initial increase in the intensity of fluorescence is also apparent in another hydrophobic, viscous gelator: 1NapFF (Figure 6b), when ThT is present. After the initial increase in the presence of ThT in 7MeONapOFF samples, instead of remaining constant, the fluorescence intensity fluctuates between decreasing and increasing intensity, below the pK_a of the gelator. These fluctuations could be an effect of the instability of ThT at high pH. DCVJ also shows an increase around a similar period in the gelation process, at a pH of 4.4, as 7MeONapFF begins to increase again.

As previously observed for the other gelators in this Chapter, Nile Blue does not display behaviour similar to the molecular rotors. For 7MeONapFF (Figure 6a), a fluorescent signal is observed and remains relatively constant until a pH of 4.0, where a sharp decrease is noted until an intensity of almost zero is reached. This type of diminished fluorescent signal has been demonstrated above for the other gelators but is more pronounced here. Importantly, the rheological behaviour is consistent for all the gelators tested but the final mechanical strength varies significantly between the rotors present in the gel.

Rotor	Time when G' > 0 (min)	pH at Time of Event	Time of Sharp G' Increase (min)	pH at Time of Event	Time of G' Plateau (min)	pH at Time of Event
No Rotor	3	7.1	48	4.9	127 (98000 Pa)	4.0
ThT	3	7.0	43	4.9	122 (54000 Pa)	4.0
DCVJ	3	7.0	40	5.0	122 (57000 Pa)	3.9
CCVJ	3	7.1	50	4.7	150 (16000 Pa)	4.0
Nile Blue	5	6.8	44	4.9	135 (16000 Pa)	3.8

Table 4 Summary of the kinetic changes in the rheology of 7MeONapFF gelation in the presence (and absence) of various dyes

6.2.3 Study of Kinetics of Gelation with Different GdL Concentrations

From extensive study of gelation kinetics of various gelators mentioned in this Chapter, it is clear that by monitoring the fluorescence of ThT during the gelation provides vital information with regards to the process. Not only does it correlate directly to the rheology during the gelation process, but it also seems to behave as a molecular rotor. The fluorescent behaviour of ThT during the gelation process mirrored that of known molecular rotors DCVJ and CCVJ, showing an initial increase in fluorescence at approximately the pK_a of the gelator, where the self-assembly (and hence fibre formation) has been shown to occur.[38] Many have

ascertained the presence of β-sheet structures in their materials using ThT[34, 35], but the data shown here explains the reason for the increase in fluorescence when ThT is incorporated into these β-sheet structures. Stsiapura *et al.* have also demonstrated an increase in ThT fluorescence in glycerol/water mixtures (with increasing glycerol content) which they have attributed to the ThT playing its role as a molecular rotor.[37] Furthermore, ThT is a charged molecule therefore its binding ability is pH dependent.[52] Particularly, ThT has been shown to poorly bind to amyloid-type materials at acidic pH.[52, 53] Thus, the ThT fluorescence behaviour observed in this Chapter, as the pH is lowered and gelation ensues, is evidence of molecular rotor behaviour (regardless of its binding to amyloid-type structures).

To gain further insight into the gelation process of the class of LMWG studied throughout this Chapter, the amounts of GdL could be altered. Doing so would not only allow the speed of the pH decrease to be varied and hence the gelation kinetics, but also the final pH value, which will affect the bulk properties.[54] To investigate this, the gelator 2NapFF (Scheme 2f) was gelled with different GdL concentrations and the fluorescence and rheological kinetics were recorded as before. 2NapFF solutions were prepared at concentrations of 5 mg/mL as before but were diluted by half before using. 2NapFF is a hydrophobic gelator similar to 7MeONapFF and 1NapFF and gives a very viscous solution at a concentration of 5 mg/mL.[13] Diluting to 2.5 mg/mL lowers the viscosity and allows the viscosity changes in the rotor environment to be probed from a lower viscosity solution through to the gel phase. Figure 7 shows the kinetic fluorescence data collected for the gelation of 2NapFF samples in presence of ThT, *via* the additions of 0.5, 1, 1.5 and 2 mg/mL GdL, respectively.

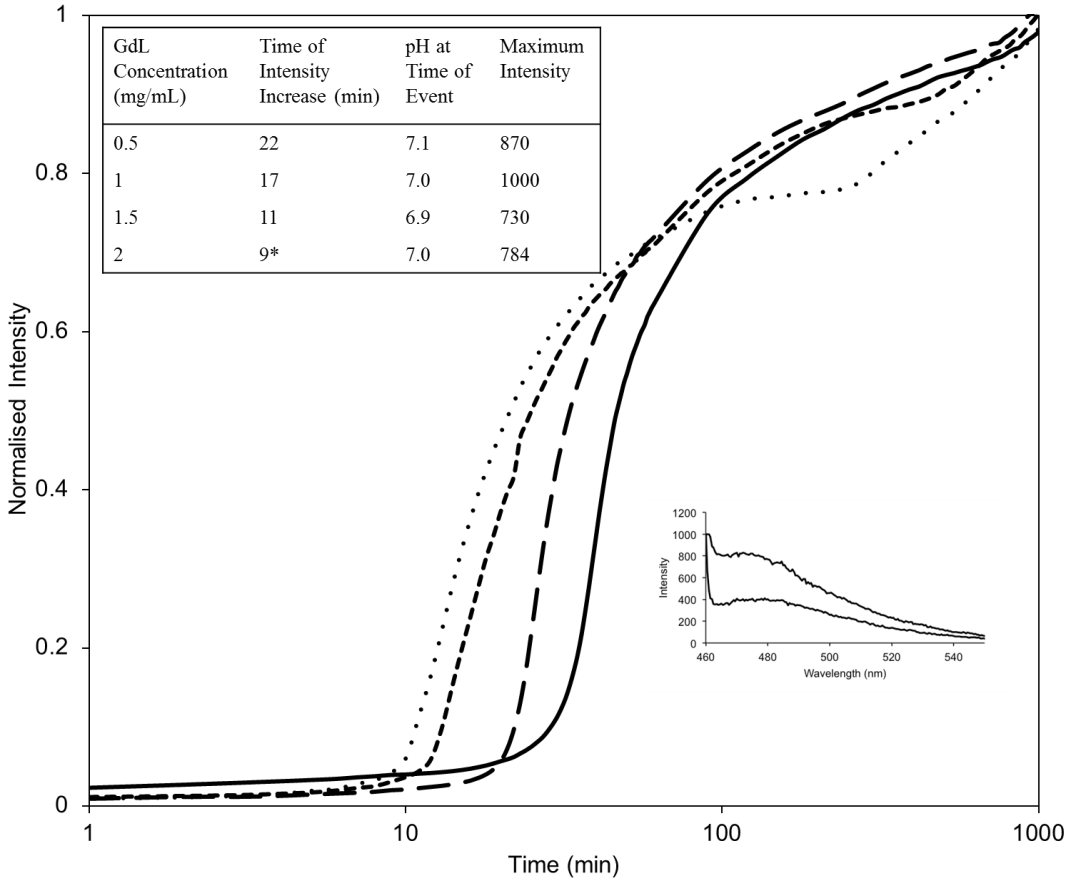

GdL Concentration (mg/mL)	Time of Intensity Increase (min)	pH at Time of Event	Maximum Intensity
0.5	22	7.1	870
1	17	7.0	1000
1.5	11	6.9	730
2	9*	7.0	784

Figure 7 Normalised changes in ThT fluorescence at 485 nm (λex = 455 nm) upon addition of 2NapFF solutions to different concentrations of GdL. GdL concentrations shown are: 0.5 mg/mL (—), 1.5 mg/mL (− −), 1.5 mg/mL (- -) and 2 mg/mL (···). Shown inset are a table of the times and pH values at which the fluorescent behaviour changes and fluorescence spectra displaying the increase in the ThT peak with time *time of increase before first plateau

A similar relationship between the ThT behaviour of the previously studied gelators in this Chapter and 2NapFF is observed. For all the 2NapFF samples shown in Figure 7, the point at which the fluorescent intensity begins to increase occurs at approximately the pK_a of the gelator (6.9). From Figure 7, it is clear that the initial increase in fluorescence intensity has a lag time which decreases as the GdL concentrations decreases, as could be expected. Clearly, the absolute pH value determines the assembly of the gelator, rather than the time taken to reach this pH. As seen for previous examples, this correlates with the generation of a measurable G' value around the same pH (Table 5). Using a GdL concentration of 2 mg/mL also shows an increase to a plateau, before increasing again and hence, indicating a two-stage kinetic process for the gelation of 2NapFF. This is not seen for the lower GdL concentrations. Although the kinetic process is shorter at higher GdL concentrations,

the final pH value (after 1000 min) is also lower. The smaller pH range change during the gelation process of 2NapFF samples with GdL concentrations lower than 2 mg/mL could be attributed to the absence of this two-stage process in the fluorescence spectra, seen for BrNapAV at higher GdL concentrations than shown in this Chapter.[38] This plateau occurs at pH 4.6 and more importantly, at point during the increase in *G'* and separation from *G"*. At this point, it is likely that 2NapFF has undergone significant assembly but is not in the gel phase. Despite this appearance of a two-stage kinetic process, the direct correlation between the kinetic rheological behaviour between 2NapFF samples with different GdL concentrations would indicate that the kinetic pathway is the same, however. When a GdL concentration of 0.5 mg/mL is added to a 2NapFF solution, ThT is sensitive enough to probe changes in viscosity as 2NapFF begins to assemble but no gelation occurs. After 1000 min, the pH had decreased to pH 6. As this is below the pK_a, some assembly will have occurred, but it would not be sufficient to form a fibrous matrix capable of sustaining the entrapment of the solvent. The intensity of fluorescence does begin to increase at the pK_a of 2NapFF as before and continues to increase to give a final intensity of 870 (a.u.) after 1000 min – higher than the final intensity of fluorescence when gelation was carried out with GdL concentrations of 1.5 and 2 mg/mL. Gelation does not occur with a GdL concentration of 0.5 mg/mL, which shows that there is no direct correlation between the absolute fluorescence intensity and *G'*. Only the kinetic process is probed, not the final mechanical properties of the gel. Fluorescence of the molecular rotors is a response to changes in local viscosity, allowing early fibre formation to be probed. This differs from the environment probed *via* rheology, as this probes the bulk material. Therefore the degrees of sensitivity to changes in the viscosity as a result of fibre formation will be dissimilar between techniques. Thus, fluorescence intensity will continue to increase as fibres being to form from 2NapFF when 0.5 mg/mL GdL is added, but the fibril growth (and hence fibrous network formation) will not be extensive enough to entrap water and produce a hydrogel. A GdL concentration of 0.5 mg/mL is too low to give a sufficient enough pH drop to allow gelation to occur. Therefore, viscosity changes on the local scale relative to the molecular rotor will change and generate a fluorescent response regardless of whether that viscosity change is significant enough to lead to gel formation on a bulk scale.

GdL Concentration (mg/mL)	Time when G' > 0 (min)	pH at Time of Event	Time of Sharp G' Increase (min)	pH at Time of Event	Time of G' Plateau (min)	pH at Time of Event
0.5	43	6.8	-[a]	-[a]	-[a]	-[a]
1.0	39	6.8	270	5.5	>1000 (19000 Pa)	4.3
1.5	37	6.8	168	5.0	700 (22000 Pa)	4.2
2.0	37	6.6	105	5.7	700 (23000 Pa)	4.2

Table 5 Summary of the kinetic changes in the rheology of 2NapFF gelation with different concentrations of GdL. [a]Sample did not form a gel

Importantly, the rheological behaviour is consistent for all the gelators tested. All gelators show an initial measurable *G'* value at the pK_a of the gelator, with a sharp increase and evolution of *G'* just below the pK_a before plateauing and thus, indicating that gelation has occurred. Again, the plateau moduli differ in the presence of the rotors. All gelators show a direct correlation between the initial increase in fluorescence of the molecular rotors with the initial evolution of the rheological properties.

6.2.4 Manipulation of Hydrogelation Kinetics using an Additive

Previous reports have shown that the incorporation of polymeric additives into low molecular weight hydrogels can affect the mechanical properties.[8, 9, 55, 56] Our group has previously shown that relatively low levels of fluorescently modified dextran materials can be incorporated without affecting the material properties.[57] However, incorporation of varying molecular weight polymeric materials can improve[6, 58] or deplete[8, 9] the mechanical properties. Javid *et al.* have demonstrated increased mechanical strength of Fmoc-dipeptide gels *via* the addition of the protein cluster β-lactoglobulin.[58] Our group has also shown in the past that kinetics of gelation can be affected by addition of a polymeric material into the hydrogel system.[9] Using this approach here, polymeric materials were incorporated into one of the aforementioned hydrogel systems (in this Chapter) and the kinetics monitored. Dextran was chosen

as its water solubility allows easy integration into the LMWG solution, and many molecular weights are also commercially available. Furthermore, it has been demonstrated to affect the kinetics of similar materials.[9] Here, the gelator 2NapFF was chosen (0.25 wt% final gelator concentration, 2 mg/mL GdL) and the kinetics of gelation were studied by utilising ThT fluorescence and rheological measurements as before. Dextran (6000 g/mol) was dissolved in water and added to the gelator solution at high pH and therefore before GdL had been added. Different final concentrations of dextran were tested: 15, 20 and 30 wt%. These were also compared to the gelation of 2NapFF alone.

As seen in Section 6.2.3 (Figure 7), 2NapFF (2 mg/mL GdL) shows no fluorescent output in the presence of ThT until around the pK_a of the gelator is reached after about 9 min. The indication of two-stage kinetic profile is also visible. The kinetic profile is similar when 15 and 20 wt% dextran is incorporated into the gelator system (Figure 8). In the presence of dextran, however, there is a fluorescence output from time zero. The gelator solutions containing dextran are visibly more viscous which could impact the fluorescent signal before gelation. 15 wt% dextran fluorescence in the presence of ThT was measured (no gelator present) and no fluorescence was detected (data not shown), thus suggesting that crowding effects[59, 60] could play a role in the increased viscosity and hence the increased fluorescent signal from time zero.

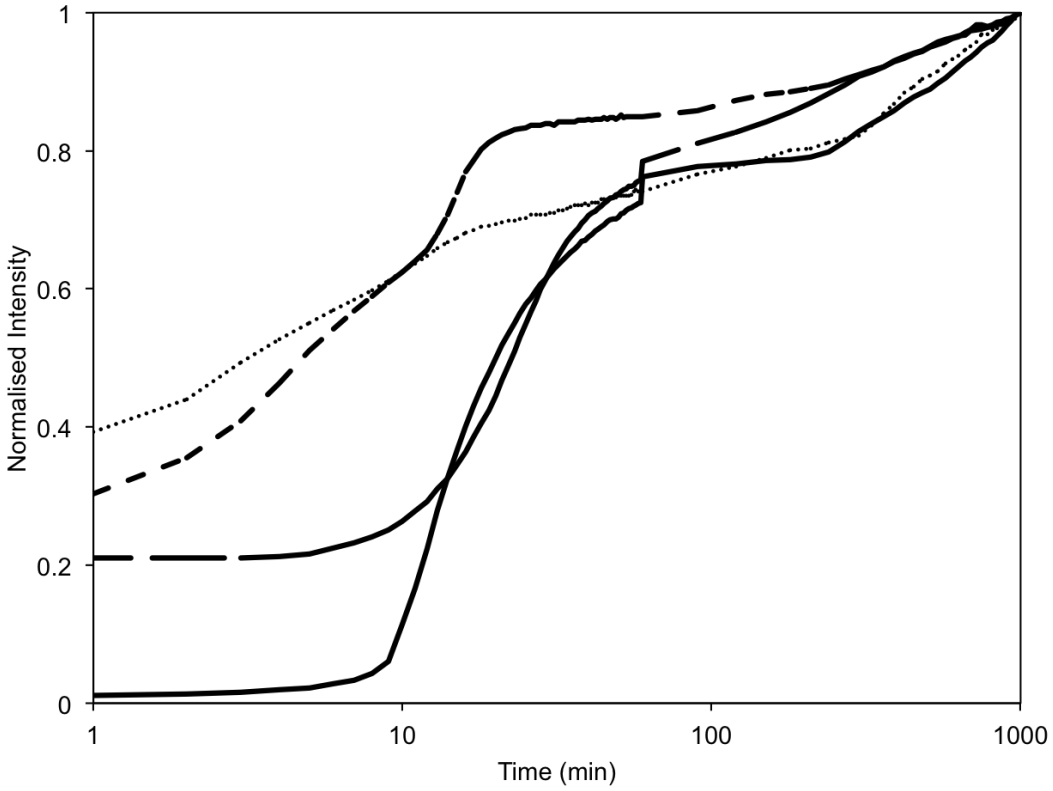

Figure 8 Normalised changes in ThT fluorescence at 485 nm (λex = 455 nm) upon addition of 2NapFF solutions containing no dextran (—), 15 wt% dextran (6K) (– –), 20 wt% dextran (- -) and 30 wt% dextran (···) to 8 mg/mL GdL. Shown inset are a table of the times and pH values at which the fluorescent behaviour changes

For a sample containing 30 wt% dextran, a steady increase in fluorescence is observed throughout the time of the experiment. In this case, the fluorescence data implies that there is a viscous environment from time zero that steadily increases, even below the pK_a of the gelator. Haidekker *et al.* have previously reported an increase in fluorescence of DCVJ in the presence of dextran.[27] A sample containing 20 wt% dextran shows a steady increase above the pK_a of the gelator (from time zero), but a sharper increase in fluorescence is noted around the pK_a, much like a 2NapFF sample containing no gelator or 15 wt% dextran. A two-stage kinetic profile is not as pronounced in the presence of 15 or 20 wt% dextran and is not observed at all in the presence of 30 wt% dextran.

Dextran Concentration (wt %)	Time when G' > 0 (min)	pH at Time of Event	Time of Sharp G' Increase (min)	pH at Time of Event	Time of G' Plateau (min)	pH at Time of Event
0	32	6.7	107	5.7	700 (23000 Pa)	4.2
15	21	6.5	191	5.5	656 (25000 Pa)	4.4
20	6	6.6	196	4.8	385 (14000 Pa)	4.2
30	10	6.6	56	5.9	340 (3200 Pa)	4.2

Table 6 Summary of the kinetic changes in the rheology of 2NapFF gelation with different concentrations of dextran added (6K)

The rheological profiles measured during the gelation process in the presence and absence of dextran also show different behaviour. Despite an immediate increase in the fluorescence after the addition of GdL in the presence of dextran, the kinetics of rheology show that *G′* begins to increase is slightly quicker in the presence of dextran, compared to 2NapFF alone (Table 6). Perhaps this is due to the increased presence of structure in solution - leading to an increase in viscosity. However, the point at which *G′* begins to sharply increase and therefore becomes increasingly larger than *G″* is slightly slower when 15 or 20 wt% dextran is present. Previous work carried out by this group using varying concentrations and molecular weight dextrans also showed this effect.[9] The previous work also demonstrated a decrease in the final *G′* with increased dextran concentration at a fixed molecular weight. This was demonstrated with a higher molecular weight dextran (2000000 g/mol) than used here (6000 g/mol), however. Conversely, the data displayed in Figure 8 shows that when an even higher concentration of dextran is added (30 wt%) to 2NapFF, the kinetics are faster than 2NapFF alone but the hydrogel is much weaker. The latter is expected due to the previous work carried out by this group.

Despite the slowing of the gelation kinetics with the introduction of dextran into the hydrogel system, it is important to note that the pH at which *G′* initially increases is similar in all systems (slightly lower when 20 wt% dextran is present). Therefore,

despite the different gelation times, the points at which self-assembly and gelation develops occur at the same pH values. *G'* always begins to evolve around the pK_a of the gelator. In general, the sharp increase in *G'* occurs at the same pH too. As the solution viscosity is increased in the presence of dextran[9], it could be interpreted that dextran act as a physical barrier working against the kinetics of assembly. The increase in solution viscosity slows the kinetics of assembly and hence gel formation at a dextran concentration of 15 and 20 wt%. Diffusion will therefore be reduced for both gelator and growing fibres. Published data from this group has shown that the fibres are thinner in the presence of dextran.[9] This implies that fibre thickening commonly observed in these systems by lateral association is not so prevalent, perhaps due to extremely reduced diffusion of the large fibrous structures. The inclusion of dextran into the gelator solution decreases the onset of the plateau on *G'* with increased dextran concentration which could be a result of thinner fibre formation giving the ability to entangle more easily, hence network formation is quickened. This may also explain the decreased mechanical strength due to thinner fibres making up the gel network. The slightly different kinetic behaviour observed for 30 wt% implies that fibril growth and association is affected by the high loading of dextran and the fibril network formation is different from that found in 2NapFF alone and in the presence of lower dextran concentrations.

6.2.5 Relationship Between Molecular Rotors and Final Hydrogel Properties

To probe the gelation process, a molecular rotor must be incorporated into the hydrogel matrix in such a way that allows it to elicit a response in the fluorescence spectrum. This could involve the rotor being non-covalently bound within the actual fibrils or within the fibrous matrix. If the former is the case, this may have a greater effect on the mechanical properties of the gel. The rotor being within the assembled chains would surely affect the mechanical strength whilst also garnering a viscous local environment for the rotor. The molecular rotors studied here contain aromatic rings and π-π stacking interactions between gelator molecules and rotor molecules could be considered entirely plausible. As seen in Sections 6.2.2, 6.2.3 and 6.2.4, incorporation of additives – whether it be a molecular rotor or a polymeric material, can have an effect on the final mechanical properties of a hydrogel. When using a molecular rotor to probe the gelation kinetics, it is important that the molecular rotor

does not have a detrimental effect on the gelation process or gel properties so that what is being probed by the rotor is a true representation of the gel alone. Section 6.2.2 shows that the presence of some of the rotors in several of the gelator systems has an effect on the values of the plateau moduli of the gels. To further study the effects of the rotor on final gel properties, several different concentrations of ThT and Nile Blue were added to gelator solutions of 7MeONapFF as before. GdL was then added and the samples were left to gel overnight before the final rheological properties were measured. Final rheological properties were measured using a vane and cup measuring system, whereas in Sections 6.2.2 and 6.2.3 a parallel plate system is used, meaning that the absolute values of *G′* cannot be directly compared. Over the concentration ranges studied for both ThT and Nile Blue (Figure 9), the mechanical properties remained relatively unchanged; with a *G′* of approximately 12000 Pa measured for all gels. This remained true even across a much larger concentration range (0.5 – 50 μM) studied for ThT.

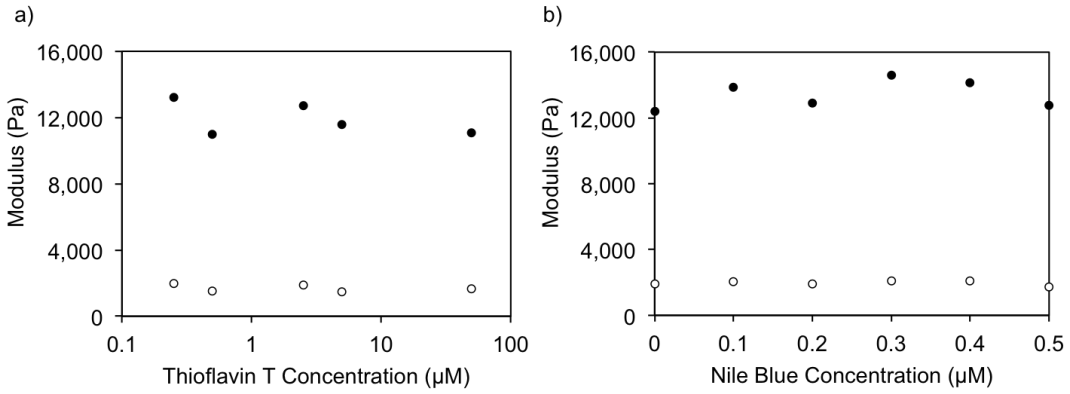

Figure 9 Final rheological properties of 7MeONapFF prepared using 8 mg/mL GdL and containing different concentrations of a) ThT and b) Nile Blue. *G′* is represented by ● and *G″* by ○

Either the presence of ThT or Nile Blue in 7MeONapFF not affecting the final mechanical properties is coincidental, or both are incorporated in the same regions of the hydrogel and thus giving rise to the same presence in the gels. Confocal microscopy suggests that both ThT and Nile Blue probe the same region of the gels as the confocal (Figure 10) images show the same fibrous material when probing the same gel. Gels containing ThT or Nile Blue show densely packed fibrous networks.

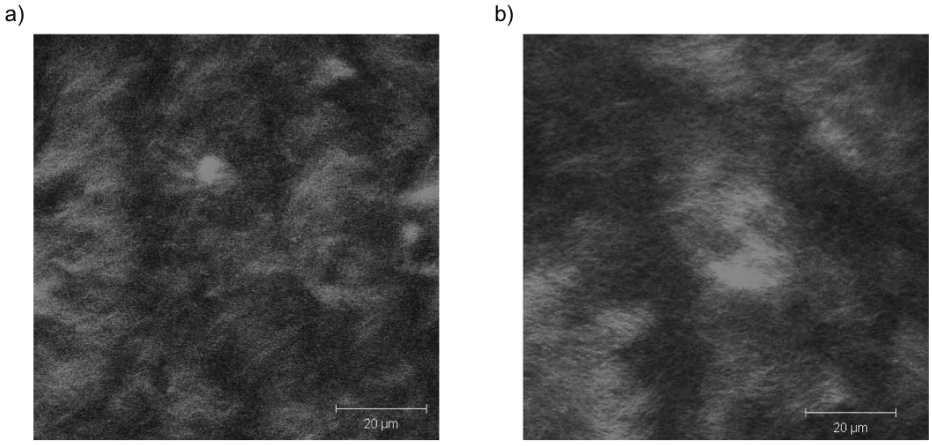

Figure 10 Confocal images of gels of 7MeONapFF containing a) Thioflavin T and b) Nile Blue

As ThT has been described to intercalate with β-sheets[34-36], ThT could be positioned within or between primary fibres. These fibres would then associate with other fibres to become thicker fibres, followed by entanglement and gelation. BrNapAV[38] and 2NapFF gelation with ThT both show a two-stage growth profile (under certain conditions), thus implying that ThT is associated with fibres during the primary fibre formation and fibre entanglement phases. As the rheological properties are affected by the presence of rotors (and Nile Blue) to different degrees may indicate that the packing of the dye material in the fibres is not as efficient in some of the gelators. Therefore, the packing will not be disrupted as much, and hence the rheological properties, if the association of the dye within the fibres is not to the same degree (weaker or less) in different gelators.

Along with final properties of 7MeONapFF being generally unaffected by the incorporation of a molecular rotor into the hydrogel system, the gelator solution is unchanged also. A solution of 7MeONapFF is viscous at high pH due to the formation of worm-like micelles at high pH.[13, 41] The addition of rotor to a 7MeONapFF solution does not affect the viscosity of the solution (Figure 11), suggesting that it does not interrupt the initial gelator structures in solution.

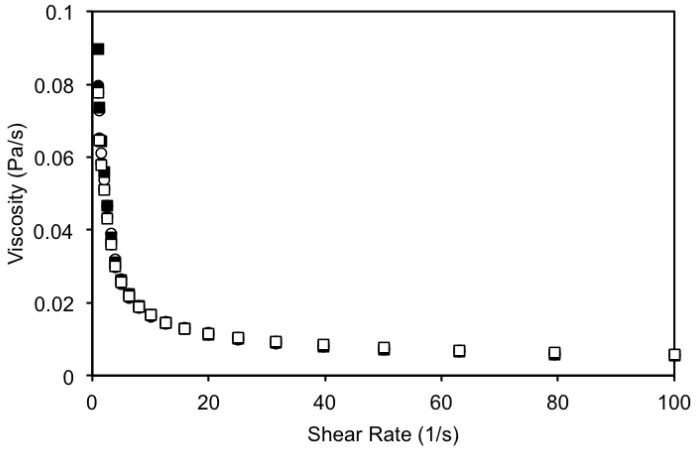

Figure 11 Viscosities of 7MeONapFF solutions containing no rotor (●), ThT (○), DCVJ (■) and Nile Blue (□)

6.3 Conclusion

Molecular rotors can effectively probe the hydrogelation kinetics of LMWG. By combining the information gathered from the fluorescence spectra of molecular rotors during the gelation process with the kinetic rheological data shows that assembly and gelation begins at the pK_a of the gelator. The rotors tested show that each rotor can provide the same kinetic information and further provides evidence that gelation is strongly related to the apparent pK_a of a LMWG. Interestingly, the kinetic information gathered from molecular rotors is mirrored by the widely reported β-sheet stain: Thioflavin T. On this basis, ThT can be thought purely as a molecular rotor in this case, showing sensitivity to changes in local viscosity just like the other rotors. ThT (and the other rotors) can probe the hydrogelation kinetics of several (similar) gelator systems and their presence do not appear to have a detrimental effect on the kinetic properties, even across a range of molecular rotor concentrations. To gain further insight into the gelation process of these materials, composite hydrogels containing dextran were studied and show a slowing down of the kinetic process which can lead to changes in the gelation behaviour at higher dextran concentrations. The sensitivity demonstrated here by ThT to changes in viscosity gives it emerging promise as viscosity sensor and probe for potential use in biosensor applications.[24, 61] Furthermore, its strongly fluorescent behaviour in these

hydrogel materials will allow future new hydrogels materials with similar mechanical properties to be probed to gain kinetic information and aid in the understanding of the gelation process.

6.4 References

1. D. J. Adams, *Macromol. Biosci.*, 2011, **11**, 160-173.
2. D. J. Adams and P. D. Topham, *Soft Matter*, 2010, **6**, 3707-3721.
3. P. Terech and R. G. Weiss, *Chem. Rev.*, 1997, **97**, 3133-3160.
4. I. W. Hamley, *Soft Matter*, 2011, **7**, 4122-4138.
5. Y. J. Adhia, T. H. Schloemer, M. T. Perez and A. J. McNeil, *Soft Matter*, 2012, **8**, 430-434.
6. J. Wang, Z. Wang, J. Gao, L. Wang, Z. Yang, D. Kong and Z. Yang, *J. Mater. Chem.*, 2009, **19**, 7892-7896.
7. E. Carretti, S. Grassi, M. Cossalter, I. Natali, G. Caminati, R. G. Weiss, P. Baglioni and L. Dei, *Langmuir*, 2009, **25**, 8656-8662.
8. G. Pont, L. Chen, D. G. Spiller and D. J. Adams, *Soft Matter*, 2012, **8**, 7797-7802.
9. L. Chen, S. Revel, K. Morris, D. G. Spiller, L. C. Serpell and D. J. Adams, *Chem. Commun.*, 2010, **46**, 6738-6740.
10. L. E. Buerkle and S. J. Rowan, *Chem. Soc. Rev.*, 2012, **41**, 6089-6102.
11. S. Roy, N. Javid, J. Sefcik, P. J. Halling and R. V. Ulijn, *Langmuir*, 2012, **28**, 16664-16670.
12. L. Chen, G. Pont, K. Morris, G. Lotze, A. Squires, L. C. Serpell and D. J. Adams, *Chem. Commun.*, 2011, **47**, 12071-12073.
13. L. Chen, T. O. McDonald and D. J. Adams, *RSC Adv.*, 2013, **3**, 8714-8720.
14. B. Ozbas, K. Rajagopal, L. Haines-Butterick, J. P. Schneider and D. J. Pochan, *J. Phys. Chem. B*, 2007, **111**, 13901-13908.
15. J. Raeburn, A. Zamith Cardoso and D. J. Adams, *Chem. Soc. Rev.*, 2013, **42**, 5143-5156.
16. J. H. van Esch, *Langmuir*, 2009, **25**, 8392-8394.
17. Z. Yang, G. Liang, M. Ma, Y. Gao and B. Xu, *J. Mater. Chem.*, 2007, **17**, 850-854.
18. J. P. Schneider, D. J. Pochan, B. Ozbas, K. Rajagopal, L. Pakstis and J. Kretsinger, *J. Am. Chem. Soc.*, 2002, **124**, 15030-15037.
19. V. Jayawarna, M. Ali, T. A. Jowitt, A. F. Miller, A. Saiani, J. E. Gough and R. V. Ulijn, *Adv. Mater.*, 2006, **18**, 611-614.
20. M. Wilhelm, C. L. Zhao, Y. Wang, R. Xu, M. A. Winnik, J. L. Mura, G. Riess and M. D. Croucher, *Macromolecules*, 1991, **24**, 1033-1040.
21. D. Das, A. Dasgupta, S. Roy, R. N. Mitra, S. Debnath and P. K. Das, *Chem. Eur. J.*, 2006, **12**, 5068-5074.
22. A. Benjelloun, A. Brembilla, P. Lochon, M. Adibnejad, M.-L. Viriot and M.-C. Carré, *Polymer*, 1996, **37**, 879-883.
23. M. L. Viriot, M. C. Carre, C. Geoffroy-Chapotot, A. Brembilla, S. Muller and J. F. Stoltz, *Clin. Hemorheol. Micro.*, 1998, **19**, 151-160.
24. M. A. Haidekker and E. A. Theodorakis, *Org. Biomol. Chem.*, 2007, **5**, 1669-1678.
25. T. Förster, G. Z. Hoffmann, *Phys. Chem.*, 1971, **75**, 63-76.

26. M. A. Haidekker, T. P. Brady, D. Lichlyter and E. A. Theodorakis, *J. Am. Chem. Soc.*, 2006, **128**, 398-399.
27. M. A. Haidekker, T. P. Brady, S. H. Chalian, W. Akers, D. Lichlyter and E. A. Theodorakis, *Bioorg. Chem.*, 2004, 32, 274-289.
28. M. A. Haidekker and E. A. Theodorakis, *J. Biol. Eng.*, 2010, **4**, 11-24.
29. K. Wang, W. Shi, J. Jia, S. Chen and H. Ma, *Talanta*, 2009, **77**, 1795-1799.
30. T. Furuno, R. Isoda, K. Inagaki, T. Iwaki, M. Noji and M. Nakanishi, *Immunol. Lett.*, 1992, **33**, 285-288.
31. K. Y. Law, *Chem. Phys. Lett.*, 1980, **75**, 545-549.
32. H.-J. Yoon, M. Dakanali, D. Lichlyter, W. M. Chang, K. A. Nguyen, M. E. Nipper, M. A. Haidekker and E. A. Theodorakis, *Org. Biomol. Chem.*, 2011, **9**, 3530-3540.
33. R. O. Loutfy and D. M. Teegarden, *Macromolecules*, 1983, 16, 452-456.
34. L. Harry, III, in *Methods in Enzymology*, ed. W. Ronald, Academic Press, 1999, vol. Volume 309, pp. 274-284.
35. S. A. Hudson, H. Ecroyd, T. W. Kee and J. A. Carver, *Febs Journal*, 2009, **276**, 5960-5972.
36. M. Groenning, L. Olsen, M. van de Weert, J. M. Flink, S. Frokjaer and F. S. Jørgensen, *J. Struct. Biol.*, 2007, **158**, 358-369.
37. V. I. Stsiapura, A. A. Maskevich, V. A. Kuzmitsky, V. N. Uversky, I. M. Kuznetsova and K. K. Turoverov, *J. Phys. Chem. B*, 2008, **112**, 15893-15902.
38. L. Chen, K. Morris, A. Laybourn, D. Elias, M. R. Hicks, A. Rodger, L. Serpell and D. J. Adams, *Langmuir*, 2010, **26**, 5232-5242.
39. Y. Pocker and E. Green, *J. Am. Chem. Soc.*, 1973, **95**, 113-119.
40. D. J. Adams, M. F. Butler, W. J. Frith, M. Kirkland, L. Mullen and P. Sanderson, *Soft Matter*, 2009, **5**, 1856-1862.
41. J. Raeburn, T. O. McDonald and D. J. Adams, *Chem. Commun.*, 2012, **48**, 9355-9357.
42. L. Chen, S. Revel, K. Morris, L. C. Serpell and D. J. Adams, *Langmuir*, 2010, **26**, 13466-13471.
43. K. A. Houton, K. L. Morris, L. Chen, M. Schmidtmann, J. T. A. Jones, L. C. Serpell, G. O. Lloyd and D. J. Adams, *Langmuir*, 2012, **28**, 9797-9806.
44. V. Foderà, M. Groenning, V. Vetri, F. Librizzi, S. Spagnolo, C. Cornett, L. Olsen, M. van de Weert and M. Leone, *J. Phys. Chem. B*, 2008, **112**, 15174-15181.
45. J. Jose and K. Burgess, *Tetrahedron*, 2006, **62**, 11021-11037.
46. C. Tang, A. M. Smith, R. F. Collins, R. V. Ulijn and A. Saiani, *Langmuir*, 2009, **25**, 9447-9453.
47. Z. Yang and B. Xu, *J. Mater. Chem.*, 2007, **17**, 2385-2393.
48. A. Z. Cardoso, A. E. Alvarez Alvarez, B. N. Cattoz, P. C. Griffiths, S. M. King, W. J. Frith and D. J. Adams, *Faraday Discuss.*, 2013, **166**, 101-116.
49. Z. A. C. Schnepp, R. Gonzalez-McQuire and S. Mann, *Adv. Mater.*, 2006, **18**, 1869-1872.
50. L. Chen, S. Revel, K. Morris and D. J. Adams, *Chem. Commun.*, 2010, **46**, 4267-4269.
51. http://www.molinspiration.com/cgi-bin/properties
52. R. Mishra, D. Sjolander and P. Hammarstrom, *Mol. Biosys.*, 2011, **7**, 1232-1240.

53. M. Lindgren, K. Sörgjerd and P. Hammarström, *Biophys. J.*, 2005, **88**, 4200-4212.
54. T. Liebmann, S. Rydholm, V. Akpe and H. Brismar, *BMC Biotechnol.*, 2007, **7**, 88-98.
55. X. Y. Liu and P. D. Sawant, *Angew. Chem. Int. Ed.*, 2002, **41**, 3641-3645.
56. B. Adhikari and A. Banerjee, *Soft Matter*, 2011, **7**, 9259-9266.
57. S. Sutton, N. L. Campbell, A. I. Cooper, M. Kirkland, W. J. Frith and D. J. Adams, *Langmuir*, 2009, **25**, 10285-10291.
58. N. Javid, S. Roy, M. Zelzer, Z. Yang, J. Sefcik and R. V. Ulijn, *Biomacromolecules*, 2013, **14**, 4368-4376.
59. D. M. Hatters, A. P. Minton and G. J. Howlett, *J. Biol. Chem.*, 2002, **277**, 7824-7830.
60. L. A. Munishkina, E. M. Cooper, V. N. Uversky and A. L. Fink, *J. Mol. Recognit.*, 2004, **17**, 456-464.
61. M. E. Nipper, M. Dakanali, E. Theodorakis and M. A. Haidekker, *Biochimie*, 2011, **93**, 988-994.

CHAPTER 7

Conclusions

The design of dipeptide-based LMWG can be modified to give different final hydrogel properties. Altering the amino acid choice and sequence has an influence over gelation which can be correlated with the hydrophobicity of the gelator. Here in this Thesis, the relationship between the hydrophobicity of the gelators and the final properties show that more hydrophobic gelators such as FmocFF can form gels across a wider range of assembly conditions and concentrations. When the amino acid sequence is altered from FF to a more hydrophilic sequence, the range of gelation parameters becomes narrower using a solvent-mediated gelation trigger, and the gels formed are mechanically weaker in comparison. Solvent-triggered gels also show that both the solvent choice and $\Phi_{solvent}$ affect the final properties of the gel by impacting the gelation process. During the initial stage of gelation, a turbidity event was observed, with the duration of this event dependent on the solvent composition. The turbidity change suggests the formation of larger structures which reorganise to later form smaller structures that make up the final hydrogel composition. Turbidity events were not observed for gels prepared from any of the other assembly methods described in this Thesis. To investigate the proposed nucleation and growth process for solvent-mediated gelation further, confocal microscopy images at early time points could be of worth. They could give kinetic information about initial fibre formation and possibly deduce any changes in the growth of fibres between changes in the hydrogel composition. Data correlating the rheological properties with the concentration of gelator to provide information about the hydrogel network suggested that there are changes in the network formed with compositional changes in the hydrogel. A further confocal microscopy study could possibly show any differences in microstructure resulting in the different networks being formed. Probing the mesh size of the gel networks by NMR diffusion studies may also point out any differences in the networks formed when the hydrogel composition is altered.

Along with hydrophobicity, the influence of the pK_a of the LMWG studied in this Thesis is vital to the hydrogelation of these materials. Generally related to the hydrophobicity, higher pK_a materials tend to be more hydrophobic. As it has been previously reported that gelation occurs below the pK_a of a gelator, pH-triggered

gelation is commonly utilised. Like for solvent-mediated gelation triggers, changes in the pH trigger conditions have an effect on the final properties of a gel. Here in this Thesis, two very different methods of altering the pH to trigger gelation were demonstrated. The first of these, to the best of our knowledge, was the first example of UV-triggered gelation of a LMWG using a PAG to generate protons. The gels prepared using this protocol had similar fibril composition as gels prepared *via* other methods but were mechanically different at the same pH. The second pH-triggered method demonstrated in this Thesis utilised the electrochemically-triggered oxidation of HQ to liberate protons and induce gelation at an electrode surface. Both of these pH-triggered methods have the ability to spatially and temporally control gelation, giving promise for biosensing and cell culturing applications. The UV-triggered method could focus light to a particular region *via* a simple lithography technique. Further work could be carried out to develop multi-component gels using this setup. If two gelators in solution with different pK_a values were to be irradiated with UV light but only in a specific region for a controlled time, it could be envisaged that there would be the possibility to gel only one of the gelators in this region whilst the other (and some of the remaining gelator from the first material) remains in solution. This could also be used to entrap material in a specific region and with a specific hydrogel composition. UV-triggered gelation could also be of promise for cell culturing not only for the fact that it could potentially be grown on a surface (and patterned if need be) but UV light would afford sterile, ready to use gels for implanting cells for culture. Electrochemically-triggered gels did also show the ability to be patterned onto a surface and initial data demonstrated that they could also be used to support cell proliferation and growth in the future. However, due to the pK_a of most gelators being lower than physiological pH, hydrogel stability over longer periods of time under physiological conditions can become an issue. To overcome this, the development of gelators with higher pK_a values would be ideal. The presence of HQ under these conditions could also be eradicated by using different currents during the gelation process, to those demonstrated in this Thesis, which would oxidise the water already present in the system and could liberate protons to decrease the pH at the electrode surface.

It was clear from detailed studies of several assembly methods that the gelation process has a profound effect on the final properties of a gel. Molecular rotors

allowed the gelation process to be probed. They showed that self-assembly and gelation always occurred around the pK_a of the gelator. This was consistent for a number of gelator systems and using different molecular rotors. ThT could behave as a molecular rotor in the small number of gelators tested. However, these gels all consist of β-sheet type structures and ThT is a known stain for these types of materials. Further testing of the validity of ThT's role as a molecular rotor could be tested by probing the gelation kinetics of gelators that are known to not form β-sheets. Introducing additives into the hydrogel did affect the kinetics but the attributes associated with the gelation process were unaffected (at the lower concentrations tested) i.e. self-assembly and gelation still occurred around the pK_a despite a slowing of the kinetics of gelation. As molecular rotors are viscosity sensors, further study into the fluorescent output detected and gelation could be analysed to see if there is a fluorescent intensity threshold over which a gel forms. If so, it could be possible to use a high throughput approach to initially screen many samples prepared by any method of trigger to see if gelation is successful or if some assembly occurs (leading to an increase in viscosity and hence, fluorescence intensity) but not gelation.

Here, it has been highlighted that the gelation process is of importance to the final properties of dipeptide-based low molecular weight hydrogels. Systematic changes in the gelation conditions, including choice of self-assembly trigger and the conditions of the trigger itself can have an impact on the mechanical properties of the resulting gel. Even subtle changes in these protocols can result in different final mechanical properties. Although the absolute rules for designing gels with specifically desired properties are not fully understood, there is an increased wealth of understanding as to how to control gelation of these materials to provide gel properties required for a potential application.